

CARDIFF UNIVERSITY

SCHOOL OF CHEMISTRY



**Novel Colorimetric Mustard Sensing
in Surfactant and Microemulsion Systems**

Thesis submitted for the degree of Doctor of Philosophy by

Bria Shannon Thomas

April 2022



CARDIFF UNIVERSITY
SCHOOL OF CHEMISTRY

Abstract

Doctor of Philosophy

By Bria Shannon Thomas

Chemical warfare agents (CWAs) have an unfortunately long history with various military and terrorist groups choosing to employ these highly toxic chemicals. The unrestricted stockpiling and development of CWAs led to the introduction of the Chemical Weapons Convention (CWC) in 1993 which outlawed these practices. Despite this, their unlawful deployment has continued resulting in substantial threat levels of possible chemical attack by international terrorists. This has led to an increased interest in the development of colorimetric sensors for the determination of these chemicals. Current methods of CWA verification are predominantly equipment-based and thus suffer from limitations including non-portability, high cost and complicated operations. Hence, there is high demand for inexpensive and lightweight colorimetric sensors that are simple to use for first responders. The development of sensitive and selective colorimetric devices for blister agents is investigated in this thesis.

The first section of the thesis focuses on the development of sensors for mustard detection. Firstly, this research aimed to improve the mustard detection response of 4-(4-nitrobenzyl)pyridine (NBP) reported by Epstein. The incorporation of reagents in an anionic microemulsion eliminated the stepwise addition of reagents and the need for elevated temperatures. Exposure to various interfering agents revealed the high selectivity of NBP towards mustard simulants.

Furthermore, the alkylation of NBP by anionic surfactant initiated an investigation into an alternative anionic surfactant to improve the shelf-life of the formulation. Furthermore, the preliminary research into self-assembled sensors for mustard detection was reported. An alternative merocyanine chromophore exhibited a moderate colour response upon exposure to CEES. However, the initial yellow-brown colour of the merocyanine in solution is undesirable and demonstrated the further work required to create a reliable analyte-induced sensor.

The second section of the thesis presents the development of smart devices containing the NBP anionic microemulsion formulation, reported in Chapter 2, for use in real-life scenarios. Swab technologies were manufactured and tested with CEES alongside the detection of contaminated soil.

Acknowledgements

I would first like to thank my principal supervisor Professor Ian Fallis for allowing me to be involved in such an interesting research project. Your knowledge and dedication to the subject has greatly contributed to the project's progress and the work in this thesis. Thank you for your continued support and guidance throughout my postgraduate studies.

I would also like to thank KESS2 and the European Social fund together with David Fraser and Dr Peter Corish at BBI, my industrial partner. I would also like to show my appreciation for all the technical and support staff at CHEMY who have allowed my project to run smoothly. I am very grateful to Simon Waller and Dr Robert Jenkins for their assistance with mass spectrometry measurements and their generosity in allowing me to undertake training to use the spectrometers. A very grateful thanks goes to Hygiena for their interest in the project and supply of swab components and also the Southampton Crystallography Service.

I am very grateful to my colleagues in the IAF group for generously sharing their knowledge and advice. In particular, I would like to thank Andy, Ashley, Siôn, Ibrahim, Mauro and Nuha. Special recognition must go to Andy for his continued encouragement and his dedication to passing on his knowledge, to Siôn for being so generous with his time and for always making me laugh especially when I needed cheering up, and to Owaen for answering all my questions without judgment, especially those concerning IT problems. My postgraduate experience would not have been as rewarding without you and I am very fortunate to have you as friends. I have many fond memories of my time at Cardiff University to look back on thanks to you all.

A huge thank you goes to the ChemChickas, Jessica, Marina, Rebekah and Sophie. Your friendship throughout my university journey has meant a great deal to me but your endless support has been instrumental during my PhD.

I would not have achieved so much during my life without the backing and encouragement of my family. Mam and Dad, I am so grateful that you have always inspired me to push myself in everything I do and thank you to Mamgu for motivating me to always do my best. Your constant love and support have always been felt despite you all not fully understanding what it is I am doing. I hope I have made you all, including Dadgu, proud and continue to do so in the future.

And finally, a huge thank you must go to my wonderful fiancé Peter. You have been by my side throughout most of my university journey and your never-ending support has given me much needed strength through the highs and lows of my academic career and personal life.

Table of Contents

Chapter 1. Introduction	1
1.1. A Brief History of Chemical Warfare Agents.....	2
1.2. Chemical Warfare Agents (CWAs)	3
1.3. Blister Agents.....	3
1.3.1. Lewisite Agents.....	4
1.3.2. Mustard Agents.....	5
1.3.2.1. Sulfur Mustard	6
1.3.2.2. Mode of Action of Sulfur Mustard	9
1.3.2.3. Nitrogen Mustard Agents	10
1.4. Nerve Agents	11
1.4.1 Mode of Action of Nerve Agents	19
1.5. Treatment of CWA poisoning.....	22
1.6. Simulants	24
1.7. Sulfur Mustard Sensors	25
1.7.1. Sulfur-Based Sensors.....	25
1.7.1.1. Thiol-Based Sensors	25
1.7.1.2. Thiocarbonyl-Based Sensors.....	26
1.7.2. Oxygen-Based Sensors.....	28
1.7.3. Nitrogen-Based Sensors.....	28
1.8. Nerve Agent Sensors.....	29
1.8.1. Sensors for the Determination of G-series Nerve Agents.....	29
1.8.1.1. Primary Alcohol-Based Sensors	29
1.8.1.2. Oxime-Based Sensors.....	31
1.8.2. Sensors for the Determination of V-series Nerve Agents	31
References	33
Chapter 2. The Rapid and Selective Detection of Sulfur and Nitrogen Mustards by a One-Pot Method	41
2.1. Introduction	42
2.1.1. Surfactants.....	42
2.1.2. Micellisation	44
2.1.3. Microemulsions.....	45
2.1.4. Development of the NBP Assay	46
2.2. Aims.....	51
2.3. Results and Discussion	52

2.3.1. Mustard (CEES) Detection in Solution and Anionic Microemulsion Solution	52
2.3.2. Performance of Anionic Aggregation Colloid Systems.....	56
2.3.3. Performance of Cationic Aggregation Colloid Systems.....	58
2.3.4. Performance of Non-ionic Aggregation Colloid Systems	60
2.3.5. Determination of Molar Extinction Coefficient of NBP-CEES Dye.....	61
2.3.6. Quantitative Absorbance Spectra of NBP Surfactant Formulations	63
2.3.7. Determination of NBP decomposition product	67
2.3.8. Development of Anionic Aggregation Colloid Systems	70
2.3.9. Selectivity studies.....	73
2.3.10. Mass Spectrometry Analysis of Anionic SDS-5T Aggregation Colloid System	78
2.3.11. Performance Comparison of SDS and SDBS	79
2.3.12. Investigating CEES Hydrolysis in Ionic Microemulsions	88
2.3.13. Investigating the pK_a of Alkylated NBP in SDS-5T Formulations	92
2.3.14. Measurement of NBP Location in SDS-5T Microemulsion.....	95
2.3.15. Evidence for the Proposed Mode of Action	98
2.4. Experimental	100
2.4.1. Preparation of surfactant mixtures	100
2.4.1.1. Anionic surfactant mixtures	100
2.4.1.2. Cationic surfactant mixtures	101
2.4.1.3. Non-ionic surfactant mixtures.....	101
2.4.2. Procedure for simulant and analyte testing	101
Synthesis of 1-(2-(Ethylthio)ethyl)-4-(4-nitrobenzylidene)-1,4-dihydropyridine (4)	102
2.5. References	103

Chapter 3. Self-Assembled Sensors for The Detection of Sulfur Mustards 107

3.1. Introduction.....	108
3.1.1. Merocyanine Dyes.....	108
3.1.2. Dye-Surfactant Interactions.....	109
3.2. Aims	111
3.3. Results and Discussion	112
3.3.1. Self-Assembled Sensors	112
3.3.2. X-Ray Structure of Alkylated Merocyanine Dye	114
3.3.3. Electronic Spectra of Merocyanines.....	115
3.3.4. <i>In-Situ</i> Merocyanine Formation	118

3.3.5. An Alternative Self-Assembled Sensor (SAS)	118
3.5. Experimental	121
3.5.1. Procedure for simulant and analyte testing	122
3.5.2. Synthesis of 1-(2-(Ethylthio)ethyl)-4-methylpyridinium chloride (1a)	122
General Procedure 1. Synthesis of Pyridinium Salts	122
Synthesis of 1-Ethyl-4-methylpyridinium bromide (1b)	123
Synthesis of 1-Propyl-4-methylpyridinium bromide (1c)	123
Synthesis of 1-Isopropyl-4-methylpyridinium bromide (1d).....	123
Synthesis of 1-Butyl-4-methylpyridinium bromide (1e)	124
Synthesis of 1-Pentyl-4-methylpyridinium bromide (1f)	124
General Procedure 2. Synthesis of Merocyanine Dyes	124
Synthesis of 4-(3,5-Di- <i>tert</i> -butyl-4-hydroxystyryl)-1-methylpyridinium (2a).....	125
Synthesis of 2,6-Di- <i>tert</i> -butyl-4-(2-(1-ethylpyridinium-4-yl)vinyl)phenolate (2b) ..	125
Synthesis of 2,6-Di- <i>tert</i> -butyl-4-(2-(1-propylpyridinium-4-yl)vinyl)phenolate (2c)	126
Synthesis of 2,6-Di- <i>tert</i> -butyl-4-2-(1-isopropylpyridinium-4-yl)vinyl)phenolate (2d)	126
.....	126
Synthesis of 2,6-Di- <i>tert</i> -butyl-4-2-(1-butylpyridinium-4-yl)vinyl)phenolate (2e)....	127
Synthesis of 2,6-Di- <i>tert</i> -butyl-4-(2-(1-pentylpyridinium-4-yl)vinyl)phenolate (2f) .	128
Synthesis of 2,6-di- <i>tert</i> -butyl-4-(2-(pyridin-4-yl)vinyl)phenol (MCP, 3).....	128
References	130
Chapter 4. Smart Devices for Chemical Warfare Agent (CWA) Detection.....	132
4.1. Introduction	133
4.1.1. Existing field detectors.....	133
4.1.3. Colorimetric swab technology.....	135
4.2. Aims.....	136
4.3. Results and Discussion	137
4.3.1. Detection in real-life scenarios.....	137
4.3.2. Sensing Mustard Agents in Soil.....	137
4.3.3. Sensing on surfaces	138
4.3.3.1. Swab Device for The Detection of Mustard Agents	140
4.4. Experimental.....	140
4.4.1. Procedure for CEES testing.....	140
4.4.2. Procedure for preparation of spiked soil sample	141
4.4.3. Manufacture of swab devices	141
4.4.4. Procedure for swabbing a CEES contaminated surface.....	142
References	143

Chapter 5. Concluding Remarks	144
5.1. Conclusion and Future Remarks	145
References	149
Appendix	150

Abbreviations

Spectroscopy and Techniques

CMC	Critical Micelle Concentration
ESI	Electrospray Ionisation
HRMS	High Resolution Mass Spectrometry
LD ₅₀	Lethal dose
LRMS	Low Resolution Mass Spectrometry
MS	Mass Spectrometry
NMR	Nuclear Magnetic Resonance
SANS	Small-Angle Neutron Scattering
UV-vis	Ultraviolet-visible spectroscopy

Units

ϵ	Extinction coefficient, L mol ⁻¹ cm ⁻¹
°C	Degrees Celsius
g	Gram
H	Hour
kV	Kilovolt
m/z	Mass-to-charge ratio
mg	Milligram, 1 x 10 ⁻³ g
min	Minute
mJ/Pulse	MegaJoule per pulse
mL	Millilitre, 1 x 10 ⁻³ L
mM	Millimolar, 1 x 10 ⁻³ molesL ⁻¹
mmol	Millimoles, 1 x 10 ⁻³ moles
mol	Moles
nm	Nanometres, 1 x 10 ⁻⁹ metres
Ns	Newton second
ppm	Parts per million
v/v	Volume by volume
w/w	Weight by weight
wt%	Weight percent
ϵ_r	Relative permittivity (dielectric constant)
μ L	Microliter, 1 x 10 ⁻⁶ L
μ M	Micromolar, 1 x 10 ⁻⁶ molesL ⁻¹

Solvents, Chemicals and Compounds

AChE	Acetylcholine esterase
BAL	British Anti-Lewisite
Brij 35	Polyoxyethylene (23) and lauryl ether
CEEE	2-Chloroethyl ethyl ether
CEES	2-Chloroethyl ethyl sulfide
CEES-OH	2-(Ethylmercapto)-ethanol
CHCl ₃ - <i>d</i>	Deuterated chloroform
DCM	Dichloromethane
DCNP	Diethyl cyanophosphate
DCP	Diethyl chlorophosphate
DFP	Diisopropylfluorophosphate
DMSO- <i>d</i> ₆	Deuterated dimethylsulfoxide
DNA	Deoxyribonucleic acid
GA	Tabun
GB	Sarin
GD	Soman
GF	Cyclosarin
HD	Sulfur mustard
HN	Nitrogen mustard
L	Lewisite
MeOH- <i>d</i> ₄	Deuterated methanol
MTT	Thiazolyl blue tetrazolium bromide
NBP	4-(4-nitrobenzyl)pyridine
PhCES	2-Chloroethyl phenyl sulfide
SDBS	Sodium Dodecylbenzenesulfonate
SDBS-5T	Sodium dodecylbenzenesulfonate microemulsion containing 5 wt% toluene
SDS	Sodium Dodecyl Sulfate
SDS-0T	Sodium dodecyl sulfate microemulsion containing 0 wt% toluene
SDS-1T	Sodium dodecyl sulfate microemulsion containing 1 wt% toluene
SDS-2T	Sodium dodecyl sulfate microemulsion containing 2 wt% toluene
SDS-3T	Sodium dodecyl sulfate microemulsion containing 3 wt% toluene
SDS-4T	Sodium dodecyl sulfate microemulsion containing 4 wt% toluene
SDS-5T	Sodium dodecyl sulfate microemulsion containing 5 wt% toluene
SM	Sulfur mustard
TBAF	Tetrabutylammonium fluoride

TBAOH	Tetrabutylammonium hydroxide
TPT	2,3,5-Triphenyltetrazolium salt
TVC	Tetrazolium violet chloride
VE	O-ethyl-S-2-diethylaminoethyl ethyl phosphonothioate
VG	O,O-diethyl S-2-diethylaminoethyl phosphorothioate
VM	O-ethyl S-2-diethylaminoethyl methylphosphonothiate
VR	<i>N</i> -diethyl-2-(methyl-(2-methylpropoxy)phosphoryl)sulfanylethanamine
VX	O-ethyl S-2-diisopropylaminoethyl methyl phosphonothiolate

Miscellaneous

CWA	Chemical Warfare Agent
O/W	Oil-in-Water
PET	Photoinduced Electron Transfer
SAS	Self-Assembled Sensor
W/O	Water-in-Oil

Chapter 1. Introduction

1.1. A Brief History of Chemical Warfare Agents

Chemical warfare agents (CWAs) have a long history however their use has been a particularly contentious topic since the 20th century. The first large scale use of chemical weapons occurred in Ypres, Belgium, in 1915.¹ German forces released one hundred and sixty tonnes of chlorine, an asphyxiating gas, against allied soldiers. It was estimated that 5,000 men were killed and another 10,000 were wounded.² Fritz Haber, a German scientist, was responsible for the weaponization of chlorine. He is known to many as a Nobel Prize winner for his invention of the Haber-Bosch Process however, he is also labelled as the ‘father of chemical warfare’ for his work on the development and weaponization of poisonous gases during World War I (WWI). In his acceptance speech as Nobel Laureate he referenced chemical warfare saying *“In no future war will the military be able to ignore poison gas. It is a higher form of killing”*.³ Ypres was chosen again by the Germans in 1917 for the release of Yperite, a new chemical weapon named after the Belgian city.⁴ This chemical is more commonly known as sulfur mustard and was first used against British forces resulting in a total of 150,000 casualties in the British Army alone.⁵

In 1925, the Geneva protocol⁶ was drafted to prohibit the use of chemical and biological weapons in war. Unfortunately, the protocol only banned the use of these weapons and did not restrict their stockpiling and research. Despite the condemnation of chemical weapons by the public,⁷ the use and development of these agents continued. Notable uses of these chemical weapons include the Iran-Iraq War between 1980-1988^{8,9} and the Gulf War between 1990-1991¹⁰. It wasn't until 1993 that the development, production and stockpiling of chemical weapons was outlawed in the Chemical Weapons Convention (CWC) which was signed by 193 state parties.¹¹ Despite this, there have been many examples of chemical weapon use. More notably, the G-series nerve agent attacks in Matsumoto, Japan in 1994¹² and on the Tokyo subway in 1995.¹³ The Tokyo subway sarin attack was responsible for killing 12 people and injuring more than 5,000 others with some victims reporting temporary vision problems. Recent uses of V-series nerve agents include the 2017 assassination of Kim Jong-nam, half-brother of North Korean leader Kim Jong-un, by VX poisoning in Malaysia and the attempted assassination of the former Russian military intelligence officer, Sergei Skripal, in England in 2018. In the latter incident, an undeclared high purity nerve agent poisoned and hospitalised three people.¹⁴ The name and structure of this nerve agent is classified as it belongs to a new class of agent developed in Russia.^{15,16}

1.2. Chemical Warfare Agents (CWAs)

Chemical weapons are defined in the CWC as 'any chemical which through its chemical action on life processes can cause death, temporary incapacitation or permanent harm to humans or animals'.¹¹ There are several classes of CWAs including blood agents, choking agents, psychomimetic agents, nerve agents, riot-control agents, toxins and vesicants (blister agents). However, this thesis will focus on blister and nerve agents. It is the physical and chemical properties of CWAs that determine how they are deployed and their effect on the body. In general, CWAs are liquids, and they can be further categorised by their environmental persistency based on their vapour pressures. Non-persistent agents like some G agents have relatively high vapour pressures therefore they are able to vaporise easily upon dissemination. On the other hand, blister agents and V agents have lower vapour pressures and as such are environmentally persistent. These agents can be disseminated as droplets or aerosols and its harmful effects can be intensified by incorporating a polymer thickening agents to further complicate its removal and decontamination from the environment or skin.

1.3. Blister Agents

As their name implies, blister agents or vesicants are a group of chemicals that damage skin tissue causing inflammation and painful blisters.¹⁷ Figure 1.1 illustrates the two categories of blister agent; lewisites and mustards.

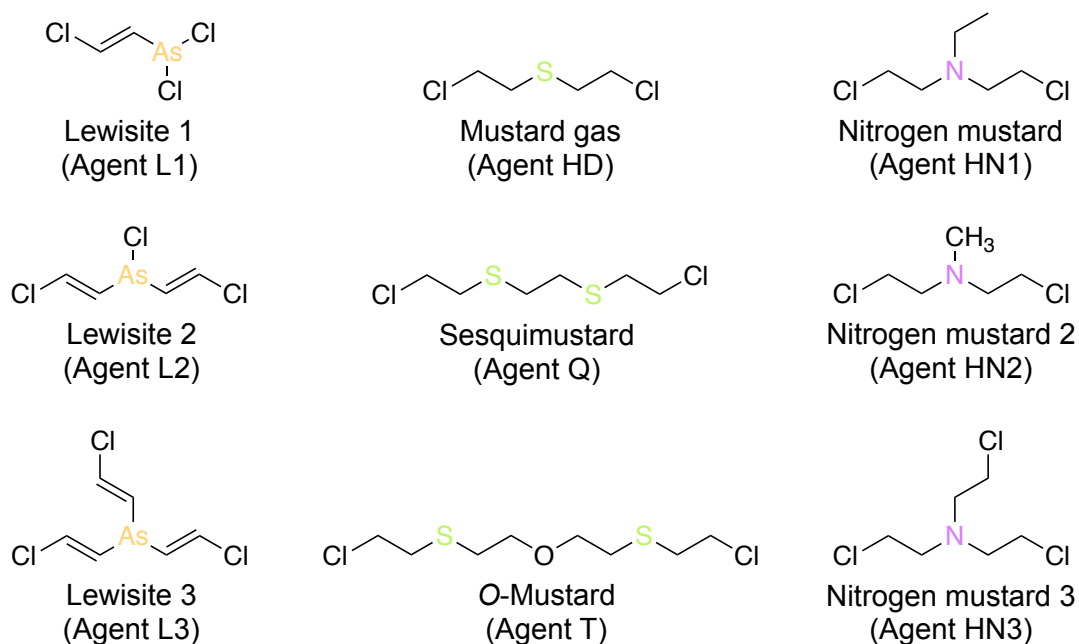


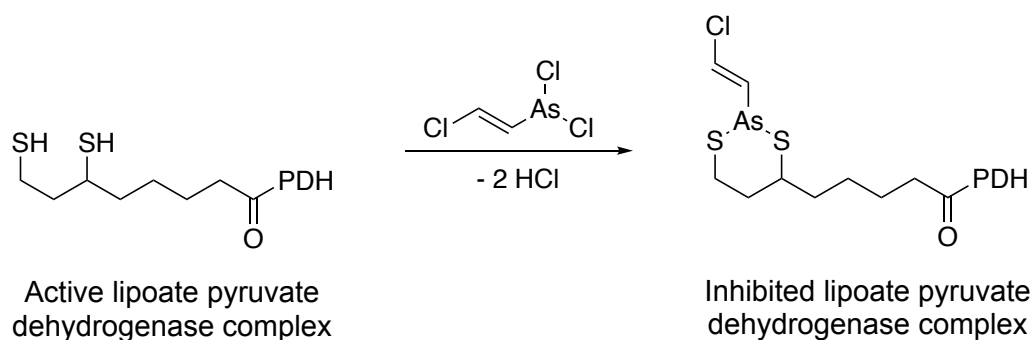
Figure 1.1. Chemical structures of the arsenic, nitrogen and sulfur blister agents.

Folded and moist regions of skin are more liable to blistering with the armpits, knees, elbows, neck and genitalia being some of the most vulnerable regions of the body.^{18,19} Eyes are particularly susceptible to vesicants with symptoms involving irritation, lacrimation and blepharospasm.¹⁷ Upon inhalation, these agents irritate the respiratory tract and lungs causing the accumulation of fluid and ultimately resulting in death by pulmonary edema.²⁰

1.3.1. Lewisite Agents

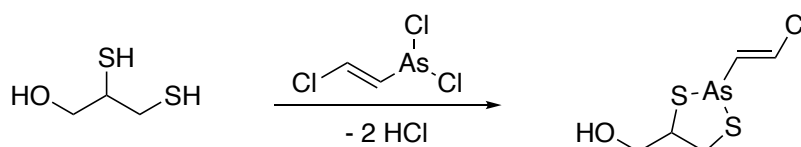
Lewisite (L) is a potent organoarsenic vesicant known for its significant systemic toxicity. Lewisite was first synthesised in 1908²¹ by the addition of acetylene to arsenic trichloride in the presence of a suitable Lewis-acid catalyst.^{22,23} Lewisite is a mixture predominantly comprised of trans isomers of 2-chlorovinylchloroarsine (L1), bis(2-chlorovinyl)chloroarsine (L2), tris(2-chlorovinyl)arsine (L3). A typical composition of a synthesised lewisite mixture is a 10:90 ratio of *cis*- and *trans*-isomers.²⁴

Due to its lipophilic nature, the main route of lewisite exposure is through skin absorption inducing painful cutaneous blistering and inflammation.²¹ However, other exposure routes are known with the eyes and respiratory tract also vulnerable.²⁵ The toxicological properties of trivalent arsenic are attributed to its interactions with thiol groups of proteins, particularly enzymes. Specifically, lewisite forms covalent bonds with vicinal thiol groups of dihydrolipoic acid, a co-factor of pyruvate dehydrogenase by forming stable cyclic arsenical structures as seen in Scheme 1.1. This inhibits the formation of acetyl coenzyme A by the oxidative decarboxylation of pyruvate. The enzymatic inhibition effect of lewisite prevents the metabolism of glucose and fatty acids by the cell thus, preventing ATP production. As a result, apoptosis occurs due to the rapid loss of energy.²⁶



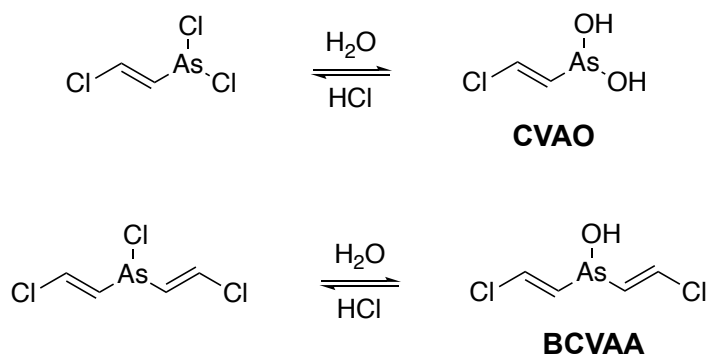
Scheme 1.1. Inhibition of pyruvate dehydrogenase complex by lewisite through the formation of stable arsenical structures. Adapted from Epure *et al.*²⁷

British anti-lewisite (BAL), also known as dimercaprol, was developed by Peters *et al.* in 1945 as an antidote treatment of acute lewisite exposure. Its effectiveness is based on the affinity of lewisite for thiol groups.²⁸ Lewisite preferentially binds to the dithiol moiety of BAL to generate a stable 5-membered chelate product as illustrated in Scheme 1.2.



Scheme 1.2. Chemical reaction of the antidote BAL with lewisite. Adapted from Peters *et al.*²⁸

Though Lewisite has limited solubility in water (0.5 g L^{-1})²⁹, hydrolysis of L1 and L2 occurs rapidly. L1 undergoes conversion to the mildly vesicant water-soluble 2-chlorovinylarsonous acid (CVAO) which also possesses toxic properties, whilst L2 forms bis(2-chlorovinyl)arsinous acid (BCVAA) (Scheme 1.3). On the other hand, L3 is relatively stable to reaction with nucleophiles such as water.^{24,30}



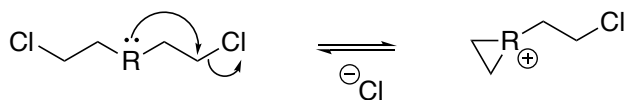
Scheme 1.3. Mechanism of the hydrolysis of L1 and L2. Adapted from Munro *et al.*²⁴

Lewisite can be readily decontaminated by a number of oxidants such as chloramines, hydrogen peroxide, hypochlorous acid and iodine to yield 2-chlorovinylarsenic acid.^{31,32} In the presence of sodium hydroxide, the *trans*-isomer is cleaved to yield acetylene and inorganic sodium arsenite. Whereas, the *cis*-isomer requires at least 40°C heat to react in basic conditions to yield acetylene, sodium arsenite and vinyl chloride.²⁹

1.3.2. Mustard Agents

Mustard agents can be divided further into two groups; sulfur mustards and nitrogen mustards. Both types exhibit vesicant properties, and both have a history of weaponization.³³ The reactivity and inherent instability of mustard agents is attributed to

their ability to form three-membered heterocycles, whereby sulfur mustard forms an episulphonium cation and nitrogen mustard forms an aziridinium cation (Scheme 1.4). This happens in the presence of polar solvents such as water.³⁴

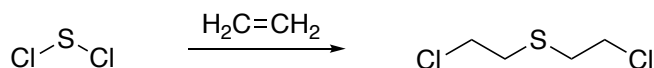


Scheme 1.4. Formation of three-membered cyclic cations by sulfur and nitrogen mustards via intramolecular nucleophilic attack. R = S or N. Adapted from Yang *et al.*³⁴

These highly reactive intermediates can undergo further reactions with nucleophiles to generate hydrolysis and polymerisation products and formation of alkylated DNA adducts. As bifunctional alkylating agents, these vesicants can undergo a second intramolecular cyclisation reaction making them potent CWAs.

1.3.2.1. Sulfur Mustard

One of the most well-known examples of blister agents is bis(β -chloroethyl) sulfide, more commonly known as sulfur mustard, was synthesised in the 1800s by Despretz whereby sulfur dichloride was treated with ethylene.³⁵ The toxic characteristics of sulfur mustard were not described until a few decades later.^{36,37} There are other synthetic routes for the preparation of sulfur mustard however, these involve the formation of impurities. For example, mustard produced by the Levenstein method involves the reaction of ethylene with sulfur chloride however there are often sulfur impurities present alongside sulfur mustard (Scheme 1.5).³⁸ As its name implies, impure sulfur mustard has a mustard or garlic-like odour however, its purification by vacuum distillation generates distilled mustard (HD) which is both colourless and odourless.



Scheme 1.5. Synthetic route of sulfur mustard via the Levenstein method.

Although this blister agent is often referred to as “mustard gas” it is a liquid at ambient temperature and capable of persisting in the environment due to its low water solubility and oily nature. Sulfur mustard vaporises at 30 °C and is able to penetrate clothes in its vaporised form. Additional chemical and physical properties of sulfur mustard are outlined in Table 1.1.

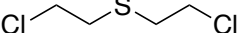
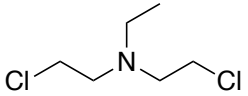
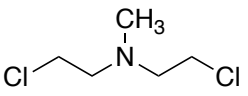
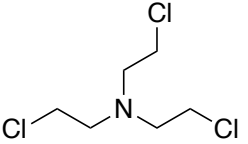
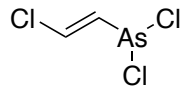
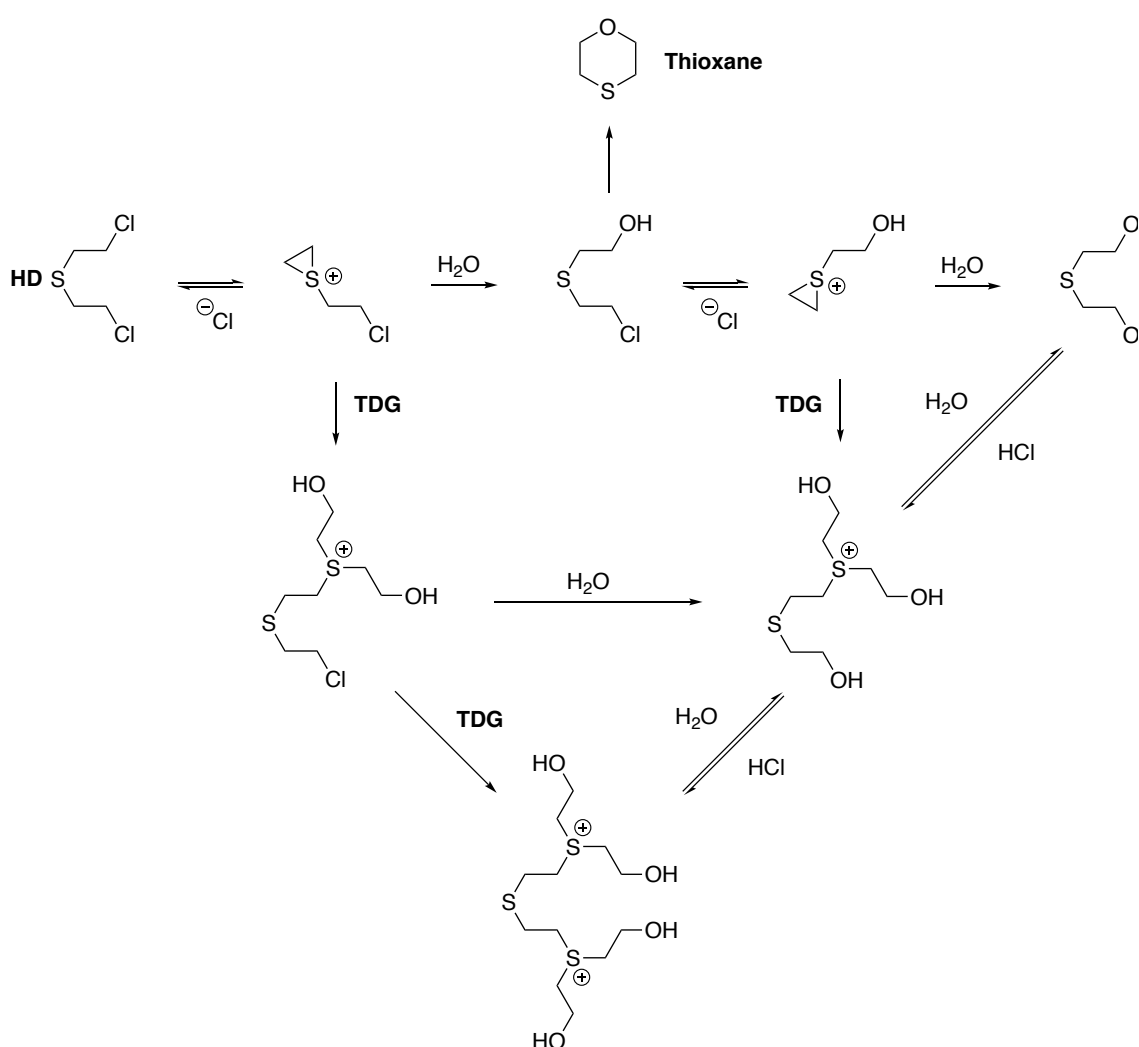
Property / parameter	Agent				
	HD	HN1	HN2	HN3	L1
Chemical formula	C ₄ H ₈ Cl ₂ S	C ₆ H ₁₃ Cl ₂ N	C ₅ H ₁₁ Cl ₂ N	C ₆ H ₁₂ Cl ₃ N	C ₂ H ₂ AsCl ₃
Structure					
Mode of action	Vesicant alkylator	Vesicant alkylator	Vesicant alkylator	Vesicant alkylator	Vesicant alkylator
Physical state at 20 °C	Colourless to pale yellow liquid	Colourless to dark liquid	Dark liquid	Dark liquid	Colourless to brown liquid
Melting point / °C	14	-34	-70	-3.9	-1.7
Boiling point / °C	217	194	75	256	190
Density at 20 °C / g cm ⁻³	1.27	1.09	1.15	1.24	1.89
Vapour pressure at 20 °C / mm Hg	0.72	0.24	0.29	0.0109	0.394
Volatility at 20 °C / mg m ⁻³	610	1520	3580	121	4480
Vapour density	5.5	5.9	5.4	7.1	7.1
LD ₅₀ / mg kg ⁻¹	100	20	10	10	30

Table 1.1. Physicochemical properties of blister agents. Data from opcw.org,³⁹ Handbook of Chemical and Biological Warfare Agents¹⁷.

Sulfur mustard is insoluble in water however when it is previously dissolved in organic solvent, it can react with water at the interface to form a complex set of water-soluble ionic products, as seen in Scheme 1.6. The kinetics of sulfur mustard hydrolysis has been previously investigated.^{34,40,41} These studies have established that the first step of this process is the equilibrium formation of a transient cyclic episulfonium cation via an intramolecular cyclisation reaction. Subsequently, this unstable intermediate undergoes an additional equilibrium process of hydrolysis to form the alcohol derivative, or alternatively reacts with nearby thioether nucleophiles to generate dimerised products. The hydrolysis of sulfur mustard has been reported to occur with a half-life of five minutes at 25 °C via an S_N1 mechanism.⁴⁰



Scheme 1.6. Mechanism of the hydrolysis and polymerisation of sulfur mustard. TDG denotes thiodiglycol; Adapted from Yang *et al.*³⁴ and Fallis *et al.*⁴¹

1.3.2.2. Mode of Action of Sulfur Mustard

Sulfur mustard is a potent alkylating agent. As a β -halothioether, HD can undergo S_N1 intramolecular cyclisation to form an episulfonium cation through cleavage of a chloride anion. This highly reactive species alkylates DNA⁴² causing inhibition of DNA replication. There have been many in vitro studies showing the formation of alkylated DNA adducts with sulfur mustard.^{43,44} Incubation studies involving calf thymus DNA or human blood with ³⁵S-labeled sulfur mustard identified the most commonly targeted alkylation sites on DNA. These included N7-[2-[(2-hydroxyethyl)thio]ethyl]guanine (I), bis[2-(guanin-7-yl)ethyl] sulfide (II), N3-[2-[(2-hydroxyethyl)thio]ethyl]adenine (IV), O6-[2-[(2-hydroxyethyl)thio]ethyl]-guanine (III) and its 2'-deoxyguanosine derivative (V).⁴⁵ These adducts are presented in Figure 1.2.

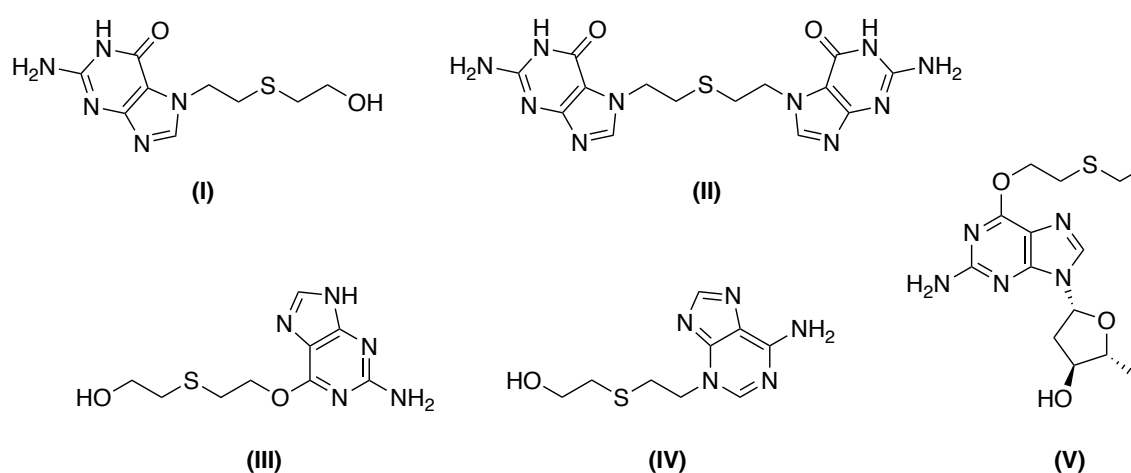


Figure 1.2. Chemical structures of common sulfur mustard-nucleobase adducts (I – IV) and sulfur-mustard-deoxynucleotide adduct (V). Adapted from Fidler *et al.*⁴⁵

The most common location for DNA alkylation is the N7 atom of guanine. Approximately 65% of the monofunctional DNA alkylation products are adducts on the N7 position of guanine nucleotides whereas adducts on the N3 position of adenine nucleotides make up only 17% of products.⁴⁶ As a bifunctional alkylating agent, sulfur mustard can undergo a second intramolecular cyclisation reaction making it possible to form cross-links within the DNA helix to yield di-(guanin-7-yl) derivatives in addition to monofunctional 7-alkylguanine products.⁴⁷ Bifunctional cross-links make up only 17% of the total alkylation products and are only formed between guanine nucleotides on the N7 position. Furthermore, in the case of mammalian cells, these bifunctional cross-links can occur between both the same and opposing DNA strands with intrastrand cross-links contributing the greatest at 75%.⁴⁶ Cross-linking of guanine nucleotides on the same

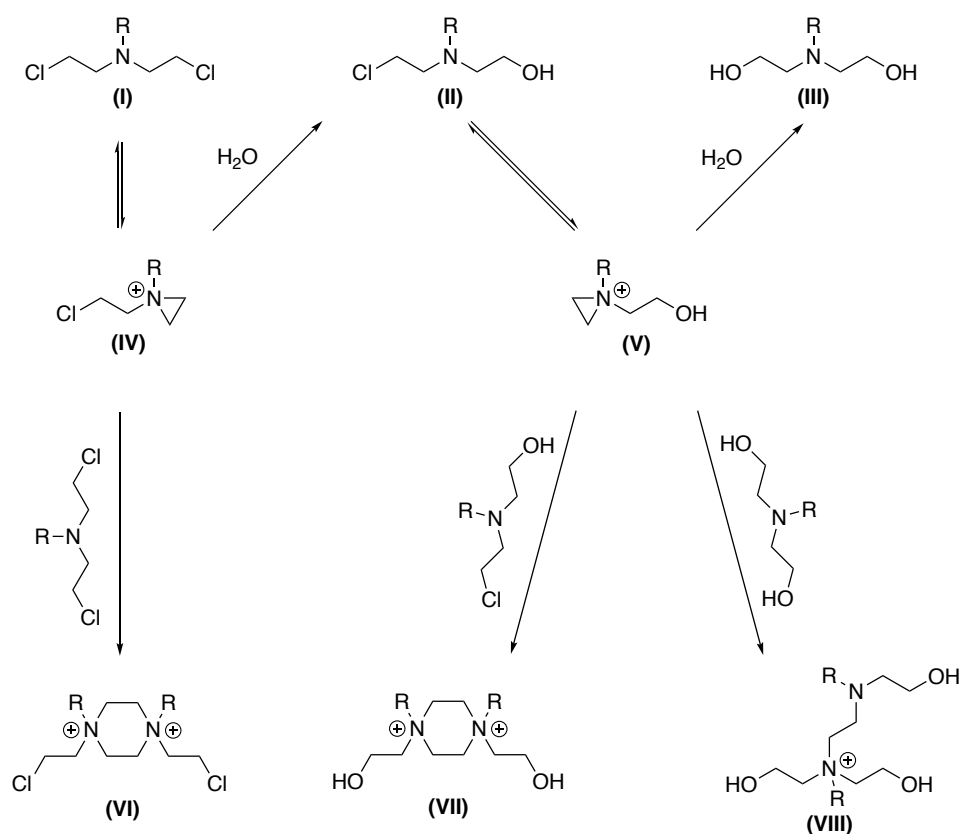
DNA strand is less likely than cross-links between guanine moieties on different strands due to the unfavourable configuration adopted by sulfur mustard.⁴⁸

The LD₅₀ value for sulfur mustard administered topically is 100 mg kg⁻¹.⁴⁹ The symptom pattern of sulfur mustard poisoning is firstly erythema, the superficial reddening of the skin, followed by blister formation and then ulceration. Erythema can be seen 4-8 hours after exposure whereas blister formation only occurs at higher doses (liquid: 40-100 μg cm⁻²).⁵⁰

1.3.2.3. Nitrogen Mustard Agents

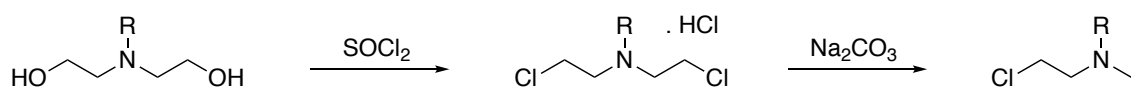
Nitrogen mustards are tertiary bis(2-chloroethyl)amines that contain at least two β-chloroethyl groups linked by a nitrogen atom. Their structure resembles sulfur mustard therefore, they have structural and toxicological similarities.⁵¹⁻⁵³ Common examples of nitrogen mustards include HN1 (bis(2-chloroethyl)ethylamine), HN2 (bis(2-chloroethyl)methylamine) and HN3 (tris(2-chloroethyl)amine).⁵⁴ Due to their toxicity and physical and chemical properties (Table 1.1), their application as CWAs grew during World War II (WWII). However, nitrogen mustard and its derivatives such as chlorambucil⁵⁵, cyclophosphamide^{56,57} and melphalan⁵⁸ are alkylating agents used as chemotherapeutic drugs.⁵⁹⁻⁶³ Ironically, mustard agents have prolonged more lives that they have truncated.

Nitrogen mustards undergo complex hydrolysis reactions leading to some heterocyclic products. Various hydrolysis conditions have been used to investigate the mechanisms of the chemistry of nitrogen mustards⁶⁴⁻⁶⁶ and a general representation of these findings is illustrated in Scheme 1.7 however the general routes of hydrolysis are similar to sulfur mustard. As previously mentioned, nitrogen mustards readily form a reactive aziridinium three-membered cyclic intermediate, which can undergo hydrolysis to form monohydroxyl and dihydroxyl products (Scheme 1.7, (II) and (III)), with other aziridinium intermediates consequently generated (Scheme 1.7, (IV) and (V)). Dimerisation processes also occur to yield 1,4-dialkyl-piazinium cations (Scheme 1.7, (VI) and (VIII)), which can be isolated in either cis- or trans-isomer form, and extended non-cyclic polymers (Scheme 1.7, (VIII)).⁶⁷



Scheme 1.7. Mechanism of the hydrolysis and polymerisation of nitrogen mustards. Adapted from Wang *et al.*⁶⁸

Nitrogen mustards are prepared by treating the appropriate amine with thionyl chloride to generate the corresponding vesicant as the hydrochloride salt which is then treated with an aqueous solution of sodium carbonate. This yields the nitrogen mustard as a viscous oil which is separated from the aqueous layer and purified by vacuum distillation (Scheme 1.8).



Scheme 1.8. Synthetic route for the preparation of nitrogen mustards; R = -CH₂CH₃ (HN1), -CH₃ (HN2) or -CH₂CH₂OH (HN3).

1.4. Nerve Agents

Nerve agents are a group of highly lethal organophosphate esters that can be categorised by their chemical structures into the G- or V-series. These agents are commonly known by either their chemical names or two-letter NATO codenames where 'G' denotes the country of origin, Germany, and 'V' stands for venomous.⁶⁹ Characteristically, nerve agents contain a pentavalent phosphorus centre bound to a

terminal oxide and three different substituents. The first nerve agent, Tabun (O-ethyl N,N-dimethyl phosphoramidocyanidate; GA), was isolated in 1936 by Dr Gerhard Schrader of IG Farben whilst developing novel insecticides. Subsequently, Sarin (O-isopropyl methylphosphonofluoridate; GB), Soman (O-pinacolyl methylphosphonofluoridate; GD) and Cyclosarin (O-cyclohexyl methylphosphonofluoridate; GF) were prepared by German scientists in 1938, 1944 and 1948, respectively.^{2,70} With the exception of the cyanide-containing agent Tabun, all G-series agents have a fluoride functionality as the leaving group. The G-agent structures are summarised in Figure 1.3.

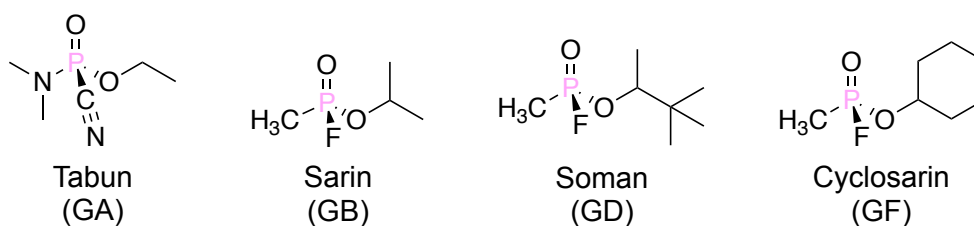
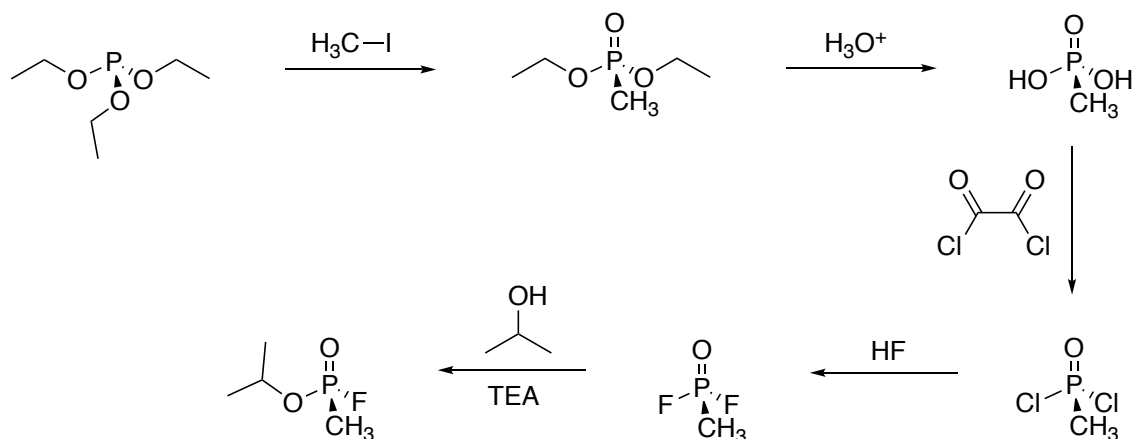
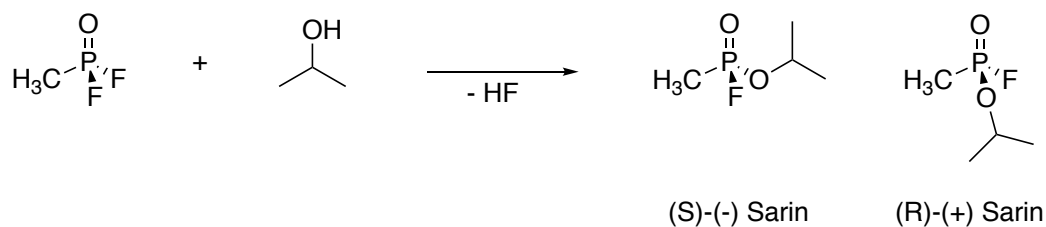


Figure 1.3. Chemical structures of G-series nerve agents.

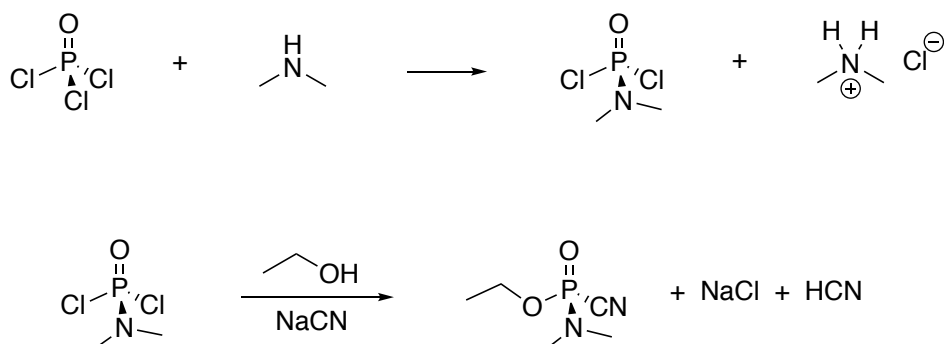
There are many possible synthetic routes for the production of G- and V-series agents. Depending on the precursors used for the synthesis of nerve agents the synthetic route can involve few to many steps. Typically, the synthesis of methylphosphonic dichloride as a precursor is common in most of these routes. Fluoride-containing G-agents can be prepared by treating methylphosphonyl difluoride with the appropriate alcohol in the presence of an amine base. For instance, sarin is prepared by treating methylphosphonyl difluoride with isopropyl alcohol and isopropyl amine or alternatively can be prepared by a five-step synthetic route which begins with the treatment of triethyl phosphite with methyl iodide.^{71,72} Both synthetic routes are presented in Scheme 1.9.

Sarin contains a chiral centre therefore a racemic mixture is generated from its synthesis and these enantiomers have varying toxicity. The P_S-enantiomer is more toxic and is able to inhibit acetylcholinesterase at approximately 5×10^4 times the rate of the P_R-enantiomer.^{73,74} A typical by-product formed from the synthesis of soman, sarin and cyclosarin is O,O-diisopropyl methyl phosphonate, O,O-dipinacolyl methyl phosphonate and O,O-dicyclohexyl methyl phosphonate. These impurities have a less potent effect on acetylcholinesterase compared to their live agent counterparts.



Scheme 1.9. Synthetic routes for the preparation of sarin. Adapted from Norlin *et al.*⁷² and Abou-Donia *et al.*⁷¹

As tabun does not contain a fluoride leaving group, its synthetic procedure differs from the other G-series nerve agents.⁷⁵ Tabun is prepared from four precursor chemicals: phosphorus oxychloride, sodium cyanide, dimethylamine and ethyl alcohol. The synthetic process for the manufacture of tabun consists of a two-step process (Scheme 1.10).



Scheme 1.10. Synthetic route for the preparation of tabun.

The first step is the treatment of phosphoryl chloride with gaseous dimethylamine to form dimethylamidophosphoric dichloride and dimethylammonium chloride. Dimethylamidophosphoric dichloride is subsequently treated with excess sodium

cyanide to yield the dimethylamidophosphoric dicyanide intermediate, which is treated with ethanol to generate tabun alongside the by-products, sodium chloride and hydrogen cyanide.

In the early 1950s, researchers at Porton Down, the British government research facility, synthesised the first V-series nerve agent, VX (O-ethyl S-2-diisopropylaminoethyl methyl phosphonothiolate). This agent was discovered as part of a British programme to develop new insecticides.^{2,70} There are four other V-agents that are commonly described; VE (O-ethyl-S-2-diethylaminoethyl ethyl phosphonothioate), VG (Amiton, O,O-diethyl S-2-diethylaminoethyl phosphorothioate), VM (O-ethyl S-2-diethylaminoethyl methylphosphonothiate) and VR (*N*-diethyl-2-(methyl-(2-methylpropoxy)phosphoryl)sulfanylethanamine). V-agents contain a P-S single bond and long-chain lipophilic tertiary amine leaving groups. The chemical structures of V-agents are summarised in Figure 1.4.

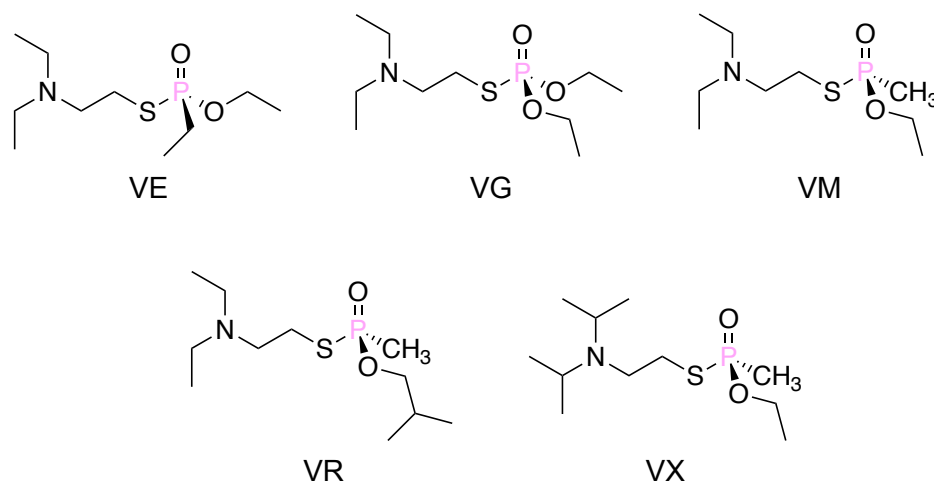
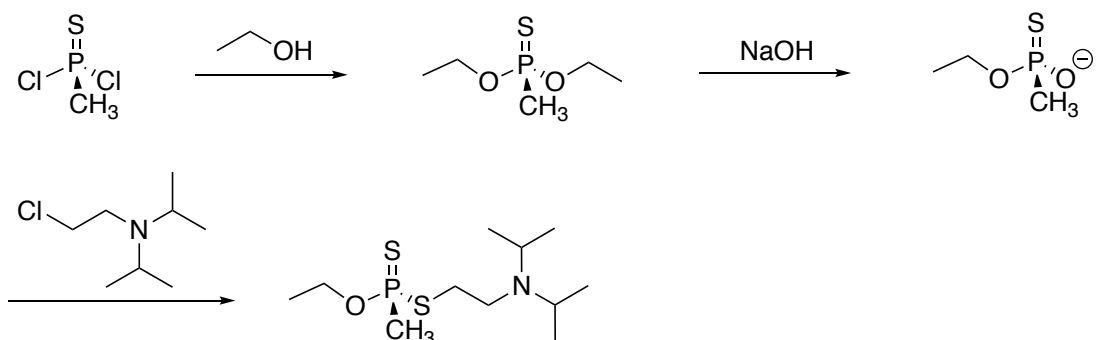


Figure 1.4. Chemical structures V-series nerve agents.

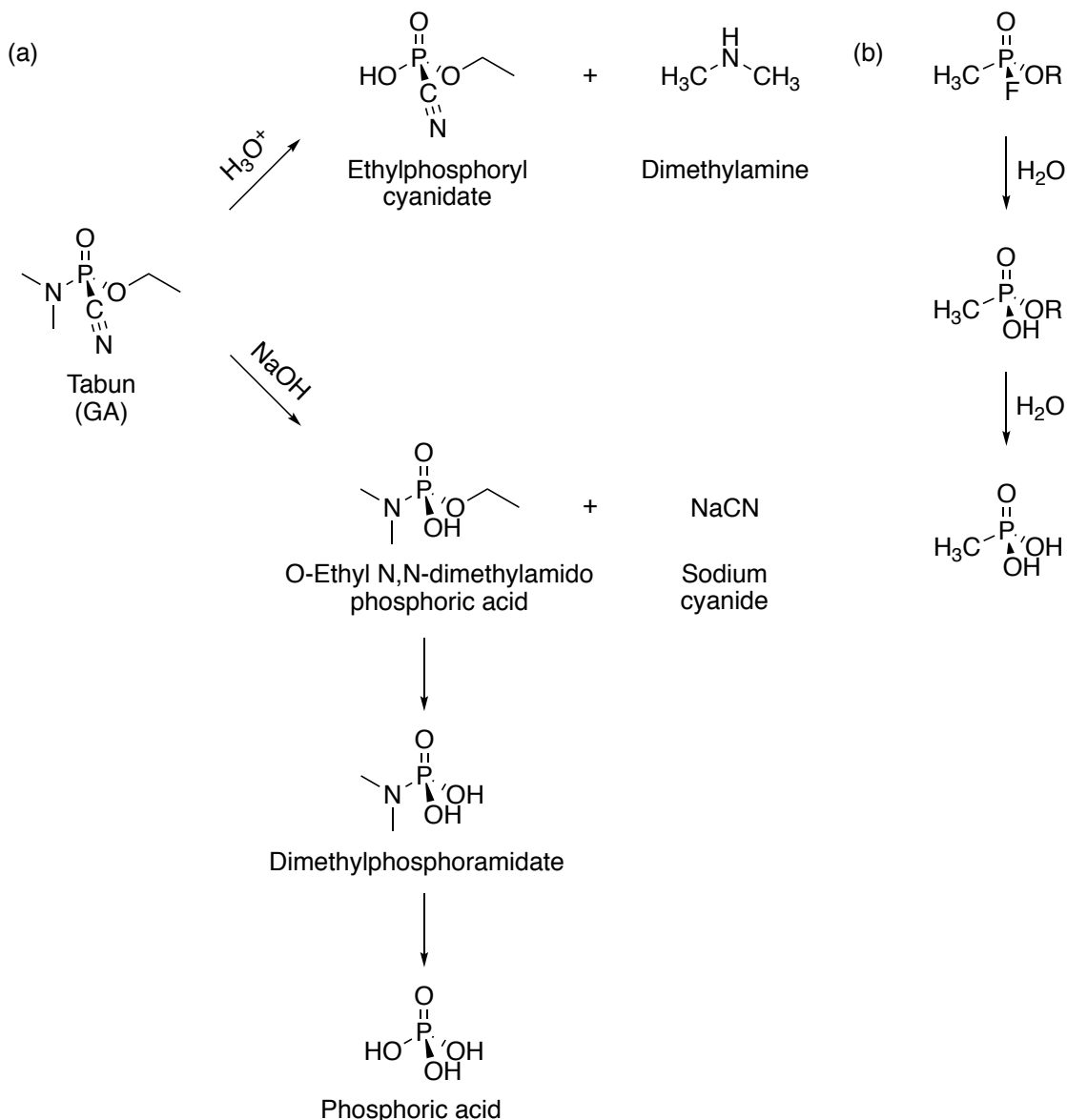
V agents can be prepared in three steps, which is presented in Scheme 1.11. The first involves the transesterification of methylphosphonothioic dichloride, followed by the hydrolysis of the formed diester with aqueous sodium hydroxide base. The resulting phosphonothioate sodium salt intermediate is treated with the appropriate aminoethyl chloride to yield the final nerve agent. This final step also involves the in-situ isomerisation of the phosphonothioate whereby the P=S transforms to the P=O.⁷⁶ VE and VG have different chemical structures to the other V-series nerve agents and therefore require different precursors for their synthetic routes: ethylphosphonic dichloride and phosphoryl trichloride, respectively. Impurities can be generated in the synthesis of V agents by the isomerisation of the diester product and the production of

various by-products during the second step, including formamide and alkyl amine derivatives.



Scheme 1.11. Synthetic route for the preparation of VX. Adapted from Gravett *et al.*⁷⁶

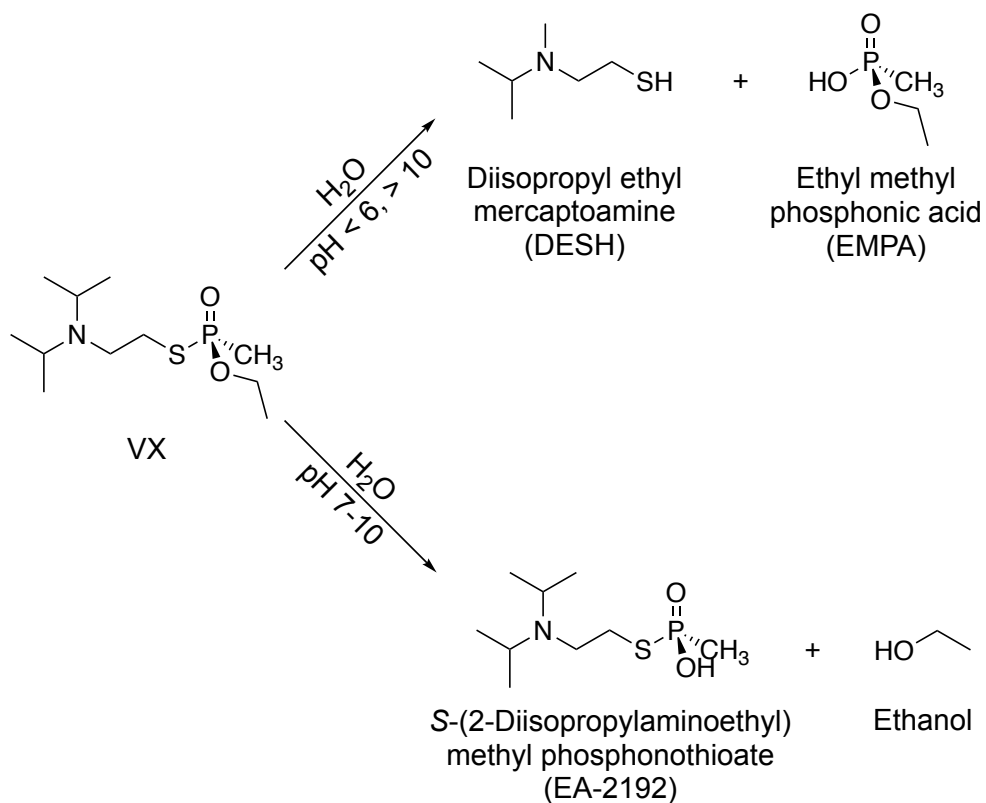
The P-X bond of G-agents is more readily hydrolysed than the P-S bond of V-agents. As a result, V-agents are less volatile and thus more persistent in the environment than the G-series nerve agents. Upon hydrolysis, nerve agents produce distinctive decomposition products (Scheme 1.12).³⁴ Hydrolysis of nerve-agents occurs via a phosphorus S_N2 nucleophilic attack. Hydrolysis rate is both pH- and temperature-dependant with basic conditions and higher temperatures increasing the reaction rate.^{77,78} Under basic and neutral pH, the hydrolysis of tabun produces O-ethyl-N,N-dimethylamidophosphoric acid and hydrogen cyanide. However, under acidic conditions dimethylamine and ethylphosphoryl cyanidate are formed. Phosphoric acid is the final product formed in the hydrolysis of tabun. The hydrolysis of sarin, soman and cyclosarin gives methylphosphonic acid (MPA) and the associated alcohol as the final products. As a result of acid formation, the pH decreases causing a reduction in hydrolysis rate. Hence, in order to maintain reaction rates an excess of base is necessary.



Scheme 1.12. Hydrolysis pathways of a) tabun and b) fluoride-containing G-series nerve agents. Adapted from Munro *et al.*²⁴

The hydrolysis of V-agents is more complicated than that of G-agents with two reaction pathways involved (Scheme 1.13). For example, VX hydrolysis is intramolecularly catalysed by the amino group and either P-O or P-S bond cleavage occurs however, this is pH-dependent. At pH < 6 and > 10, P-S bond cleavage is favoured resulting in the production of diisopropyl ethyl mercaptoamine (DESH) and ethyl methylphosphonic acid (EMPA). At a pH range of 7-10, VX is hydrolysed to S-(2-diisopropyl-aminoethyl) methylphosphonothioic acid (EA-2192) and ethanol. These products can undergo further hydrolysis with EMPA forming MPA and ethanol, while EA-2192 hydrolysis yields DESH and MPA.⁷⁹ EA-2192 is known to be just as toxic as VX and its hydrolysis at room temperature is extremely slow. As a result, VX cannot be decontaminated using base-

catalysed hydrolysis like G-agents. Instead VX is oxidatively detoxified with aqueous bleach containing either sodium hypochlorite or calcium hypochlorite.^{80,81}



Scheme 1.13. Hydrolysis pathways of VX. Adapted from Munro *et al.*²⁴

The physicochemical properties of selected G- and V-series nerve agents are presented in Table 1.2.

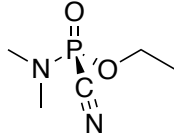
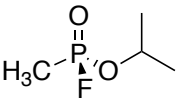
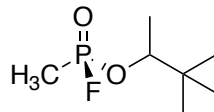
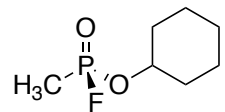
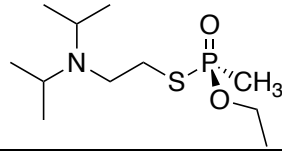
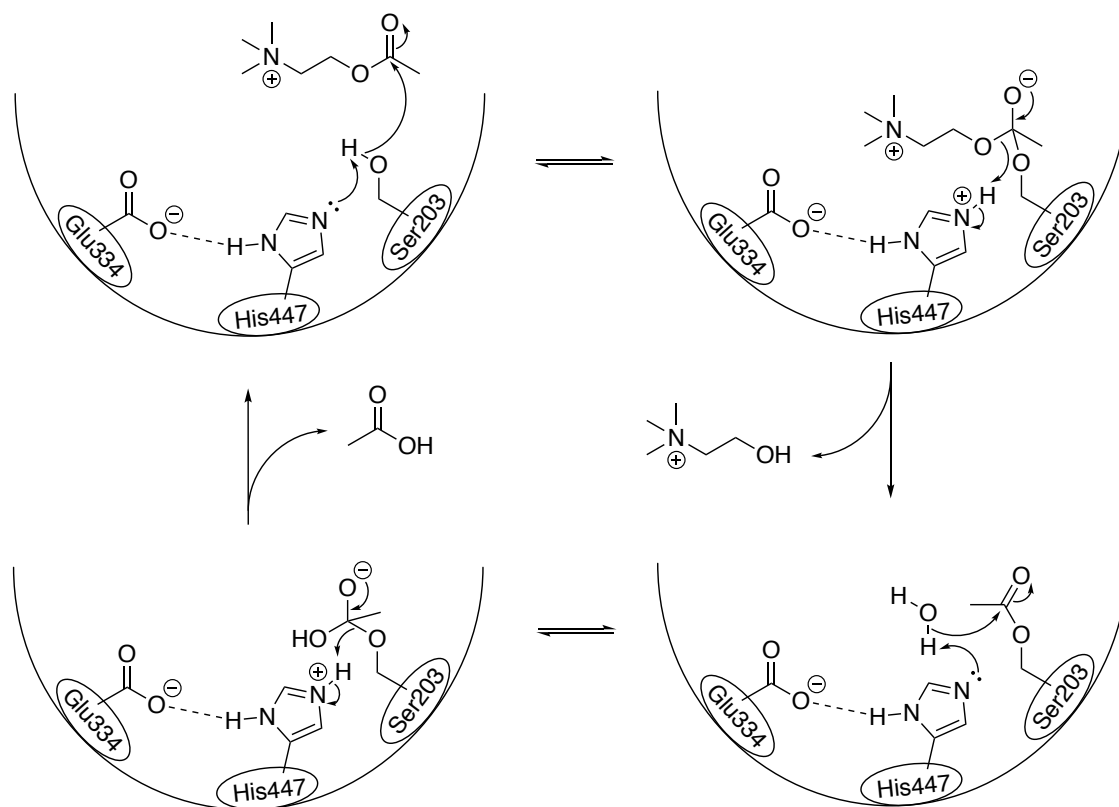
Property / parameter	Agent				
	Tabun (GA)	Sarin (GB)	Soman (GD)	Cyclosarin (GF)	VX
Chemical formula	C ₅ H ₁₁ N ₂ O ₂ P	C ₄ H ₁₀ FO ₂ P	C ₇ H ₁₆ FO ₂ P	C ₇ H ₁₄ FO ₂ P	C ₁₁ H ₂₆ NO ₂ PS
Structure					
Mode of action	AChE inhibitor	AChE inhibitor	AChE inhibitor	AChE inhibitor	AChE inhibitor
Physical state at 20 °C	Colourless to brown liquid	Colourless liquid	Colourless to brown liquid	Colourless liquid	Colourless to amber liquid
Melting point / °C	-50	-56	-42	-12	-39
Boiling point / °C	240	158	198	239	298
Density at 25 °C / g cm ⁻³	1.073	4.86	1.022	1.133	1.0083
Vapour pressure at 20 °C / mm Hg	0.037	2.10	0.40	0.044	0.0007
Volatility at 25 °C / mg m ⁻³	610	22000	3900	438	10.5
Vapour density	5.6	4.8	6.2	6.2	9.2
LD ₅₀ / mg kg ⁻¹	21.42	24.28	0.71	0.42	0.071
Aging half-time	19.2 h	3.0 h	6 min	7 h	1.5 d

Table 1.2. Physicochemical properties of nerve agents. Data from opcw.org,³⁹ Handbook of Chemical and Biological Warfare Agents,¹⁷ Worek and Thiermann⁸².

1.4.1 Mode of Action of Nerve Agents

The toxicity of nerve agents is attributed to their inhibition of acetylcholinesterase, an enzyme responsible for the hydrolysis of the neurotransmitter acetylcholine at cholinergic synapses. It can inhibit enzymatic function because the inhibition mechanism is analogous to the hydrolysis of acetylcholine. The mechanism of enzymatic acetylcholine hydrolysis is presented in Scheme 1.14.

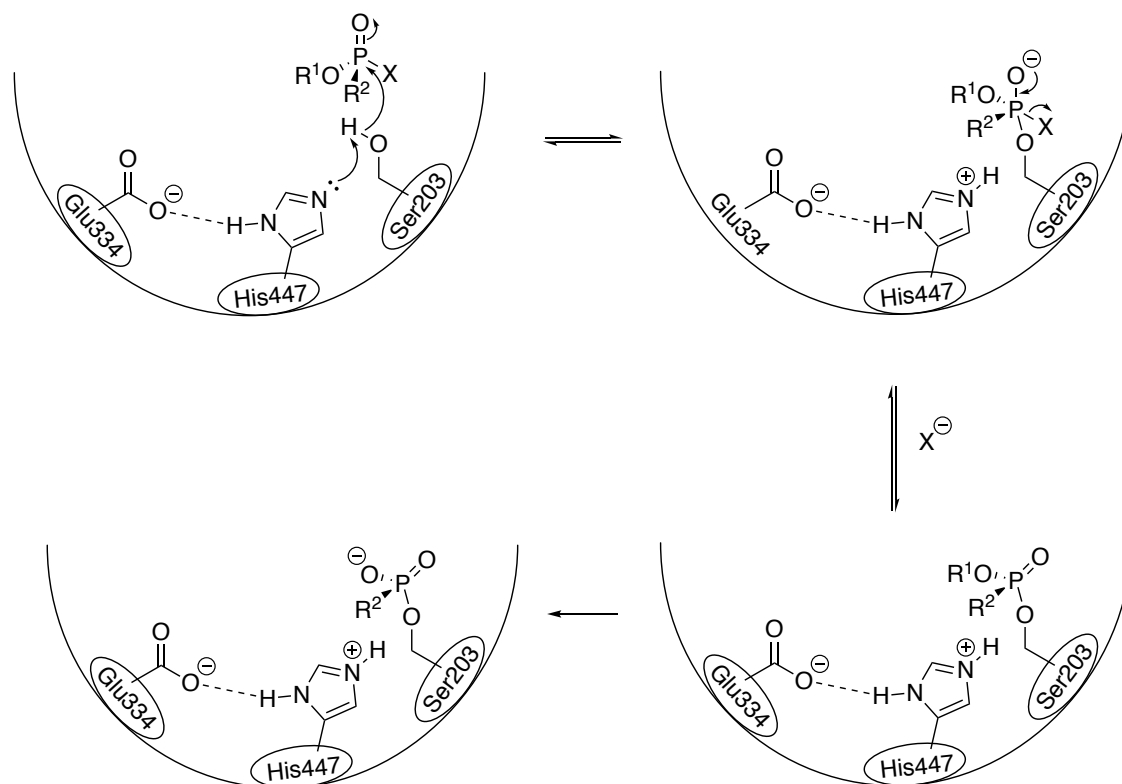


Scheme 1.14. Mechanism of acetylcholine hydrolysis by AChE.

These reactions involve a catalytic triad in the active site of the enzyme which is situated at the bottom of a deep and narrow electronegative gorge ($\sim 20 \text{ \AA}$). There are three amino acids that make up the triad: serine (Ser203), histidine (His447) and glutamic acid (Glu334). The active site is divided into two subsites denoted anionic and esteratic. With an overall negative charge, the anionic site attracts the positively charged quaternary ammonium group of acetylcholine and the esteratic site is responsible for catalytic substrate hydrolysis. Each amino acid of the catalytic triad plays a role in the hydrolysis of the substrate. Following the formation of an enzyme-substrate complex between acetylcholinesterase and acetylcholine, acetylation of the serine hydroxyl group is catalysed by the imidazole moiety of histidine. This reaction is facilitated by the simultaneous transfer of a proton from serine to histidine, to form a tetrahedral

intermediate transition state which is stabilised through electrostatic interactions with glutamic acid. Subsequently, the acetylated enzyme is hydrolysed generating the free enzyme and inactive choline and acetic acid.

Acetylcholinesterase is a primary target for organophosphate nerve agents as they can phosphorylate the active site of the enzyme by forming covalent adducts with the reactive hydroxyl group of the serine residue of the triad. This inhibition is often irreversible resulting in the accumulation of acetylcholine, which leads to the continuous stimulation of cholinergic synapses. In the case of nerve agent poisoning, the enzyme becomes phosphorylated instead of acetylated. Studies have shown that phosphorylation is a two-step process involving an addition-elimination mechanism, with the addition step being rate-determining in comparison to the subsequent rapid steps. Cleavage of the appropriate organophosphorus leaving group occurs after the agent is bound to the enzyme to form a stable organophosphorus-enzyme complex however, two secondary processes can occur. Firstly, the enzyme can be reactivated by hydrolysis of the complex. This process is slower than the hydrolysis rate of an acetylated AChE.⁴ Alternatively, dealkylation of the alkoxy group of the agent can occur in a process known as 'aging'.⁸³⁻⁸⁵ This aging process causes antidote treatments to be ineffective against enzyme reactivation due to the dealkylation reaction generating a negatively charged phosphorylated serine residue, making it resistant to nucleophilic attack by reactivators. This negatively charged adduct participates in strong hydrogen bonding with His447 and therefore stabilises the anionic phosphorylated serine residue.⁸⁵ Scheme 1.15 illustrates the inhibition and irreversible aging of acetylcholinesterase by organophosphorus nerve agent. The aging mechanism of tabun is slightly different with P-N bond cleavage.^{86,87} However, an alternative mechanism has also been proposed.⁸⁸



Scheme 1.15. Reaction schemes describing the inhibition and irreversible aging of acetylcholinesterase by organophosphorus nerve agent. R^1 = alkyl chain, R^2 = $-\text{CH}_3$ or $-\text{N}(\text{CH}_3)_2$ and $X = \text{F}$ or CN .

The electron-donating ability of the alkoxy group is proportional to the rate of ageing with the potential for reactivation decreasing with time.⁸⁹ Each nerve agent has a different AChE aging rate however increasing the number of methyl groups of the alkoxy moiety increases the aging rate. The aging half-times of selected V-agents are presented in Table 1.3.

	Tabun	Sarin	Soman	Cyclosarin	VX	VR
Aging half-time ⁹⁰	19.2 h	3.0 h	6 min	7.00 h	1.5 d	5.8 d

Table 1.3. Aging half-times of V-series nerve agents.

Nerve agent poisoning has a multitude of symptoms affecting the entire body⁹¹ however, the respiratory and nervous systems are greatly affected. Large exposures of nerve agent can cause sudden loss of consciousness, convulsions and flaccid paralysis. Mucus secretions and ventilatory failure are also typical, with asphyxiation being the common cause of death.^{8,92} Most nerve agents possess a chiral centre about the phosphorus (V) atom generating both S_p and R_p isomers. AChE nerve agent inhibition

has been shown to be stereoselective with S_p enantiomers exhibiting increased inhibition potency compared to the R_p isomer.^{93–97} In addition to the chiral phosphorus atom, soman contains a second chiral centre at the carbon atom in the pinacolyl group which leads to four stereoisomers.

1.5. Treatment of CWA poisoning

For the purposes of medical triage, it is imperative that all detection technologies are capable of selectively distinguishing between different classes of CWAs as the treatment of patients poisoned by HD and nerve agents differ considerably.

Treatment of mustard poisoning is primarily symptomatic as there is no available antidote. Alternatively, the priority lies heavily on the treatment and decontamination of blistered skin. Thorough decontamination of HD-poisoned skin is important to reduce HD absorption and thus reducing the blistering effect to the victim and reduces the secondary exposure to medical staff.⁹⁸ The whole body area, not just the HD-affected regions of the body should be washed with large amounts of water and 0.5 % hypochlorite solution.^{99,100} The treatment of hairless guinea pigs exposed to undiluted HD with 0.5 % hypochlorite solution caused a 68% reduction of skin HD content.¹⁰¹

Therapeutic antidotes for organophosphate-inhibited AChE are developed based on a class of oxime reactivators. Standard treatment for organophosphate poisoning involves the combined administration of atropine (anti-muscarinic), diazepam (anticonvulsive) and oxime.¹⁰² Atropine and diazepam are used to reduce symptoms however oximes are able to restore the physiological function of AChE through the cleavage of the P-O bond of the organophosphate-enzyme adduct. Since the discovery of pralidoxime (2-pyridinealdoxime methiodide) or 2-PAM as an efficient reactivator of phosphorylated AChE in 1955 by UK and US researchers^{103,104}, many oxime structures have been synthesised. Initially, AChE reactivators were designed based on the structure of acetylcholine therefore early examples of oximes contain a quaternary ammonium group to give mono-pyridinium (2-PAM) and bis-pyridinium reactivators. The latter class of reactivators contain oximes such as asoxime (HI-6), obidoxime (LüH-6), trimedoxime (TMB-4), methoxime (MMB-4) and HLö-7. Chemical structures of these oxime reactivators can be seen in Figure 1.5. Unfortunately, the clinical use of the aforementioned oximes is limited as their efficacy is unequal against structurally different nerve agents thus, they cannot be regarded as effective broad-spectrum reactivators. As an antidote, 2-PAM is very efficient at reactivating AChE inhibited by sarin and VX¹⁰⁵ with calculated reactivation half-times of approximately 10 minutes, however it is ineffective at reactivating soman-inhibited, cyclosarin-inhibited, and tabun-inhibited enzymes¹⁰⁶. A

study involving 2-PAM, obidoxime, HI-6, and HLö-7 identified obidoxime as the most potent reactivator of human AChE inhibited by organophosphates and organophosphoramidates whereas, HLö-7 was most effective at reactivating phosphorylated AChE. Extremely low values for oxime reactivation were documented for tabun-inhibited AChE with all oximes however, no significant reactivation was recorded for HI-6-treated samples.¹⁰⁷ Tabun is one of the most difficult nerve agents to treat due to the resistance of tabun-inhibited AChE to reactivation by antidotes. The crystal structures of tabun-inhibited *Mus musculus* (mouse) AChE (mAChE) before the aging process sheds light on this unique resistance. The non-aged tabun conjugate undergoes a structural change in the active site of the enzyme. Specifically, the catalytic triad is uncoupled which positions the imidazole side chain of His447 into a conformation where hydrogen bonding to a nearby water molecule is favoured. Furthermore, the phenyl side chain of Phe338 is displaced thus moving it into the active site gorge resulting in reduced accessibility of reactivators.¹⁰⁸ Charged oximes cannot pass the blood-brain barrier (BBB) therefore recent advances in reactivator development has been centred around uncharged oxime and non-oxime structures.¹⁰⁹

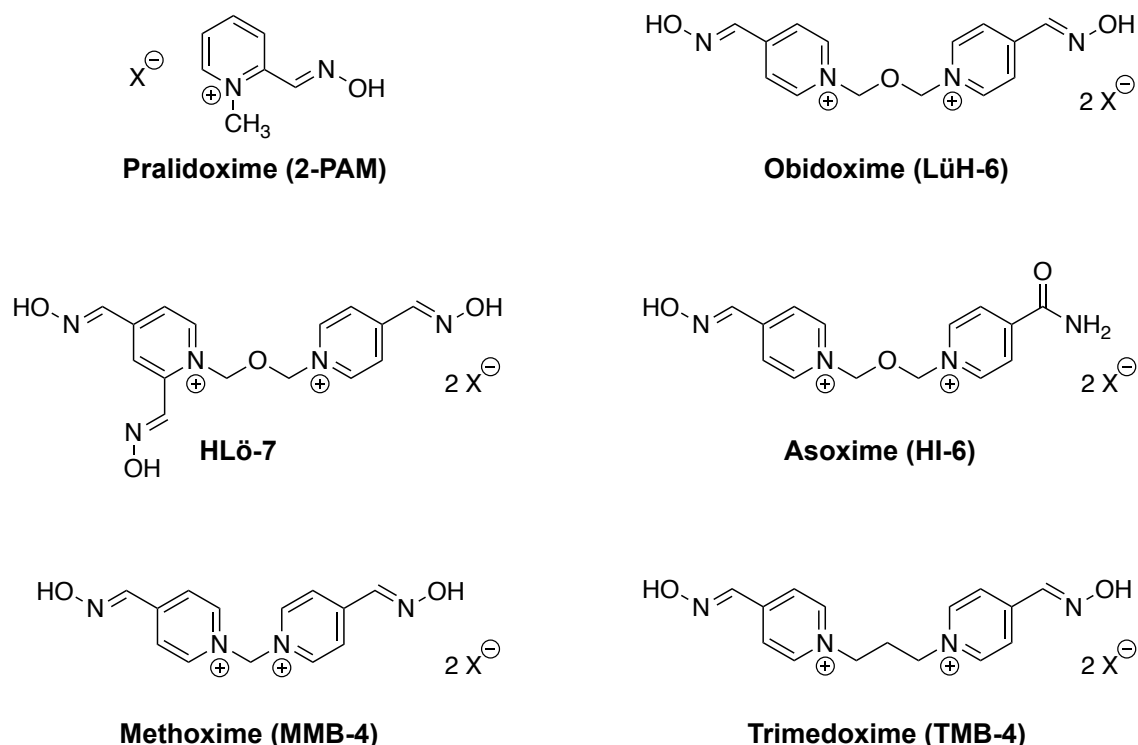
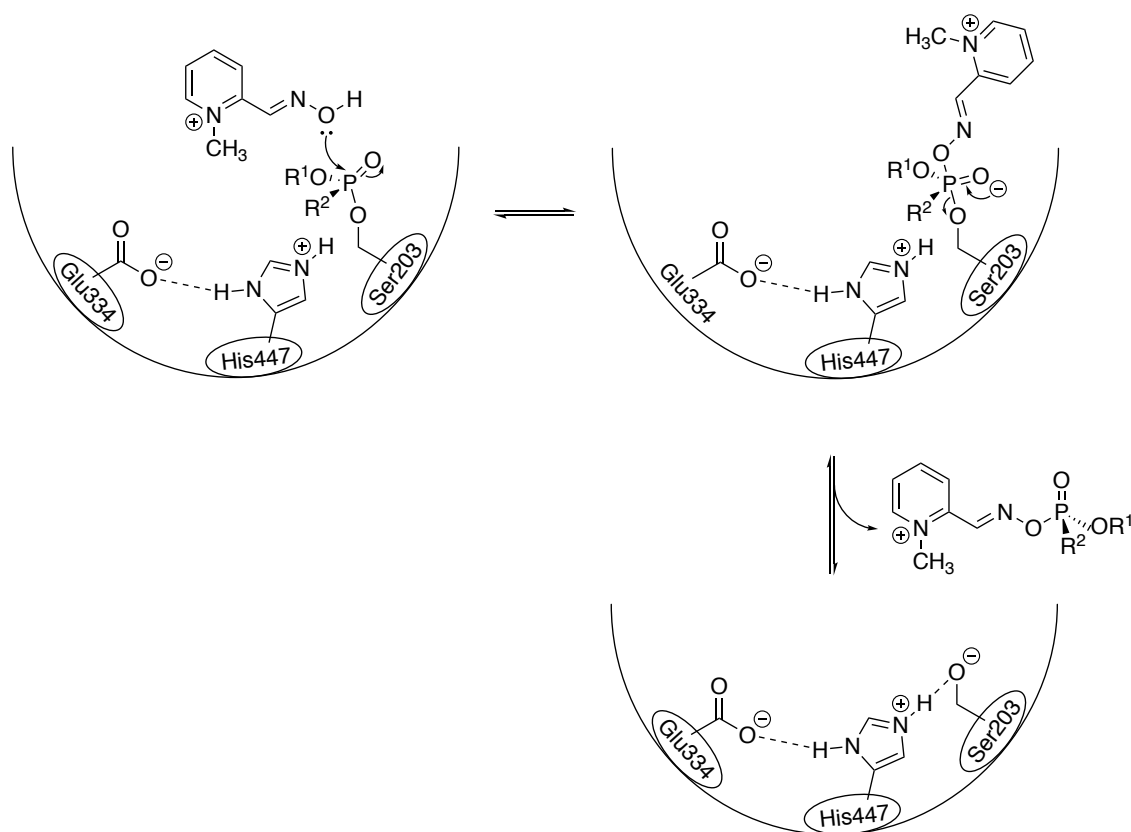


Figure 1.5. Chemical structures of pyridinium oxime antidotes for nerve agent poisoning.

Due to their high affinity for the enzyme, oximes can displace the organophosphorus nerve agent and reactivate AChE by nucleophilic attack of the oxime group on the

phosphorus atom of the nerve agent.¹¹⁰ The enzyme reactivation reaction is outlined in Scheme 1.16 whereby the mechanism occurs via a two-step reaction. Firstly, the nucleophilic hydroxyl group of the oxime attacks the phosphorus atom of the covalently bound nerve agent forming a reversible oxime-organophosphate-enzyme conjugate. Secondly, the resulting organophosphate-antidote complex is cleaved via a pentacoordinate transition state.^{111,112} Furthermore, studies have shown that the resulting phosphorylated oximes formed during the reactivation process are capable of inhibiting AChE.^{113,114}



Scheme 1.16. Reaction scheme for the reactivation of organophosphorous inhibited acetylcholinesterase with 2-pralidoxime.

1.6. Simulants

Due to the high toxicity of live agents, they are classified as schedule 1 substances by the CWC. This classification concerns chemicals which can either be used as chemical weapons or used in the manufacture of chemical weapons. Alternatively, simulants with similar chemical and physical properties to live agents but decreased toxicity are used for research purposes. Although these compounds can mimic the chemistry of live agents, no simulant can behave completely the same therefore a degree of incomplete utility is always present. Thus, licensed chemical weapons facilities such as Porton Down

in Salisbury are locations used for authorised live agent testing. There are many common examples of simulants chosen to substitute live agents in research. For this research, we chose 2-chloroethyl ethyl sulfide, diethyl chlorophosphonate (DCP), diethyl cyanophosphonate (DCNP), diisopropylfluorophosphate (DFP) and profenofos for H, G, and V agents respectively (Figure 1.6).

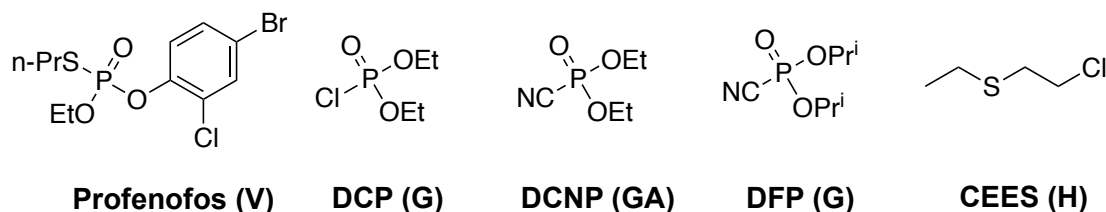


Figure 1.6. Chemical structures of simulants

1.7. Sulfur Mustard Sensors

Due to the relatively weak electrophilicity of sulfur mustard, there have been fewer reported sensors for blister agents and their simulants compared to nerve agents^{115–117}. Thus far, a multitude of chemical probes have been reported by various research groups constructed with various nucleophilic sites for the detection of sulfur mustard and its simulants. The most common nucleophilic centres include sulfur^{118–129}, nitrogen^{130–134}, and oxygen^{135,136}. Those with a sulfur atom active site can be further divided into two groups: thiol-based sensors^{118–121} and thiocarbonyl-based sensors^{122–129}.

1.7.1. Sulfur-Based Sensors

1.7.1.1. Thiol-Based Sensors

In 2013, Kumar and Anslyn reported the first turn-on fluorescent sensor for sulfur mustard simulant, CEES, in hot water (80 °C) based on a displacement mechanism involving a dithiol and a Cd²⁺-indicator complex (Figure 1.7, left). Unfortunately, an intermediary step was required to cap any unreacted dithiol before detection of simulant. The probe was found to selectively detect CEES at a concentration of 0.2 mM within 1 minute in solution, soil and on surfaces.¹²¹ This sensing protocol was later optimised by introducing a squaraine dye to eliminate the need for the capping step. The absence of CEES caused the dithiol to react with the dye causing bleaching of the colour. However, the chromogenic and fluorogenic properties of the squaraine dye were retained in the presence of CEES. The detection of CEES was found to be selective and sensitive with chromogenic and fluorogenic detection limits of 50 μM and 10 μM, respectively.¹²⁰

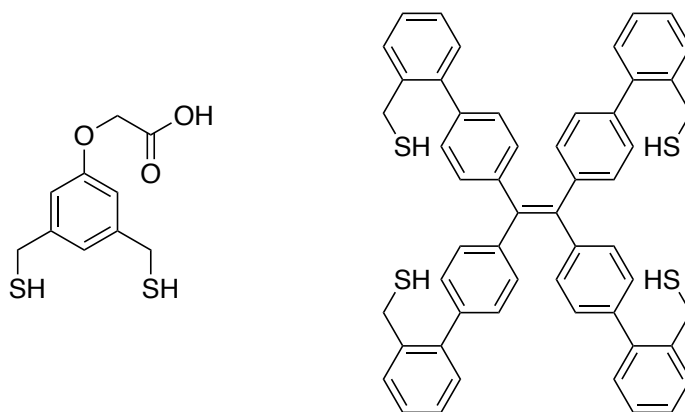


Figure 1.7. Structures of sulfur-based sensors reported by Kumar and Anslyn (left) and Wang *et al.* (right).

Despite this elegant effort, the instability of the dye in the presence of excess base was a potential source of false positive responses. To overcome this, both phenolic functional groups were removed from the dye rendering it non-responsive to basic conditions. This adapted sensing protocol was found to be selective at detecting sulfur mustard over other live nerve agents in multiple matrices including in solution, in soil, on surfaces, and in the vapour phase. The detection limit was found to be 18 μM and 40 μM by fluorescence and visual inspection, respectively.¹¹⁸ Wang and co-workers designed and synthesised a non-emissive mercaptomethylphenyl-modified tetraphenylethene multisite probe for sulfur mustard detection (Figure 1.7, right). This probe generated aggregation-induced emission (AIE) upon reaction with CEES at 80°C for 5 minutes in the presence of Hg^{2+} metal ions because of the production of a sandwich-type complex, which restricted the phenyl ring rotation of tetraphenylethene. This sensing protocol exhibited high selectivity and sensitive for CEES in solution and in soil samples with a detection limit of 1.10 μM .¹¹⁹

1.7.1.2. Thiocarbonyl-Based Sensors

In this group of thiocarbonyl sensors, sulfur is incorporated into the probe as either a thioamide or a thioketone. Those with thioamide moieties are largely designed on a rhodamine core structure with a thiolactam functionality (Figure 1.8, left).^{122,128} An example of this type of sensor was designed by Pardasani and co-workers. Their rhodamine chemodosimeter with a thioamide functional group was capable of selectively detecting sulfur and nitrogen mustards within 15 minutes at room temperature. In the presence of sulfur mustard, the thioamide group of the chemodosimeter underwent S-alkylation followed by ring opening of the spirothiolactum, resulting in the production of a highly conjugated salt. The detection limit for sulfur mustard in the solution and gas phase was 4.75 μM and 6.25 ppm, respectively.¹²⁹ Song *et al.* designed four fluorescent

probes based on a thioquinolone structure for both solution and gas phase detection of sulfur mustard and its analogues via a fluorescent ‘turn-on’ reaction (Figure 1.8, right). Two probes containing trifluoromethyl groups were identified for their superior sensing performance, displaying high selectivity, rapid response times (1 minute), and nM-levels of sensitivity at an elevated temperature of 60°C. The field application of mustard gas detection was shown using probe-fabricated test strips which selectively detected CEES vapour at 0.2 ppm within 4 minutes.¹²³

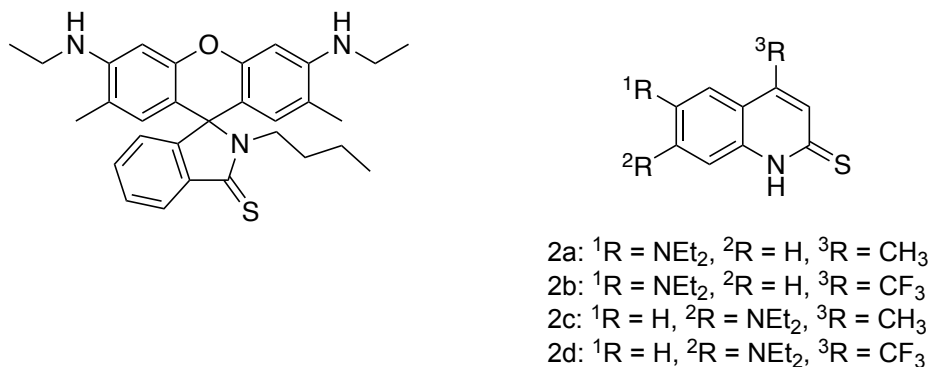


Figure 1.8. Structures of thiocarbonyl-based sensors reported by Pardasani *et al.* (left) and Song *et al.* (right).

Gupta *et al.* developed the first chromogenic and fluorogenic sensor for the detection of sulfur mustard in solution, in soil and on surfaces (Figure 1.9, left). The turn-on fluorescent xanthene-9-thione derivative was able to selectively detect sulfur mustard and its simulant within 1 minute of exposure at a temperature of 60 and 50°C, respectively. The level of sensitivity displayed by visual inspection (0.04 mg mL^{-1}), fluorescence ($0.0005 \text{ mg mL}^{-1}$), and UV spectroscopy (0.02 mg mL^{-1}), makes this approach a strong field-deployable option, particularly with the fabrication of a portable chemosensor kit.¹²⁵ Interestingly, Tian *et al.* later optimised this probe by replacing the trimethylamine groups with piperidine moieties, which improved the detection limit of CEES in solution from 0.2 mg mL^{-1} to $1.2 \mu\text{M}$ and was also capable of detecting CEES vapour at a concentration of 0.5 ppm (Figure 1.9, right). This probe underwent a selective transformation in the presence of CEES to form a fluorescent thiopyronin derivative, which also generated a noticeable colour change.¹²⁷

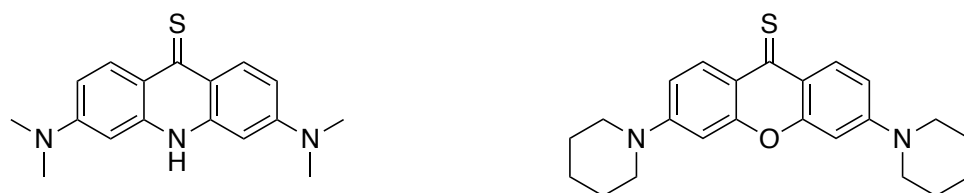


Figure 1.9. Structures of thiocarbonyl-based sensors designed by Gupta *et al.* (left) and Tian *et al.* (right).

1.7.2. Oxygen-Based Sensors

Broome and Jiang constructed a salicylic acid derivative containing a pyrene functionality for the detection of alkylating agents. The sensing protocol took advantage of the aggregation of the probe in aqueous solution which caused pyrene excimer fluorescence emission in the presence of CEES. Unfortunately, the response time was lengthy at 48 hours at a temperature of 40°C. Efforts to reduce the reaction time with the introduction of a phase-transfer catalyst at an elevated temperature of 90°C were unsuccessful with a time of 2 hours.¹³⁵ Gupta *et al.* reported a luminol-based turn-on fluorescent probe in combination with an ionic liquid for the selective detection of ppm levels of sulfur mustard in soil, in solution, on surfaces, and in the gas phase. The introduction of the ionic liquid improves the nucleophilicity of the probe and enhances the electrophilicity of sulfur mustard, allowing detection to occur at an ambient temperature of 25°C within 1 minute in solution and 2 minutes in the gas phase. The LOD for sulfur mustard was determined to be 6 ppm.¹³⁶ These probe structures are presented in Figure 1.10.

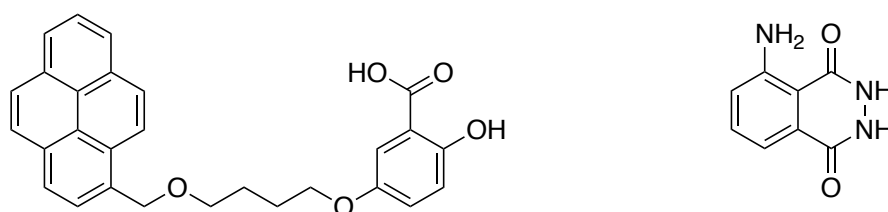


Figure 1.10. Structures of oxygen-based sensors reported by Broome and Jiang (left) and Gupta *et al.* (right).

1.7.3. Nitrogen-Based Sensors

Chu *et al.* developed six affinity ionic liquids incorporating a reactive azobenzene derivative for the chemoselective detection of gaseous CWA mimics by quartz crystal microbalance, in solution and on filter paper discs. These discs were capable of detecting DCP at room temperature and CEES at 60°C, within 10 minutes.¹³⁰ Zhao *et al.*¹³¹ studied the relationship between CEES and fluorescent multicarbazole co-assembled

nanofibers. The photostability of their previously reported carbazole-based nanofiber¹³⁷ was improved with the introduction of fluorenone-based nanofibers as a Förster Resonance Energy Transfer (FRET) acceptor. The unique fluorescence quenching behaviour observed for CEES vapour enabled the rapid discrimination of this simulant in the presence of other CWA mimics within 3 seconds. The detection limit of CEES vapour was measured at 0.3 ppm. The structures of these sensors are presented in Figure 1.11.

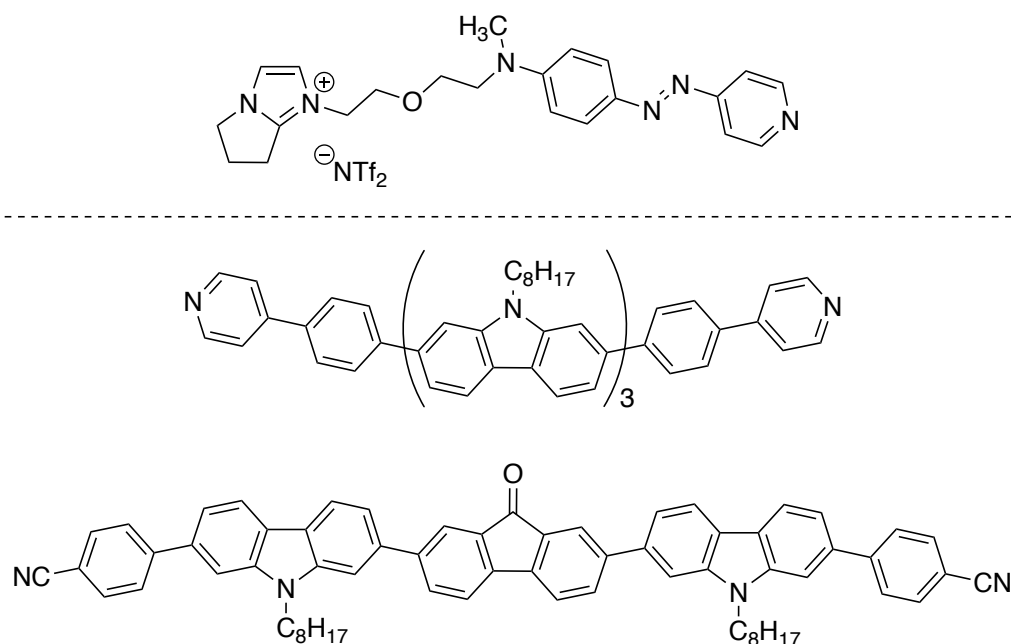


Figure 1.11. Structures of nitrogen-based sensors reported by Chu *et al.* (top) and Zhao *et al.* (bottom).

1.8. Nerve Agent Sensors

Due to the inherent electrophilicity of nerve agents, there are more reported sensors in the literature compared to those of mustards. Many elegant sensors have been developed based on chromogenic and fluorogenic detection.

1.8.1. Sensors for the Determination of G-series Nerve Agents

1.8.1.1. Primary Alcohol-Based Sensors

Sensors containing a purposely positioned hydroxyl moiety undergo phosphorylation and subsequent intramolecular cyclisation upon exposure to organophosphate resulting in a spectrophotometrically detectable species. Some of these sensors also generate a colorimetric response detectable by the naked eye. Dale and Rebek developed a collection of fluorescent sensors for the determination of DCP via a photoinduced electron transfer (PET) mechanism (Figure 1.12, left). The fluorescence of the tertiary

amine probes at an excitation wavelength of 340 nm was quenched by transfer of the amine lone pair to the pyrene fluorophore via a PET process. Upon exposure to DCP, the primary alcohol was phosphorylated followed by a rapid intramolecular cyclisation reaction to form the quaternarised ammonium salt. This species was no longer able to quench the pyrene fluorescence due to the absence of a lone pair of electrons and thus the emission was enhanced. It was found that increasing the spacer length (n) reduced the quenching efficiency. Using a large excess of DCP, a rate constant of $k = 0.07 \text{ M}^{-1} \text{ min}^{-1}$ was determined.¹³⁸

In a similar approach, Zhang and Swager developed a fluorescent naphthalene-based sensor for the sensitive and selective detection of nerve agent simulants DCP and DFP (Figure 1.12, middle). The restricted conformation of the naphthalene ring accelerated the cyclisation step after formation of the phosphate ester intermediate. The reaction kinetics exhibited were too rapid to measure accurately however it was estimated to be $k_{\text{obs}} > 0.024 \text{ s}^{-1}$. This sensor was developed into thin films that exhibited a bathochromic shift in emission wavelength from 375 to 438 nm upon formation of the cationic cyclised product.¹³⁹

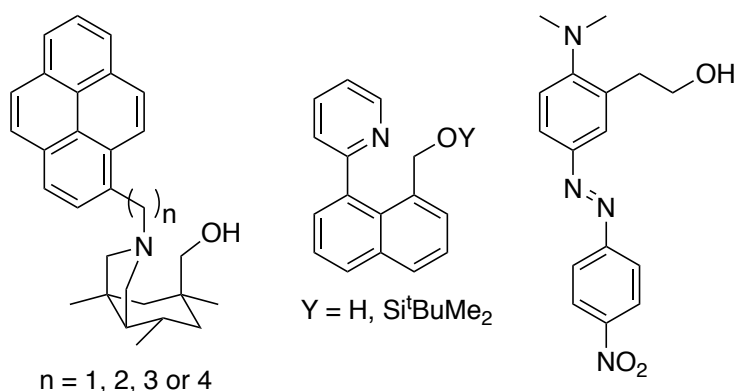


Figure 1.12. Structures of sensors containing hydroxyl moieties reported by Dale and Rebek (left), Zhang and Swager (middle) and Royo *et al.* (right).

Royo *et al.* designed an azo dye (Figure 1.12, right) with a similar mechanism to that of Zhang and Swager. Here, the dye was derivatised with a 2-(2-(dimethylamino)phenyl)ethanol (DAPE) moiety where the nucleophilic hydroxyl functional group undergoes phosphorylation in the presence of simulant which facilitates the intramolecular N-alkylation to generate the final quaternary ammonium salt. This cyclisation reaction can be observed spectrophotometrically and visually whereby the yellow-coloured probe shows an absorbance peak at 410 nm and undergoes bleaching to the cyclised salt generating a peak at 325 nm. This azo was able to determine the

presence of DCP, DCNP and DFP at rate constant (k) values of 0.013 s^{-1} , 0.061 s^{-1} and 0.20 s^{-1} , respectively.¹⁴⁰

1.8.1.2. Oxime-Based Sensors

A common limitation of some PET sensors is the relatively slow phosphorylation of the nucleophilic moiety by a target organophosphate. As a result, sensors have been developed with highly nucleophilic moieties to increase the kinetics of this rate-limiting step. Hence, probes have been developed with oxime functional groups. For example, Dale and Rebek developed their previously reported fluorescent sensor by synthesising four oxime-based probes with coumarin, naphthalene, pyrene and pyridine cores (Figure 1.13, left). Upon treatment with DCP, the sensors underwent a cyclisation reaction to form the desired arylisoxazole structures thus causing measurable shifts in the absorption and emission peaks. The naphthyl-based sensor was identified as the highest performing with a 62-fold increase in fluorescent enhancement.¹⁴¹

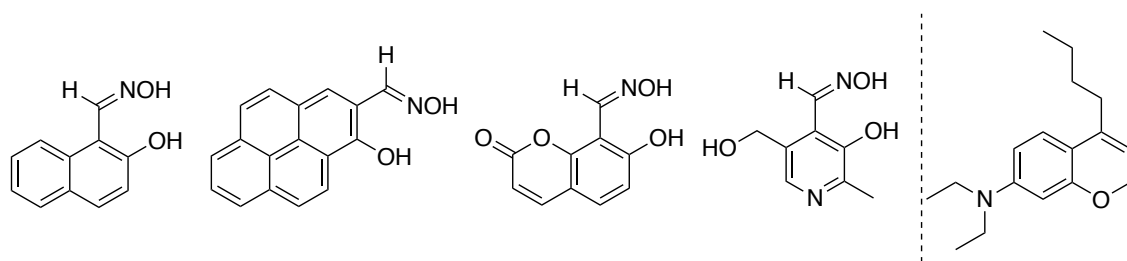


Figure 1.13. Structures of oxime-based sensors reported by Dale and Rebek (left) and Anslyn (right).

Anslyn *et al.* developed a “turn-on” PET fluorescent probe capable of detecting DFP within a ms timeframe in the presence of a non-nucleophilic base (Figure 1.13, right). The oximate anion quenched the fluorescence of the probe via a PET mechanism resulting in a very weak fluorescence intensity. Subsequent addition of simulant prevented this quenching and causes a rapid increase in fluorescence intensity.¹⁴² This study showed that introducing highly nucleophilic moieties substantially increases the response time of PET-based sensors.

1.8.2. Sensors for the Determination of V-series Nerve Agents

There are relatively fewer sensors for the detection of V-series nerve agents in comparison to that of G-agents. Furthermore, a higher proportion of the literature concerning V-agents involve colorimetric sensors with responses that can be visually observed by the naked eye. For example, Kumar and Rana developed a squaraine dye

capable of selectively detecting VX and tabun. A fluoride source reacts with tabun and VX to generate their respective leaving group anions, cyanide and thiolate. These nucleophilic anions attack the blue-coloured dye resulting in the bleaching of colour only in the presence of simulant. This system required the subsequent addition of Hg (II), a thiophilic metal ion, to cleave the thiol from the dye complex in order to visually discriminate between VX from tabun by the restoration of colour. The limit of detection (LOD) for the visual and fluorescence detection of tabun was determined to be 50 μM and 8 μM , respectively, and 80 μM and 8 μM for VX, respectively.¹⁴³

Gupta *et al.* later reported a chromogenic ferrocene dye with a dicyanovinyl moiety. The sensing mechanism requires a diketoxime reagent that reacts with a nerve agent to generate the phosphonylated intermediate which then decomposes under basic conditions to produce cyanide ions that react with the dye resulting in the bleaching of colour. This sensor was found to be selective towards tabun, sarin and VX over other potential interfering agents. The detection limits for these agents were determined to be 1.0 mM and 0.15 mM by visual and UV-vis detection.¹⁴⁴ The sensor structures are presented in Figure 1.14.

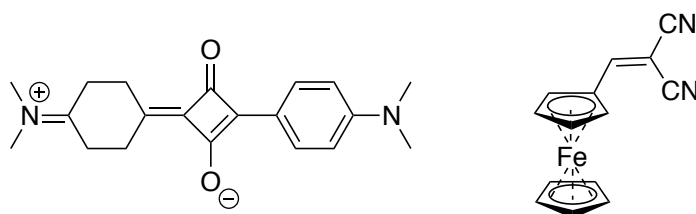


Figure 1.14. Structures of VX sensors reported by Kumar and Rana (left) and Gupta *et al.* (right).

Despite the wide variety of detection systems for the determination of blister and nerve agents, the lack of purely colorimetric systems creates a demand for selective and sensitive probes that can be interpreted without the requirement of complicated equipment. This thesis will focus mainly on sensor development for mustards as it was concluded to be the most challenging CWA type to detect due to its water immiscibility.

References

- 1 J. L. McWilliams; R. J. Steel, *Gas! The Battle for Ypres, 1915*, Vanwell Publishing Limited, Canada, 1985.
- 2 R. Harris and J. Paxman, *A Higher Form of Killing: The Secret History of Chemical and Biological Warfare*, Arrow Books, London, 2010.
- 3 K. Coleman, *A History of Chemical Warfare*, Palgrave Macmillan UK, London, 2005.
- 4 T. T. Marrs, R. L. Maynard and F. Sidell, *Chemical Warfare Agents : Toxicology and Treatment*, John Wiley & Sons Ltd, England, Second Edi., 2007.
- 5 J. B. S. Haldane, *Callinicus: A Defence of Chemical Warfare*, E. P. Dutton & Company, New York, 1925.
- 6 Protocol for the Prohibition of the Use in War of Asphyxiating, Poisonous or Other Gases, and of Bacteriological Methods of Warfare, https://unoda-web.s3-accelerate.amazonaws.com/wp-content/uploads/assets/WMD/Bio/pdf/Status_Protocol.pdf, (accessed 9 April 2020).
- 7 J. Goldblat, *The Problem of Chemical and Biological Warfare Volume IV: CB Disarmament Negotiations, 1920-1970*, Paul Elek Limited, London, 1971.
- 8 F. R. Sidell, E. T. Takafuji and D. R. Franz, *Medical Aspects of Chemical and Biological Warfare*, Borden Institute, Walter Reed Army Medical Center, Washington, D.C., 1997.
- 9 J. Newmark, *Neurology*, 2004, **62**, 1590–1596.
- 10 L. L. Chao, J. C. Rothlind, V. A. Cardenas, D. J. Meyerhoff and M. W. Weiner, *Neurotoxicology*, 2010, **31**, 493–501.
- 11 Organisation for the Prohibition of Chemical Weapons, https://www.opcw.org/sites/default/files/documents/CWC/CWC_en.pdf, (accessed 20 April 2020).
- 12 H. Morita, N. Yanagisawa, T. Nakajima, H. Okudera, M. Shimizu, H. Hirabayashi, M. Nohara, Y. Midorikawa and S. Mimura, *The Lancet*, 1995, **346**, 290–293.
- 13 T. Okumura, K. Suzuki, A. Fukuda, A. Kohama, N. Takasu, S. Ishimatsu and S. Hinohara, *Academic Emergency Medicine*, 1998, **5**, 618–624.
- 14 Summary of the Report on Activities Carried Out in Support of a Request for Technical Assistance by the United Kingdom of Great Britain and Northern Ireland, https://www.opcw.org/sites/default/files/documents/S_series/2018/en/s-1612-2018_e_.pdf, (accessed 20 April 2020).
- 15 Letter from the UK National Security Adviser to the NATO Secretary General regarding the Salisbury attack,

https://assets.publishing.service.gov.uk/government/uploads/system/uploads/attachment_data/file/699819/Letter_from_the_UK_National_Security_Adviser_to_the_NATO_Secretary_General_regarding_the_Salisbury_incident.pdf, (accessed 20 April 2020).

- 16 S. P. Harvey, L. R. McMahon and F. J. Berg, *Heliyon*, 2020, **6**, 1–4.
- 17 D. H. Ellison, *Handbook of Chemical and Biological Warfare Agents*, CRC Press, Boca Raton, Florida, Second Edi., 2008.
- 18 K. Kehe, H. Thiermann, F. Balszuweit, F. Eyer, D. Steinritz and T. Zilker, *Toxicology*, 2009, **263**, 3–8.
- 19 S. Sezigen and L. Kenar, *Toxicol Lett*, 2020, **320**, 52–57.
- 20 K. Ganesan, S. K. Raza and R. Vijayaraghavan, *J Pharm Bioallied Sci*, 2010, **2**, 166–78.
- 21 C. Li, R. K. Srivastava, Z. Weng, C. R. Croutch, A. Agarwal, C. A. Elmets, F. Afaq and M. Athar, *American Journal of Pathology*, 2016, **186**, 2637–2649.
- 22 C. L. Hewitt, W. E. Jones, H. W. Vallender and F. N. Woodward, *Journal of the Society of Chemical Industry*, 1949, **68**, 263–268.
- 23 W. E. Jones, R. J. Rosser and F. N. Woodward, *Journal of the Society of Chemical Industry*, 1949, **68**, 258–262.
- 24 N. B. Munro, S. S. Talmage, G. D. Griffin, L. C. Waters, A. P. Watson, J. F. King and V. Hauschild, *Environ Health Perspect*, 1999, **107**, 933–974.
- 25 S. Srivastava and S. J. S. Flora, in *Handbook of Toxicology of Chemical Warfare Agents*, ed. R. C. Gupta, Academic Press, Third Edi., 2020.
- 26 R. A. Peters, H. M. Sinclair and R. H. Thompson, *Biochem J*, 1946, **40**, 516–524.
- 27 G. Epure, N. Grigoriu and D. Mosteanu, *Technical Sciences*, 2015, **2**, 226–232.
- 28 R. A. Peters, L. A. Stocken and R. H. S. Thompson, *Nature*, 1945, **156**, 616–619.
- 29 D. H. Rosenblatt, T. A. Miller, J. C. Dacre, I. Muul and D. R. Cogley, *Problem Definition Studies on Potential Environmental Pollutants. II. Physical, Chemical, Toxicological, and Biological Properties of 16 Substances. Tech Rpt 7509*, 1975.
- 30 O. Terzic, S. Bartenbach and P. de Voogt, *J Chromatogr A*, 2013, **1304**, 34–41.
- 31 C. L. Hewitt, *J Chem Soc*, 1948, **3**, 1203–1205.
- 32 D. H. Rosenblatt, A. Thomas Miller, J. C. Dacre, I. Muul and D. R. Cogley, *US Army Medical Research and Development Command Forrestal Building*, 1975.
- 33 Charles. G. Hurst and William. J. Smith, in *Chemical Warfare Agents: Chemistry, Pharmacology, Toxicology, and Therapeutics*, eds. J. A. Romano Jr, B. J. Lukey and H. Salem, CRC Press, Second Edi., 2007.
- 34 Y. C. Yang, J. A. Baker and J. R. Ward, *Chem. Rev*, 1992, **92**, 1729–1743.
- 35 M. Despretz, *Ann. Clin. Phys*, 1882, **21**, 437–438.

- 36 F. Guthrie, *Justus Liebigs Ann Chem*, 1860, **113**, 266–288.
- 37 A. Niemann, *Justus Liebigs Ann Chem*, 1860, **113**, 288–292.
- 38 Robert. A. Young and Cheryl. B. Bast, in *Handbook of Toxicology of Chemical Warfare Agents*, ed. Ramesh. C. Gupta, Academic Press, Third Edi., 2020.
- 39 W. S. Alwan, *Physicochemical Properties & Relative Toxicity of Chemical Warfare Agents*,
https://www.opcw.org/sites/default/files/documents/Science_Technology/CW_Agents.pdf, (accessed 11 May 2022).
- 40 P. D. Bartlett and C. Gardner Swain, *J Am Chem Soc*, 1949, **71**, 1406–1415.
- 41 I. A. Fallis, P. C. Griffiths, T. Cosgrove, C. A. Dreiss, N. Govan, R. K. Heenan, I. Holden, R. L. Jenkins, S. J. Mitchell, S. Notman, J. A. Platts, J. Riches and T. Tatchell, *J Am Chem Soc*, 2009, **131**, 9746–9755.
- 42 B. Papirmeister, C. L. Gross, H. L. Meier, J. P. Petrali and J. B. Johnson, *Toxicological Sciences*, 1985, **5**, 134–149.
- 43 T. Q. Niu, Z. Matijasevic, P. Austin-Ritchie, A. Stering and D. B. Ludlum, *Chem Biol Interact*, 1996, **100**, 77–84.
- 44 G. P. van der Schans, A. G. Scheffer, R. H. Mars-Groenendijk, A. Fidder, H. P. Benschop and R. A. Baan, *Chem Res Toxicol*, 1994, **7**, 408–413.
- 45 A. Fidder, G. W. H. Moes, A. G. Scheffer, G. P. van der Schans, R. A. Baan, L. P. A. de Jong and H. P. Benschop, *Chem Res Toxicol*, 1994, **7**, 199–204.
- 46 I. G. Walker, *Can J Biochem*, 1971, **49**, 332–336.
- 47 P. Brookes and P. D. Lawley, *Biochemical Journal*, 1961, **80**, 496–503.
- 48 P. Brookes and P. Lawley, *Biochemical Journal*, 1961, **80**, 496–503.
- 49 E. Raber, A. Jin, K. Noonan, R. McGuire and R. D. Kirvel, *Int J Environ Health Res*, 2001, **11**, 128–148.
- 50 K. Kehe and L. Szinicz, *Toxicology*, 2005, **214**, 198–209.
- 51 J. P. Mason and D. J. Gasch, *J. Chem. Soc*, 1935, 1217.
- 52 K. Ward, *J Am Chem Soc*, 1935, **57**, 914–916.
- 53 M. F. Sartori, *Chem Rev*, 1951, **48**, 225–257.
- 54 W. P. Anslow and D. A. Karnovsky, *J Pharmacol Exp Ther*, 1947, **91**, 224–235.
- 55 J. L. Everett, J. J. Roberts and W. C. J. Ross, *J Chem Soc*, 1953, 2386.
- 56 O. M. Friedman and A. M. Seligman, *J Am Chem Soc*, 1954, **76**, 655–658.
- 57 O. M. Friedman and A. M. Seligman, *J Am Chem Soc*, 1954, **76**, 658–661.
- 58 F. Bergel and J. A. Stock, *Br Emp Cancer Comp Annu*, 1953, **31**, 6–21.
- 59 V. T. Devita, A. A. Serpick and P. P. Carbone, *Ann Intern Med*, 1970, **73**, 881–895.

- 60 V. T. DeVita, E. DeVita-Raeburn and J. H. Moxley, *Cancer Res*, 2016, **76**, 1303–1304.
- 61 A. Gilman, *The American Journal of Surgery*, 1963, **105**, 574–578.
- 62 S. M. Somani, *Chemical warfare agents*, Academic Press, New York, 1992.
- 63 A. Haddow, G. A. R. Kon and W. C. J. Ross, *Nature*, 1948, **162**, 824–825.
- 64 C. W. Crane and H. N. Rydon, *J Chem Soc*, 1947, 527–530.
- 65 C. Golumbic and M. Bergmann, *Journal of Organic Chemistry*, 1946, **11**, 536–542.
- 66 P. D. Bartlett, S. D. Ross and C. Gardner Swain, *J Am Chem Soc*, 1949, **71**, 1415–1419.
- 67 Q. Q. Wang, R. A. Begum, V. W. Day and K. Bowman-James, *Org Biomol Chem*, 2012, **10**, 8786–8793.
- 68 Q. Q. Wang, R. A. Begum, V. W. Day and K. Bowman-James, *Org Biomol Chem*, 2012, **10**, 8786–8793.
- 69 J. B. Tucker, *War of Nerves: Chemical Warfare from World War I to Al-Qaeda*, Pantheon Books, New York, 2006.
- 70 J. A. Romano Jr, H. Salem, B. J. Lukey and B. J. Lukey, *Chemical Warfare Agents: Chemistry, Pharmacology, Toxicology, and Therapeutics*, CRC Press, Second Edi., 2007.
- 71 M. B. Abou-Donia, B. Siracuse, N. Gupta and A. Sobel Sokol, *Crit Rev Toxicol*, 2016, **46**, 845–875.
- 72 R. Norlin and G. Lindberg, *J Labelled Comp Radiopharm*, 2003, **46**, 599–604.
- 73 A. Ordentlich, D. Barak, C. Kronman, H. P. Benschop, L. P. A. De Jong, N. Ariel, R. Barak, Y. Segall, B. Velan and A. Shafferman, *Biochemistry*, 1999, **38**, 3055–3066.
- 74 H. P. Benschop and L. P. A. De Jong, *Acc Chem Res*, 1988, **21**, 368–374.
- 75 K. Lohs, *Deutscher Militärverlag*, 1967, 327.
- 76 M. R. Gravett, F. B. Hopkins, A. J. Self, A. J. Webb, C. M. Timperley and J. R. Riches, *Anal Bioanal Chem*, 2014, **406**, 5121–5135.
- 77 J. R. Ward, Y. C. Yang, R. B. Wilson, W. D. Burrows and L. L. Ackerman, *Bioorg Chem*, 1988, **16**, 12–16.
- 78 R. L. Gustafson and A. E. Martell, *J Am Chem Soc*, 1962, **84**, 2309–2316.
- 79 J. Epstein, J. J. Callahan and V. E. Bauer, *Phosphorus*, 1974, **4**, 157–163.
- 80 H. J. Altmann and A. Richardt, *Decontamination of Warfare Agents: Enzymatic Methods for the Removal of B/C Weapons*, 2008, **92**, 83–115.
- 81 Y. C. Yang, *Acc Chem Res*, 1999, **32**, 109–115.

- 82 F. Worek, H. Thiermann, L. Szinicz and P. Eyer, *Biochem Pharmacol*, 2004, **68**, 2237–2248.
- 83 K. Cannard, *J Neurol Sci*, 2006, **249**, 86–94.
- 84 P. Masson, F. Nachon and O. Lockridge, *Chem Biol Interact*, 2010, **187**, 157–162.
- 85 T. M. Epstein, U. Samanta, S. D. Kirby, D. M. Cerasoli and B. J. Bahnson, *Biochemistry*, 2009, **48**, 3425–3435.
- 86 D. Barak, A. Ordentlich, D. Kaplan, R. Barak, D. Mizrahi, C. Kronman, Y. Segall, B. Velan and A. Shafferman, *Biochemistry*, 2000, **39**, 1156–1161.
- 87 E. Elhanany, A. Ordentlich, O. Dgany, D. Kaplan, Y. Segall, R. Barak, B. Velan and A. Shafferman, *Chem Res Toxicol*, 2001, **14**, 912–918.
- 88 E. Carletti, H. Li, B. Li, F. Ekström, Y. Nicolet, M. Loidice, E. Gillon, M. T. Froment, O. Lockridge, L. M. Schopfer, P. Masson and F. Nachon, *J Am Chem Soc*, 2008, **130**, 16011–16020.
- 89 M. Sun, Z. Chang, M. Shau, R. Huang and T. Chou, *Eur J Biochem*, 1979, **100**, 527–530.
- 90 F. Worek, H. Thiermann, L. Szinicz and P. Eyer, *Biochem Pharmacol*, 2004, **68**, 2237–2248.
- 91 D. Grob and J. C. Harvey, *J Clin Invest*, 1958, **37**, 350–368.
- 92 U.S. Army Medical Research Institute of Chemical Defense, *Medical Management of Chemical Casualties Handbook*, Aberdeen Proving Ground, MD, Fourth Edi., 2007.
- 93 A. Ordentlich, D. Barak, C. Kronman, H. P. Benschop, L. P. A. De Jong, N. Ariel, R. Barak, Y. Segall, B. Velan and A. Shafferman, *Biochemistry*, 1999, **38**, 3055–3066.
- 94 H. C. J. V. De Bisschop, K. W. Michiels, L. B. C. Vlamincx, S. O. Vansteenkiste and E. H. Schacht, *Biochem Pharmacol*, 1991, **41**, 955–959.
- 95 A. Ordentlich, D. Barak, G. Sod-Moriah, D. Kaplan, D. Mizrahi, Y. Segall, C. Kronman, Y. Karton, A. Lazar, D. Marcus, B. Velan and A. Shafferman, *Biochemistry*, 2004, **43**, 11255–11265.
- 96 S. P. Harvey, J. E. Kolakowski, T. C. Cheng, V. K. Rastogi, L. P. Reiff, J. J. DeFrank, F. M. Raushel and C. Hill, *Enzyme Microb Technol*, 2005, **37**, 547–555.
- 97 H. P. Benschop, C. A. G. Konings, J. Van Genderen and L. P. A. De Jong, *Toxicol Appl Pharmacol*, 1984, **72**, 61–74.
- 98 T. Okumura, K. Suzuki, A. Fukuda, A. Kohama, N. Takasu, S. Ishimatsu and S. Hinohara, *Academic Emergency Medicine*, 1998, **5**, 618–624.
- 99 M. Balali-Mood and M. Hefazi, *Basic Clin Pharmacol Toxicol*, 2006, **99**, 273–282.

- 100 M. B. Gold, R. Bongiovanni, B. A. Scharf, V. C. Gresham and C. L. Woodward, *Drug Chem Toxicol*, 1994, **17**, 499–527.
- 101 U. Wormser, B. Brodsky and A. Sintov, *Arch Toxicol*, 2002, **76**, 517–522.
- 102 M. Eddleston, N. A. Buckley, P. Eyer and A. H. Dawson, *The Lancet*, 2008, 371, 597–607.
- 103 I. B. Wilson and S. Ginsburg, *BBA - Biochimica et Biophysica Acta*, 1955, **18**, 168–170.
- 104 A. F. Childs, D. R. Davies, A. L. Green and J. P. Rutland, *J. Pharmacol*, 1955, 462.
- 105 I. Koplovitz and J. R. Stewart, *Toxicol Lett*, 1994, **70**, 269–279.
- 106 F. Worek, L. Szinicz and H. Thiermann, *Chem Biol Interact*, 2005, **157–158**, 349–352.
- 107 F. Worek, H. Thiermann, L. Szinicz and P. Eyer, *Biochem Pharmacol*, 2004, **68**, 2237–2248.
- 108 F. Ekström, C. Akfur, A. K. Tunemalm and S. Lundberg, *Biochemistry*, 2006, **45**, 74–81.
- 109 C. L. Cadieux, H. Wang, Y. Zhang, J. A. Koenig, T. M. Shih, J. McDonough, J. Koh and D. Cerasoli, *Chem Biol Interact*, 2016, **259**, 133–141.
- 110 M. Jokanović and M. P. Stojiljković, *Eur J Pharmacol*, 2006, **553**, 10–17.
- 111 B. Sanson, F. Nachon, J.-P. Colletier, M.-T. Froment, L. Toker, H. M. Greenblatt, J. L. Sussman, Y. Ashani, P. Masson, I. Silman and M. Weik, *J Med Chem*, 2009, **52**, 7593–7603.
- 112 Y. Ashani, Z. Radic, I. Tsigelny, D. C. Vellom, N. A. Pickering, D. M. Quinn, B. P. Doctor and P. Taylor, *Journal of Biological Chemistry*, 1995, **270**, 6370–6380.
- 113 Y. Ashani, A. K. Bhattacharjee, H. Leader, A. Saxena and B. P. Doctor, *Biochem Pharmacol*, 2003, **66**, 191–202.
- 114 S. Herkenhoff, L. Szinicz, V. K. Rastogi, T. C. Cheng, J. J. DeFrank and F. Worek, *Arch Toxicol*, 2004, **78**, 338–343.
- 115 L. Chen, D. Wu and J. Yoon, *ACS Sens*, 2018, **3**, 27–43.
- 116 M. Burnworth, S. J. Rowan and C. Weder, *Chemistry - A European Journal*, 2007, **13**, 7828–7836.
- 117 S. Royo, R. Martínez-Máñez, F. Sancenón, A. M. Costero, M. Parra and S. Gil, *Chemical Communications*, 2007, 0, 4839–4847.
- 118 V. Kumar and H. Rana, *RSC Adv*, 2015, **5**, 91946–91950.
- 119 H. Wang, D. E. Wang, J. Guan, X. Han, P. Xue, W. Liu, M. Sen Yuan and J. Wang, *J Mater Chem C Mater*, 2017, **5**, 11565–11572.
- 120 V. Kumar and E. V. Anslyn, *Chem Sci*, 2013, **4**, 4292–4297.

- 121 V. Kumar and E. V. Anslyn, *J Am Chem Soc*, 2013, **135**, 6338–6344.
- 122 W. Meng, H. Zhang, L. Xiao, X. Chen, M. Sun, Q. Xu, Y. Cao, K. Xiao and Z. Li, *Sens Actuators B Chem*, 2019, **296**, 126678.
- 123 W. Feng, H. Li, M. J. Xue, Q. L. Zhang, S. L. Liu and Q. H. Song, *Anal Chim Acta*, , DOI:10.1016/j.aca.2021.338440.
- 124 W. Meng, M. Sun, Q. Xu, J. Cen, Y. Cao, Z. Li and K. Xiao, *ACS Sens*, 2019, **4**, 2794–2801.
- 125 V. Kumar, H. Rana, G. Raviraju and A. K. Gupta, *Anal Chem*, 2018, **90**, 1417–1422.
- 126 H. Wang, J. Guan, X. Han, S. W. Chen, T. Li, Y. Zhang, M. Sen Yuan and J. Wang, *Talanta*, 2018, **189**, 39–44.
- 127 Y. Zhang, Y. Lv, X. Wang, A. Peng, K. Zhang, X. Jie, J. Huang and Z. Tian, *Anal Chem*, 2018, **90**, 5481–5488.
- 128 D. Li, H. Xi, S. Han and S. Zhao, *Analytical Methods*, 2021, **13**, 484–490.
- 129 D. R. Goud, A. K. Purohit, V. Tak, D. K. Dubey, P. Kumar and D. Pardasani, *Chemical Communications*, 2014, **50**, 12363–12366.
- 130 C. Y. Chen, K. H. Li and Y. H. Chu, *Anal Chem*, 2018, **90**, 8320–8325.
- 131 W. Xiong, Y. Gong, Y. Che and J. Zhao, *Anal Chem*, 2019, **91**, 1711–1714.
- 132 R. C. Knighton, M. R. Sambrook, J. C. Vincent, S. A. Smith, C. J. Serpell, J. Cookson, M. S. Vickers and P. D. Beer, *Chemical Communications*, 2013, **49**, 2293–2295.
- 133 Neelam, V. Singh and T. Gupta, *Anal Chim Acta*, 2014, **812**, 222–227.
- 134 K. S, S. M and F. SJ, *Appl Biochem Biotechnol*, 2013, **171**, 1405–1415.
- 135 Y. L. Jiang and A. M. Broome, *ACS Sens*, 2019, **4**, 1791–1797.
- 136 V. V. Singh, V. Kumar, U. Biswas, M. Boopathi, K. Ganesan and A. K. Gupta, *Anal Chem*, 2021, **93**, 1193–1199.
- 137 C. Sun, W. Xiong, W. Ye, Y. Zheng, R. Duan, Y. Che and J. Zhao, *Anal Chem*, 2018, **90**, 7131–7134.
- 138 T. J. Dale and J. Rebek, *J Am Chem Soc*, 2006, **128**, 4500–4501.
- 139 S. W. Zhang and T. M. Swager, *J Am Chem Soc*, 2003, **125**, 3420–3421.
- 140 A. M. Costero, S. Gil, M. Parra, P. M. E. Mancini, R. Martínez-Mañez, F. Sancenón and S. Royo, *Chemical Communications*, 2008, **0**, 6002–6004.
- 141 T. J. Dale and J. Rebek, *Angewandte Chemie*, 2009, **121**, 7990–7992.
- 142 K. J. Wallace, R. I. Fagbemi, F. J. Folmer-Andersen, J. Morey, V. M. Lynth and E. V. Anslyn, *Chemical Communications*, 2006, **0**, 3886–3888.
- 143 V. Kumar and H. Rana, *Chemical Communications*, 2015, **51**, 16490–16493.

144 V. Kumar, G. Raviraju, H. Rana, V. K. Rao and A. K. Gupta, *Chemical Communications*, 2017, **53**, 12954–12957.

Chapter 2. The Rapid and Selective Detection of Sulfur and Nitrogen Mustards by a One-Pot Method

2.1. Introduction

2.1.1. Surfactants

Surfactants (surface active agents)¹ are amphiphilic compounds comprised of a hydrophobic 'tail' group and a hydrophilic 'head' group. Surfactants can be divided into four main categories based on the chemical structure of their 'head' group: anionic, cationic, non-ionic and zwitterionic. These classes are summarised in Figure 2.1.

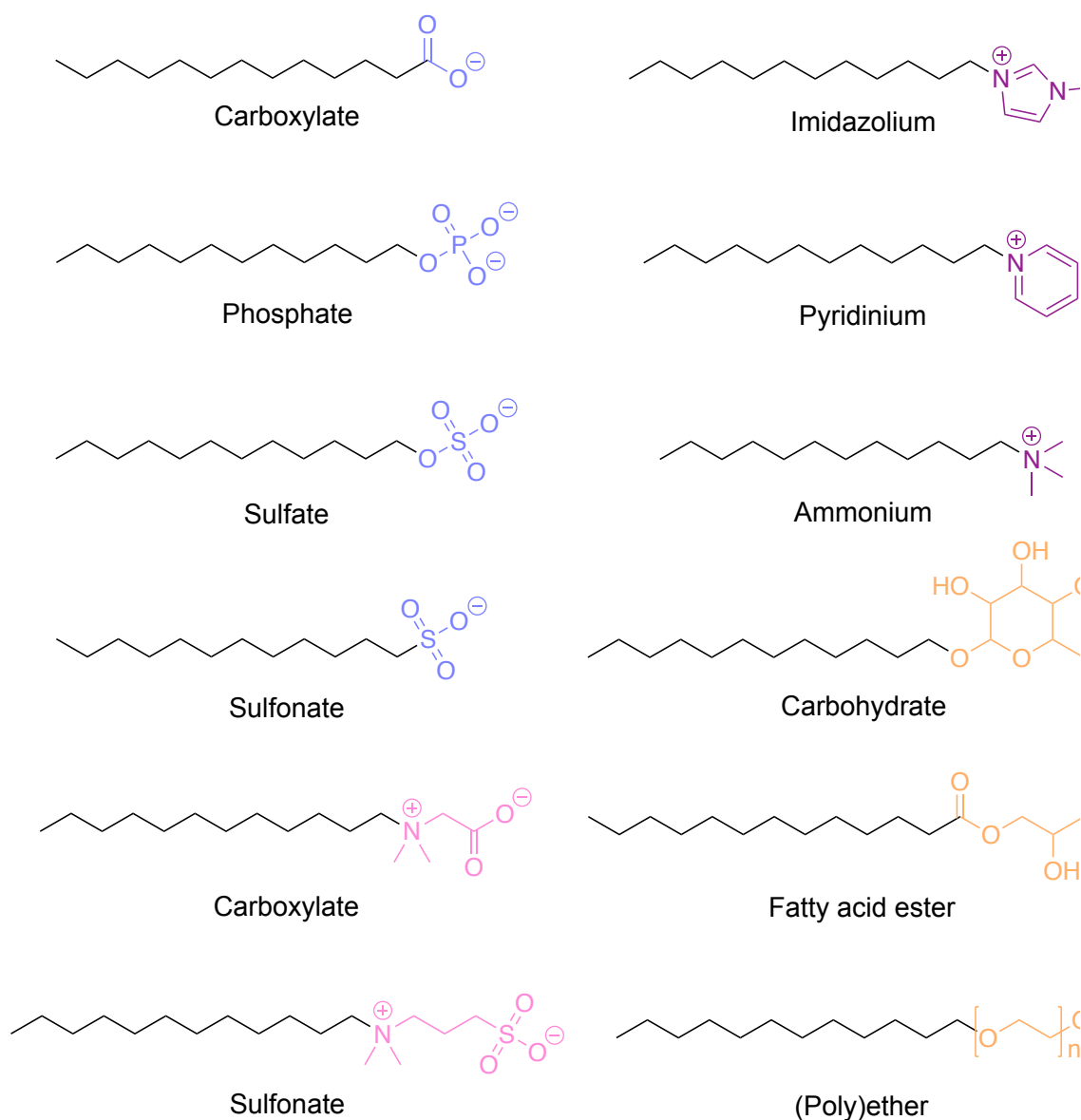


Figure 2.1. General structures of surfactants are grouped into categories based on their 'head' groups. Blue: anionic surfactants; pink: zwitterionic surfactants; purple: cationic surfactants; orange: non-ionic surfactants.

In detail, examples of anionic surfactant 'head' groups include carboxylates,² phosphates,³ sulfates⁴ and sulfonates⁵. Conversely, the structures of cationic surfactants typically contain amine groups such as imidazolium cations,⁶ pyridinium cations⁷ and quaternary ammonium cations⁸.

Typically, non-ionic surfactants are based on carbohydrates,⁹ fatty acid esters,¹⁰ and (poly)ethers,¹¹ with the water solubility of the latter being the result of hydrogen bonding between the ether oxygen atoms of the oxyethylene 'head' groups and the water molecules of the aqueous phase. They also possess a unique property whereby micellar solutions develop a turbid appearance at a certain temperature. This phenomenon is known as the cloud point, above which the system phase separates into a micelle-rich phase and a micelle-poor phase creating a density difference between the two phases.¹² This separation is caused by an increase in aggregation number due to the aggregation of small micelles to form large secondary aggregates and a reduction in intermicellar repulsions.¹³ These much larger micellar structures are able to scatter light sufficiently to create a turbid mixture.^{14,15} The temperature at which this phenomenon occurs is dependent on the surfactant, surfactant concentration, and ionic strength of the aqueous phase^{16,17}. For example, for polyethylene oxide non-ionic surfactants, an increase in ethylene oxide chain length increases the cloud point due to a decrease of intermicellar repulsion as a consequence of the dehydration of the hydrophilic 'head' groups with rising temperature.^{18,19} At constant ethylene oxide chain length, the cloud point may be lowered by increasing the hydrocarbon tail length, branching of the hydrocarbon chain, and a broad range of hydrocarbon chain lengths.²⁰

Zwitterionic surfactants are amphoteric as their structures contain both anionic and cationic groups within their structure. The cationic component is typically based on primary, secondary or tertiary amines or quaternary ammonium cations with a sulfonate²¹ or carboxylate²² group as the anionic component. The 'tail' groups of surfactant molecules remain fairly unaltered and typically consist of hydrocarbon chains which can be either linear, branched, or aromatic. Commonly, these hydrophobic chains are at least eight carbon atoms in length.²³⁻²⁵ Alternatively, surfactants with perfluoroalkyl²⁶ and polysiloxane²⁷ hydrophobic chains have been reported. These traditional surfactants are considered chemically "innocent" as their properties are a result of their structurally amphiphilic nature. Metallosurfactants are a subdivision of surfactants in which the incorporation of a metal centre at the polar 'head' group introduces new properties such as variable charge, catalytical activity, and magnetic properties.²⁸⁻³⁰

2.1.2. Micellisation

At specific concentrations, surfactant molecules can adsorb at interfaces to form micelles thereby significantly changing the physical properties of the interface. The word interface describes the boundary between two phases in gas/liquid, liquid/liquid, and solid/liquid systems. The concentration at which aggregation occurs is specific to the individual surfactant compound and is termed the critical micelle concentration (CMC). This process of self-assembly occurs spontaneously whereby surfactant monomers form thermodynamically stable and ordered structures. The adsorption behaviour of surfactants is a result of the amphiphilic nature of the molecules. In an aqueous solution, surfactant molecules form micelle structures in which the hydrophobic 'tails' are positioned in the interior of the micelle and the hydrophilic 'head' groups are in contact with the aqueous phase (Figure 2.2). Micelles can exist in a variety of shapes however spheres are the simplest of these self-assembled structures.

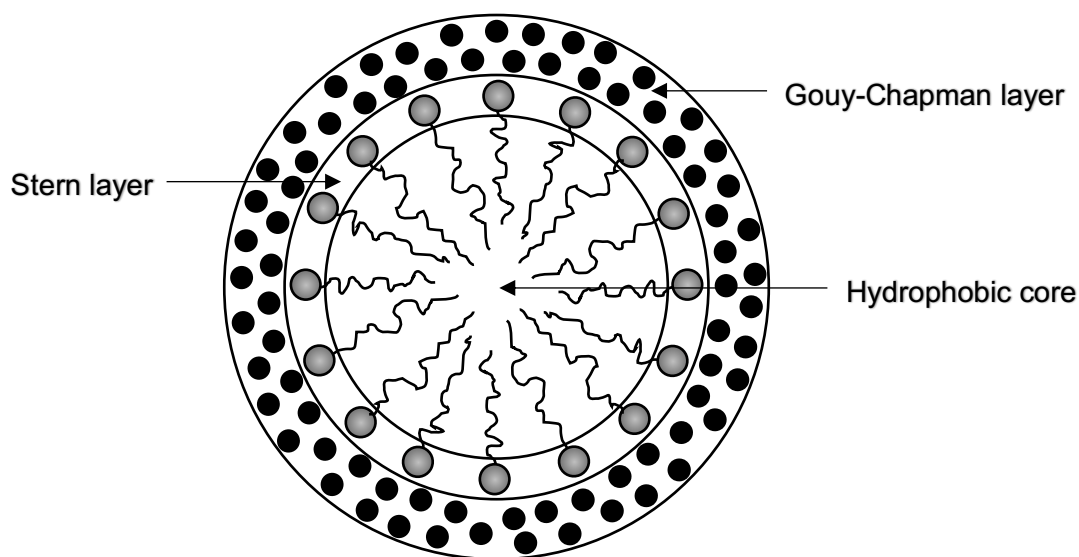


Figure 2.2. Two-dimensional illustration of the adsorption of surfactant molecules into a micelle of an oil-in-water (O/W) microemulsion.

The micelle radius is dependent upon the length of the surfactant hydrocarbon chain.³¹ Furthermore, increasing the hydrocarbon chain length linearly increases the aggregation number of surfactants whilst lowering the CMC.³² Non-ionic micelles with surfactants containing zwitterionic or uncharged 'head' groups have significantly lower CMCs compared to their analogous ionic surfactants of the same carbon chain length due to a reduction in intramicellar electrostatic repulsion between the polar 'head' groups.³³ Ionic strength has little influence on the CMC of non-ionic surfactants compared to that of ionic

surfactants.^{34,35} The addition of salt decreases the repulsion between the charged 'head' groups of ionic surfactants which reduce the CMC; however, the ionic strength effect is less pronounced for non-ionic surfactants due to the absence of electrostatic repulsion between the uncharged 'head' groups. Many additional factors affect the CMC including pH,³⁶ pressure,³⁷ temperature³⁸ and the type of counter ion³⁸. Furthermore, increasing the alkyl chain length also increases the distance between 'head' groups at the micelle interface. The adopted shape of a micelle is dependent on the packing and interactions of surfactant 'head' groups.^{32,39,40} Other complex self-assembled structures are favoured at surfactant concentrations above the CMC such as rod-like and lamellar micelles. At greater surfactant concentrations, a variety of complex liquid crystalline structures can be adopted such as cubic phases, hexagonal phases and vesicles.⁴¹ The aggregate structures described are in relation to systems existing in aqueous solutions; however, micellisation can also occur in organic media where surfactants aggregate to form reverse micelles. This micellar structure consists of the hydrophobic 'tails' interacting with the organic phase at the exterior of the micelle whilst the hydrophilic 'head' groups form the centre of the structure (Figure 2.3).⁴¹

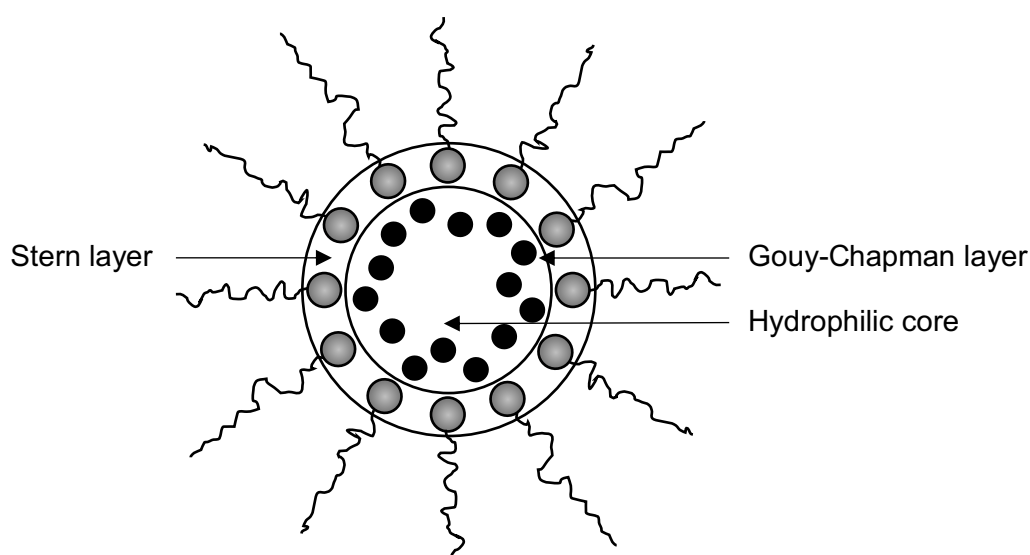


Figure 2.3. Two-dimensional illustration of the adsorption of surfactant molecules into a micelle of a water-in-oil (W/O) microemulsion.

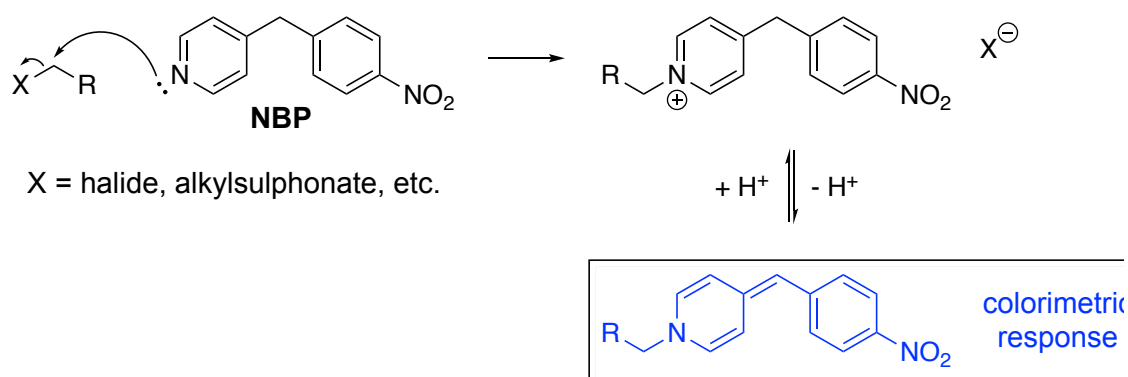
2.1.3. Microemulsions

An emulsion is a dispersed system of liquid phases which are usually immiscible or partially miscible. Microemulsions are a subclass of emulsions with small droplet diameters in the range of approximately 0.01-0.1 μm . Their characteristically small

diameter size means that these systems are of low turbidity.⁴² Microemulsions can be classified into three main categories based on their structure: water-in-oil (W/O), oil-in-water (O/W) or bicontinuous systems. The latter arises when oil and water nanochannels are interspersed by flexible surfactant monolayers.⁴³ Microemulsions are clear, thermodynamically stable, optically isotropic systems typically containing at least three components: oil phase, aqueous phase and surfactant.^{44,45} The formation of stable microemulsions involves creating a system whereby the interfacial tension between the oil and water phases approaches zero. However, single surfactants are often unable to sufficiently lower the interfacial tension between the two phases of the microemulsion even after the CMC or solubility limit has been reached.⁴² To overcome this problem, co-surfactants can be introduced to achieve the desired lowering of the interfacial tension.^{46,47} Typically, medium chain length alcohols are employed due to their amphiphilic nature and preference to adsorb at the water/oil interface compared to shorter or longer chain length alcohols.^{48–51}

2.1.4. Development of the NBP Assay

The employment of 4-(4-nitrobenzyl)pyridine (NBP) in the detection of alkylating agents was first described by Koenigs *et al.*⁵² in 1925 and was later developed by Epstein *et al.*⁵³ in 1955 for the quantitative determination of alkylating agents such as alkyl halides. In this two-step laboratory process, NBP is treated with a suitably reactive electrophile under elevated temperature resulting in the formation of a cationic salt, which upon subsequent treatment with a strong base produces an intensely blue-purple coloured dye through deprotonation at the benzylic methylene group (Scheme 2.1).

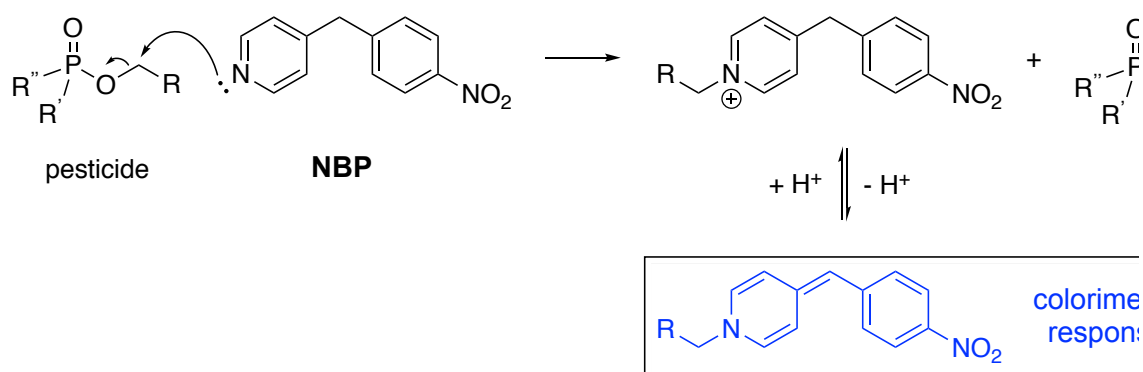


Scheme 2.1: Detection of alkylating agents by NBP (Epstein's method.)

The Epstein method is a reliable procedure because it is sensitive and reproducible. However, there are some notable drawbacks as detailed here:

1. The relatively poor nucleophilicity of NBP requires it to be heated with the analyte at a high reaction temperature of 100 °C.
2. The sensing protocol is a two-step process with the addition of a strongly basic developing solution that can only be added after the NBP is alkylated due to its base sensitivity. This competitive reaction produces a red colour change which could render the positive colour change indistinct in the presence of an alkylating agent.
3. Sulfur mustard is essentially insoluble in water therefore high boiling point organic solvent mixtures are required.
4. This protocol requires the user to have previous knowledge and education in laboratory chemistry and therefore renders this method to a laboratory setting only. Thus, we cannot call this a “point-of-use” sensor as it is not practicable for use in the field.

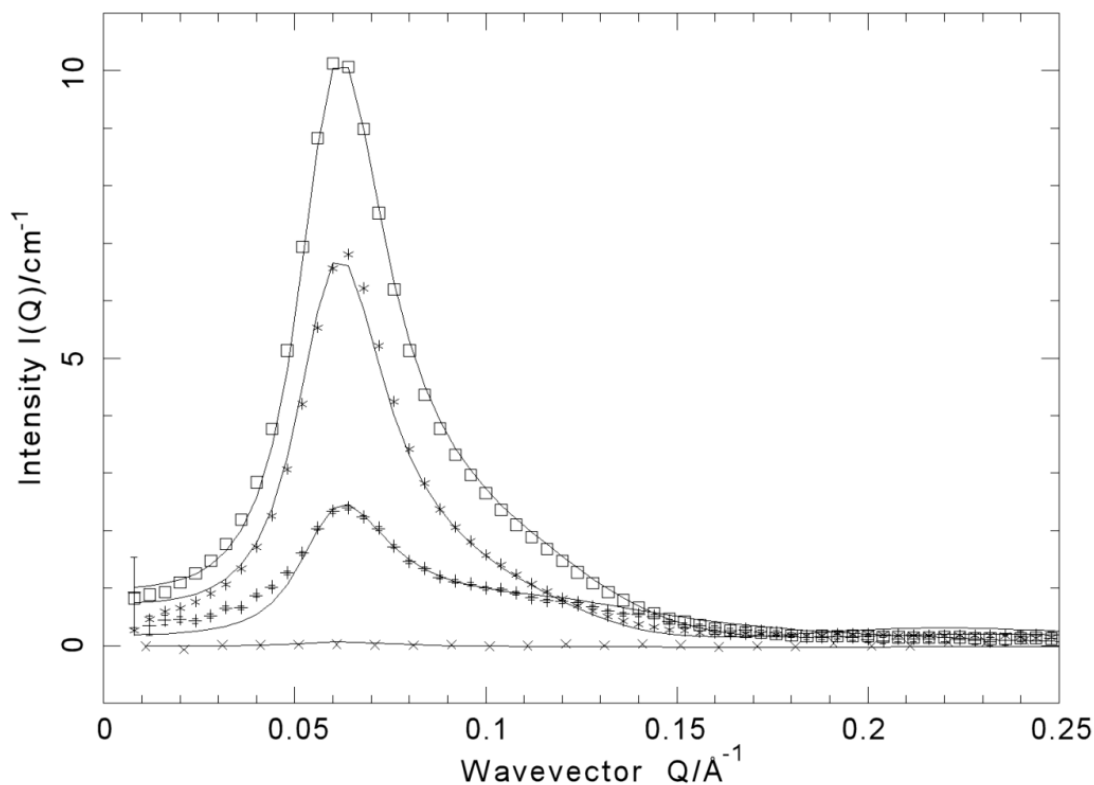
NBP has also been used as a colorimetric sensor for the determination of organophosphate pesticides by UV-vis spectrophotometry.⁵⁴ Turner’s method uses a lower reaction temperature along with lower boiling point solvents compared to other pesticide determination protocols involving NBP.^{55–57} This method was shown to be suitable for many organophosphate pesticides. However, like Epstein’s method, this sensing protocol suffers many of the same limitations. For example, since this method treats pesticides as alkylating agents the reaction conditions are again forcing, requiring a 100 °C heating step to produce the quaternarised dye precursor. Furthermore, the sensing protocol again requires a step-wise addition of analyte and a strong base, tetraethylenepentamine, in this case, to produce the colour change. These limitations restrict the potential development of Turner’s method as a field-deployable sensor. Scheme 2.2 depicts the mechanism of pesticide determination by NBP.



Scheme 2.2. Detection of pesticides as alkylating agents by NBP (Turner’s method.)

Previous work in the Fallis group involved the study of episulfonium chemistry in a O/W anionic microemulsion.⁵⁸ Sodium dodecyl sulfate was used as the surfactant with toluene as the oil phase, n-butanol as co-surfactant and distilled water as the aqueous phase. This microemulsion was denoted SDS-5T with "5T" indicating 5% (wt%) of toluene present as an oil sub-phase. Mass spectrometry analysis of HD and its simulants in SDS-5T showed the expected hydrolysis products with the negatively charged interface of the anionic microemulsion accelerating the hydrolysis of mustards and by doing so proved the formation of the characteristic episulfonium cation intermediate. The unexpected alcoholysis products from the nucleophilic substitution by n-butanol co-surfactant molecules observed in the mass spectrometry data implies that sulfur mustards become more electrophilic in the anionic microemulsion medium as these compounds do not readily react with pure alcohols.

Small-angle neutron scattering (SANS) was employed to study the partitioning of simulants within the microemulsion structure (Figure 2.4). The SANS data shows that there is a net negative charge associated with the SDS-5T microemulsion droplets. Furthermore, the expected droplet volume fraction shows that much of the total material present on average is contained in these droplets. Note that this value decreases upon dilution as water-soluble components of the microemulsion partition to the larger aqueous phase of the system. Given the small radius of the droplets, the surface area is extremely high resulting in the high decontamination performance of the system. This paper also demonstrates that 2-chloroethyl ethyl sulfide (CEES) has a very similar reactivity to sulfur mustard (HD) in microemulsion solutions. Hence, CEES is an ideal simulant for HD.



	x 3 dilution	x 5 dilution
R_{core} (mean) (Å)	14.3	11.6
S(Q) effective radius (Å)	31.1	29.1
Effective charge (e)	17.6	13.5
Expected droplet volume fraction	0.095	0.061

Figure 2.4. SANS contrast variation study from a three-fold dilution of SDS-5T. Plots (contrasts) refer to drop (\square), shell ($*$), core ($+$, scaled $\times 5$) and perdeuterated microemulsion (\times , scaled $\times 5$). The data were fitted by Prof. Peter Griffiths using the parameters in the table. See reference 58 for full details.

Figure 2.5 shows the SANS data of perdeuterated SDS-5T microemulsion samples containing 1 wt% simulant and $[\text{MnCl}(\text{salen})]$ catalyst along with a control sample containing no analyte. The presence of peaks for both the lipophilic 2-chloroethyl phenyl sulfide (PhCES) and catalyst suggests that these compounds are both localised in the droplet's oil phase and do not partition to other areas of the microemulsion structure. The absence of a structured peak for CEES shows that it does not partition into the oil core of the droplet which is a reasonable observation due to the rapid self-reaction of mustards to form the episulfonium cation which rapidly partitions to the aqueous phase.

This data indicates that CEES undergoes rapid hydrolysis while PhCES hydrolyses more slowly. The lipophilic catalyst remains localised in the droplets. This published work can be utilised to create a new NBP sensing system for mustards through the exploitation of the evident enhancement of the electrophilicity of HD and its simulant in a microemulsion. Thus, we aim to explore the reactivity of NBP with mustards and other selected electrophiles in a range of microemulsion media.

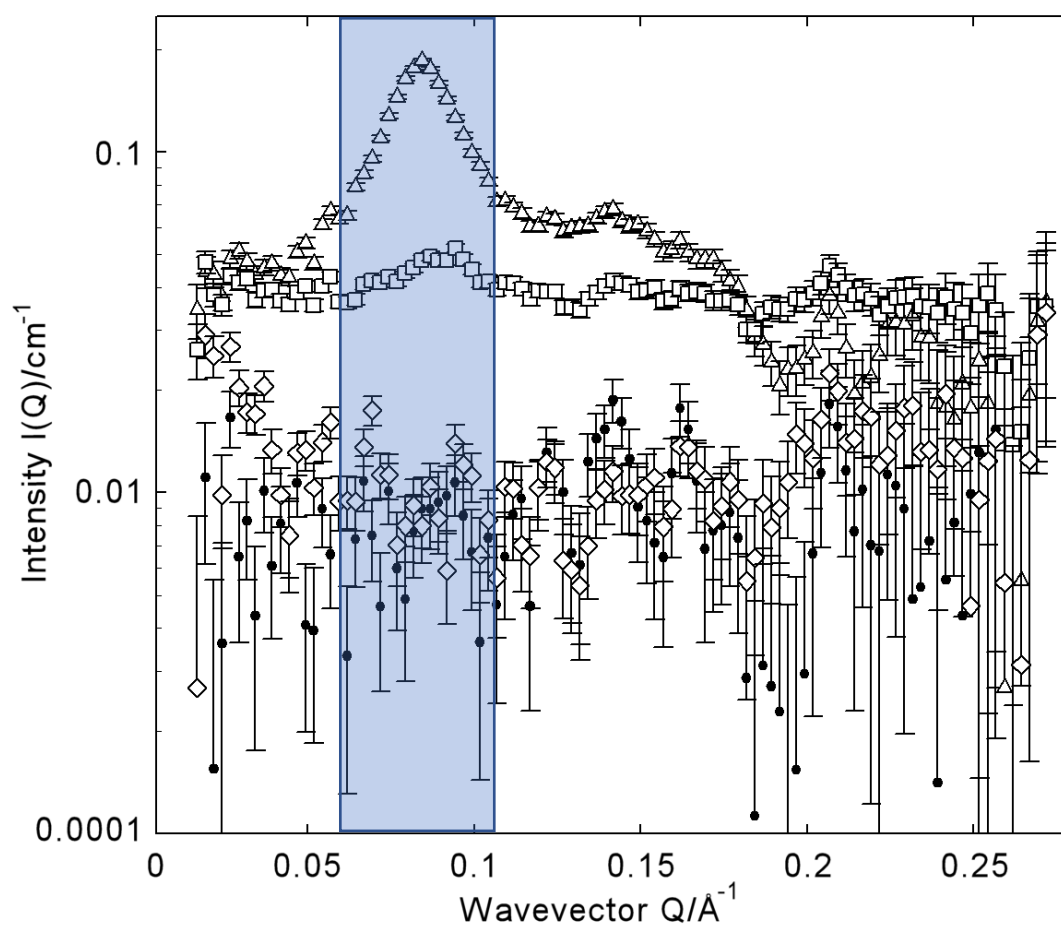


Figure 2.5. SANS of CEES (\diamond), PhCES (\square) and a lipophilic [MnCl(salen)] catalyst (Δ) in a per-deuterated microemulsion (control, \bullet). Note that the scattering intensity (Q) axis is logarithmic. The highlighted region shows the peaks arising from droplet-droplet scattering.

2.2. Aims

The purpose of this work was to devise a low-cost colorimetric sensor for sulfur and nitrogen mustard vesicants that may be used at point-of-use by non-experts (e.g. war-fighters and first-responders). The development of sensor systems for mustards is challenging due to its low reactivity characterised by its relatively weak electrophilicity under normal circumstances; there are considerably fewer sensors reported in the literature for mustard type agents in comparison to that of nerve agents. To date, there are no suitable field-deployable systems for mustards that meet our threshold design criteria. In this work, we sought to develop a colorimetric test system that was based solely upon commercial-off-the-shelf materials. This not only reduces the costs of the system but also truncates the development processes by circumventing lengthy custom synthetic reagent development. The design criteria are summarised as follows in Table 2.1.

Point-of-Use Sensor Design Criteria			
	Target	Threshold	Comment
1	Detection of 0.1 μL of deposited hazard	Detection of 2 μL of deposited hazard	The limit of detection is normally limited by visual detection of the deposited liquid
2	Colorimetric response persists with high analyte loading (100 μL)	Colorimetric response persists with high analyte loading (20 μL)	High loads of mustard agents are likely to be contaminated with HCl
3	Commercial-off-the-shelf component formulation	Non- commercial-off-the-shelf reagents must meet the price per unit threshold (determined by market forces)	Commercial-off-the-shelf reagents have established supply chains and alternative suppliers
4	Formulation to remain colourless upon exposure to negative	Formulation to remain colourless for 30 minutes upon exposure to negative	Colour detection may have to be performed at a remote location under poor lighting conditions.
5	Formulation to remain coloured upon exposure to positive	Formulation to remain coloured for 1 hour upon exposure to positive	
6	Effective against all common false positives	Unaffected by decontamination reagents	Essential for operational effectiveness.
7	5-year shelf-life	2-year shelf life	Essential for product viability.

Table 2.1. Design criteria for point-of-use sensors.

2.3. Results and Discussion

2.3.1. Mustard (CEES) Detection in Solution and Anionic Microemulsion Solution

2-Chloroethyl ethyl sulfide (CEES), also known as “half-mustard”, was used as a sulfur mustard (HD) simulant since it has very similar physicochemical properties to the live agent without the associated severe toxicological properties. CEES has a relatively high LD₅₀ of 300 mg/kg⁵⁹ (dermal, predicted) in comparison with that of HD (100 mg kg⁻¹, dermal)⁶⁰, and is an appropriate substitution of HD for laboratory studies of an academic nature. However, it must be handled with extreme caution as it is carcinogenic and mutagenic, and capable of causing sensitisation.

The reactivity of NBP and other weak bases towards CEES was first investigated by low-resolution ESI+ mass spectrometry (ESI+ LRMS) in an anionic microemulsion. 10 µL of CEES was added to anionic microemulsion solutions (1 mL) containing 2 equivalents of NBP, 4-picoline and 2-bromopyridine, respectively. The solutions were allowed to stand at room temperature for 16 h and were diluted with methanol (10 µL mL⁻¹) before analysis. The mass spectra obtained for these solutions along with a control of anionic microemulsion are presented in Figures 2.6, 2.7, 2.8 and 2.9.

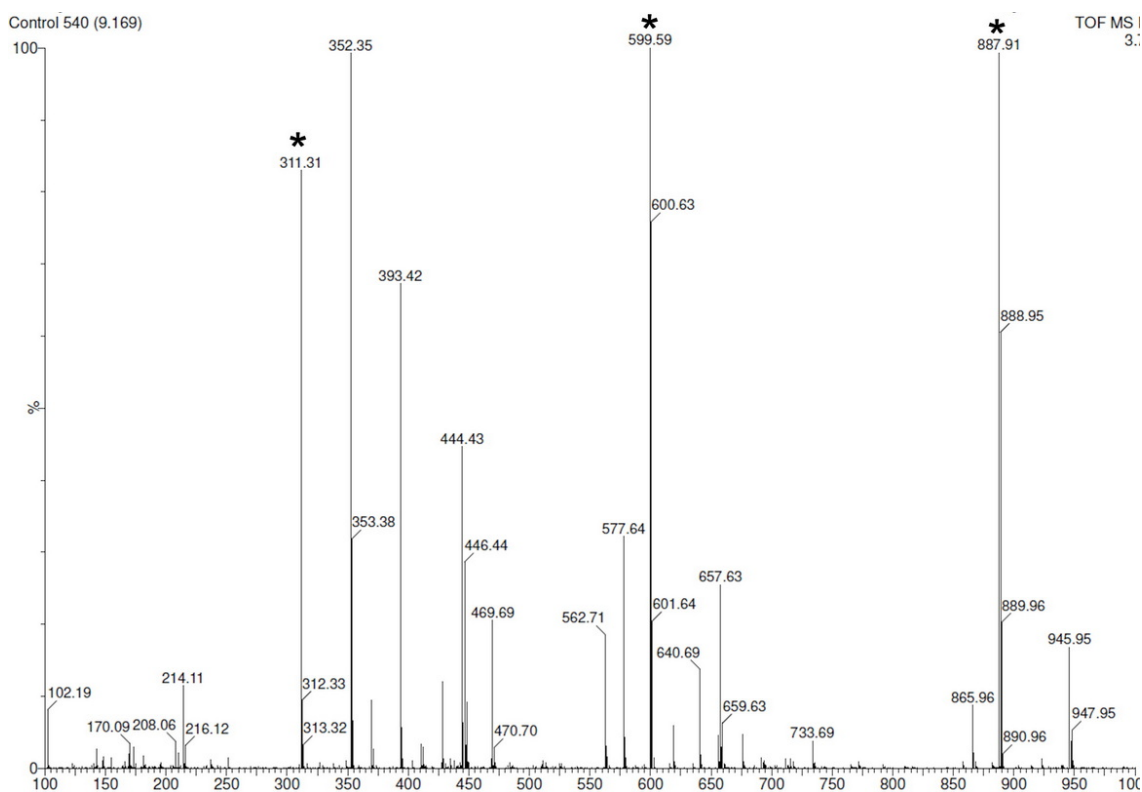


Figure 2.6. ESI MS (+ve mode) of control SDS-5T. *Clusters arising from the surfactant are marked.

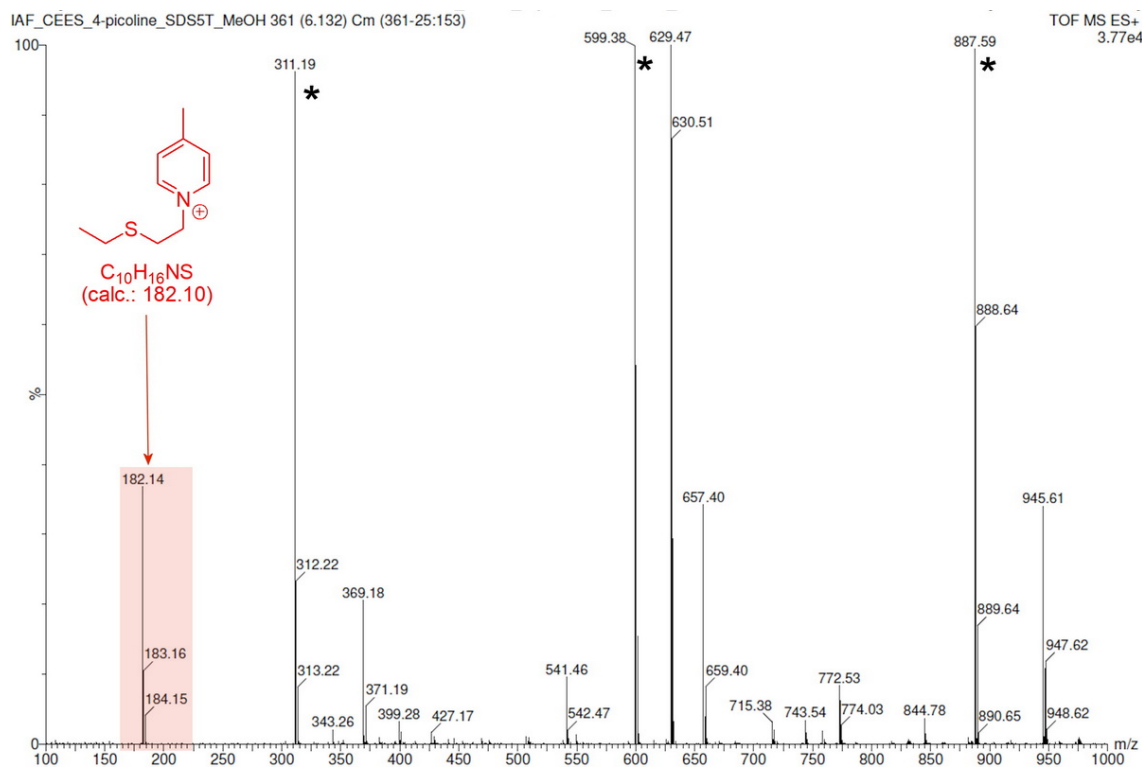


Figure 2.7. ESI MS (+ve mode) of SDS-5T and 4-picoline with CEES. *Clusters arising from the surfactant are marked.

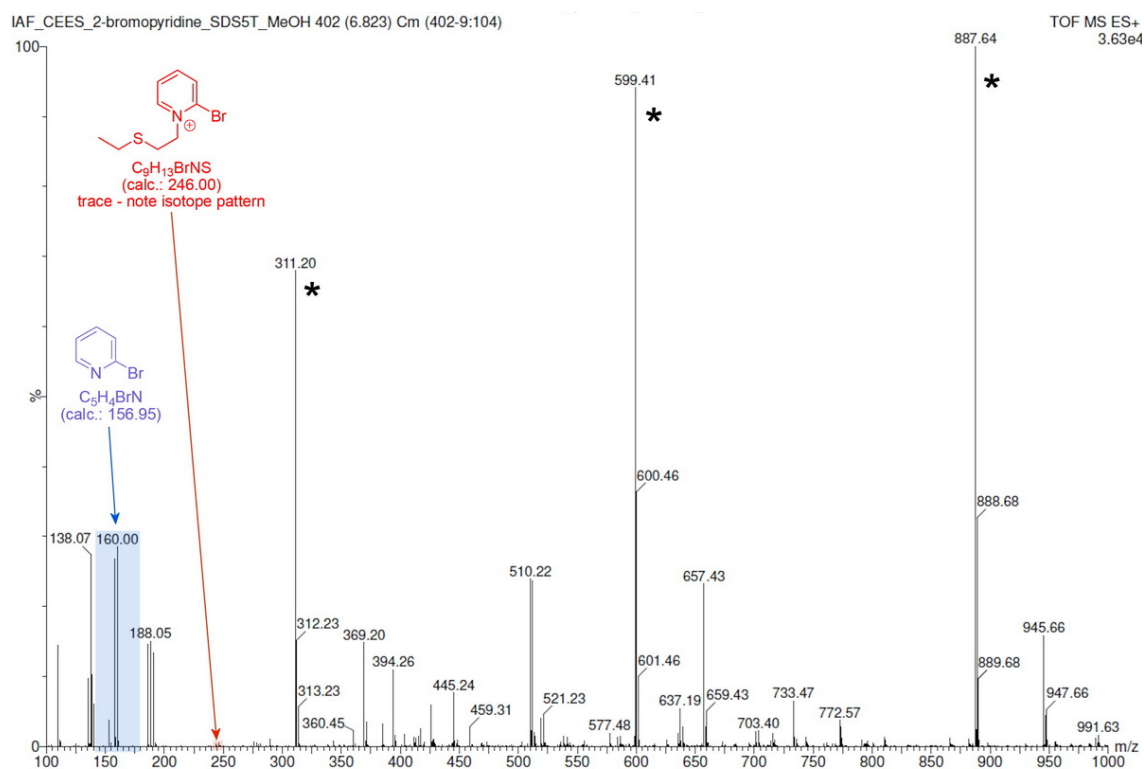


Figure 2.8. ESI MS (+ve mode) of SDS-5T and 2-bromopyridine with CEES. Not the trace amount of product arising from the sterically hindered substrate. *Clusters arising from the surfactant are marked.

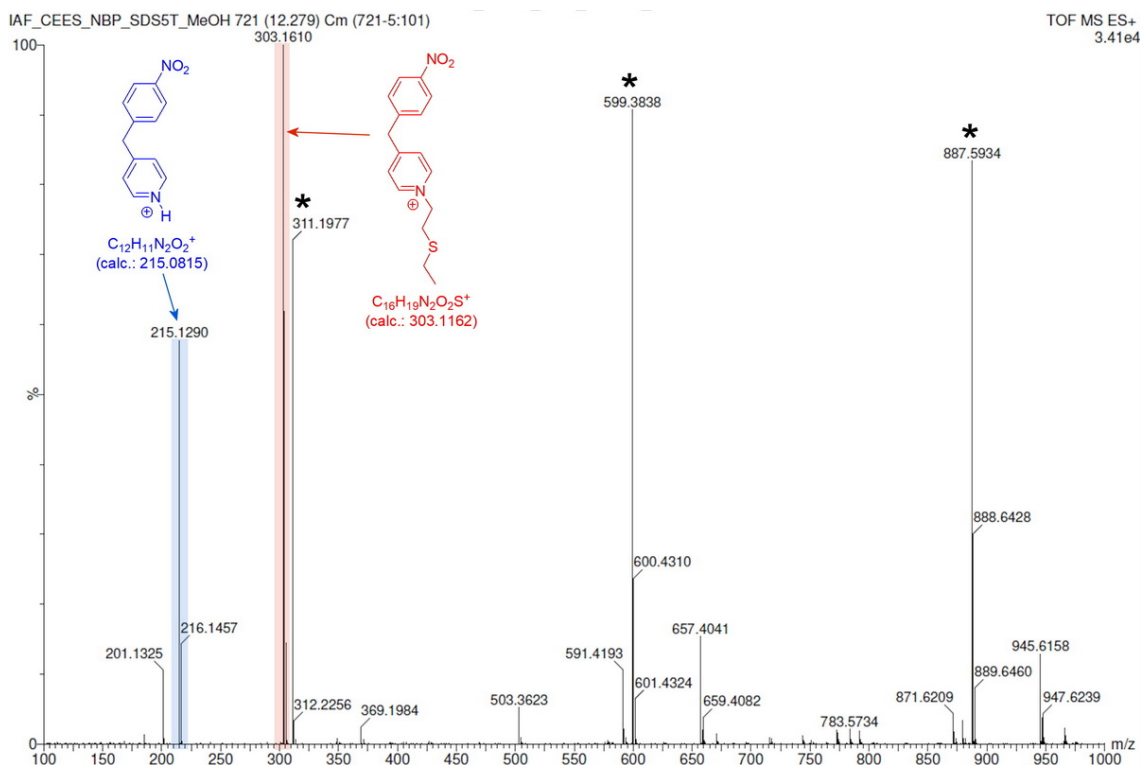
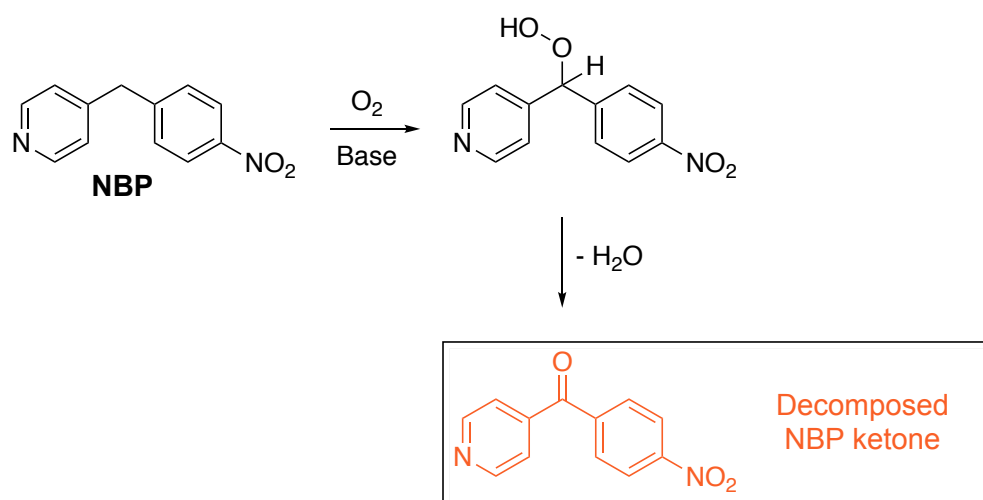


Figure 2.9. ESI MS (+ve mode) of SDS-5T and NBP with CEES. *Clusters arising from the surfactant are marked.

These mass spectra show characteristic peaks for SDS, and its sodium addition clusters. The peaks at m/z 311 correspond to sodium dodecyl sulfate clustered with a sodium cation to create a positively charged adduct. Each subsequent cluster peak denotes an adduct with an additional sodium dodecyl sulfate molecule. Analysis of the mass spectrometry data shows that both NBP and 4-picoline are alkylated by CEES in anionic microemulsion. This is apparent from the peaks at m/z 215.1290 and 182.14, respectively. However, the alkylated product of 2-bromopyridine was not observed at an expected m/z of 260.01 ($C_{10}H_{15}BrNS^+$). The bromine substituent in the 2-position on the pyridine ring has both steric and electronic effects on the alkylation reaction. Bromine in this position creates a sterically hindered environment around the pyridine nitrogen atom, in addition to withdrawing electron density away from the nitrogen atom. These combined effects suppress the nucleophilicity of this weak base. Thus, the data suggests that both unhindered pyridine nucleophiles such as NBP and 4-picoline are selective towards sulfur mustard analytes.

To examine the detection performance of NBP as a reagent for mustard (CEES) detection, the reaction time was first investigated at ambient temperature using anionic, cationic, and non-ionic surfactant mixtures as the reaction media with ethanol solutions as a control system. The formulations outlined in Table 2.2 are varying combinations of

NBP solution in ethanol (0.4 M) with aqueous sodium hydroxide solution (0.4 M) along with the appropriate solvent. This value of sodium hydroxide concentration allowed the adjustment of the pH without inducing side reactions which cause the yellowing of the mixtures. We speculate that this yellowing reaction is the base promoted aerobic oxidation of NBP to the corresponding ketone ((4-nitrophenyl)(pyridine-4-yl)ketone) (Scheme 2.3).



Scheme 2.3. Aerobic oxidation of NBP to the corresponding ketone.

Table 2.3 outlines the volumes used for each component of the formulation. CEES was added as a limiting reagent in each test solution, thus an excess of 2.33 equivalents of NBP was present relative to CEES. All reactions were monitored for a maximum of five minutes and digital photographs were taken immediately after CEES addition and at 1, 3 and 5 minutes of exposure. Data is presented at the 5-minute timepoint to highlight any non-positive (i.e. non blue-purple) responses.

Since the pH of the system is crucial to the operation of NBP as a reagent, the pH values of the surfactant mixtures were recorded before and after the addition of NBP and NaOH and are presented in Table 2.4.

	Volume of stock solution added (μL)	Moles of stock solution added (mol)	Final concentration (M)
NBP (0.4 M)	100	4.0×10^{-5}	2.0×10^{-2}
NaOH (0.4 M)	200	8.0×10^{-5}	4.0×10^{-2}

Table 2.2. Components of NBP formulation.

Component	Vial 1	Vial 2	Vial 3	Vial 4
NBP (0.4 M) / μL	100	100	100	100
NaOH (0.4 M) / μL		200		200
Solvent / μL	1900	1700	1900	1700
CEES / μL			2	2

Table 2.3. Quantities for NBP formulations for CEES sensing in solution.

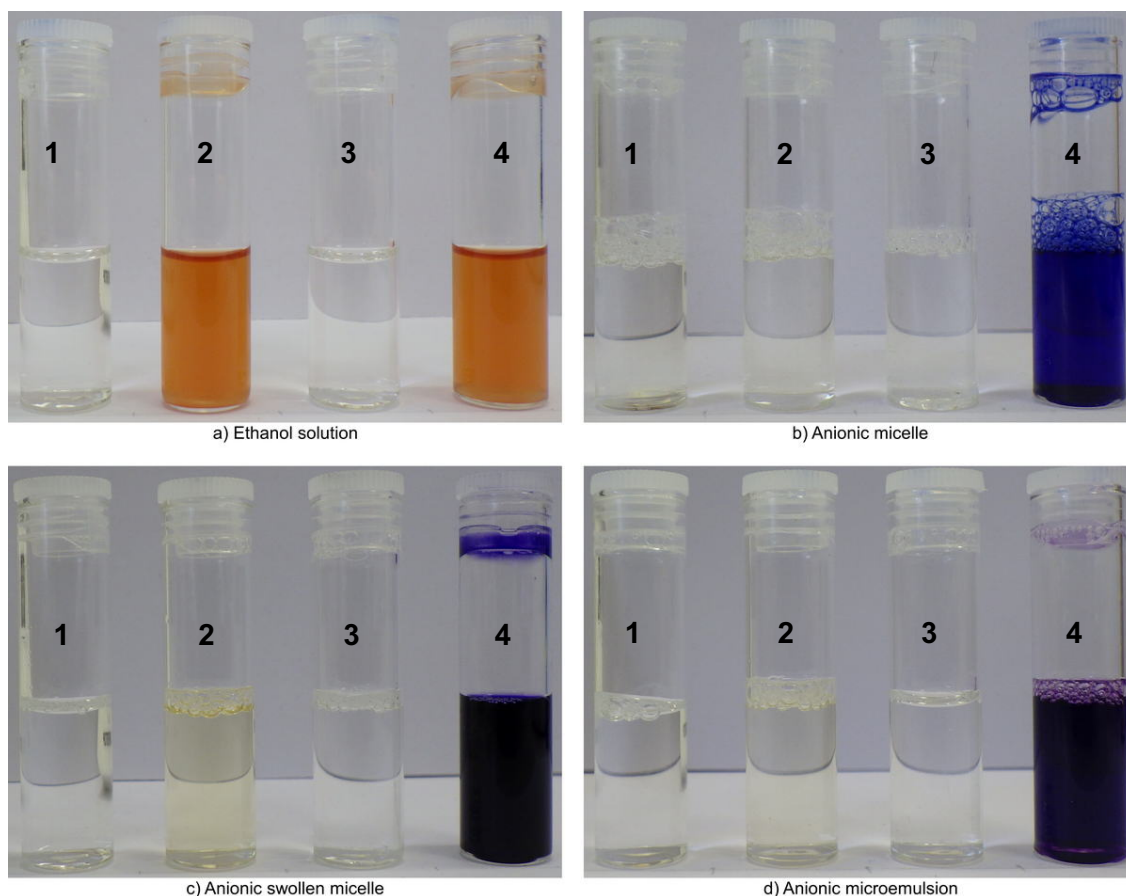
System	pH		
	No reagent	+ NBP (0.4 M)	+ NaOH (0.4 M)
Anionic micelle	5.70	8.25	12.41
Anionic swollen micelle	6.38	7.53	12.42
Anionic microemulsion	5.94	7.34	12.20
Cationic micelle	3.66	5.62	12.53
Cationic swollen micelle	3.74	5.89	12.63
Cationic microemulsion	3.78	5.68	12.65
Non-ionic micelle	3.67	4.96	12.48
Non-ionic swollen micelle	5.89	6.45	12.73

Table 2.4. pH values of surfactant mixtures before and after the addition of reagents.

2.3.2. Performance of Anionic Aggregation Colloid Systems

The response of anionic surface-active systems and an ethanol control is presented in Figure 2.10. It is evident from the images that the reaction medium is an important factor in the operation of the system. The responses are discussed in the following sections. Ethanol was chosen as a control since all the reagents were freely soluble. Using ethanol as the bulk solvent, no reaction took place resulting in no change in the perceived colour (Figure 2.10). Even upon standing for extended periods, this system failed to yield the desired blue-purple positive response. Thus, it is likely that a simple solvent (ethanol) system does not afford the pre-organisation of reagents and analytes (NBP and CEES) at ambient temperature to yield the desired characteristic blue-purple colour of the dye. We tentatively suggest that this implies the rate-limiting step is the attack by NBP on the alkylating agent (CEES). This was verified by the rapid colour response of alkylated NBP reagents to alkaline ethanol solutions. In addition, this system also depicts the instability of NBP in basic conditions due to the production of an orange colour. The production of colour upon exposure to no analyte is unsatisfactory for colorimetric detection as a positive colour change in the presence of an analyte would be less defined and therefore

perceived as ambiguous by the naked eye, especially in operational scenarios of poor ambient lighting.



Component	Vial 1	Vial 2	Vial 3	Vial 4
NBP (0.4 M) / μL	100	100	100	100
NaOH (0.4 M) / μL		200		200
Solvent / μL	1900	1700	1900	1700
CEES / μL			2	2

Figure 2.10. Comparison of the performance of the solution and anionic surfactant mixtures with simulant after 5 mins of exposure. Vials are numbered 1 to 4 from left to right in each image.

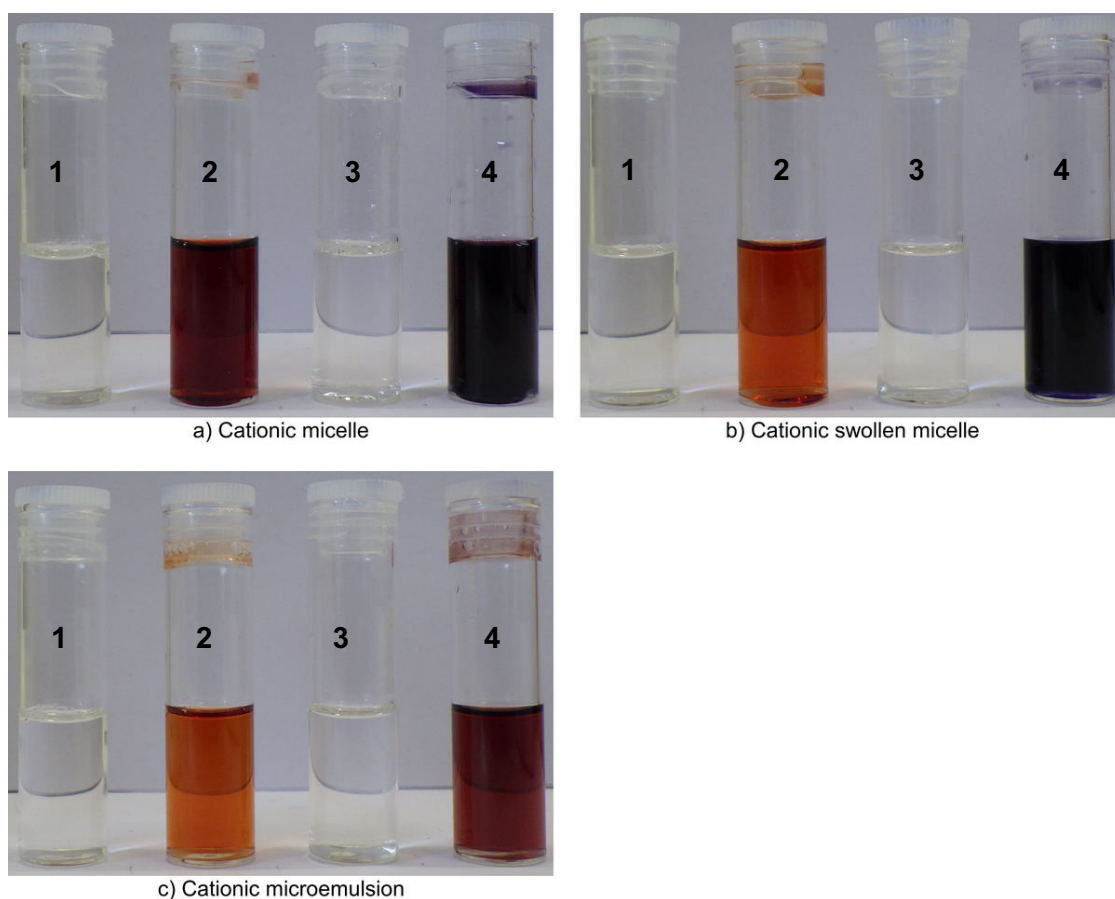
From inspection of Figure 2.10, it is apparent that the introduction of various anionic surfactant components has a significant impact on the reactivity of the system. Firstly, formulation 2 produced a very pale-yellow colour upon exposure to negative in all three SDS mixtures, which was a substantial improvement upon the orange colour seen in the ethanol system. This colour was attributed to small amounts of NBP-ketone that is present in commercial sources of the reagent. This colour is lost if NBP is freshly

recrystallised from butanone/hexane. We postulate that this observation arises from the anionic interface of the micelles/droplets repelling the hydroxide ions from the interfacial region, thus protecting the NBP reagent from decomposition. Secondly, very high reaction rates were observed with the rapid production of intense blue or purple colour within seconds which intensified over 5 minutes upon exposure to CEES. Incorporating SDS in the form of micelles resulted in a colour change from nearly colourless to an intense blue in the presence of CEES. The addition of an *n*-butanol co-surfactant to create a swollen micelle system caused a slight impact on the analyte-free colour with an increase in the depth of yellowing. However, this can be considered negligible compared to that of the ethanol system. The addition of toluene as an oil-phase to generate an SDS-5T microemulsion system also gave rise to a negligible pale-yellow negative response. It is clear to see that there is a change in positive colour production from blue to purple upon the addition of toluene. Since the dye is solvatochromic and produced a red colour when dissolved in toluene, we can argue that a weighted average microenvironment response yields a colour combination of red and blue, resulting in the final purple colour produced in the anionic microemulsion formulation. In these systems, likely, the micelles and droplets are effectively concentrating the reagents and analytes into a small volume (see SANS data above) with a corresponding increase in the reaction rates. The enhanced production of episulfonium species in these systems also provides further reaction rate benefits, while the surface activity of the alkylated NBP species will expose the dye precursor to the alkaline aqueous continuous phase, hence developing the colour response.

2.3.3. Performance of Cationic Aggregation Colloid Systems

The behaviour of NBP was further studied by varying the nature of the microemulsion medium. The response of cationic formulations after treatment with CEES is presented in Figure 2.11, and it is apparent that the system was negatively impacted by utilising a cationic surfactant. Upon formulation with no analyte present, all systems produced a red colour similar, but more intense, to that observed in the ethanol system. Again, this is of course an undesirable response, as it would reduce the fidelity of the colour response observed with a true positive. It was hypothesised that the net positive charge of the cationic droplets should suppress episulfonium cation formation resulting in poor reactivity. Interestingly, both the cationic micelle and swollen micelle formulations exhibited good activity towards CEES exposure resulting in a significant colour change. However, this change was more difficult to observe in the micelle formulation due to the inherent intense red colour of the blank solution. This may suggest that the positively

charged interface suppresses the formation of episulfonium cation in the interfacial region and thus remains localised in the droplet core where it is vulnerable to nucleophilic attack by NBP. However, the cationic interface will also undergo facile bromide-hydroxide exchange, thus concentrating hydroxide in the vicinity of the NBP. It is feasible to assume that this is the origin of the 'enhanced' red colour observed in the analyte free control sample. Interestingly, the cationic microemulsion exhibited the worst performance of the cationic systems with only a slight deepening of the red colour observed upon the addition of CEES. This may be indicative of the more dilute microenvironment in the droplet core, reducing the rate of the second-order (bimolecular) NBP-CEES interaction.

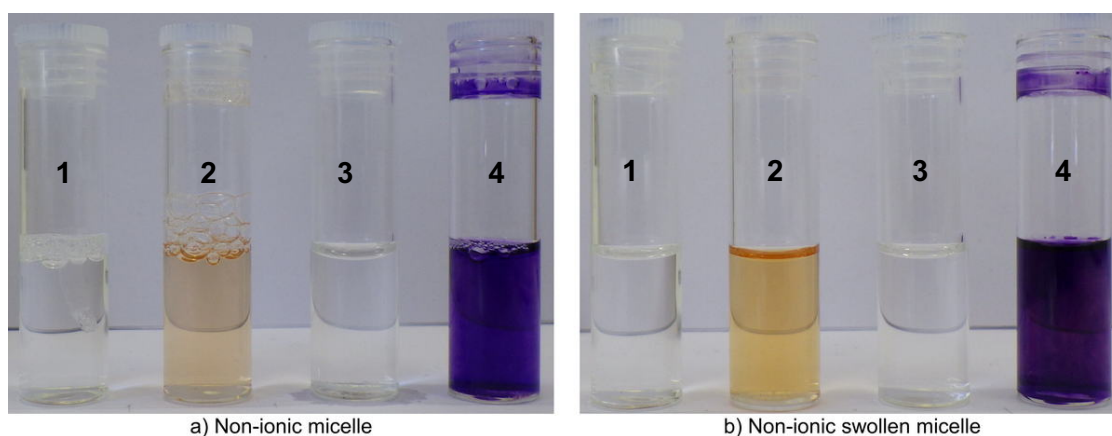


Component	Vial 1	Vial 2	Vial 3	Vial 4
NBP (0.4 M) / μL	100	100	100	100
NaOH (0.4 M) / μL		200		200
Solvent / μL	1900	1700	1900	1700
CEES / μL			2	2

Figure 2.11. Comparison of the performance of cationic surfactant mixtures with simulant after 5 mins of exposure. Vials are numbered 1 to 4 from left to right in each image.

2.3.4. Performance of Non-ionic Aggregation Colloid Systems

Once more, it is visible from the images of non-ionic surfactant mixtures that these formulations were unstable and formed a pale orange colour upon exposure to base (Figure 2.12). Although this colour is less intense compared to that of the cationic surfactant formulations, it is unfavourable and reduces the impact of the perceived colour change. Despite this, they both exhibited moderate performances to generate clear colour changes, but the final purple colour was less intense compared to the anionic formulations. This suggests that the equilibrium between CEES and episulfonium formation is less favourable in non-ionic systems compared to anionic systems. Here, the images presented are for non-ionic micelle and swollen micelle formulations as the microemulsion was unstable with 5 wt% toluene and formed a cloudy suspension. Thus, no formulations were prepared with non-ionic microemulsions for treatment with CEES. The stability of non-ionic surfactants is a common problem with these amphoteric compounds exhibiting a unique property called the “cloud point” which results in phase separation.



Component	1	2	3	4
NBP (0.4 M) / μL	100	100	100	100
NaOH (0.4 M) / μL		200		200
Solvent / μL	1900	1700	1900	1700
CEES / μL			2	2

Figure 2.12. Comparison of the performance of non-ionic surfactant mixtures with simulant after 5 mins of exposure. Vials are numbered 1 to 4 from left to right in each image.

It is apparent from the images in Figure 2.13 that all systems experienced a colour change upon simulant exposure but only the anionic and non-ionic formulations

displayed a strong purple colour response. However, it is clear that the anionic formulations have a markedly high performance for CEES determination, not only in terms of colour contrast but also in the speed of response. Furthermore, we also observed that only anionic surfactant mixtures were able to protect the NBP reagent from base-catalysed degradation as essentially no production of colour was observed in the basic analyte free system. Although the colour of the blank formulation was pale and near colourless in the anionic surfactant systems, the NBP used in all formulations was slightly yellow. However, the desire to use all commercial-off-the-shelf reagents as much as possible has meant that the NBP was not recrystallised before use. The purification of NBP via recrystallisation in butanone/hexane gives a white crystalline solid, which generated colourless formulations in anionic surfactant mixtures.

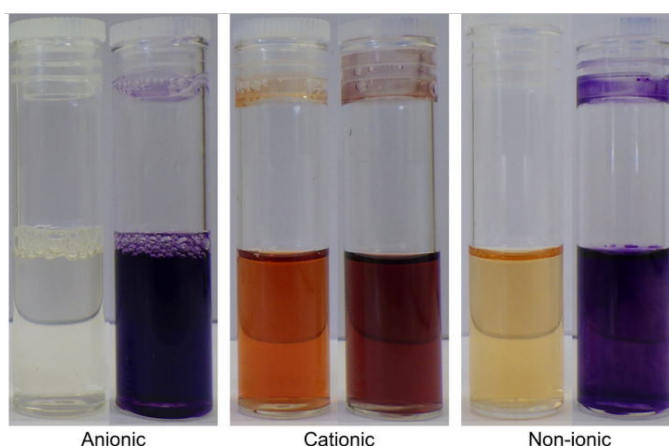


Figure 2.13. Comparison of the performance of anionic and cationic microemulsion and non-ionic swollen micelle mixtures with simulant. Vials are from left to right in each image: Blank; CEES. Note that these experiments were performed with commercially sourced NBP and used as received.

2.3.5. Determination of Molar Extinction Coefficient of NBP-CEES Dye

Due to the variation in molar extinction coefficient values reported for alkylated NBP in the literature^{61,62}, this parameter was investigated using an aprotic solvent due to the pH sensitivity of the dye. The molar extinction coefficient of the alkylated adduct was investigated by UV-vis spectroscopy at ambient temperature at a wavelength range of 200-800 nm (Figure 2.14). Solutions of the dye in acetonitrile previously dried over potassium carbonate were measured in triplicate to generate a plot of average molar absorptivity against wavelength (Figure 2.15). Potassium carbonate was also added to each sample to maintain a high pH throughout the UV-vis measurement.

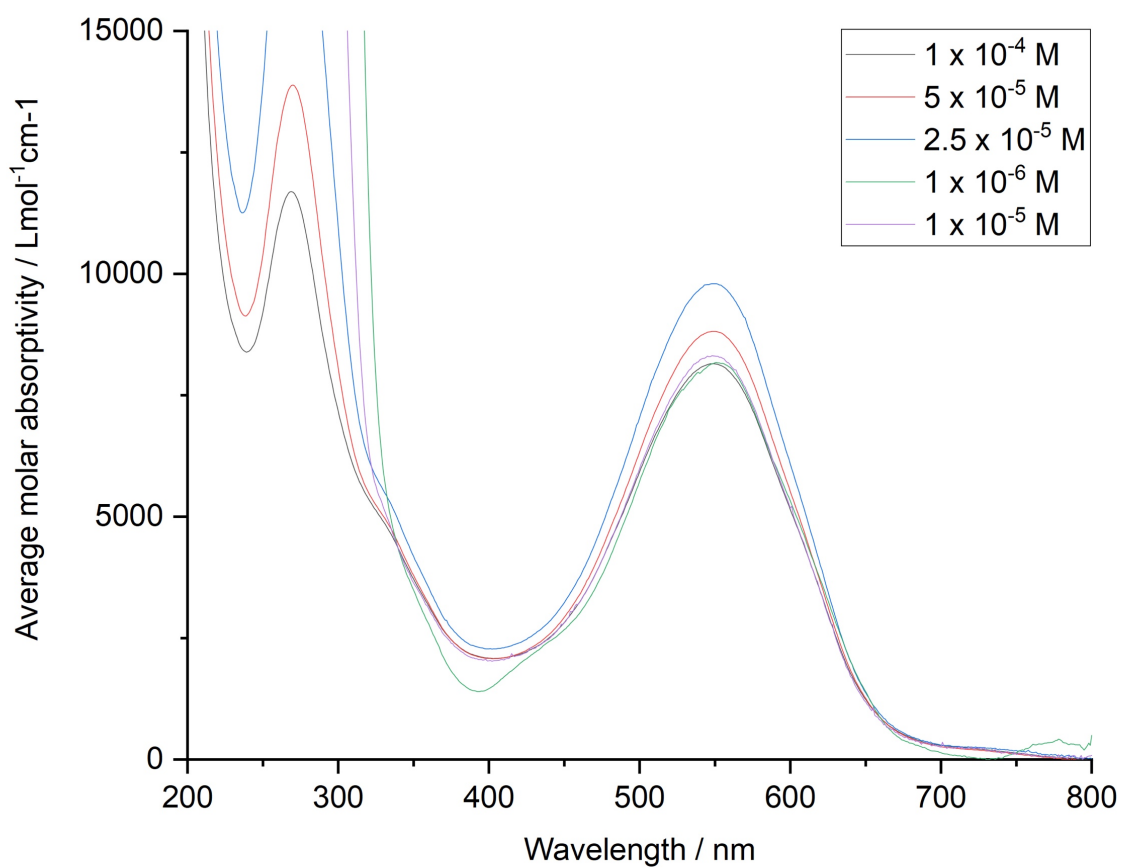
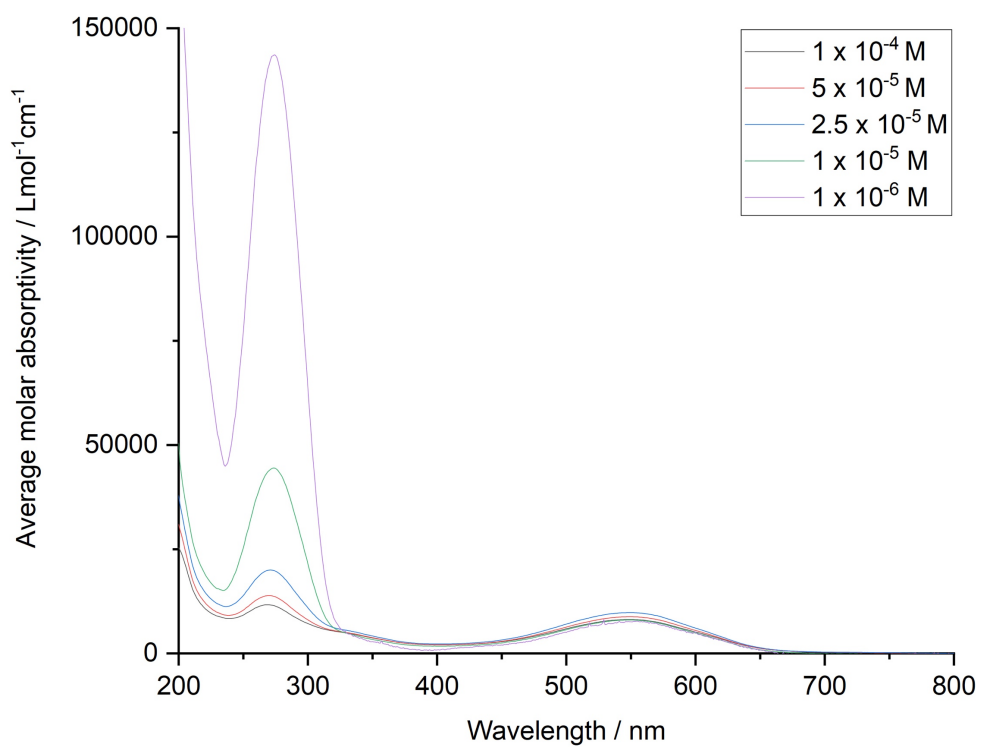


Figure 2.14. UV-vis spectra of NBP-CEES adduct at various concentrations in acetonitrile.

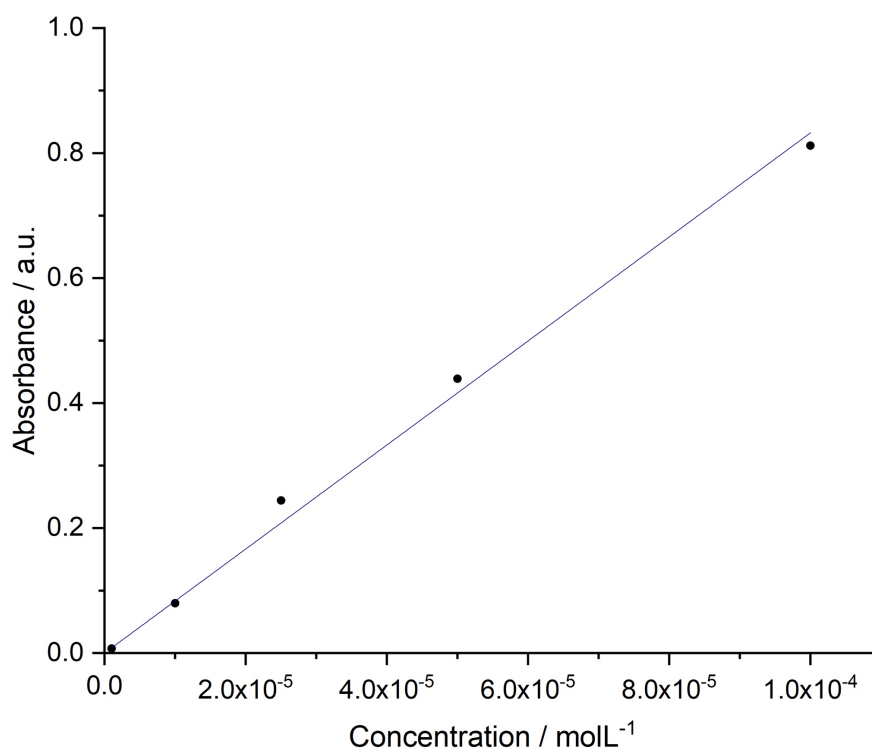


Figure 2.15. Average maximum absorbance versus concentration plot of each solution.

From this triplicate data set, a maximum wavelength of 551 nm was identified and absorbance values at this wavelength were plotted against dye concentration to obtain a linear equation with an R^2 value of 0.99753 (Figure 2.15). The gradient of this line corresponds to the average molar extinction coefficient multiplied by the path length thus allowing an extinction coefficient value of $8350 \text{ L mol}^{-1} \text{ cm}^{-1}$ to be calculated.

2.3.6. Quantitative Absorbance Spectra of NBP Surfactant Formulations

The electronic spectra of the anionic, cationic and non-ionic surfactant formulations before and after simulant exposure are presented in Figures 2.16, 2.17 and 2.18, respectively. All solutions were measured after 5 minutes of exposure to either negative or simulant. Each solution was analysed in the appropriate surfactant mixture containing NaOH ($4 \times 10^{-2} \text{ M}$) to maintain a high pH, at a concentration of $7.5 \times 10^{-5} \text{ M}$.

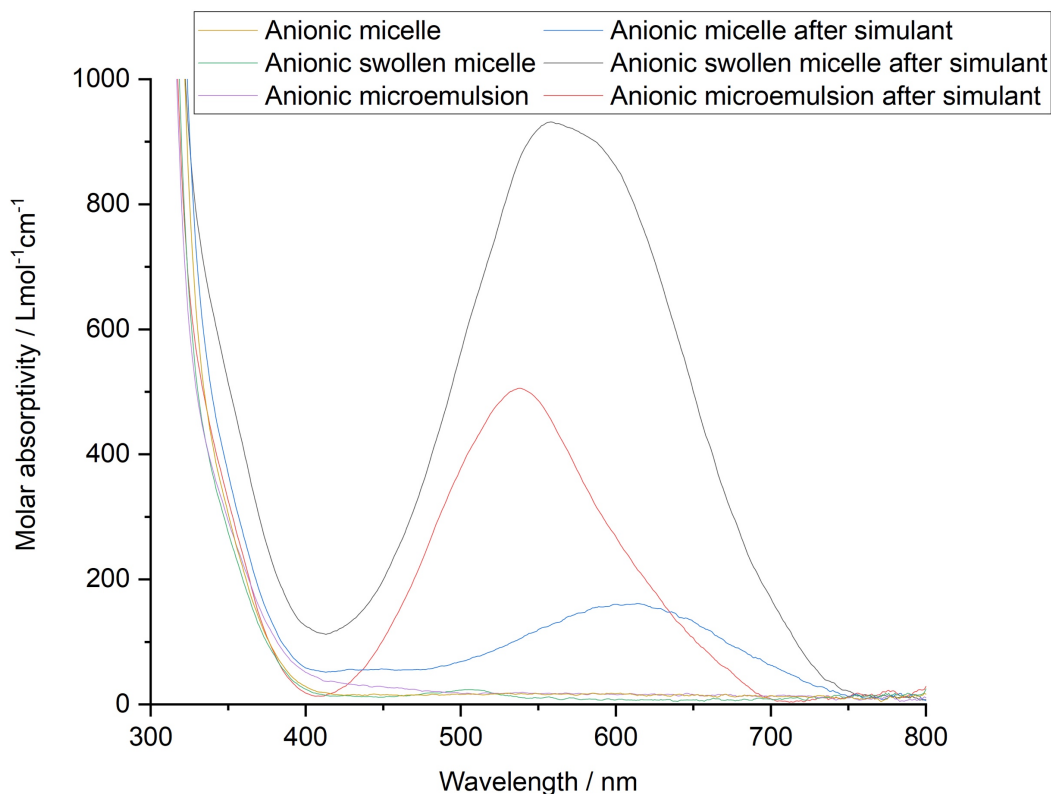


Figure 2.16. UV-vis spectra of anionic surfactant formulations before and after exposure to simulant. Solutions were diluted to 7.5×10^{-5} M in anionic surfactant mixtures containing NaOH (4×10^{-2} M) and measured after 5 mins.

It is apparent from the electronic spectra of anionic surfactant formulations in Figure 2.16 that all blank solutions were essentially non-absorbing over the typical human eye visible region (380-750 nm). The response of the system to CEES yielded spectra with a broad peak with shoulders centred in the 540-640 nm region. In the context of this project, this is a very useful response since the maximum human visual acuity is centred at ~ 555 nm. Upon comparison, it is clear to see that the anionic micelle formulation gave the poorest performance in terms of colour intensity with a molar absorptivity of $163 \text{ L mol}^{-1} \text{ cm}^{-1}$ at an absorbance of 615 nm. The addition of n-butanol as a co-surfactant to generate the anionic swollen micelle formulation caused the peak to shift hypsochromically from 615 to 557 nm. This system exhibited the best performance of all the anionic formulations generating the highest molar absorptivity of $934 \text{ L mol}^{-1} \text{ cm}^{-1}$. The incorporation of 5 wt% toluene to create the anionic microemulsion formulation also resulted in a hypsochromic shift. However, the change in wavelength was smaller with a shift from 557 to 539 nm. The molar absorptivity for the microemulsion formulation lay in the middle with a value of $509 \text{ L mol}^{-1} \text{ cm}^{-1}$.

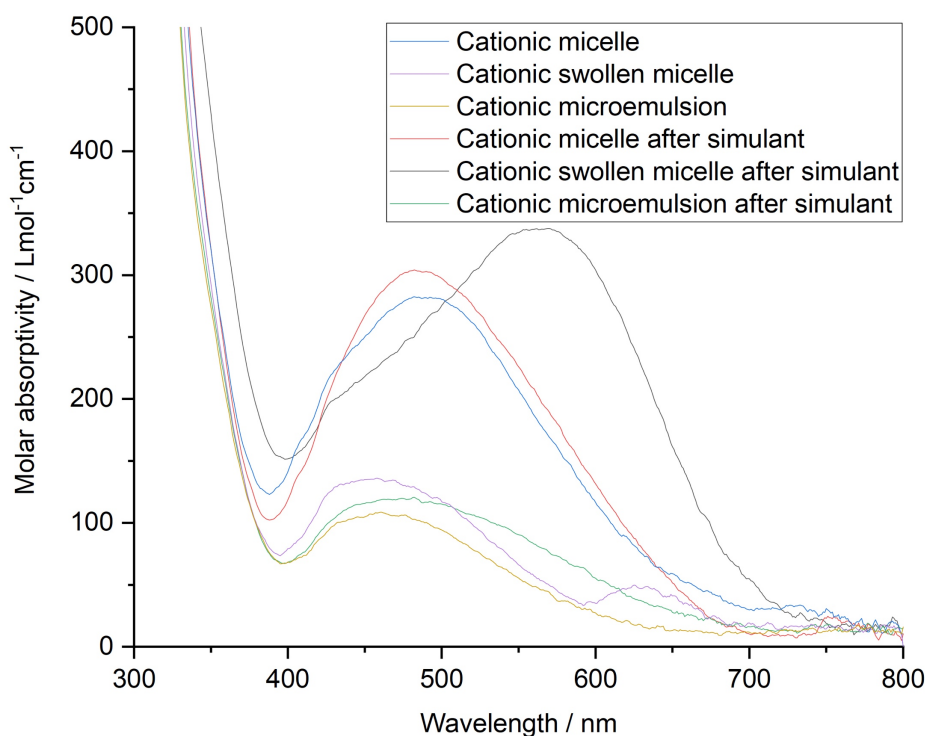


Figure 2.17. UV-vis spectra of cationic surfactant formulations before and after exposure to simulant. Solutions were diluted to 7.5×10^{-5} M in cationic surfactant mixtures containing NaOH (4×10^{-2} M) and measured after 5 mins.

The electronic spectra of the performance of cationic surfactant formulations before the addition of simulant (Figure 2.17) display the production of the colour seen in the testing images for all systems as a result of the decomposition of NBP. The cationic micelle generated the greatest colour production upon exposure to the added base, to such an extent that it had a comparable molar absorptivity to some solutions exposed to simulant. The performance of the cationic surfactant formulations upon exposure to CEES followed a slightly different trend from the anionic formulations. Here, the cationic micelle formulation exhibited an intermediate performance with a molar absorptivity of $304 \text{ L mol}^{-1} \text{ cm}^{-1}$ at 492 nm. The addition of *n*-butanol to create the cationic swollen micelle formulation resulted in an absorbance peak at 571 nm. Similar to the anionic formulations, this system continued to give the best performance with a molar absorptivity of $339 \text{ L mol}^{-1} \text{ cm}^{-1}$. The addition of toluene to generate the cationic microemulsion system greatly reduced the intensity of the response of the formulation with a large decrease in molar absorptivity generating a value of $123 \text{ L mol}^{-1} \text{ cm}^{-1}$ at 483 nm.

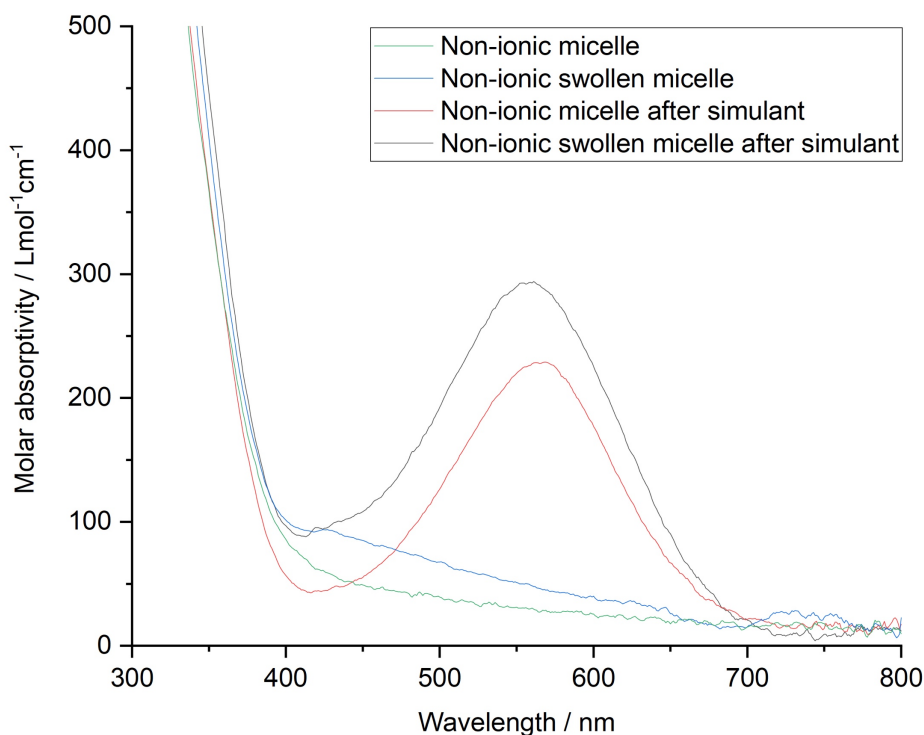


Figure 2.18. UV-vis spectra of non-ionic surfactant formulations before and after exposure to simulant. Solutions were diluted to 7.5×10^{-5} M in non-ionic surfactant mixtures containing NaOH (4×10^{-2} M) and measured after 5 mins.

The electronic spectra of non-ionic surfactant formulations in Figure 2.18 support the evidence of limited NBP degradation in non-ionic micelle and swollen micelle systems with the absence of absorbance peaks in the visible region after 5 minutes of exposure to negative. There was little difference in the colour intensity produced in both formulations upon exposure to CEES. However, the non-ionic micelle formulation had an absorbance peak at 569 nm and lower molar absorptivity of $230 \text{ L mol}^{-1} \text{ cm}^{-1}$ compared to the swollen micelle system with a molar absorptivity of $296 \text{ L mol}^{-1} \text{ cm}^{-1}$. Incorporation of co-surfactant caused a slight hypsochromic shift of the absorbance peak from 569 to 559 nm.

From the electronic spectra of the above systems, the conversion of NBP to the NBP-CEES dye responsible for the colour production was calculated for each surfactant system. These values are presented in Table 2.5.

System	Conversion (%) at 5 mins	Comment / Interpretation
Anionic micelle	4.5	CEES is poorly soluble in the micellar system. Contact area is low between analyte and reagents.
Anionic swollen micelle	26.0	CEES rapidly dispersed and fully solubilised.
Anionic microemulsion	14.2	CEES and toluene are 'competing' for solubilisation.
Cationic micelle	8.5	CEES is moderately well solubilised. Intermediate reaction rate.
Cationic swollen micelle	9.4	
Cationic microemulsion	3.4	CEES is very well solubilised in microemulsion core, low propensity to episulfonium formation.
Non-ionic micelle	6.4	CEES is moderately well solubilised. Episulfonium formation is a less favourable equilibrium.
Non-ionic swollen micelle	8.2	

Table 2.5. Calculated conversion (%) values of NBP to NBP-CEES dye in surfactant formulations at 5 mins.

The calculated conversions clearly show the superior performance exhibited by the anionic swollen micelle formulation with a 26.0 % conversion of NBP to the dye. The anionic microemulsion generated just under half the amount of dye with a 14.2 % conversion. The anionic micelle exhibited the poorest performance of the anionic systems with a 4.5 % conversion. This is not unexpected since the intensity of colour produced in the micelle system was noticeably weaker than that of the swollen micelle and microemulsion formulations. On the other hand, the cationic and non-ionic systems had similar conversion values with all formulations exhibiting less than 10 % conversion of NBP to the coloured dye. However, there is a notable increase in conversion when *n*-butanol co-surfactant was introduced to the micelle formulations. This trend was seen in all surfactant systems. Upon comparison of the anionic and cationic systems, there was a considerable reduction in conversion upon the addition of toluene to the swollen micelle formulation.

2.3.7. Determination of NBP decomposition product

The decomposition of NBP was investigated by UV-vis spectroscopy and mass spectrometry in each of the surfactant mixtures. The electronic spectra of all the surfactant formulations before exposure to simulant are combined in Figure 2.19 for ease of comparison. It is clear to see from the UV-vis spectra that cationic surfactant formulations produced the most colour upon exposure to negative compared to anionic and non-ionic formulations. This suggests that NBP undergoes the most decomposition

in cationic surfactant which is evident in previously presented formulation images in Figure 2.11. Thus, only the anionic surfactant systems were effective at protecting NBP from degradation as the anionic interfacial region shields the droplet-solubilised NBP from the high hydroxide levels present in the aqueous continuous phase.

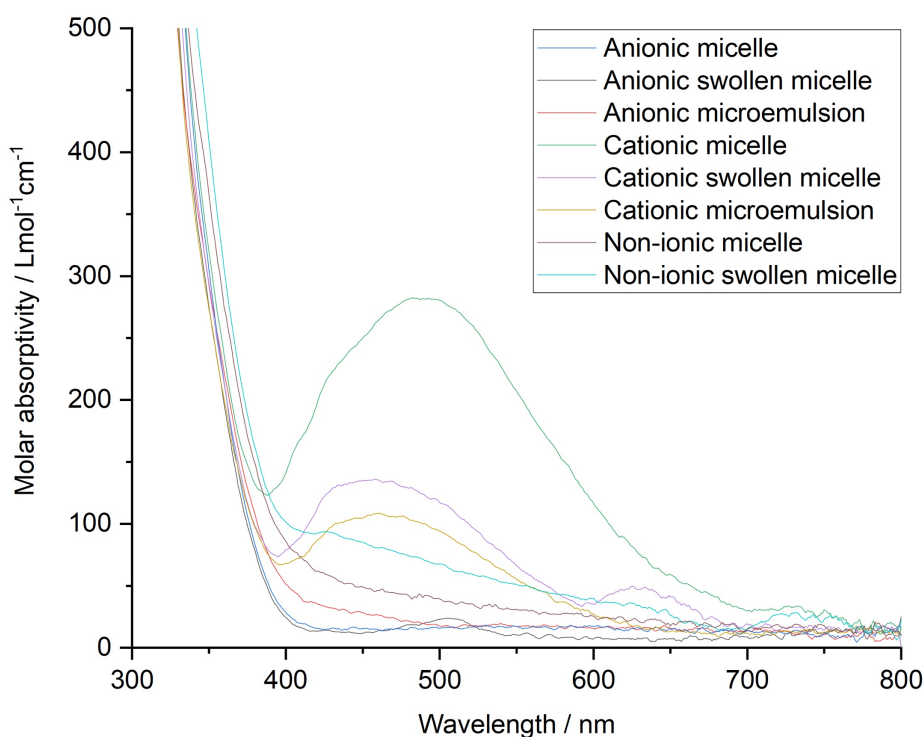


Figure 2.19. UV-vis spectra of anionic, cationic and non-ionic surfactant formulations after 5 mins exposure to base.

Mass spectrometry was utilised to investigate the identity of the NBP decomposition product responsible for creating the peach to orange colour in the blank formulations. The cationic swollen micelle formulation was chosen for analysis by ESI mass spectrometry as this solution generated the most intense orange colour of all the surfactant formulations upon exposure to no analyte.

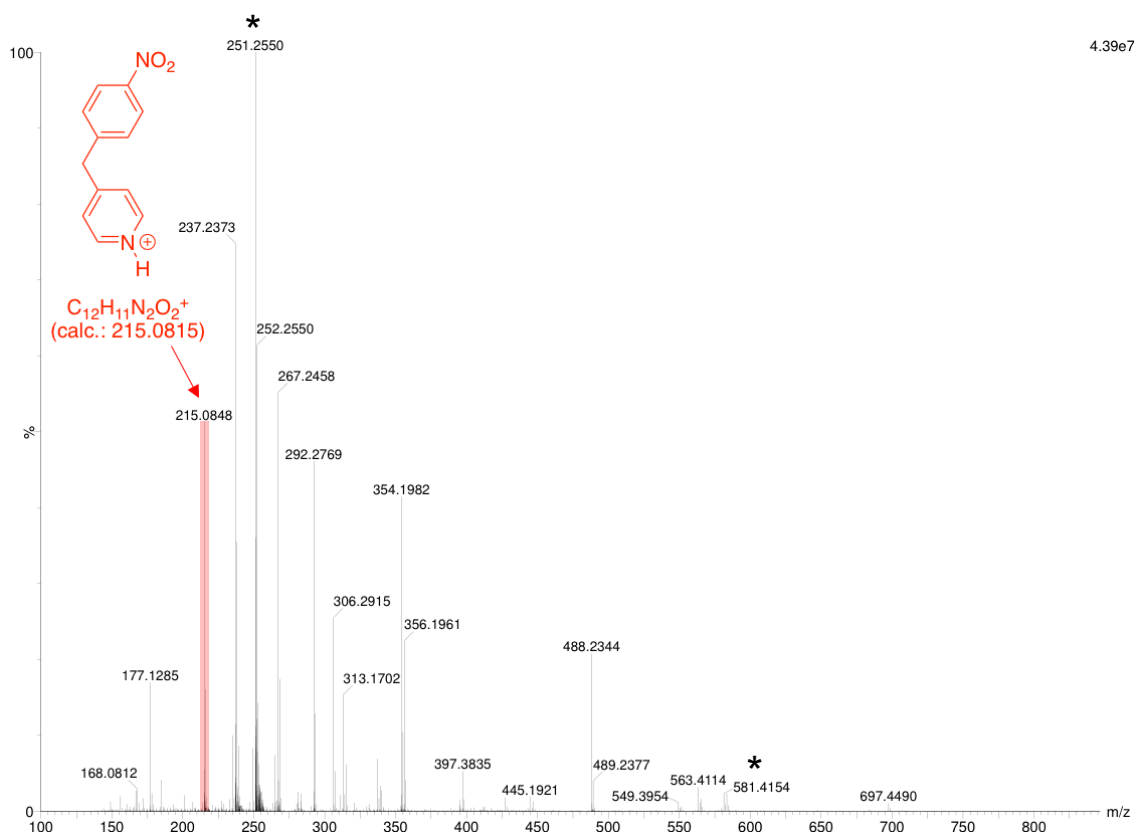


Figure 2.20. Mass spectrum of NBP and NaOH in cationic micelle formulation.

The mass spectrometry data of the cationic micelle formulation in Figure 2.20 shows no peak for the expected ketone at m/z 229.0608. However, the presence of this ketone has been found in previous unpublished work by the IAF group. The proposed decomposition reaction of NBP in surfactant systems has been previously outlined in Scheme 2.3. Firstly, NBP undergoes base-catalysed oxidation at the benzylic methylene group resulting in the addition of a hydroperoxide functional group (ROOH). Subsequently, a ketone is produced upon the loss of water. Unlike NBP, this ketone is unable to undergo the required deprotonation step to produce the intensely coloured dye. Hence, the NBP ketone is not a sensor for CEES determination and its production in a formulation reduces the amount of NBP present for alkylation by CEES. As a result, the reactivity of the formulation is reduced causing a decrease in the production of colour. This effect is greatly seen in the cationic surfactant systems where the colour change upon CEES addition is perceived as ambiguous to the naked eye. The peak at m/z 488.2344 is postulated to be an adduct of NBP and the cationic surfactant in its sodium salt form whereby the imidazolium undergoes a carbene C-H insertion of the methylene group of NBP.

2.3.8. Development of Anionic Aggregation Colloid Systems

On account of the instability of cationic and non-ionic formulations with the generation of noticeable colour before CEES addition, it was concluded that these systems do not meet the design criteria and thus were not pursued further as mustard detection systems. Instead, the SDS anionic formulations were identified as the best performing systems and were further studied to understand the behaviour of the surfactants and the location of the components within the microemulsion structure. The images of the ethanol solution and anionic surfactant mixtures after 5 minutes of CEES exposure have been combined for ease of performance comparison and are presented in Table 2.6.





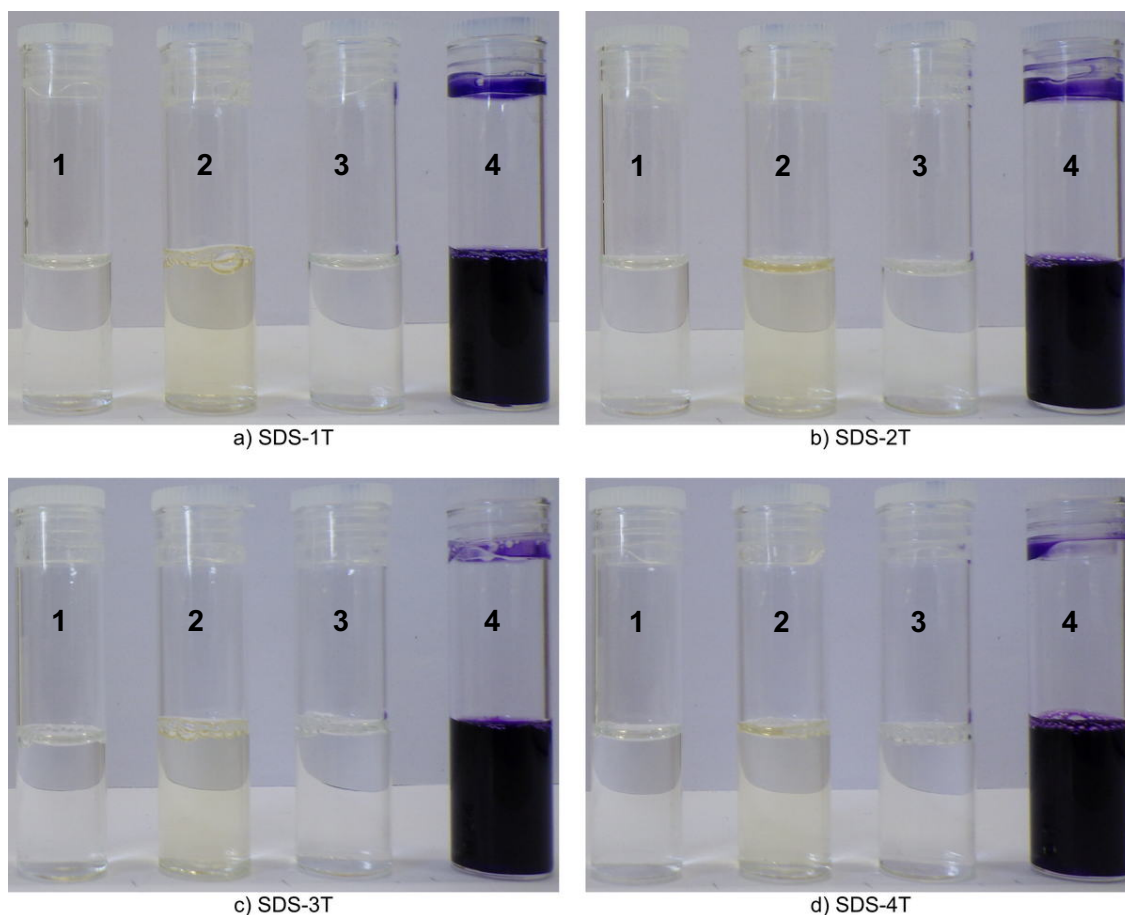
System	Solution	Anionic micelle	Anionic swollen micelle	Anionic microemulsion
CEES response	×	✓	✓✓✓	✓✓✓
Image				

Table 2.6. Comparison of the performance of the solution and anionic surfactant mixtures after 5 minutes of exposure to CEES.

The toluene content of anionic SDS microemulsions was varied to investigate the mustard detection performance of the microemulsion. Four microemulsions were prepared with 1, 2, 3 and 4 wt% toluene and denoted SDS-1T, SDS-2T, SDS-3T and SDS-4T, respectively. Images of these microemulsion formulations after 5 minutes of exposure to CEES are presented in Figure 2.21. Microemulsions prepared with higher toluene concentrations were not further investigated due to their temperature sensitivity. Upon cooling, these microemulsion experienced phase separation and thus cannot be deployed in real-life scenarios due to their poor temperature stability.



Component	Vial 1	Vial 2	Vial 3	Vial 4
NBP (0.4 M) / μL	100	100	100	100
NaOH (0.4 M) / μL		200		200
Anionic microemulsion / μL	1900	1700	1900	1700
CEES / μL			2	2

Figure 2.21. Comparison of the performance of anionic microemulsions with varying amounts of toluene (wt%) as oil-phase. Vials are numbered 1 to 4 from left to right in each image.

It is interesting to observe that the toluene content did not have an appreciable effect on the colour intensity detectable by the naked eye. However, it was observed that microemulsions with a toluene content of less than 4 wt% were unable to sufficiently solubilise CEES with noticeable droplets of the simulant sitting at the bottom of the vial even after the 5-minute monitoring period. Progressing forward, anionic microemulsion (SDS-5T) was chosen over the anionic swollen micelle formulation based on its rapid and intense response and superior solubilisation of simulant. Although the swollen micelles exhibited higher conversions than the micelles and microemulsion, the swollen

micelle systems tend to phase separate with large amounts of mustards. On the other hand, microemulsions are adept at dissolving hydrophobic materials. Additionally, previous studies have fully characterised this type of SDS, H₂O, *n*-butanol, toluene anionic microemulsion.⁵⁸

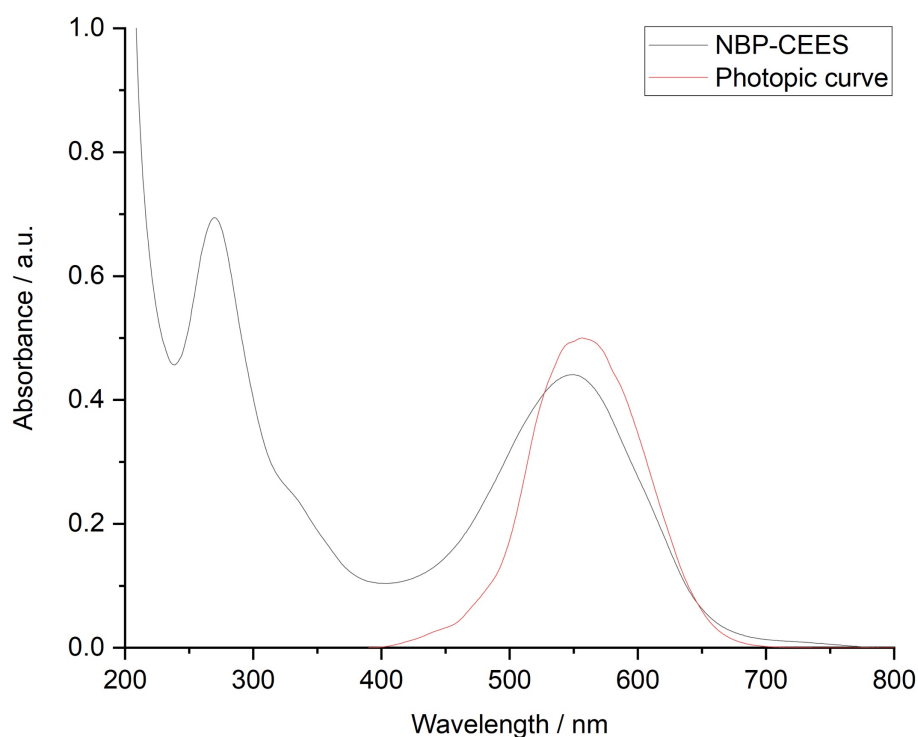


Figure 2.22. UV-vis spectra of NBP-CEES dye at 5×10^{-5} M in acetonitrile with the photopic curve overlaid.

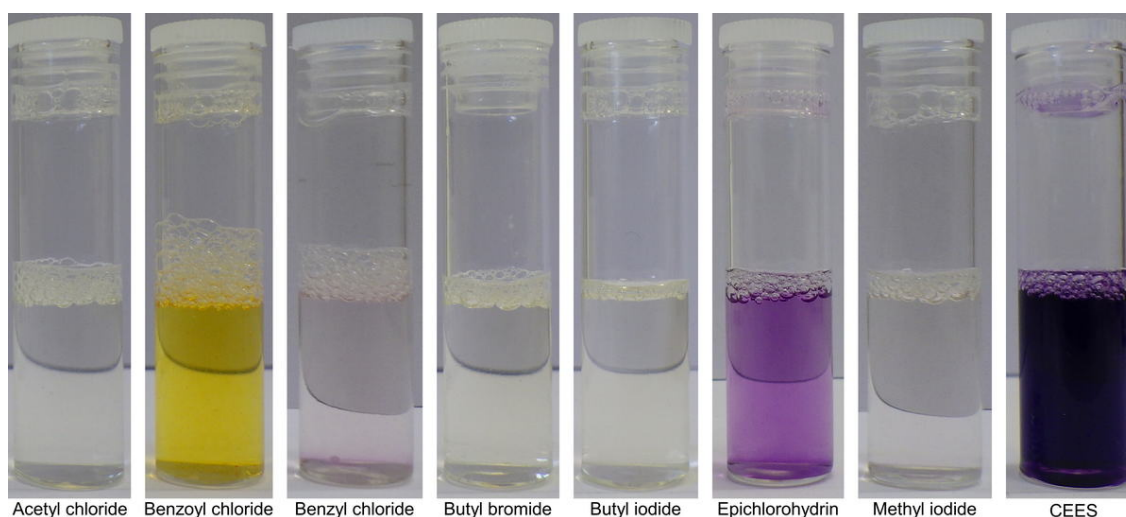
Figure 2.22 displays the UV-vis response of NBP-CEES dye in acetonitrile at a concentration of 5×10^{-5} M. In addition, the photopic curve is recorded. The photopic curve, more formally known as the luminous efficiency function, is a theoretical construct derived from empirical data that is effectively a plot of human eye sensitivity against wavelength under ambient lighting conditions.⁶³ This function has a maximum at 555 nm and corresponds to the green region of the visible spectrum. Notably, there is a strong similarity between these two curves, which is indicative of why NBP is such a good colorimetric sensor despite a rather modest extinction coefficient of the dye.

2.3.9. Selectivity studies

One of the common complications in the development of new sensor systems is the interference of common everyday chemicals (e.g. bleach). More important for this study, is the ability to distinguish other analytes such as reactive electrophiles and various chemical nerve agents, since in real-world scenarios the decontamination protocols and medical remediation for these species differ from that of blister agents. Sensors with high selectivity are crucial in designing a reliable detection system that does not experience meaningful false-positive responses. Thus, a colorimetric study was performed with electrophiles, mustard simulants, nerve agent simulants and several known false positives of commercially available colorimetric chemical detection papers which were previously used by the US military. When the paper encounters a CWA, the colour observed will change according to the type of agents present. For example, H-agents produce a red colour, G-agents produce a yellow colour and V-agents produce a green colour. These chemical papers have now been discontinued as the impregnated dyes used were found to be carcinogenic. Furthermore, these papers suffered from many false positives caused by various common chemicals usually found in civilian and military environments such as diesel, brake fluid, blood, dish detergent and a wide range of common solvents. Thus, it was determined appropriate to study the selectivity of NBP by also exposing the formulation to the colorimetric paper false positives. The images of the formulation after exposure to various false positives are presented in Figures 2.23, 2.24 and 2.26. The performance of the formulation was examined by the addition of 2 μL of an analyte, which was allowed to react at ambient temperature for 5 minutes.

It is evident from these images that benzoyl chloride, benzyl chloride and epichlorohydrin are the three electrophiles to induce a colour change. Benzoyl chloride produced a bright yellow colour after exposure. However, as this response is not the distinctive purple colour associated with the dye, this colour can be confidently accepted, and benzoyl chloride can be considered a nuisance positive. For our purposes, a nuisance positive is a positive that does not specifically identify the target analyte but gives a positive response that may in some scenarios be useful. Since benzyl chloride is hardly benign, and not commonly encountered in operational scenarios, we do not regard this response as significantly deleterious to overall performance. Benzyl chloride also produced a response with the production of a very pale purple colour after 5 minutes of exposure. However, it can be seen in the image that the analyte sits at the bottom of the vial in the form of droplets. Furthermore, the poor reactivity with benzyl chloride and the slow production of colour further accentuates its low impact as a nuisance positive for this system. From its moderate reactivity, epichlorohydrin may be considered a false positive

for this system due to its clear purple colour response. Despite these undesirable responses, these electrophilic analytes are toxic chemicals in their own right and their detection by this sensor cannot be considered undesirable. Acetyl chloride, 1-bromobutane, 1-iodobutane and methyl iodide did not generate a colour change suggesting that NBP is not alkylated by these analytes as the characteristic purple colour of the dye is not observed. This is an interesting observation, particularly in the case of methyl iodide since this reagent normally yields a rapid reaction. For methyl iodide, a similar microemulsion system has been reported, but in this case, additional Ag(I) ions were required to effect methyl iodide detection.⁶⁴ Hence the commercially useful result here is that the current system is likely to be very selective against simple alkyl halides, which have been previously used as fumigation agents (e.g. methyl bromide).



Component	Volume (μL)
NBP (0.4 M)	100
NaOH (0.4 M)	200
Anionic microemulsion	1700
Electrophile	2

Figure 2.23. Comparison of the selectivity performance of anionic microemulsion formulation with reactive electrophiles.

It is important as a sensor that NBP is selective as a mustard detection system therefore it must not give a response when treated with nerve agents. This is crucial since the medical remediation protocols for nerve and blister agent toxicity are very different and due to their nature likely to be harmful. Organophosphate simulants including profenofos, diethyl chlorophosphate (DCP), diethyl cyanophosphate (DCNP), diisopropylfluorophosphate (DFP) and mephosfolan (an organophosphorus insecticide)

were used to investigate the selectivity of NBP (Figure 2.24). The simulant structures are presented in Figure 2.25.

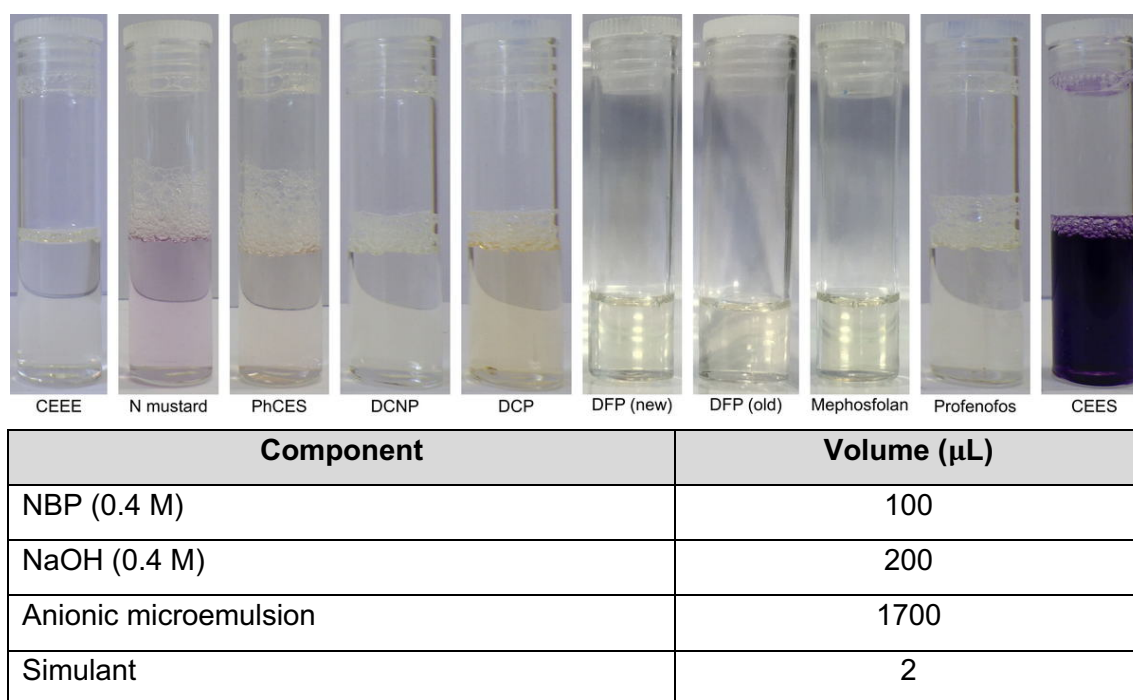


Figure 2.24. Comparison of the selectivity performance of anionic microemulsion formulation with blister and nerve agent simulants. Note that the N-mustard was added as a hydrochloride salt.

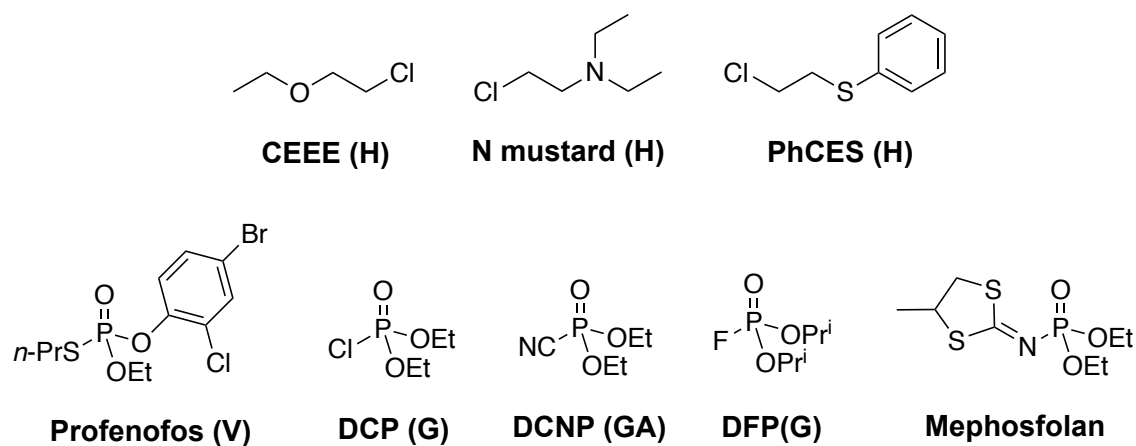
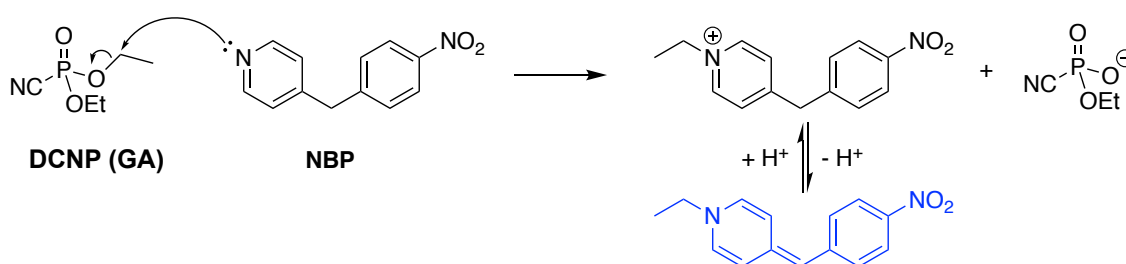


Figure 2.25. Simulants used in the false-positive screen.

Reassuringly, these nerve agent simulants did not generate a colour change. These results contrast the previous work of Turner where NBP was used for the determination of pesticides.⁵⁴ This suggests that the anionic microemulsion does not sufficiently enhance the electrophilicity of organophosphate simulants, which is inconsistent with its effect on both HD and CEES.⁵⁸ In the case of organophosphates, nucleophilic attack by

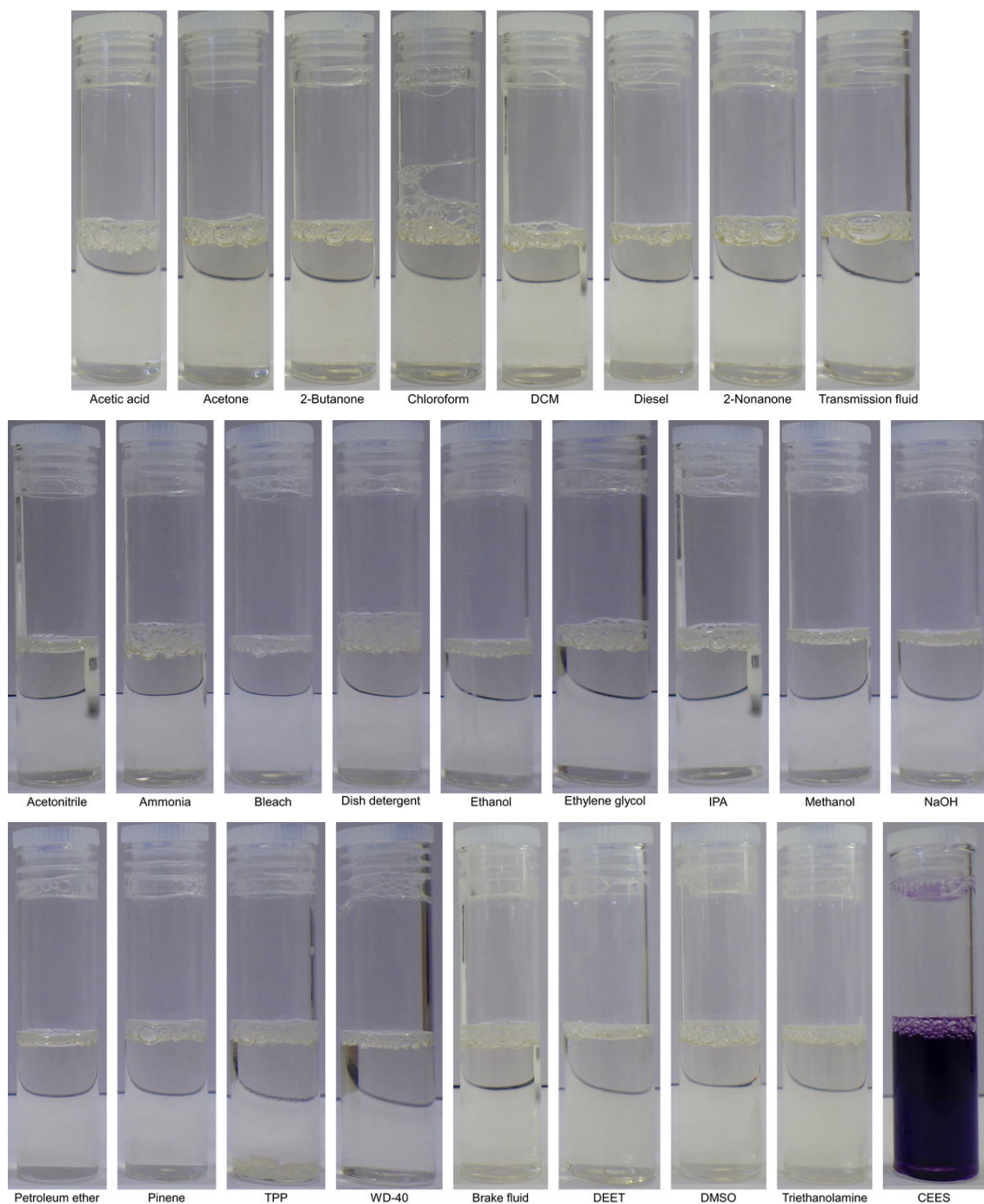
NBP occurs at the carbon atom of the ester group. The suggested mechanism for this reaction is illustrated in Scheme 2.5. Unlike the reaction with HD, the determination of organophosphates does not occur through an ionic intermediate. Instead, upon attack of the ester carbon atom, an anionic leaving group is generated to yield ethyl phosphorocyanidate anion and alkylated NBP cation. The latter species can subsequently be deprotonated in a basic environment to produce the characteristic blue colour of the dye. However, this reaction is not enhanced in anionic microemulsion whereby the net negative charge of the droplet interface would suppress the formation of the anion. This suggests that a cationic microemulsion would enhance the reactivity by which the net cationic charge of the droplet interface creates a favourable environment for the formation of the phosphorocyanidate anion. It is worth noting that this method of Turner also used forcing conditions and extended reaction times to generate significant colorimetric responses.



Scheme 2.5. The suggested mechanism of the Turner method for organophosphorus agent detection.

At first glance, the poor response for 2-(diethylamino)ethyl chloride (N mustard) may be considered an unsatisfactory result. However, this simulant is a hydrochloride salt which changes the pH of the system to create a less basic environment. The addition of NaOH base to this solution resulted in the colour intensification of the dye similar to the response with CEES, hence it is likely that live-agent mustards such as HN1, HN2 or HN3 would yield good positive responses.

The common analytes to produce a false positive response for the H-, G- and V-agent dyes of the discontinued commercial colorimetric chemical papers were tested with the anionic microemulsion formulation. The images of these treated formulations after subsequent exposure to simulant are presented in Figure 2.26.



Component	Volume (μL)
NBP (0.4 M)	100
NaOH (0.4 M)	200
Anionic microemulsion	1700
Analyte	2

Figure 2.26. Comparison of the selectivity performance of anionic microemulsion formulation with several common false positives for discontinued colorimetric chemical detection papers.

Reassuringly, no response was indicated by all solutions treated to the analyte. Thus, these chemicals are unreactive in this formulation suggesting that they are not false positives for the sensing system. Additionally, each formulation solution was treated with CEES (2 μL) after exposure to each interference agent and all solutions generated a purple colour response similar to test solutions exposed to CEES only. This clearly demonstrates the specificity of NBP for mustards and we can confidently conclude that this formulation can detect the target analyte in the presence of other CWAs and potential reactive interfering agents present in the environment.

2.3.10. Mass Spectrometry Analysis of Anionic SDS-5T Aggregation Colloid System

The mass spectrometry data of the anionic microemulsion formulation before and after the 5-minute exposure to CEES can be seen in Figure 2.27a and 2.27b.

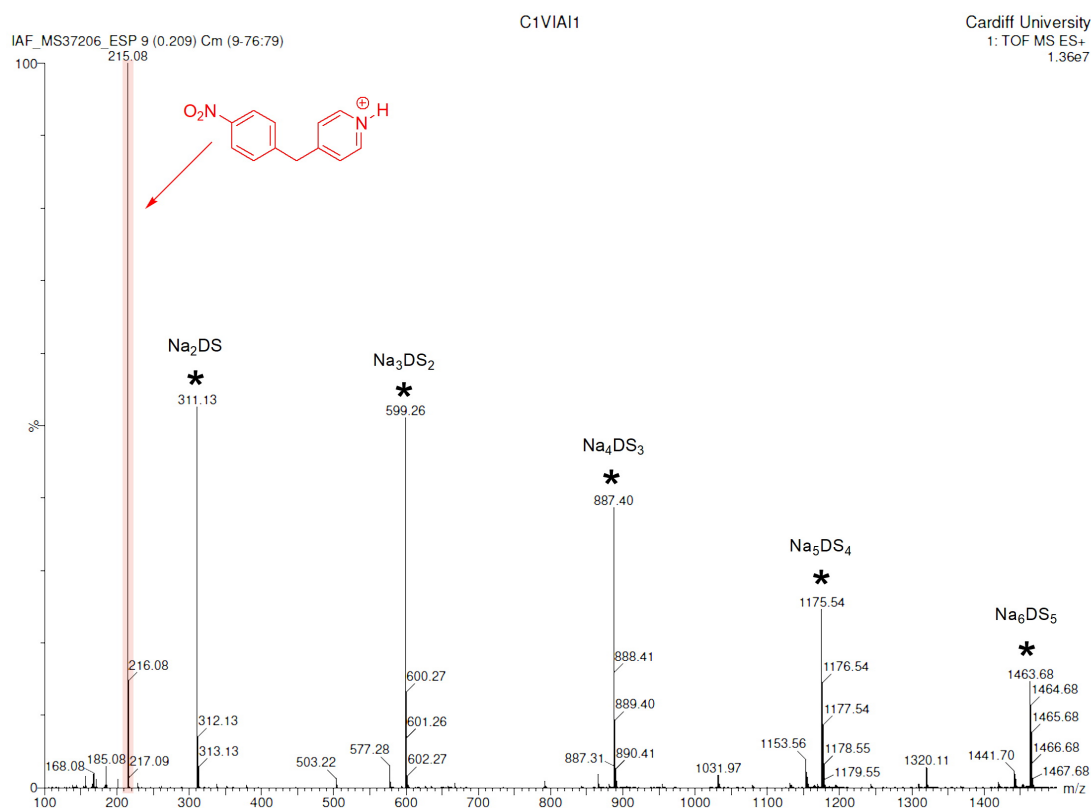


Figure 2.27a. ESI MS (+ve mode) of anionic microemulsion formulation before exposure to simulant. *Clusters arising from the surfactant are marked.

To prevent overloading the detector with microemulsion, the solutions were diluted with methanol (10 $\mu\text{L mL}^{-1}$) prior to mass spectrometry analysis. This also breaks the microemulsion structure, rendering it into a simple solution which essentially prevents

any further reaction from occurring. Thus, the spectra obtained are a good representation of the species present in the formulation at 5 minutes. Analysis of the spectra show a strong peak for $[\text{NBP}+\text{H}^+]$ at m/z 215.08. As expected, the formulation treated with CEES generated a peak for CEES-alkylated NBP adduct $[\text{NBP-CEES}]^+$ observed at m/z 303.12.

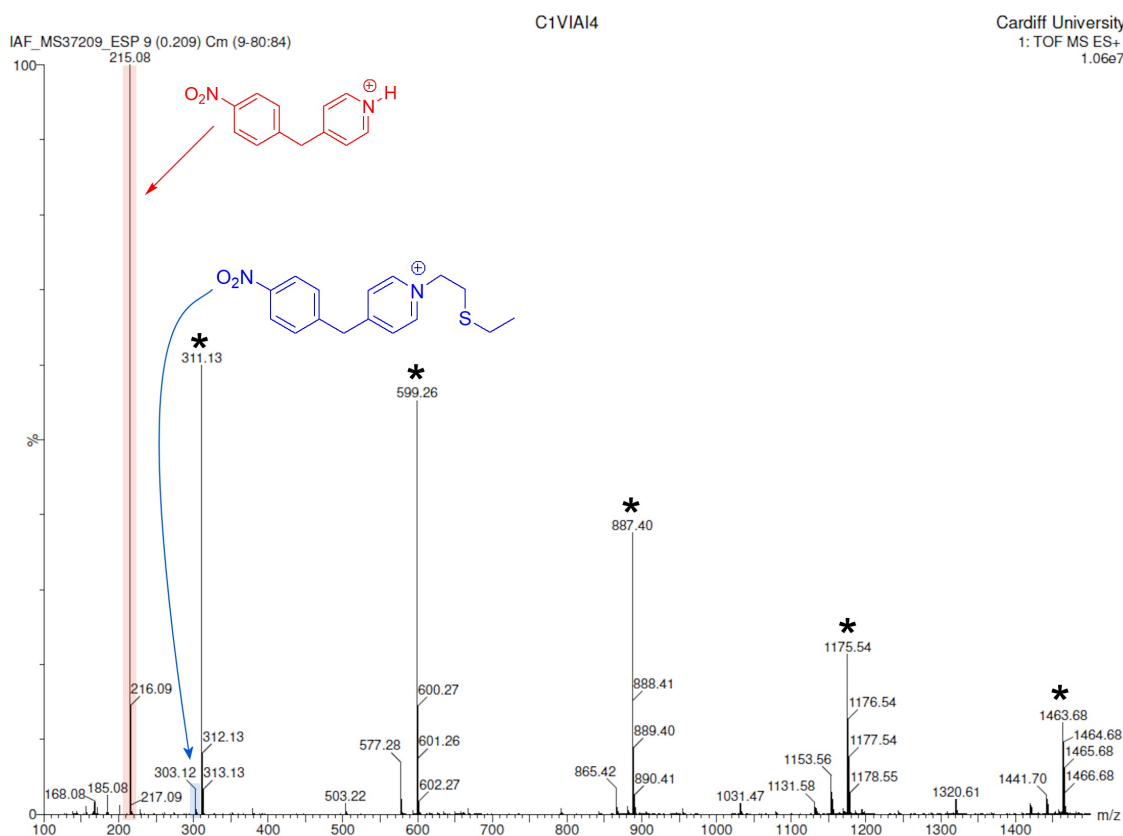
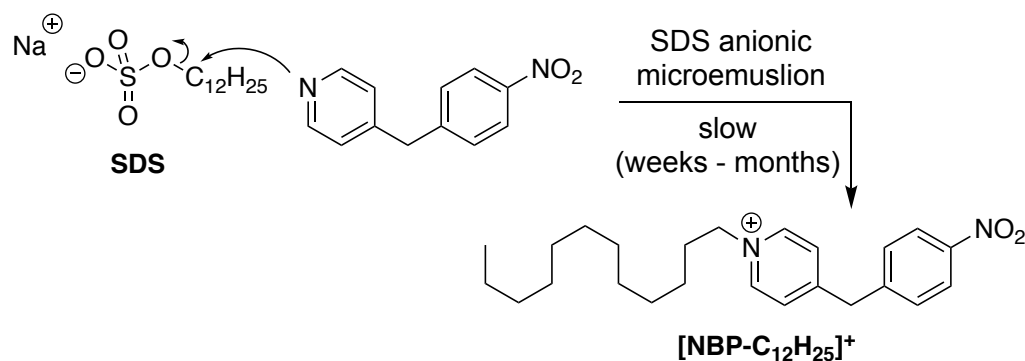


Figure 2.27b. ESI MS (+ve mode) of anionic microemulsion formulation after exposure to simulant. *Clusters arising from the surfactant are marked.

2.3.11. Performance Comparison of SDS and SDBS

Given that one of our target design criteria relates to the shelf life of the system, mass spectrometry was used to establish the inherent stability of the SDS microemulsion NBP system as means of identifying any unwanted reactions occurring within the microemulsion media. NBP was added to SDS-5T and the solution was stored for 4 weeks and then subjected to ESI-MS. The analysis of these spectra shows the formation of NBP alkylated by the dodecyl chain of SDS after 4 weeks at ambient temperature (Figure 2.28), as indicated by the peak at m/z 383.2710 (calculated for $\text{C}_{24}\text{H}_{35}\text{N}_2\text{O}_2^+$ = 383.2693, 4.4 ppm, $[\text{H}_{25}\text{C}_{12}\text{-NBP}]^+$). This reaction is likely to proceed via the mechanism illustrated in Scheme 2.6. This shows that the SDS system is unstable to one-pot storage

and cannot meet the 2-year shelf-life design criterion. In designing a point-of-use system this observation had important implications for the manufacturability of the system.



Scheme 2.6. Proposed mechanism of NBP alkylation in anionic microemulsion media.

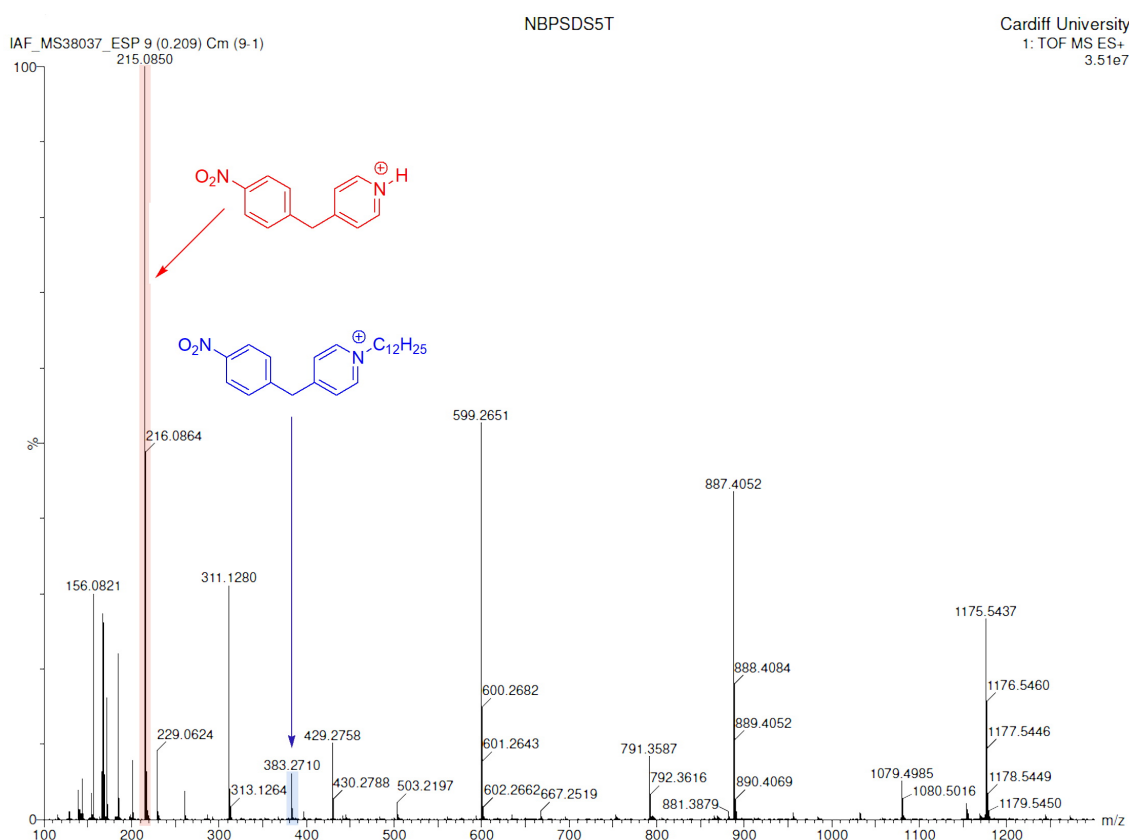


Figure 2.28. ESI MS (+ve mode) of a stock solution of SDS-5T (10 mg mL^{-1}) left at ambient temperature for 4 weeks. The sample ($10 \mu\text{L}$) was diluted with 1 mL MeOH before analysis.

To overcome this limitation, SDS was replaced by sodium dodecylbenzenesulfonate (SDBS) which has a different structure with a phenyl ring making it less susceptible to

nucleophilic attack by NBP. The structures of SDS and SDBS are combined in Figure 2.29 for comparison.

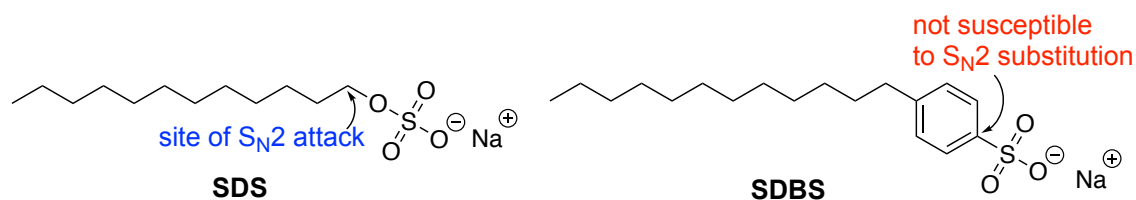


Figure 2.29. Structures of anionic surfactants SDS and SDBS and their susceptibility to nucleophiles.

Mass spectrometry analysis of an aged (~1 year) sample of NBP in SDBS-5T shows no production of NBP- $C_{12}H_{25}$ alkylation product (Figure 2.30) as SDBS is resistant to nucleophilic attack due to the lack of electrophilic site and the insufficient leaving group. This shows that NBP is stable in SDBS microemulsion and this system may be formulated as a single component on a point-of-use system.

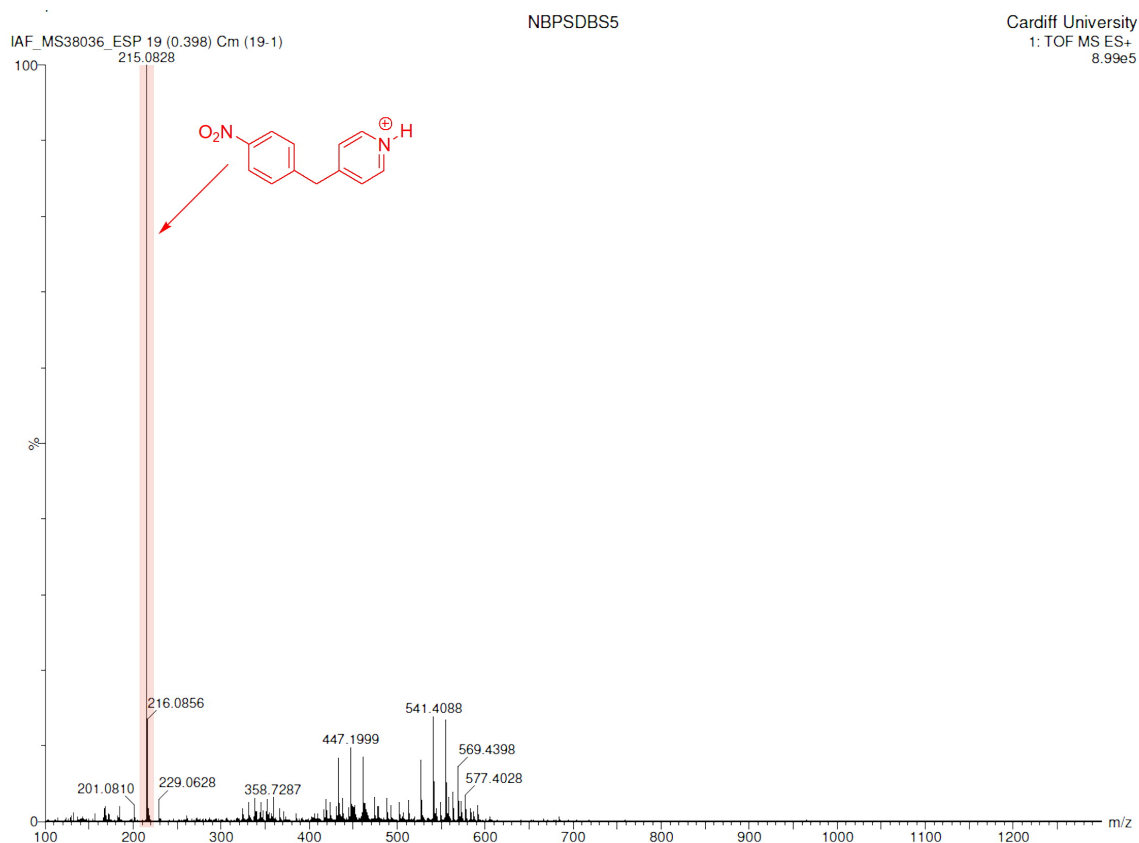
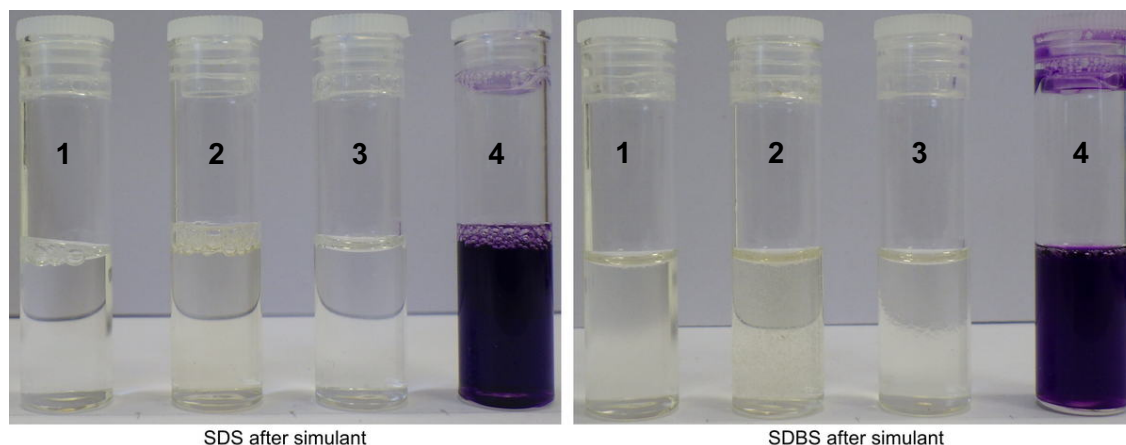


Figure 2.30. ESI MS (+ve mode) of a stock solution of SDBS-5T (10 mg mL^{-1}) left at ambient temperature for ~1 year. The sample ($10 \mu\text{L}$) was diluted with 1 mL MeOH before analysis. Note the reduced tendency for ion clustering in comparison to SDS based systems.

Following this, the reactivity of NBP was examined in SDBS microemulsion to determine its CEES detection performance. The compositions of the formulations tested and the images of the colorimetric responses with CEES simulant are presented below in Figure 2.31. Again, photographs were taken at 5 minutes to permit any discolouration of the control samples to develop. Intense colours were produced immediately that grew in intensity during the experiment.



Component	1	2	3	4
NBP (0.4 M) / μL	100	100	100	100
NaOH (0.4 M) / μL		200		200
Anionic microemulsion / μL	1900	1700	1900	1700
CEES / μL			2	2

Figure 2.31. Comparison of the performance of SDS and SDBS microemulsion with simulant. Vials are numbered 1 to 4 from left to right in each image.

It is evident from these images that SDBS microemulsion exhibits a similar naked eye colorimetric response to SDS microemulsion after 5 minutes of exposure to CEES. It should be noted that the SDBS-5T formulation is considerably more viscous than SDS. Unfortunately, we were unable to quantify the viscosity characteristics of the systems under study. It is sufficient to note that the rheological properties of the system do not impede the reactivity of NBP or the performance of the system. It is noteworthy that this formulation is also less susceptible to foaming, which is beneficial for swab system design and formulation (see Chapter 4).

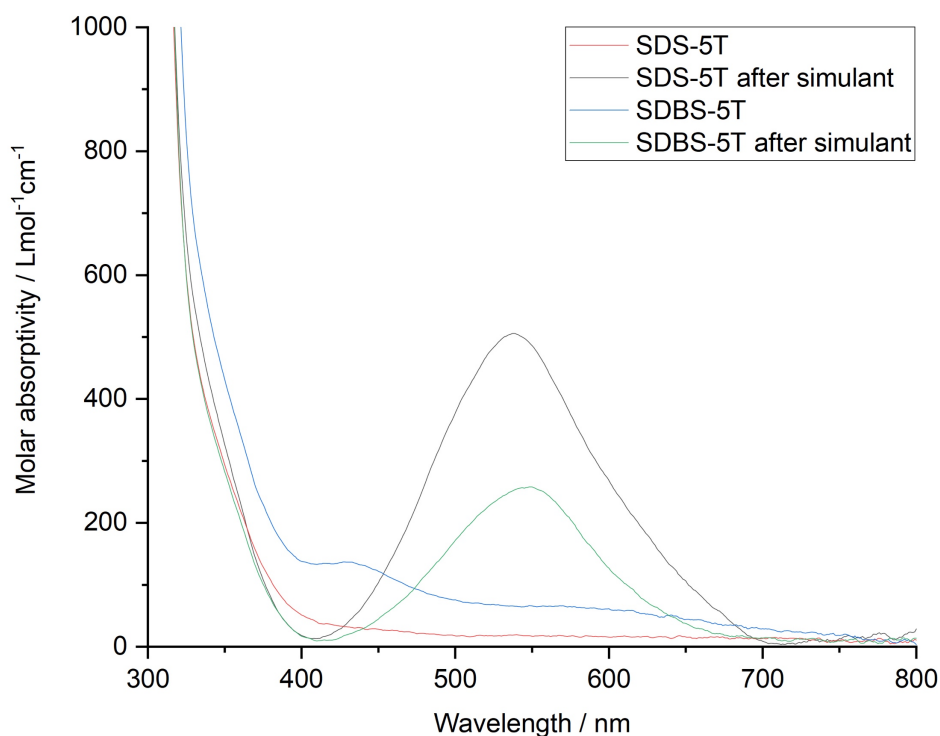
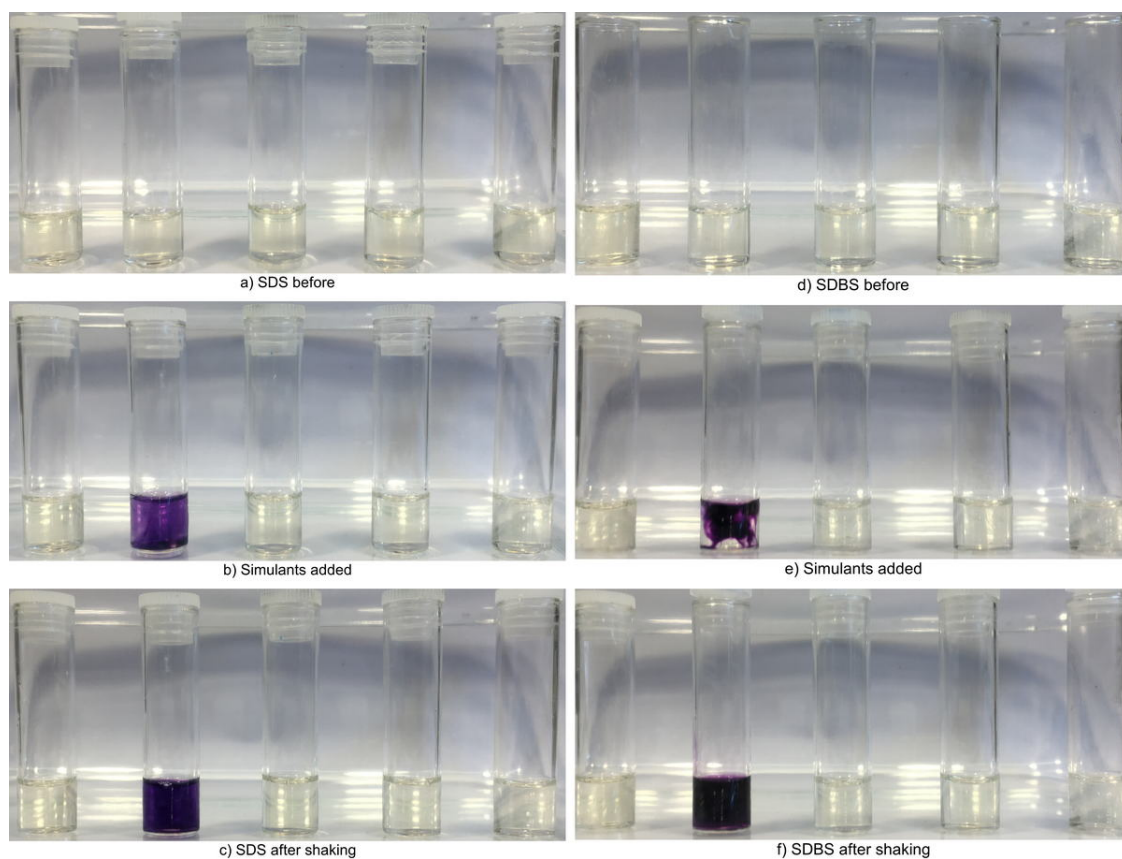


Figure 2.32. UV-vis spectra of SDS and SDBS microemulsion formations after 5 mins of exposure to CEES.

The electronic spectra of the SDS-5T and SDBS-5T formulations before and after simulant addition are presented in Figure 2.32. The absorbance data shows the lack of colour production associated with the decomposition of NBP. Although the colorimetric responses of these systems were indistinguishable by eye, it is apparent that the SDS-5T formulation produces a more significant colour production than that of SDBS-5T with a molar absorptivity of $509 \text{ L mol}^{-1} \text{ cm}^{-1}$ at 539 nm compared to $258 \text{ L mol}^{-1} \text{ cm}^{-1}$ at 550 nm, respectively. The conversion of NBP to NBP-CEES dye was again calculated using the above electronic spectra to give 14.2 % and 7.2 % conversion for SDS-5T and SDBS-5T, respectively. We postulate that the increased viscosity of the SDBS system may be the cause of this reduction in conversion.



Component	Volume (μL)
NBP (0.4 M)	100
NaOH (0.4 M)	200
Anionic microemulsion	1700
Analyte	2

Figure 2.33. Comparison of the performance of SDS and SDBS microemulsion with simulants. Vials are from left to right in each image: Blank; CEES; mephosfolan; DFP (new); DFP (aged). Note the turbidity of the more viscous SDBS sample in image b).

SDS and SDBS microemulsions, prepared here at a total volume of 1 mL for ease of testing severely hazardous analytes, were exposed to organophosphorus AChE inhibitor simulants DFP and mephosfolan (Figure 2.33). Two samples of DFP were used for these interference tests with new and aged simulants employed. Aged DFP contains the hydrolysis product diisopropyl hydrogen phosphate and contains varying amounts of hydrofluoric acid. These potential organophosphate interferants did not produce a colour change thus we can confidently eliminate mephosfolan and DFP as potential false positives of both the SDS and SDBS sensing system. Only CEES initiated the sensing mechanism to produce the intensely colourful dye. The increase in viscosity upon substituting SDS for SDBS, can be seen in image e) of Figure 2.33 where the dispersion

of colour is much slower before shaking compared to the SDS system in image b). However, this increased viscosity of the system in repeat runs was again found not to impede the reactivity or the ability to disperse the simulant with gentle shaking by the user.

CWAs may be present as mixtures and it is deemed important to examine the H-detection capability of the system after exposure to other simulants or agents (Figure 2.34).

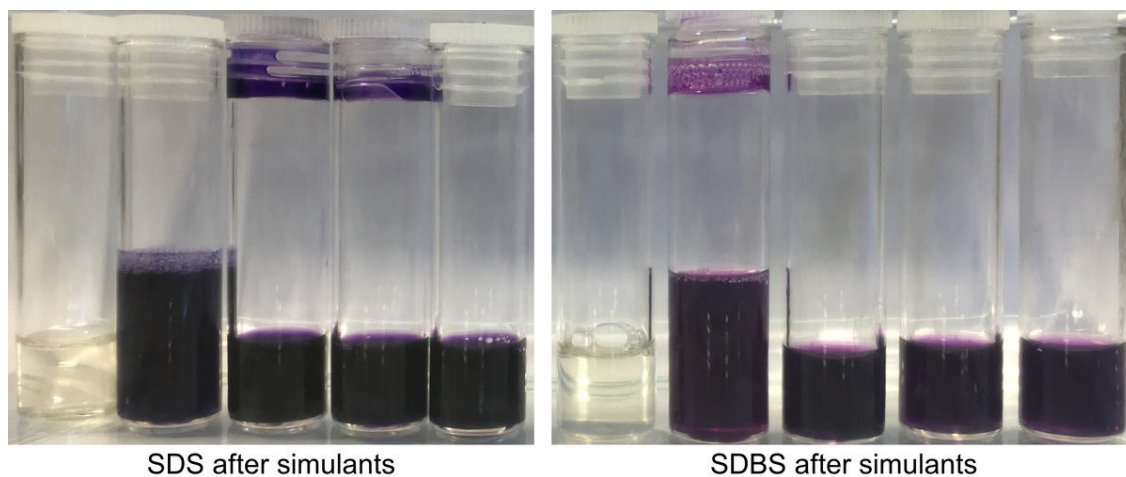


Figure 2.34. Comparison of the performance of SDS and SDBS microemulsions with CEES addition to formulations previously exposed to simulants. Vials are from left to right in each image: Blank; CEES with H₂O (1 mL); mephosfolan; DFP (new); DFP (aged).

Figure 2.34 shows that previous exposure to simulants does not interfere with the sensing mechanism when CEES (2 μ L) is added. Furthermore, no impact on the colour intensity after 5 minutes of exposure was seen by the naked eye. This suggests that the formulation was not compromised by previous simulant exposure.

To dilute the observed colour, 1 mL of distilled water was added to each vial after CEES exposure. Upon dilution of the formulations, the colours were immediately distinguishable by the naked eye, and this was further improved with the aid of illumination by a light bulb. It can be seen in Figure 2.35 that the SDS formulation produced a purple colour however, the SDBS formulation produced a magenta colour. This may suggest that the SDBS formulation experiences a phase change in the microemulsion system or a change in the location of the dye. Thus, we interpret this as a solvatochromic effect reflecting the different microenvironments of the dye. Since the perceived colour is very important in colorimetric detection systems, further studies were undertaken to examine the origins of this solvatochromic effect.

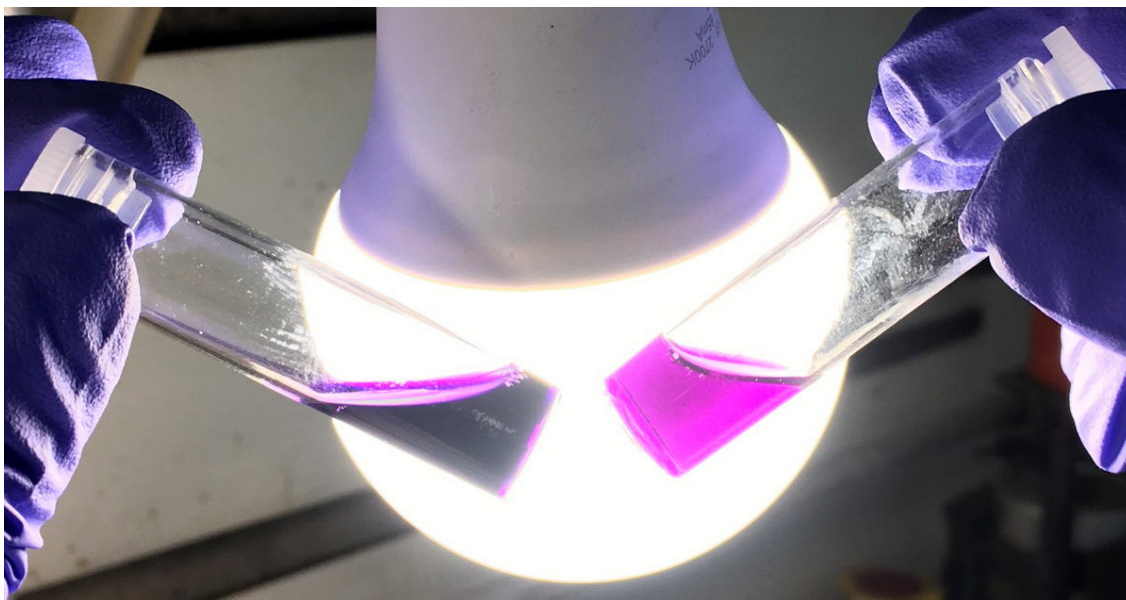


Figure 2.35. Comparison of the performance of SDS and SDBS microemulsions with CEES. Vials are from left to right: SDS-5T; SDBS-5T. Note these samples contain identical amounts of reagents and analytes.

The electronic spectra of the dye in toluene/*n*-butanol solvent mixtures show that the solvatochromic dye gives a different colour depending on the polarity of the solvent (Figure 2.36). For example, in a non-polar solvent such as toluene, the dye is a purple colour but in a more polar solvent like *n*-butanol, it displays a red colour. Note that in the 'water rich' micellar systems described above the colour appeared blue. These discussions have more than aesthetic importance since a colorimetric dosimeter that has a variable colour must be used with caution to avoid misidentification of target analytes. The electronic spectra suggest that the dye in SDS-5T remains localised in the toluene oil phase however in SDBS-5T the dye is accessible to the interface where the *n*-butanol molecules are located. Further studies are required to fully investigate this hypothesis. We may conclude here that whilst SDBS based formulations are more useful from a shelf-life perspective, those based on SDS have superior response where the human eye perceived colour is concerned.

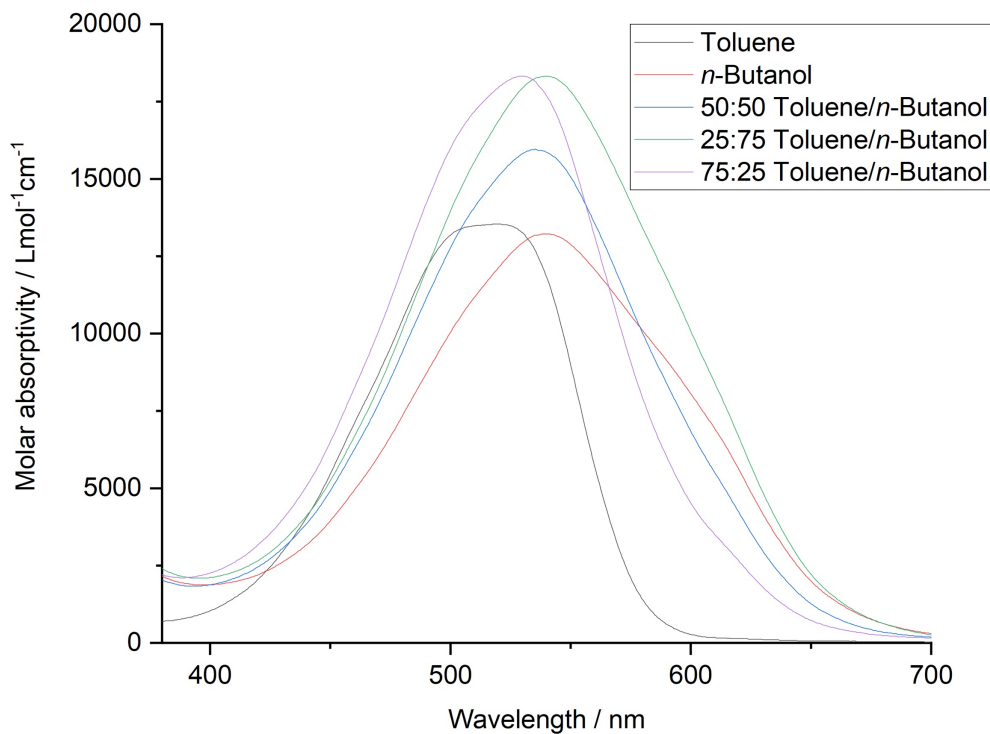


Figure 2.36. UV-vis spectra of NBP-CEES dye in toluene/*n*-butanol solvent mixtures of varying ratios.

To explore this phenomenon the absorbance spectra for SDS-5T and SDBS-5T formulations after exposure to CEES are presented alongside the photopic curve in Figure 2.37. Upon comparison, it is apparent to see that the absorbance peaks for both formulations exhibit a similar λ_{max} to the photopic curve. This data elegantly shows why the perceived colour response is so strong and easily detectable by the naked eye. However, it is apparent that the extent of reaction is much less in the SDBS system implying a low level of conversion of analyte to colorimetric dye response. This is an important consideration when we consider our target detection limit of 0.1 μL .

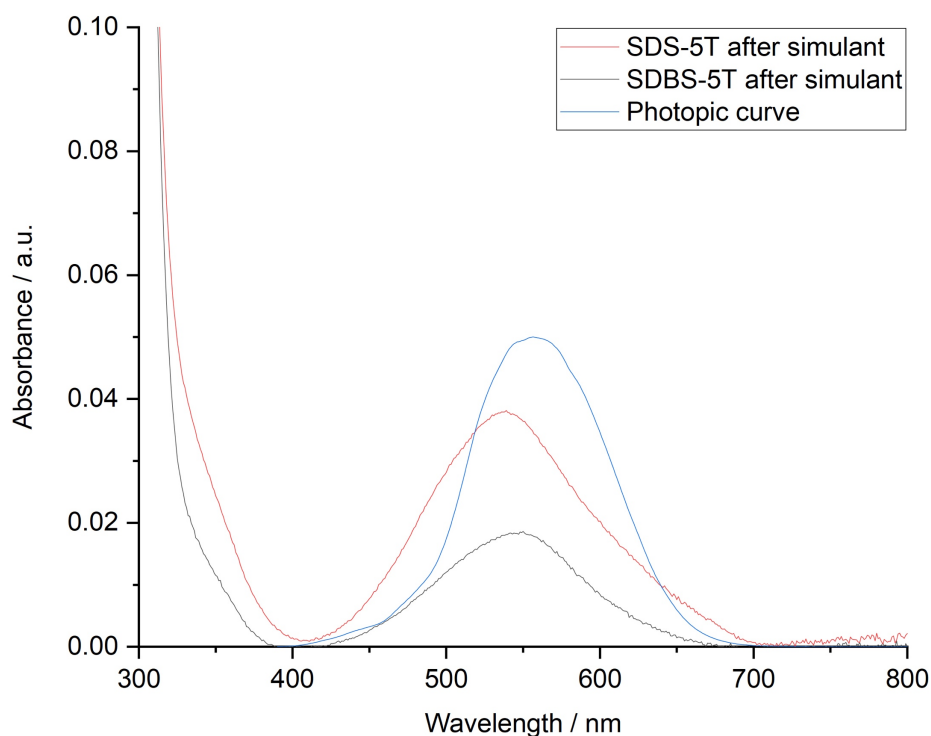


Figure 2.37. UV-vis spectra of SDS-5T and SDBS-5T after exposure to simulant with the photopic curve overlaid.

2.3.12. Investigating CEES Hydrolysis in Ionic Microemulsions

Mustard agents are known to hydrolyse in water to yield a complex mixture of the corresponding alcohols and sulfonium species^{65,66} with the concomitant release of HCl and a lowering of the pH. In formulating point-of-use devices it is deemed important to establish the pH behaviour of mustard agents in microemulsion media.

Initially, the volume of CEES that could be solubilised in SDS-0T was determined to give a best-case scenario of a microemulsion system in which the oil content of the system was solely derived from the analyte. This has the advantage of generating a system in which the organic oil phase could be omitted. This is not only more cost-effective but is likely to yield a system with a better shelf-life. The measurement of CEES loading using 100 mL SDS-0T was carried out at ambient temperature with CEES added in 100 μ L increments and the pH was monitored after each addition of CEES. SDS-0T was also used here so that a maximal loading value could be obtained without the toluene 'competing' for the solubilising power of the microemulsion. Recording of pH values was stopped at the point where the microemulsion became turbid in appearance, indicative of phase separation. The hydrolysis product of CEES is 2-(ethylmercapto)-ethanol,

which will be denoted CEES-OH, which was also used as a co-surfactant (Scheme 2.7). This was done to account for the *in-situ* generations of a co-surfactant, namely CEES-OH, from CEES hydrolysis since additional co-surfactant can significantly alter the structure of microemulsions, such as changes in droplet morphology and viscosity.

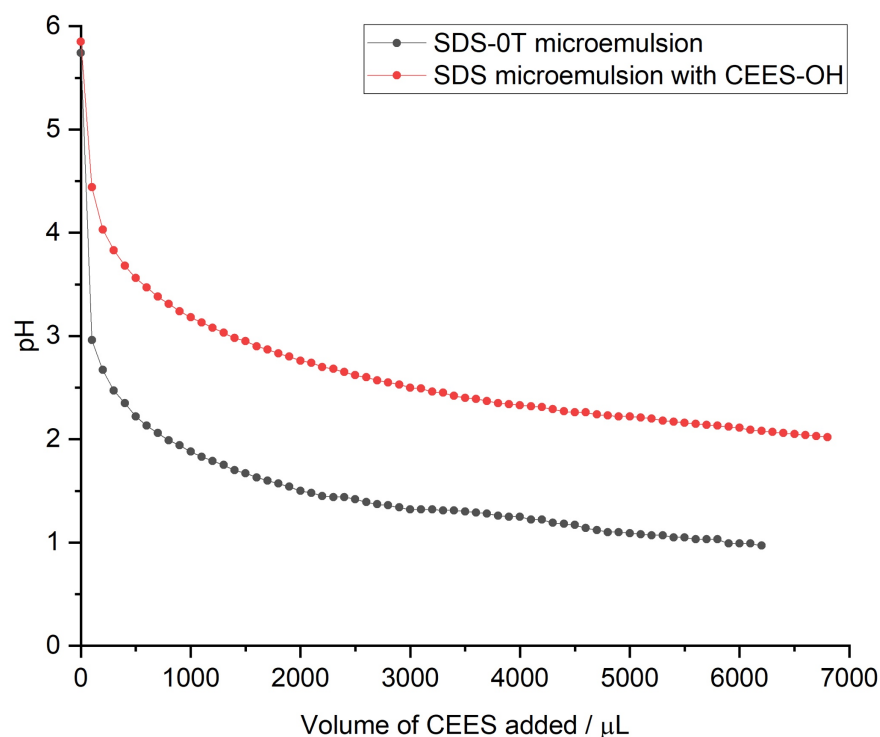
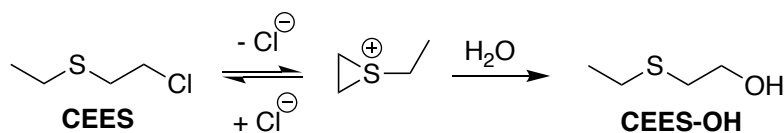


Figure 2.38. CEES hydrolysis in SDS-0T and SDS swollen micelle with CEES-OH as co-surfactant. Simulant was added in increments of 100 μL to the microemulsion (100 mL) and allowed to stir for 1 minute before measuring the pH.

Figure 2.38 shows that the starting pH of SDS-0T is 5.74 (arising from CO_2 absorption from the air) with the first addition of CEES decreasing the pH to an acidic value of 2.96. This suggests that the equilibrium between CEES and its hydrolysis product, CEES-OH, is favourable in an anionic swollen micelle system as the production of HCl reduces the pH, creating an acidic medium. The continued addition of CEES gradually decreased the pH to a final value of 0.97. At this point, pH measurements were stopped as the microemulsion became turbid upon a CEES loading of 6.2 mL. It is worth noting that the hydrolysis is likely to be suppressed at higher loadings of sulfur mustards since the back reaction of the intermediate episulfonium species will begin to increase in its importance at higher chloride concentrations (Scheme 2.7).



Scheme 2.7. The CEES-episulfonium chloride equilibrium and hydrolysis of CEES to CEES-OH.

To address the possibility that CEES hydrolysis yields a co-surfactant, an SDS swollen micelle with the n-butanol co-surfactant replaced with equimolar CEES-OH was prepared and the hydrolysis of CEES in this new microemulsion was investigated similarly to that of SDS-0T (Figure 2.38).

The pH decreases less significantly with CEES addition compared to in SDS-0T, whereby the pH decreases to 4.44 from an initial value of 5.85. This suggests that incorporation of CEES-OH as the co-surfactant creates an unfavourable environment for the formation of the hydrolysis product by suppressing the forward reaction of the episulfonium intermediate. Interestingly, this microemulsion can solubilise more CEES than SDS-0T, with 6.8 mL incorporated before the system becomes turbid in appearance. The results of these hydrolysis experiments suggest that by simple formulation manipulations the hydrolysis behaviour of sulfur mustards can be influenced. This is an important practical consideration since a lower rate of hydrolysis implies that more mustard agent is available for detection and hence the effective limit of detection is more likely to fulfil our target criterion of 0.1 μ L.

The hydrolysis of CEES was also investigated in both anionic and cationic microemulsions containing 4 wt% toluene. CEES was added in either 0.1 or 1 wt% and the pH was monitored every minute for over 1 hour. Furthermore, the pH of the system was investigated with the addition of NBP and the effect of ionic strength was studied using NaCl. These graphs are presented in Figure 2.39.

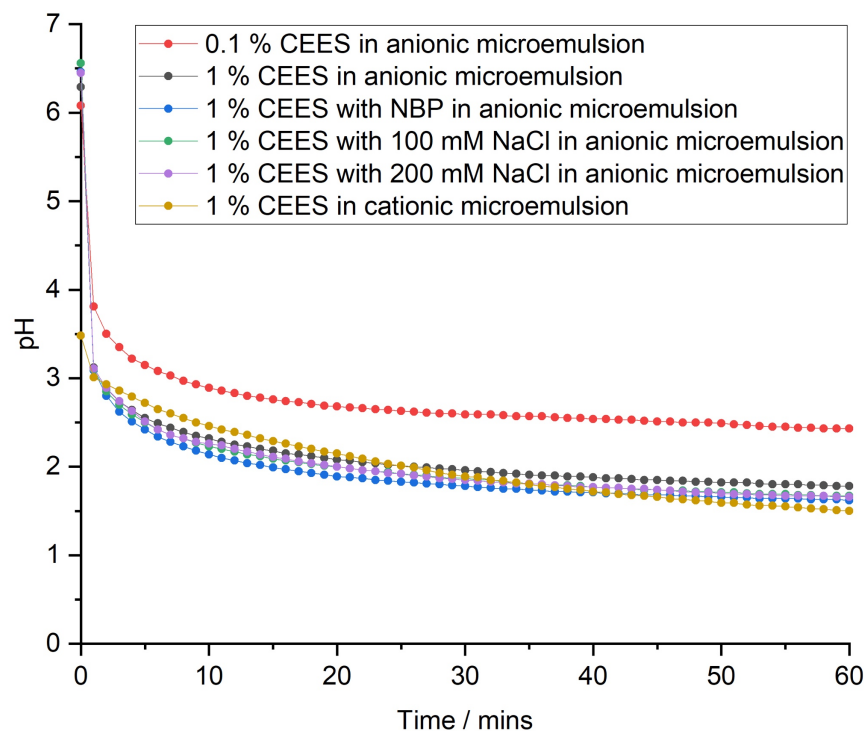


Figure 2.39. Comparison of CEES hydrolysis in anionic and cationic microemulsions with various additives.

The pH begins at 6.29 for 1% CEES and quickly drops to 3.12 after the first minute. This shows that CEES hydrolysis is a rapid reaction as the production of HCl quickly creates an acidic environment. At approximately 20 mins, the rate of hydrolysis begins to decline with the pH decreasing at an approximate rate of 0.01 min^{-1} for the remainder of the time. The change in pH over the 1-hour period is 6.29 to 1.78. As expected, decreasing the amount of CEES present from 1 wt% to 0.1 wt% means that less CEES is available to undergo hydrolysis to CEES-OH. Thus, HCl production is reduced which causes the pH to decrease at a lower rate. However, the data follows the same trend as that of 1 wt% CEES, particularly with the rate of the pH decrease in the last 40 minutes. The change in pH over the 1-hour period is 6.08 to 2.43. NBP (5 mg) was added to SDS-4T with 1 wt% CEES. The amount of NBP added was calculated from the previously calculated extinction coefficient of the dye ($8350 \text{ L mol}^{-1} \text{ cm}^{-1}$) at an absorbance of 2 using the Beer-Lambert law. With the presence of NBP, the pH decreases more than when NBP is absent. However, this change is subtle which indicates that the weakly basic NBP localised in the oil core of the droplet has little effect. Changing the ionic strength of the aqueous phase of the microemulsion by introducing NaCl at concentrations of 100 mM

and 200 mM is expected to cause a less dramatic reduction in pH compared to the 1 wt% CEES data as it should suppress the hydrolysis of CEES. This is due to Le Chatelier's principle. As a consequence of the presence of salt, a higher concentration of chloride ions is present in the aqueous phase which causes the hydrolysis equilibrium to lie on the episulfonium side to re-establish the equilibrium. As a result, less hydrolysis would occur and the production of HCl by-products would reduce causing the pH to be less acidic. However, this is not what is observed. Although the difference is small, the addition of NaCl causes the pH to decrease. By adding NaCl to the system we are changing its composition which might be changing the size of the droplets. Big aggregates tend to get smaller with increasing ionic strength therefore the surface area increases thus the rate of hydrolysis increases. Furthermore, increasing the concentration of NaCl from 100 to 200 mM has an insignificant impact on the pH. Substitution of the anionic microemulsion to a cationic microemulsion causes a change in the overall charge of the droplet interface from negative to positive. It is believed that a net positive charge would suppress the production of the episulfonium cation and therefore diminish CEES hydrolysis. However, upon addition of CEES to cationic microemulsion, the pH is reduced considerably to 3.48, which is the lowest recorded value of all previously monitored samples.

2.3.13. Investigating the pK_a of Alkylated NBP in SDS-5T Formulations

The requirement for an elevated pH in NBP colorimetric systems is an important consideration when designing field-deployable devices. The need in our current formulations for an additional base (NaOH) has cost implications, not only arising from reagent costs but also, given the sensitivity of NBP to high hydroxide concentrations may necessitate the compartmentalisation of a device before its use. Hence it is important to quantify the interaction of hydroxide and alkylated NBP derivatives to achieve a better understanding of the mode of action of the sensor and hence instigate design improvements. This has required a determination of the pK_a value of alkylated NBP derivatives.

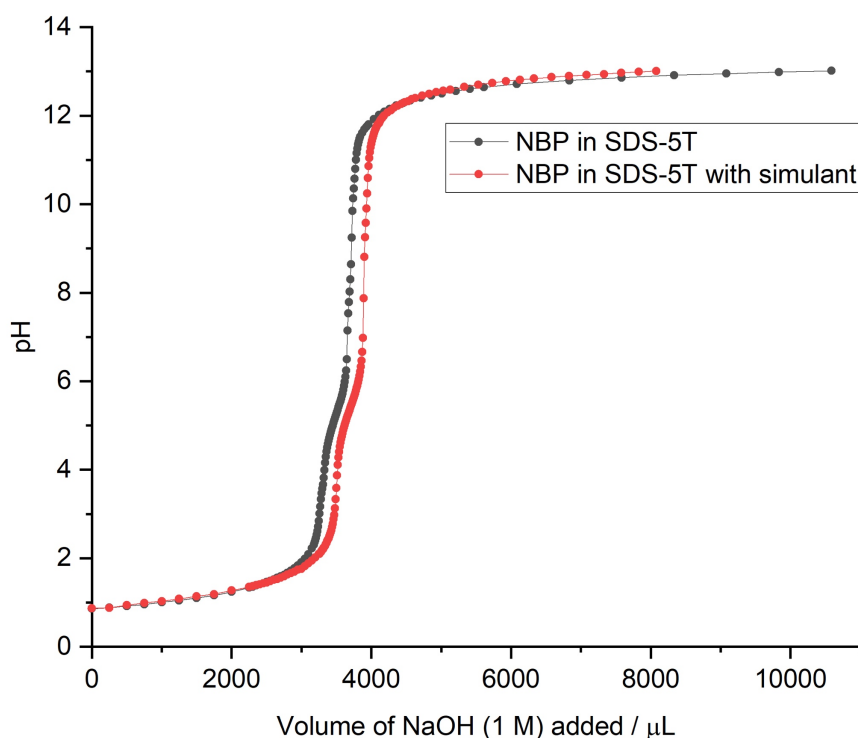


Figure 2.40. Averaged pH titration curve for NBP in SDS-5T at a total concentration of 2×10^{-2} M with the titration curve for this formulation after exposure to simulant overlaid.

The acid-base equivalence point of the SDS-5T formulation was investigated by executing a pH titration with an aqueous 1 M NaOH solution (Figure 2.40). A stock solution of NBP in SDS-5T was prepared at a concentration of 2×10^{-2} M to reflect its concentration in the previous testing formulations. A 20 mL portion of this solution was first acidified with 6 M HCl solution to achieve a low starting pH of below 1 and subsequently treated with aliquots of 1 M NaOH at ambient temperature until a pH of approximately 13 was reached. The pH was monitored after each addition of NaOH. The titrations were run in duplicate, and the data were averaged to create the pH titration curve. The reaction conditions were kept constant for the titration involving CEES (20 μ L) (Figure 2.41). Interestingly, the pH titration curve with simulant present follows the same pattern as that of NBP only, implying that the pK_a value of NBP and alkylated NBP are comparable. Additionally, the system with CEES added requires a lower amount of base to reach a pH of approximately 13. This indicates that small amounts of CEES do not considerably change the pH of the formulation, implying that the alkylation reaction is rapid in comparison to the rate of sulfur mustard hydrolysis. Given that CEES

hydrolysis results in the production of HCl, which would normally lower the pH it is clear from this data that this is not occurring in substantial amounts.

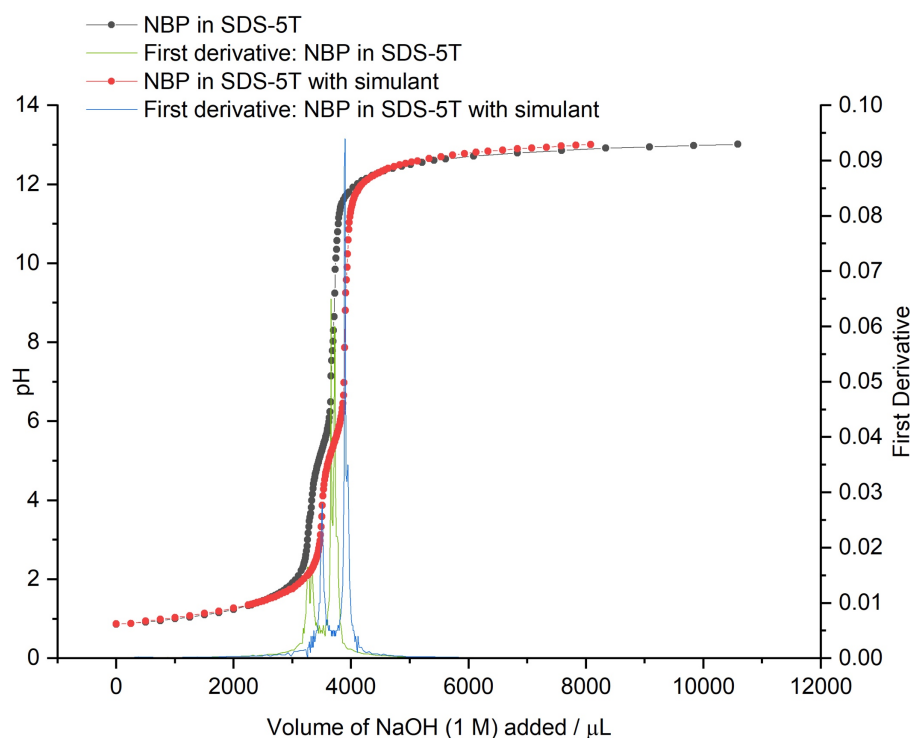
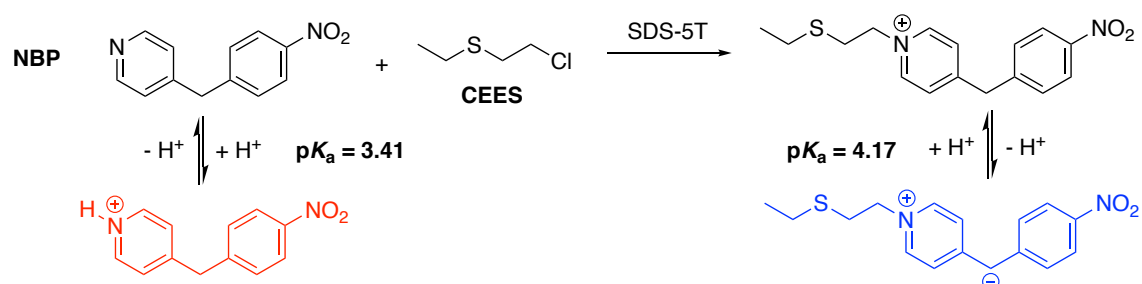


Figure 2.41. Titration curves of SDS-5T formulation before and after exposure to simulant along with their corresponding first derivative plots.

The half-equivalence points of these titration curves were found using the first derivative. The half-equivalence point represents the point at which the pK_a of the acid is equal to the pH of the solution. This value represents the pK_a value of the methylene proton of NBP in the anionic microemulsion system in both the absence and presence of stimulant. The pK_a values calculated were 3.41 and 4.17 for formulations before and after exposure to simulant, respectively. Thus, we can conclude that under these conditions the pyridyl based pK_a of NBP is 3.41 and that of alkylated NBP has a methylene group pK_a value of 4.17 (Scheme 2.8). *The experimentally calculated pK_a of 3.41 is lower than expected for the pyridinium cation, which has a value of approximately 5.3. This suggests that the conjugate acid of NBP is more acidic in the anionic microemulsion. Similarly, the pK_a value of the methylene group of NBP is considerably lower than the expected value of approximately 26.7. This suggests that the resonance effect increases the stability of the*

conjugate base through the delocalisation of the negative charge, thus lowering the pK_a value.



Scheme 2.8. The acid-base behaviour of the SDS-5T/CEES/NBP system.

2.3.14. Measurement of NBP Location in SDS-5T Microemulsion

The localisation of NBP in SDS microemulsion was studied using the fluorescence of pyrene through the efficiency of the nitro group of NBP to quench the fluorescence of pyrene. As a hydrophobic compound, pyrene has been widely employed to study the micellisation of surfactants. The unique characteristics of pyrene fluorescence were exploited to investigate the locus of NBP. Specifically, the calculation of the ratio of the third to first vibronic peaks provides a direct measure of the polarity of the solvent that the probe resides in and the fluorescence intensity as a function of quencher concentration. Pyrene was added to the microemulsion at a concentration of 2 μM and the emission was measured between 370-600 nm using the following parameters: λ_{ex} of 340 nm with an emission slit of 2.5 nm.

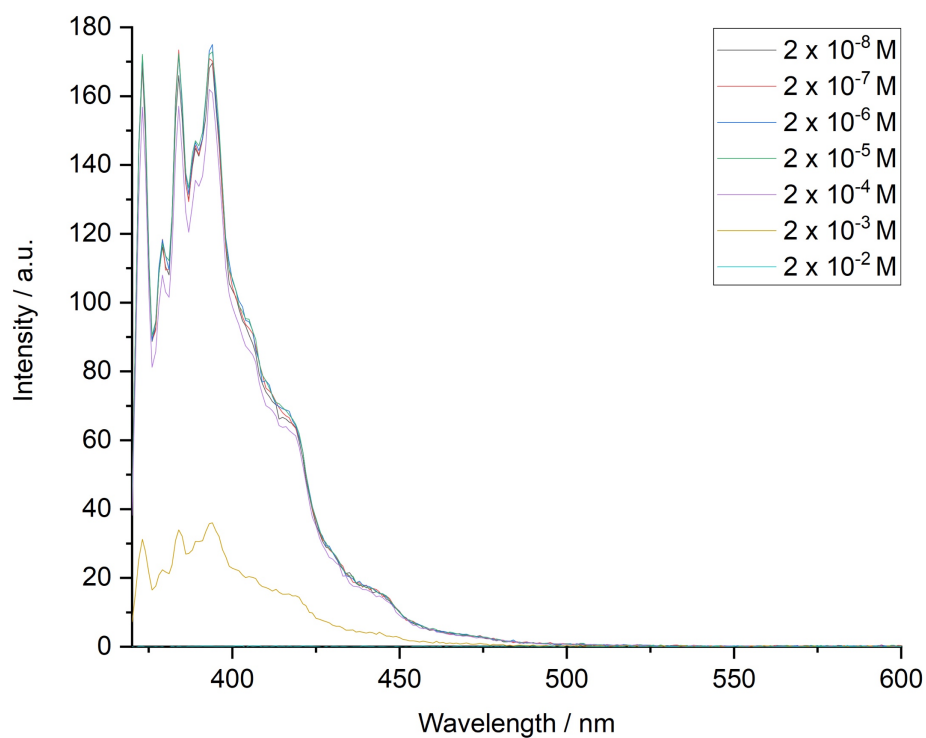


Figure 2.42. The intensity of SDS-5T solubilised pyrene emission as a function of quencher concentration.

Figure 2.42 clearly shows that pyrene fluorescence is quenched by the presence of NBP, with the fluorescence decreasing with an increase in quencher concentration. This suggests that the pyrene is located in the same environment as NBP and thus resides in the toluene oil phase of the droplet. The fluorescence intensity does not change considerably below an NBP concentration of 2×10^{-4} M.

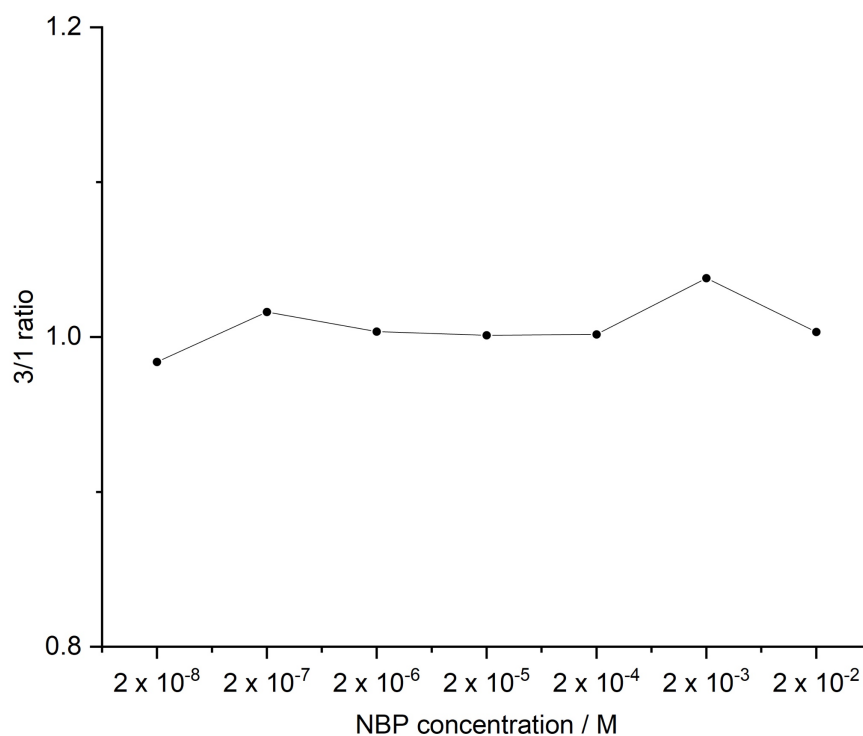


Figure 2.43. Ratio of the third to first vibronic peak of the pyrene probe of the same data.

Figure 2.43 shows the 3/1 ratio of the vibronic peaks of pyrene as a function of quencher (NBP) concentration. The relatively unvarying 3/1 ratio values with NBP concentration clearly demonstrates that the pyrene probe remains in a constant hydrophobic environment. This suggests that NBP and pyrene both reside in the same environment and therefore NBP must occupy the oil core of the microemulsion droplet.

2.3.15. Evidence for the Proposed Mode of Action

In designing the colorimetric sensor system we have generated sufficient data to propose a mode of action (a mechanism) for the sensor system. This is illustrated in Figure 2.44 below.

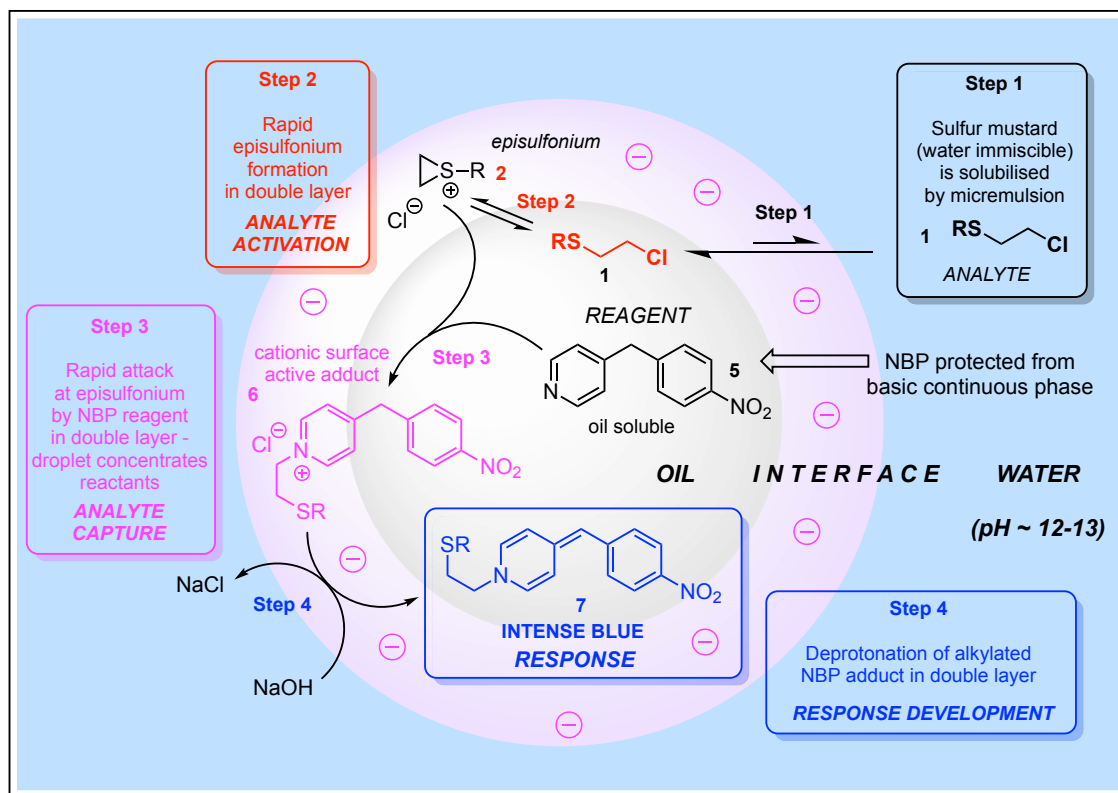


Figure 2.44. Proposed mode of action of mustard detection in an anionic microemulsion.

Step 1 - The first step of the detection of sulfur mustard is the solubilisation of analyte 1 by the microemulsion droplet in the toluene oil phase. This is verified by the intermediate self-diffusion coefficient observed by Fallis *et al.*⁵⁸

Step 2 - Here is the rapid formation of the episulfonium cation 2 at the interface of the droplet. The episulfonium formation is driven by the net negatively charge of the anionic microemulsion droplet interface. This is evidenced by the observation of CEES self-addition products in microemulsion solutions by mass spectrometry studies in the work of Fallis *et al.*⁵⁸ Reaction with further analyte will yield acyclic sulfonium species (3, not shown) or hydrolysis to CEES-OH (4, not shown) will reduce the concentration of analyte in the system.

Step 3 - Here the nucleophilic attack of the episulfonium cation by the nitrogen atom of the oil-soluble NBP **5** produces an alkylated adduct. This step is rapid with the reaction rate decreased with help from the microemulsion bringing the analyte and sensor molecule in close proximity. This effectively gives the reactants a higher concentration locally and thus improves the rate of reaction. This is evidenced by the observation of CEES-NBP adduct in the +ESI-MS. Furthermore, the anionic interface of the droplet protects the oil-soluble NBP and the interracial bound episulfonium species from nucleophilic attack by the hydroxide ion base located in the continuous aqueous phase. This step is also likely since the direct reaction of sulfur mustards and NBP in normal solutions (see ethanol data above) is observed to be exceedingly slow under ambient conditions and a more reactive electrophile, the episulfonium, is needed to explain the observed high rate of reaction.

Step 4 - The final step is the deprotonation of the alkylated adduct which produces a highly coloured conjugated dihydropyridine dye **7**. This is the visually detected colorimetric response arising from the π to π^* transition within the chromophore. This is a reasonable postulate since the alkylated NBP species **6** will be surface active. This places **6** at the interface where it is exposed to the high pH of the continuous aqueous medium.

The rate-limiting step can only be postulated as additional kinetic studies are required. Based on the available evidence, there are two possible rate-limiting steps in the mustard detection. Firstly, the dispersion of CEES in the microemulsion may be the slowest step as gentle shear force is occasionally required to accelerate the dispersion of simulant. Secondly, the deprotonation of the cationic dye precursor is a plausible rate-limiting chemical step as this adduct must be in proximity to a sodium hydroxide molecule in order for the final step of the detection to occur.

2.4. Experimental

Reagents were purchased from commercial suppliers and used as received without further purification unless stated otherwise. ^1H and ^{13}C NMR spectra were run on Bruker Ultrashield FT-NMR spectrometers with a field strength of 300 MHz. NMR chemical shifts (δ) are reported in ppm and are referenced to the residual solvent signal. Spin-spin coupling constants J are given in Hz. Mass spectra were performed by the Analytical Services staff at Cardiff University School of Chemistry on a Waters Xevo G2-XS QToF mass spectrometer. UV-vis studies were performed on an Agilent Technologies Cary 60 UV-vis spectrophotometer using quartz cells. Fluorescence studies were performed on an Agilent Technologies Cary Eclipse Fluorescence spectrophotometer using quartz cells. pH measurements were performed on a Thermo Scientific Orion Star A111 pH meter.

2.4.1. Preparation of surfactant mixtures

Anionic, cationic and non-ionic surfactant solutions and microemulsions were prepared by mixing a surfactant, co-surfactant (n-butanol), distilled water and an organic solvent (toluene). Materials of technical or ACS reagent grades were used in all circumstances. For the purpose of this thesis, surfactant derived mixtures will be referred to by the terms in Table 2.7.

System	Components	Composition
Micelle	2	Water – surfactant mixture
Swollen micelle	3	Water – surfactant – co-surfactant (n-butanol) mixture
Microemulsion (O/W – oil-in-water)	At least 4	Water – surfactant – co-surfactant (n-butanol) – oil(toluene)* mixture
Inverse microemulsion (W/O – water-in-oil)	At least 4	Water – surfactant – co-surfactant – toluene mixture

Table 2.7. Components of micellar, swollen micellar and microemulsion systems. *Each microemulsion contains 5% (wt%) toluene.

2.4.1.1. Anionic surfactant mixtures

The compositions of sodium dodecyl sulfate (SDS) mixtures were prepared according to Table 2.8. Here, SDS-0T is the anionic swollen micelle and SDS-5T is the anionic microemulsion.

Component / system	SDS micelle	SDS-0T	SDS-5T
SDS (g)	10.1	10.1	10.1
1-Butanol (g)	-	9.1	9.1
Toluene (g)	-	-	4.8
Distilled water (g)	76	76	76

Table 2.8. Composition of anionic surfactant mixtures.

2.4.1.2. Cationic surfactant mixtures

1-Dodecyl-3-methylimidazolium bromide ($[C_{12}H_{25}ImCH_3]Br$) mixtures were prepared according to Table 2.9.

Component / system	Cationic micelle	Cationic swollen micelle	Cationic microemulsion
$[C_{12}H_{25}ImCH_3]Br$ (g)	10.0	10.0	10.0
1-Butanol (g)	-	10.0	10.0
Toluene (g)	-	-	4.5
Distilled water (g)	70	70	70

Table 2.9. Composition of cationic surfactant mixtures.

2.4.1.3. Non-ionic surfactant mixtures

Polyoxyethylene (23) and lauryl ether (Brij 35) mixtures were prepared according to Table 2.10.

Component / system	Non-ionic micelle	Non-ionic swollen micelle	Non-ionic microemulsion
Brij 35 (g)	10.0	10.0	10.0
1-Butanol (g)	-	10.0	10.0
Toluene (g)	-	-	4.8
Distilled water (g)	75	75	75

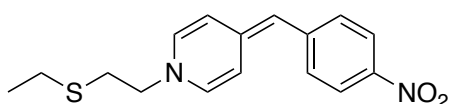
Table 2.10. Composition of non-ionic surfactant mixtures. All components are present in %(w/w).

2.4.2. Procedure for simulant and analyte testing

Prior to testing formulations with simulant or other toxic analytes, a bleach bath must be prepared to decontaminate all equipment and glassware that come in contact with hazardous chemicals during testing experiments. This decontaminating solution is prepared with thick bleach, IPA and water in a 1:1:2 ratio with NaOH pellets to maintain a high pH. Furthermore, coloured crepe paper is attached to the fume hood sash to demonstrate the level of extraction. Testing involving simulants should always be

conducted with a supervisor or other qualified person in attendance. A glass petri dish is utilised as a secondary container to store the simulant bottle. In addition to standard laboratory PPE, two pairs of gloves of opposing colours are worn to handle simulants in order to identify any tears in the material. Once the stimulant has been carefully added to the formulation and the necessary equipment contaminated in the bleach bath, gloves are inspected for contamination. If contaminated, the gloves are placed in the bleach bath for decontamination.

Synthesis of 1-(2-(Ethylthio)ethyl)-4-(4-nitrobenzylidene)-1,4-dihydropyridine (4)



4-(4-nitrobenzyl)pyridine was first recrystallised using methyl isobutyl ketone. 4-(4-nitrobenzyl)pyridine (0.833 g, 3.89 mmol) was dissolved in ethanol (15 mL) and added to SDS-5T microemulsion (50 mL). The reaction mixture was stirred at room temperature and 2-chloroethyl ethyl sulfide (0.45 mL, 3.89 mmol) was added dropwise. 0.2 M aqueous NaOH solution was added dropwise until the solution remained a purple colour. Water (~700 mL) and 0.2 M aqueous NaOH solution were added in portions sequentially until a blue-green precipitate was seen. The reaction mixture was stirred at room temperature for 16h. The product was filtered under suction to yield a blue-green solid (0.549 g, 1.82 mmol, 47%). **¹H NMR** (300 MHz, CHCl₃-*d*) δ_H (ppm) = 8.01 (2H, d, ³J_{HH} = 9.0 Hz, Ar-**H**), 7.21 (2H, d, ³J_{HH} = 9.0 Hz, Ar-**H**), 6.59 (2H, dd, ³J_{HH} = 5.4, 2.1 Hz, Ar-**H**), 6.45 (1H, dd, ³J_{HH} = 7.6, 1.8 Hz, Ar-**H**), 5.96 (1H, dd, ³J_{HH} = 7.6, 2.4 Hz, Ar-**H**), 5.37 (1H, s, R=C-**H**), 3.60 (2H, t, ³J_{HH} = 6.8 Hz, R-N-**CH**₂-), 2.75 (2H, t, ³J_{HH} = 6.8 Hz, R-N-**CH**₂-**CH**₂-S-), 2.54 (2H, q, ³J_{HH} = 7.4 Hz, R-S-**CH**₂-CH₃), 1.25 (3H, t, ³J_{HH} = 7.4 Hz, R-S-**CH**₂-**CH**₃). **¹³C NMR** (75 MHz, CHCl₃-*d*) δ_C (ppm) = 148.04, 141.37, 139.02, 135.43, 132.80, 124.70, 124.46, 116.69, 108.08, 102.75, 55.27, 32.30, 26.65, 14.86. **HRMS (ES⁺)** found *m/z* 303.1158, calcd *m/z* 302.1089 for [C₁₆H₁₈N₂O₂S]. **UV-vis** (*n*-BuOH) λ_{max} (ε / L mol⁻¹ cm⁻¹): 540 (13220) nm.

2.5. References

- 1 E. Olkowska, Z. Polkowska and J. Namieśnik, *Chemical Reviews*, 2011, **111**, 5667–5700.
- 2 Y. Li, L. Lai, P. Mei, S. J. Li, L. Cheng, Z. H. Ren, Y. C. Zheng and Y. Liu, *Journal of Surfactants and Detergents*, 2018, **21**, 845–858.
- 3 A. S. Fouda, M. A. A. El-Ghaffar, M. H. Sherif, A. T. El-Habab and A. El-Hossiany, *Protection of Metals and Physical Chemistry of Surfaces*, 2020, **56**, 189–201.
- 4 P. Li, Z. Wang, K. Ma, Y. Chen, Z. Yan, J. Penfold, R. K. Thomas, M. Campana, J. R. P. Webster and A. Washington, *Journal of Colloid and Interface Science*, 2020, **565**, 567–581.
- 5 C. Kang, J. Wu, Y. Zheng and L. Lai, *Journal of Molecular Liquids*, 2020, **320**, 114431.
- 6 A. Shaheen, A. W. Mir, R. Arif and A. L. Wani, *Colloids and Interface Science Communications*, 2020, **36**, 100257.
- 7 M. M. Shaban, A. M. Eid, R. K. Farag, N. A. Negm, A. A. Fadda and M. A. Migahed, *Journal of Molecular Liquids*, 2020, **305**, 112817.
- 8 F. Pan, Z. Zhang, X. Zhang and A. Davarpanah, *Powder Technology*, 2020, **373**, 93–98.
- 9 Saroj and L. Sharma, *Journal of Surfactants and Detergents*, 2020, **23**, 1079–1085.
- 10 M. Di Francesco, C. Celia, M. C. Cristiano, N. D’Avanzo, B. Ruozi, C. Mircioiu, D. Cosco, L. Di Marzio and M. Fresta, *ACS Omega*, 2021, **6**, 2973–2989.
- 11 C. Fang, P. Zhang, S. Rajabzadeh, N. Kato and H. Matsuyama, *Colloids and Surfaces A: Physicochemical and Engineering Aspects*, 2021, **611**, 125885.
- 12 T. Nakagawa and K. Shinoda, in *Colloidal Surfactants: Some Physicochemical Properties*, ed. E. M. Loebel, Academic Press Inc., 1963, pp. 97–178.
- 13 E. J. Staples and G. J. T. Tiddy, *Journal of the Chemical Society, Faraday Transactions 1: Physical Chemistry in Condensed Phases*, 1978, **74**, 2530–2541.
- 14 O. Glatter, G. Fritz, H. Lindner, J. Brunner-Popela, R. Mittelbach, R. Strey and S. U. Egelhaaf, *Langmuir*, 2000, **16**, 8692–8701.
- 15 J. Eastoe, in *Colloid Science: Principles, methods and applications*, ed. T. Cosgrove, Blackwell Publishing, Bristol, First Edi., 2005, p. 63.
- 16 K. S. Sharma, S. R. Patil and A. K. Rakshit, *Colloids and Surfaces A: Physicochemical and Engineering Aspects*, 2003, **219**, 67–74.
- 17 Ç. Batigöç, H. Akbaş and M. Boz, *Journal of Chemical Thermodynamics*, 2011, **43**, 1800–1803.

- 18 M. Hajy Alimohammadi, S. Javadian, H. Gharibi, A. R. Tehrani-Bagha, M. R. Alavijeh and K. Kakaei, *Journal of Chemical Thermodynamics*, 2012, **44**, 107–115.
- 19 K. Glenn, A. van Bommel, S. C. Bhattacharya and R. M. Palepu, *Colloid and Polymer Science*, 2005, **283**, 845–853.
- 20 H. Schott, *Journal of Pharmaceutical Sciences*, 1969, **58**, 1443–1449.
- 21 X. Zhong, C. Li, Y. Li, H. Pu, Y. Zhou and J. X. Zhao, *Energy and Fuels*, , DOI:10.1021/acs.energyfuels.9b04067.
- 22 H. H. Abdel Ghafar, E. K. Radwan and S. T. El-Wakeel, *ACS Omega*, 2020, **5**, 6834–6845.
- 23 A. Rodríguez, M. del Mar Graciani, A. J. Moreno-Vargas and M. L. Moyá, *Journal of Physical Chemistry B*, 2008, **112**, 11942–11949.
- 24 M. Laurenti, J. R. Retama, F. G. Blanco and E. L. Cabarcos, *Langmuir*, 2008, **24**, 13321–13327.
- 25 F. A. Maulvi, A. R. Desai, H. H. Choksi, R. J. Patil, K. M. Ranch, B. A. Vyas and D. O. Shah, *International Journal of Pharmaceutics*, 2017, **524**, 193–204.
- 26 C. A. Zentner, F. Anson, S. Thayumanavan and T. M. Swager, *Journal of the American Chemical Society*, 2019, **141**, 18048–18055.
- 27 K. Aramaki, M. Fujii and Y. Sakanishi, *Colloids and Surfaces A: Physicochemical and Engineering Aspects*, 2019, **581**, 123841.
- 28 P. C. Griffiths, I. A. Fallis, D. J. Willock, A. Paul, C. L. Barrie, P. M. Griffiths, G. M. Williams, S. M. King, R. K. Heenan and R. Görgl, *Chemistry - A European Journal*, 2004, **10**, 2022–2028.
- 29 P. C. Griffiths, I. A. Fallis, T. Tatchell, L. Bushby and A. Beeby, *Advances in Colloid and Interface Science*, 2008, **144**, 13–23.
- 30 P. C. Griffiths, I. A. Fallis, T. Chuenpratoom and R. Watanesk, *Advances in Colloid and Interface Science*, 2006, **122**, 107–117.
- 31 Charles Tanford, *The Journal of Physical Chemistry*, 1972, **76**, 3020–3024.
- 32 R. C. Oliver, J. Lipfert, D. A. Fox, R. H. Lo, S. Doniach and L. Columbus, *PLoS ONE*, 2013, **8**, 62488.
- 33 J. Aguiar, P. Carpena, J. A. Molina-Bolívar and C. Carnero Ruiz, *Journal of Colloid and Interface Science*, 2003, **258**, 116–122.
- 34 J. E. Newbery, *Colloid and Polymer Science Kolloid Zeitschrift & Zeitschrift für Polymere*, 1979, **257**, 773–775.
- 35 A. Chattopadhyay and K. G. Harikumar, *FEBS Letters*, 1996, **391**, 199–202.
- 36 E. Fuguet, C. Ràfols, M. Rosés and E. Bosch, *Analytica Chimica Acta*, 2005, **548**, 95–100.

- 37 K. Hara, H. Kuwabara, O. Kajimoto and K. Bhattacharyya, *Journal of Photochemistry and Photobiology A: Chemistry*, 1999, **124**, 159–162.
- 38 S. K. Mehta, K. K. Bhasin, R. Chauhan and S. Dham, *Colloids and Surfaces A: Physicochemical and Engineering Aspects*, 2005, **255**, 153–157.
- 39 J. Iyer and D. Blankschtein, *Journal of Physical Chemistry B*, 2012, **116**, 6443–6454.
- 40 C. Dupuy, X. Auvray, C. Petipas, R. Anthore, F. Costes, I. Rico-Lattes and A. Lattes, *Langmuir*, 1996, **12**, 3162–3172.
- 41 J. Eastoe and R. F. Tabor, in *Colloidal Foundations of Nanoscience*, eds. D. Berti and G. Palazzo, Elsevier, First Edi., 2014, pp. 135–157.
- 42 Duncan J. Shaw, in *Introduction to Colloid & Surface Chemistry*, Elsevier Science, Fourth Edi., 1992, pp. 262–276.
- 43 D. G. Hayes, R. Ye, R. N. Dunlap, D. B. Anunciado, S. V. Pingali, H. M. O'Neill and V. S. Urban, *Biochimica et Biophysica Acta - Biomembranes*, 2018, **1860**, 624–632.
- 44 M. Trotta, F. Pattarino and G. Grosa, *International Journal of Pharmaceutics*, 1998, **174**, 253–259.
- 45 R. G. Alany, T. Rades, S. Agatonovic-Kustrin, N. M. Davies and I. G. Tucker, *International Journal of Pharmaceutics*, 2000, **196**, 141–145.
- 46 S. Friberg, in *Microemulsions Theory and Practice*, ed. L. M. Prince, Academic Press Inc., New York, 1977, pp. 133–148.
- 47 D. Langevin, *Molecular Crystals and Liquid Crystals*, 1986, **138**, 259–305.
- 48 R. Aveyard, B. P. Binks and J. Mead, *Journal of the Chemical Society, Faraday Transactions 1: Physical Chemistry in Condensed Phases*, 1987, **83**, 2347–2357.
- 49 Y. Nan, W. Li and Z. Jin, *Langmuir*, 2020, **36**, 5198–5207.
- 50 H. Jia, Y. Song, D. Jiang, L. Xing, X. Leng, Y. Zhu, J. An, A. Dong, C. Jia and H. Zhou, *Colloids and Surfaces A: Physicochemical and Engineering Aspects*, 2017, **513**, 292–296.
- 51 M. Sun, Y. Wang and A. Firoozabadi, *Energy and Fuels*, 2012, **26**, 5626–5632.
- 52 E. Koenigs, K. Köhler and K. Blindow, *Ber. Dtsch. Chem. Ges.*, 1925, **58**, 933–940.
- 53 J. Epstein, R. W. Rosenthal and R. J. Ess, *Analytical Chemistry*, 1955, **27**, 1435–1439.
- 54 C. R. Turner, *The Analyst*, 1974, **99**, 431–434.
- 55 C. T. Bedford and J. Robinson, *Xenobiotica*, 1972, **2**, 307–337.
- 56 M. E. Getz and R. R. Watts, *Journal of Association of Official Agricultural Chemists*, 1964, **47**, 1094–1096.

- 57 R. Preussman, H. Schneider and F. Epple, *Arzneimittel-Forsch.*
- 58 I. A. Fallis, P. C. Griffiths, T. Cosgrove, C. A. Dreiss, N. Govan, R. K. Heenan, I. Holden, R. L. Jenkins, S. J. Mitchell, S. Notman, J. A. Platts, J. Riches and T. Tatchell, *J Am Chem Soc*, 2009, **131**, 9746–9755.
- 59 S. Aldrich, Material Safety Data Sheet Database, <https://www.sigmaaldrich.com/GB/en/sds/aldrich/242640>, <https://www.sigmaaldrich.com/GB/en/product/aldrich/242640#>.
- 60 E. Raber, A. Jin, K. Noonan, R. McGuire and R. D. Kirvel, *Int J Environ Health Res*, 2001, **11**, 128–148.
- 61 J. A. Manso, M. T. Pérez-Prior, M. Del Pilar García-Santos, E. Calle and J. Casado, *Chemical Research in Toxicology*, 2005, **18**, 1161–1166.
- 62 J. A. Manso, M. T. Pérez-Prior, M. P. García-Santos, E. Calle and J. Casado, *Journal of Physical Organic Chemistry*, 2008, **21**, 932–938.
- 63 L. T. Sharpe, A. Stockman, W. Jagla and H. Jaägle, *Journal of Vision*, 2005, **5**, 3–3.
- 64 R. A. Mackay and R. P. Seiders, *Journal of Dispersion Science and Technology*, 1985, **6**, 193–207.
- 65 Y. C. Yang, L. L. Szafraniec, W. T. Beaudry and R. J. Way, *Journal of Organic Chemistry*, 1988, **53**, 3293–3297.
- 66 Y. C. Yang, J. A. Baker and J. R. Ward, *Chem. Rev*, 1992, **92**, 1729–1743.

Chapter 3. Self-Assembled Sensors for The Detection of Sulfur Mustards

3.1. Introduction

3.1.1. Merocyanine Dyes

Merocyanine dyes are a class of neutral polymethine dyes discovered by Brooker,^{1,2} where one terminal component is electron donating while the other terminal component is electron withdrawing. The structure of Brooker's merocyanine is illustrated in Figure 3.1.

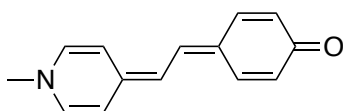


Figure 3.1. Brooker's merocyanine.

The electron accepting/donating capability of these two moieties impacts the electronic structure of the dye and thus its electronic spectrum. Merocyanines display a wide variety of colours in solution and the perceived colour can be influenced by the solvent polarity. Thus, a large number of reported literature has been devoted to understanding the solvatochromic behaviour of merocyanine dyes.³⁻⁷ The solvatochromic behaviour of merocyanines was first observed by Brooker in 1951.⁸ Thus, many of these compounds have found applications as solvent polarity indicators.^{9,10} In general, the λ_{\max} exhibits hypsochromic shifts to shorter wavelengths with increasing solvent polarity. This effect results from the stabilisation of the merocyanine ground state where the dye can exist in two resonance forms, neutral and zwitterionic, as illustrated in Figure 3.2.

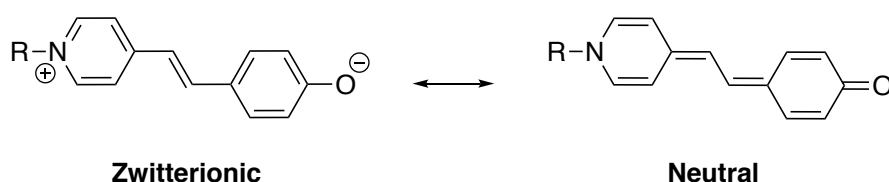


Figure 3.2. Resonance forms exhibited by merocyanine dyes. R = any alkyl chain.

In polar solvents, merocyanines exist in the zwitterionic structure which increases the energy gap between the ground state and excited states which corresponds to and absorption of shorter wavelengths of light. Research into the solvatochromic behaviour of merocyanines suggests that a major factor in the stabilisation of the zwitterion in polar solvents is the hydrogen-bonding interaction between the solvent and the oxygen atom of the dye.^{11,12} Furthermore, large functional groups placed *ortho* with respect to the oxygen atom have been found to reduce this hydrogen bonding through steric effects.¹² On the other hand, merocyanines favour the neutral resonance form in non-polar

solvents and thus longer wavelengths of light are absorbed due to the formation of a fully conjugated species which corresponds to a decrease in the energy gap.

Improving the electron donating ability of the terminal phenolate group by incorporating two tertiary butyl groups *ortho* to the oxygen atom generates more symmetrical electronic spectra with distinct vibrational structure.^{11,13,14}

Merocyanine dyes have large extinction coefficients in the order of $10^4 - 10^5$ L mol⁻¹ cm⁻¹.^{15,16} For example, Brooker's merocyanine has a molar extinction coefficient of 5.4×10^4 L mol⁻¹ cm⁻¹ in water.⁹ Owing to these large extinction coefficients, merocyanine dyes have found many applications in biology and medicine as stains for measuring cellular membrane potentials.^{17,18} Furthermore, merocyanine dyes have been applied in dye-sensitised solar cells as they are easily polarisable due to their dipole moments.¹⁹⁻²¹

3.1.2. Dye-Surfactant Interactions

The electronic spectral changes of merocyanine dyes in micellar media have been a widely researched topic.²²⁻²⁵ It has been reported that merocyanine dyes can form complexes with oppositely charged surfactants through electrostatic interactions. On the other hand, the absence of such interactions is observed for similarly charged dye and surfactant molecules as a consequence of electrostatic repulsion.^{26,27} However, the strong hydrophobic effect of merocyanine dyes has been shown to overcome these electrostatic interactions.

The spectroscopic behaviour of merocyanine dyes in anionic and cationic microemulsions has been investigated by Shah and Minch.²⁵ Sodium dodecyl sulfate and hexadecyltrimethylammonium bromide solutions were used to investigate the spectral changes of 1-alkyl-4-[(oxocyclohexadienylidene)ethylidene]-1,4-hydropyridines with varying chain lengths from methyl to decyl. The general structure of the merocyanine dyes is illustrated in Figure 3.3.

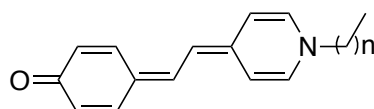


Figure 3.3. The general structure of 1-alkyl-4-[(oxocyclohexadienylidene)ethylidene]-1,4-hydropyridines investigated by Shah and Minch. $n = 0 - 9$.

The spectral shifts observed for merocyanine dyes in micelle solutions varied with solvent polarity. Thus, changes in the electronic spectra can be used to predict the location of the dyes in the micellar environment. For example, the dye can be in one of two environments; adsorbed on or near the surface or localised in the micelle droplet. Interestingly, a bathochromic shift was observed in all cases upon incorporation of the dye into micelles. This spectral shift to longer wavelengths was attributed to an increase in the localisation of dye molecules into micelles. Increasing the alkyl chain length generated more hydrophobic dyes which displayed pronounced bathochromic shifts in the electronic spectra. Additionally, more hydrophobic dyes were found to induce micellisation of both anionic and cationic surfactants which suggests that dyes with longer alkyl chains interact more strongly with surfactant molecules compared to their more hydrophilic analogues. However, it is difficult to attribute dye-surfactant interactions to a single force as there are many forces working in parallel including the combined effect of the change in microenvironment upon deaggregation of dye molecules^{28,29}, localisation of the merocyanine within the hydrophobic micellar core³⁰, electrostatic interactions³¹ and charge-transfer interactions between donor and acceptor functional groups^{32,33}.

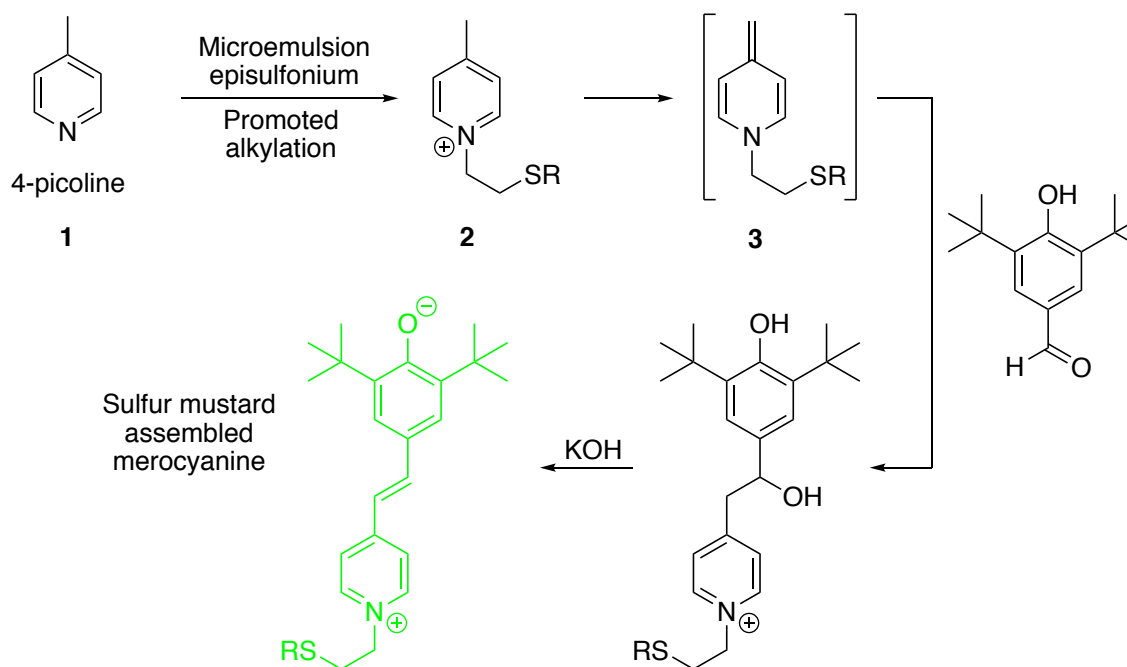
3.2. Aims

The purpose of this work was to devise a self-assembled sensor for sulfur mustard vesicants that may be used at point-of-use by non-experts (e.g. war-fighters and first-responders). There have been few reported *in-situ* sensors for chemical warfare agents with the majority involving the formation of a chemosensor via a cyclisation reaction.³⁴⁻³⁷ Most of these sensors have been designed for organophosphorus detection thus, there is an urgent requirement for mustard-selective probes. However, elevated temperatures are often required for the sensing mechanism to occur which restricts the field applications of these probes. In this work, we aim to build upon this research to develop a colorimetric sensor that can self-assemble from a reagent mixture at ambient temperature.

3.3. Results and Discussion

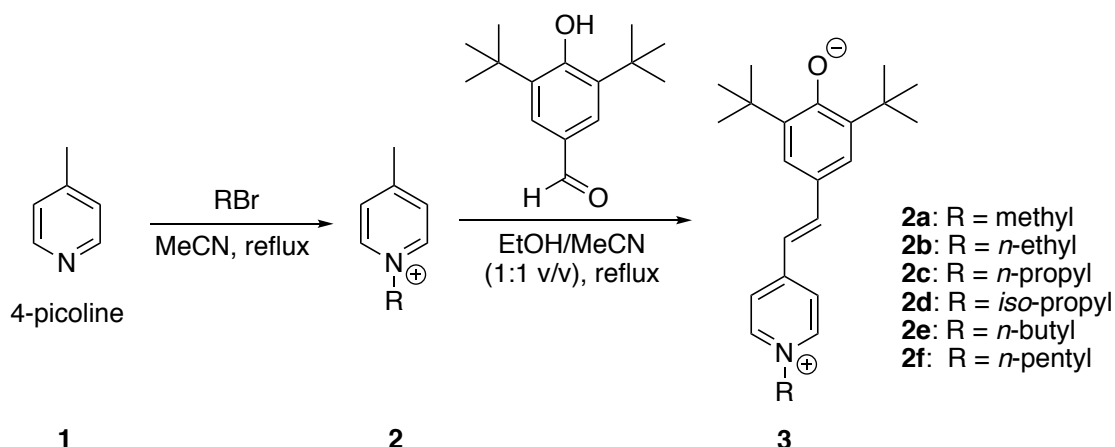
3.3.1. Self-Assembled Sensors

To improve on the selectivity of commercially available chemical detection papers, an alternative colorimetric system was explored whereby the analyte drives the assembly of the dye. Thus, this self-assembled sensor (SAS) is generated via a cascade synthesis triggered by the detection of a target hazardous chemical. Merocyanines, a class of dyes defined by their (poly)methine structures, were chosen as SAS molecules as these dyes are often intensely coloured with large extinction coefficients. Brooker's merocyanine is a well-known dye notable for its solvatochromic properties and as a result, has been extensively used as a solvent polarity indicator.³⁸ It was postulated that the formation of sulfur mustard derived episulfonium species in microemulsions could be exploited to drive the formation of a merocyanine system (Scheme 3.1). It was suggested that the alkylation of 4-picoline **1** by the analyte in an alkaline microemulsion generates first the pyridinium species **2** which upon deprotonation yields the reactive intermediate **3**. Reaction within the microemulsion with the hydroxy-benzaldehyde **4** generates the benzylic pyridinium phenol **5** which upon dehydration yields the desired colorimetric response, namely the merocyanine dye **6**. The hindered lipophilic aldehyde **4** was chosen to suppress alkylation at the phenol site and ensure partitioning of the aldehyde into the microemulsion droplets. Preliminary work (Prof Ian Fallis, private communication) indicates a red colour response with this system (**1** + **4** in pH = 12 SDS-5T), however, repeats of this experiment gave variable results (mass spectra indicated trace reaction products). While further work is needed in this area, we felt it would be informative to prepare some simple merocyanines to compare their spectroscopic properties to the dihydropyridine dyes obtained by NBP alkylation.



Scheme 3.1. Proposed analyte driven assembly of a merocyanine dye from 4-picoline.

To examine the potential of merocyanines, several non-mustard derived dyes of this class was prepared (Scheme 3.2). In a general method 4-picoline (1) was first alkylated to yield 1-alkyl-4-methylpyridinium bromides (2). Subsequent reaction in EtOH/MeCN solution with one equivalent of 3,5-di-tert-butyl-4-hydroxybenzaldehyde under reflux conditions affords the **hydrated form**. Alkaline work-up afforded the target merocyanines in modest to good yields.



Scheme 3.2. Synthetic route for the production of merocyanine dyes.

In the case of R = Et (Scheme 2.9), crystals of **2b** suitable for single-crystal X-ray diffraction were grown by slow evaporation of an acetone solution (~ 100 mL) over 72 h. Upon data collection and refinement, the solid-state structure was found to crystallise in

the monoclinic space group $P2_{1/c}$ with one molecule in the asymmetric unit (Z'); increasing to four molecules in the unit cell (Z).

3.3.2. X-Ray Structure of Alkylated Merocyanine Dye

Compound **2b** was obtained as an attractive green crystal with a yellow-gold reflex (Figure 3.1 (a)). The compound has a typical Brooker's merocyanine structure with an essentially co-planar central chromophore (Figure 2.46 (b)) and all bond lengths and angles were typical for this type of structure (Appendix, Table 1). Interestingly an examination of the packing diagram (Figure 2.46 (c)) revealed a head-to-tail dimerisation of the dye molecules, presumably driven by electrostatic forces. These dimers are in turn packed into H-bonded chains in an alternating herringbone pattern. No other significant packing interactions were found in the structure.

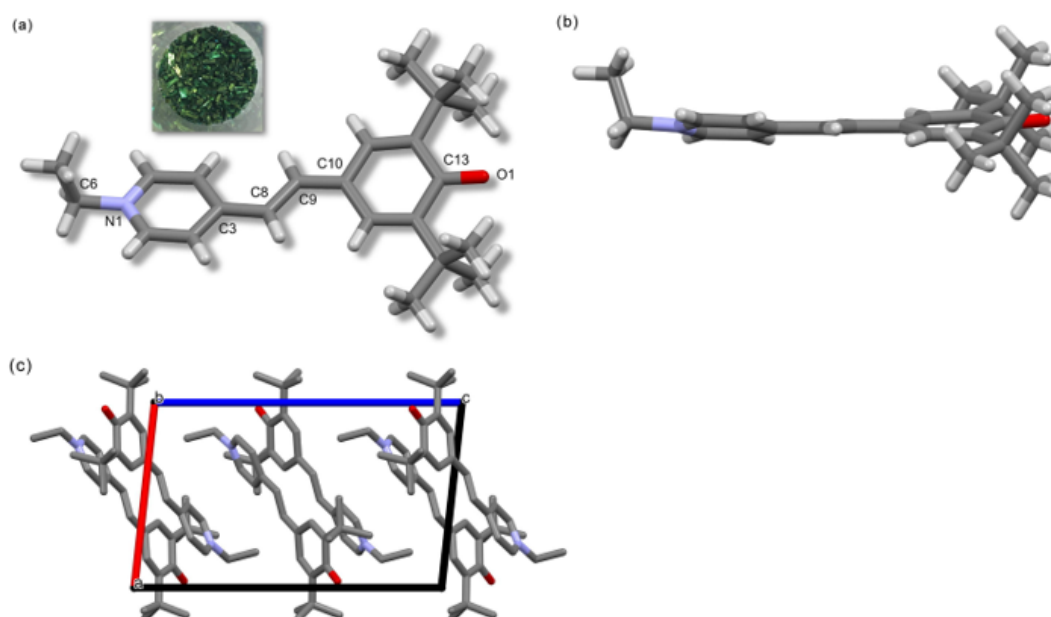
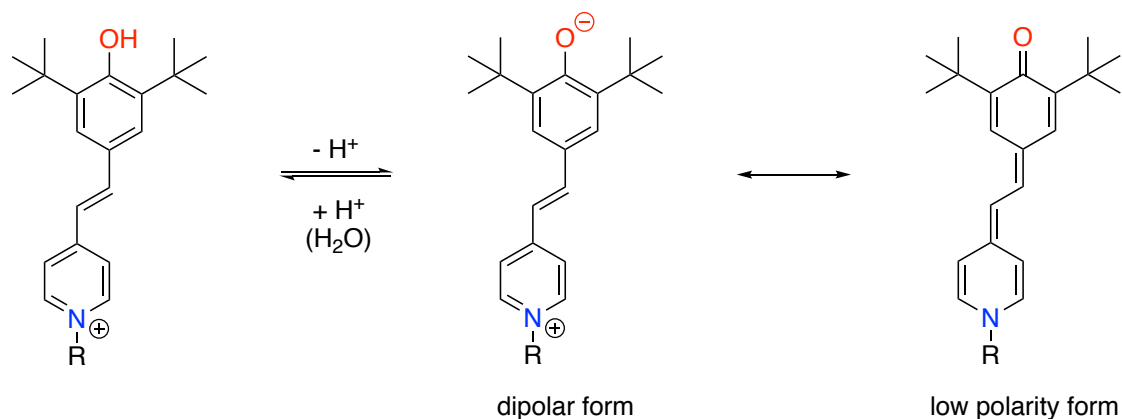


Figure 3.1. a) Crystal structure of the merocyanine dye **2b**; b) planarity of the crystal structure; c) packing diagram showing dimerization of the dye molecules.

3.3.3. Electronic Spectra of Merocyanines

The electronic spectra of a range of merocyanines were determined in toluene, chloroform, acetonitrile and methanol solution (Scheme 3.3 and Figure 3.2). It is apparent from these spectra that in common with other merocyanines these are highly solvatochromic.³⁹ In common with the parent compound Brooker's merocyanine these compounds display red absorption in low polarity media with the absorption shifting to shorter wavelengths in more polar media. Thus, in chloroform or toluene, we observe complex manifolds centred around 575 nm whilst in methanol the main absorption occurs at 395 nm for all the derivatives measured. Of note is the comparison of the spectra of methanol and acetonitrile. Here, and despite having a higher relative permittivity, the acetonitrile spectrum remains predominantly red adsorbing. We attribute this difference to the protonation of the merocyanine (Scheme 3.3) generating the protonated form in methanol arising from water in the solvent, while this occurs to a lesser extent in acetonitrile which has lower water content.



Scheme 3.3. (Top) Merocyanines in this study; (Bottom) resonance forms of merocyanines in media of differing polarities and the effect of protonation from methanol.

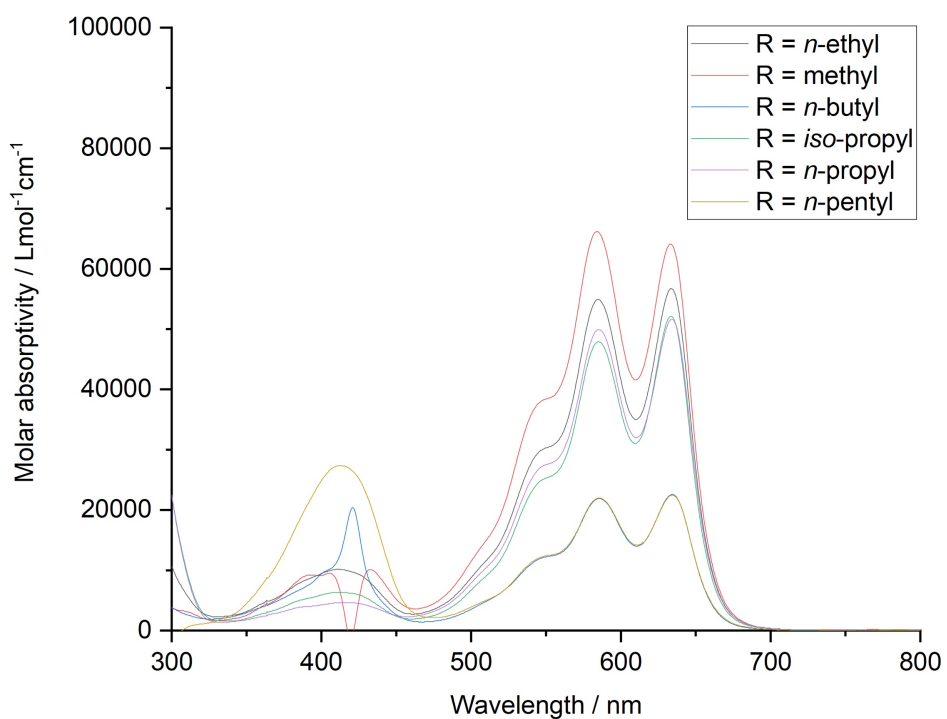
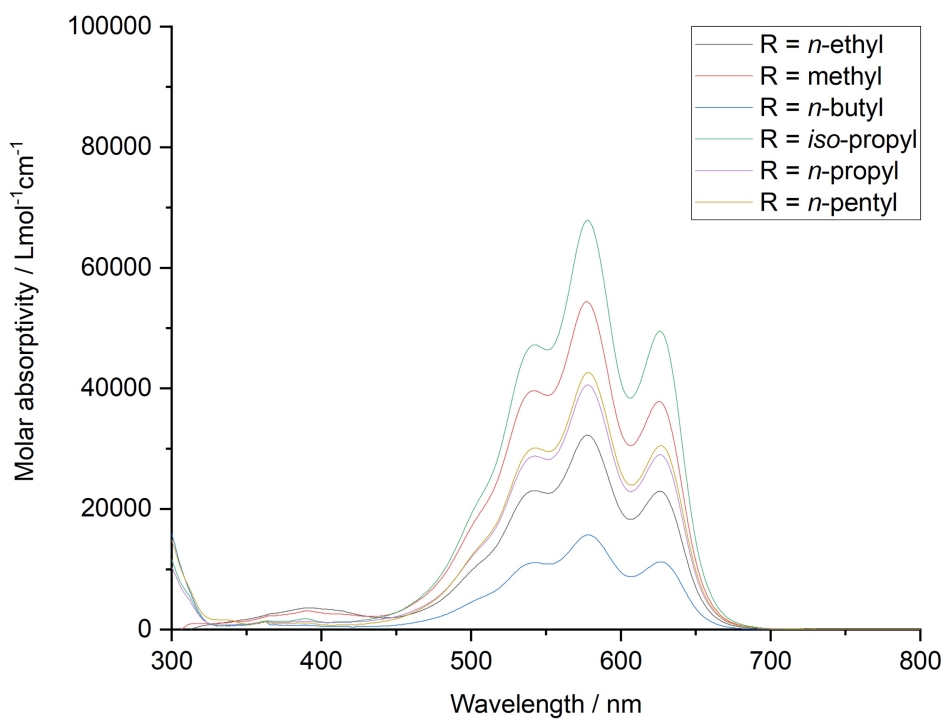


Figure 3.2a. Electronic spectra of mercyanines in solvents of differing polarity. Toluene (top) and chloroform (bottom). ϵ_r = relative permittivity (dielectric constant). ϵ_r = 2.38 (toluene) and 4.81 (CHCl_3)

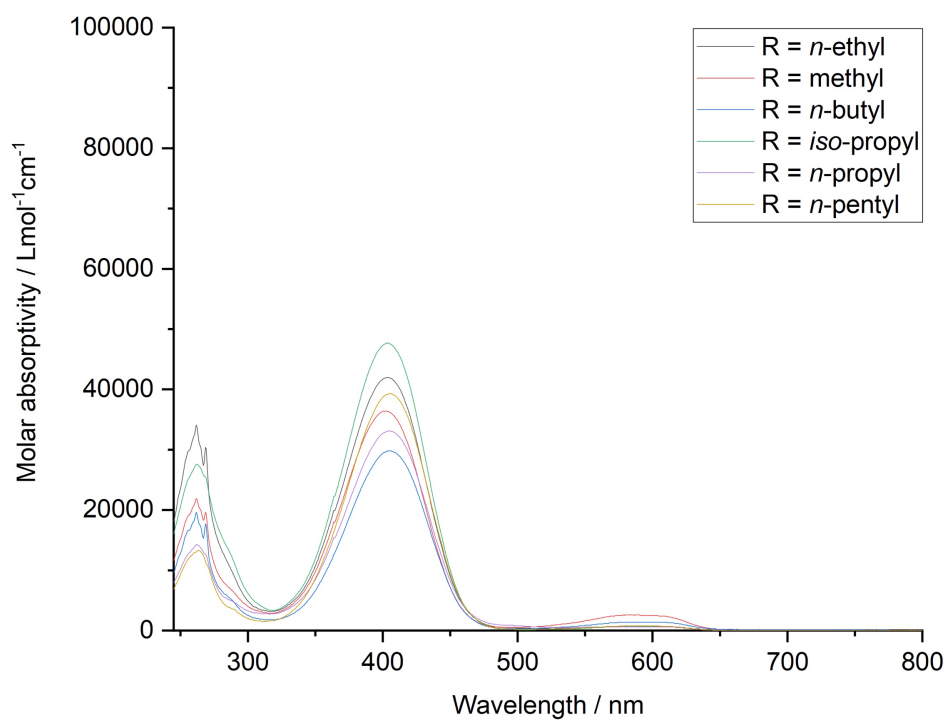
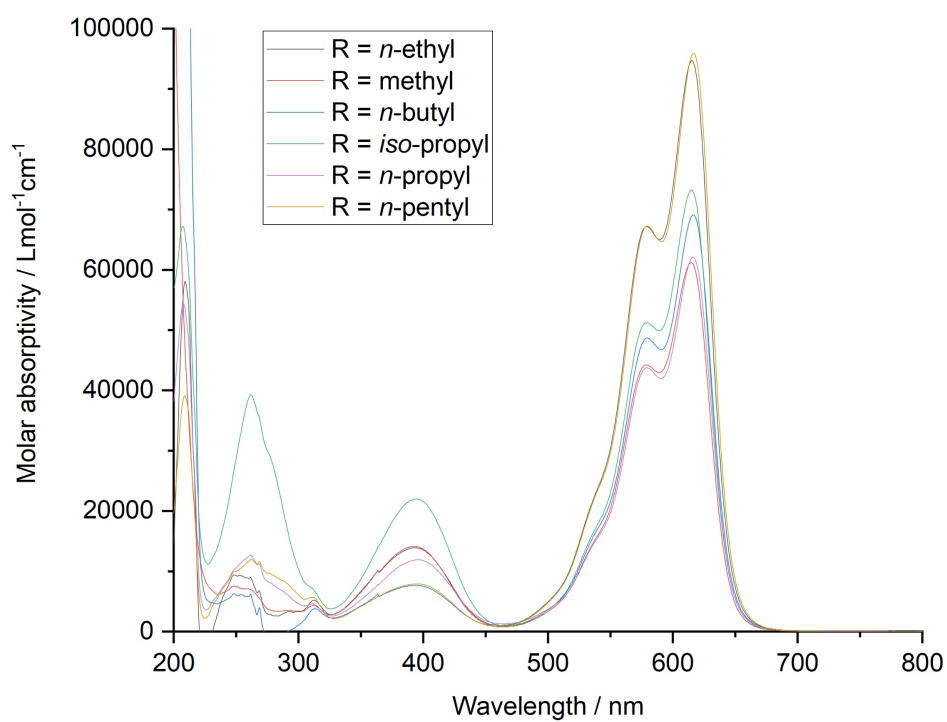
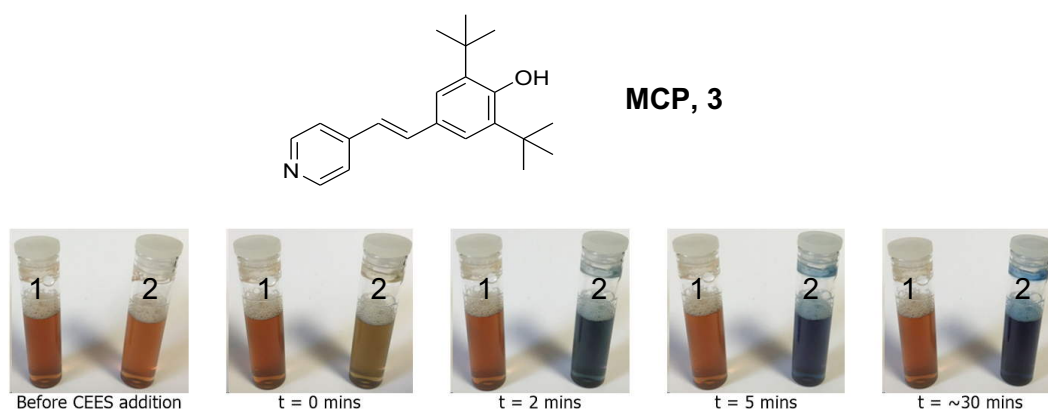


Figure 3.2b. Electronic spectra of merocyanines in solvents of differing polarity. Acetonitrile (top) and methanol (bottom). ϵ_r = relative permittivity (dielectric constant). ϵ_r = 32.6 (MeOH) and 36.6 (MeCN).

3.3.4. *In-Situ* Merocyanine Formation

Given the challenges of assembling a sensor *in-situ* from a phenolic aldehyde and an episulfonium alkylated picoline, we attempted the 'semi *in-situ*' synthesis. The merocyanine precursor illustrated in Figure 2.48 was dispersed in SDS-5T and exposed to CEES as an analyte. On all occasions, these solutions were somewhat cloudy, even after filtration, precluding the use of UV-vis spectroscopy due to scattering. However, it was apparent from visual inspection that reaction to form the merocyanine dye was taking place (Figure 3.3). Here we observe a slow but characteristic blue colour change indicated. Unfortunately, attempts at purifying this precursor (**MCP, 3**) failed to result in a strongly yellow-brown coloured analyte free solution. This colouration is likely to arise not only from the impure nature of the sample but also from the intrinsic colour of the pyridyl vinyl phenolate chromophore.



Component	Vial 1 (control)	Vial 2
Merocyanine precursor (MCP, 3)	5 mg	5 mg
SDS-5T (pH 12)	3000 μ L	3000 μ L
CEES		2

Figure 3.3. Performance of SDS-5T (pH 12) microemulsion system with the 2,6-di-*tert*-butyl-4-((*E*)-2-(pyridine-4-yl)vinyl)phenol merocyanine precursor. Notes: a) Note the blue colour of the sample vials indicating red absorption, hence localisation within the microemulsion core. b) Note the cloudiness of the sample, even after filtration.

3.3.5. An Alternative Self-Assembled Sensor (SAS)

The general observation that pyridines are rapidly *N*-alkylated by sulfur mustards in microemulsion media prompted the investigation of an alternative commercial-off-the-shelf formulation of a self-assembled sensor system (Figure 3.4). This system has the 4-picoline (**1**) reagent in common with that above and progresses through the same alkyl

pyridinium and the methyldene dihydropyridine intermediates **2** and **3**. The aldehyde acceptor has been replaced with 4-(dimethylamino)-benzaldehyde (**4**) with the intent of forming N-alkyl dimethylamino aza-stilbene chromophore (**6**) via its hydrate **5**.

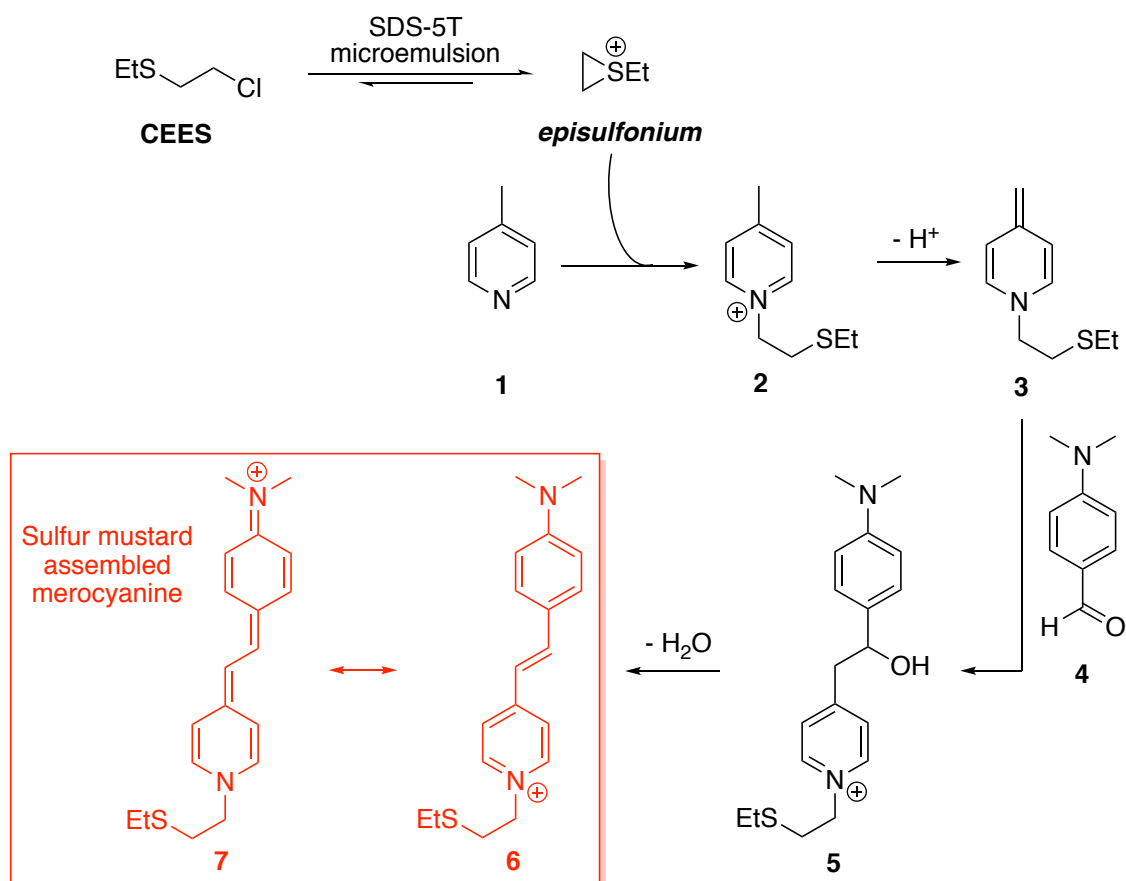


Figure 3.4. The proposed mechanism in situ of dye formation from 4-(dimethylamino)-benzaldehyde in an anionic microemulsion system.

The initial reaction of 4-picoline, 4-Me₂NC₆H₄CHO and CEES in an alkaline (pH 12) SDS-5T microemulsion gives an immediate red colour which grows in intensity over time after analyte addition and moderate agitation. The electronic spectra of this system and a control sample are illustrated in Figure 2.50. Here the control consists of a mixture of 4-picoline and CEES in an alkaline (pH 12) SDS-5T microemulsion. Only the sample containing the 4-Me₂NC₆H₄CHO reagent yields a positive response as indicated by the strong absorption in the blue part of the spectrum. Dilutions of this system with water remain blue absorbing, but the maximum in the visible spectrum shifts slightly towards the red region of the spectrum, indicative of a dipolar chromophore being exposed to an increasing polar medium. This implies that the merocyanine dye formed (resonance structures **6** and **7** in Figure 3.4) initially resides within the droplet cores, as expected

based on its cationic charge and likely lipophilicity. Unfortunately, the λ_{max} observed in this system (482 nm) is considerably shifted from the photopic maximum and hence the colour perceived is not as strong as that observed for the NBP system. The absorbance spectra of the *in-situ* formation of merocyanine from 4-picoline are illustrated in Figure 3.5.

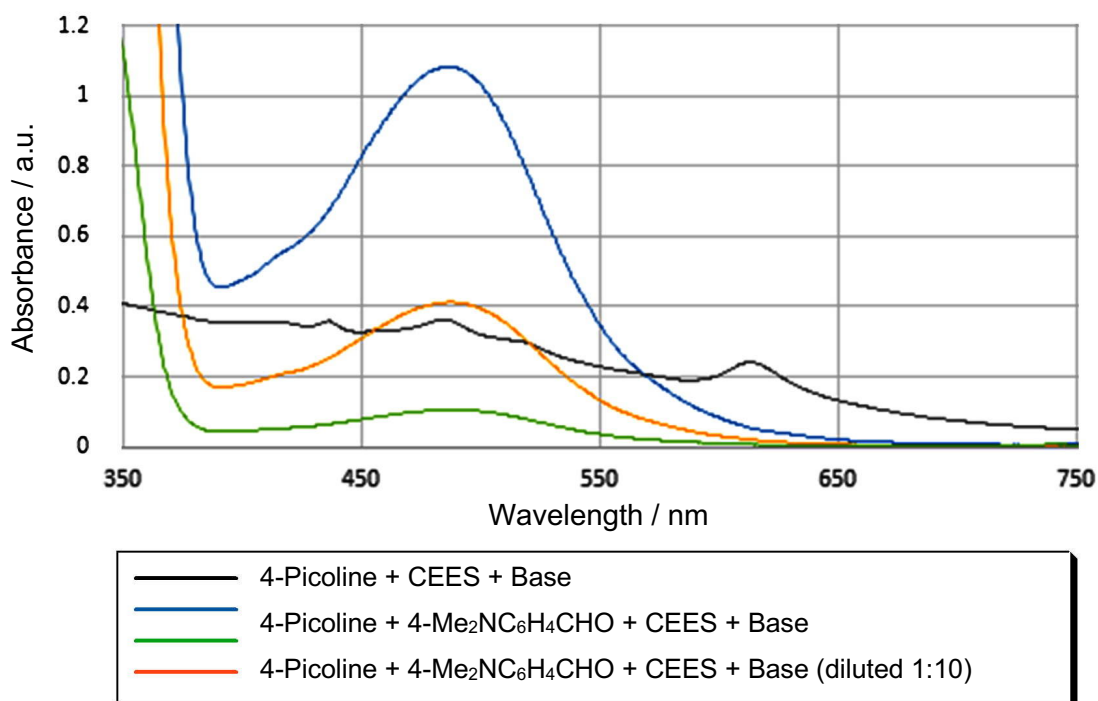


Figure 3.5. *In-situ* merocyanine formation from 4-picoline (10 μL) + 4-Me₂NC₆H₄CHO (10 mg) + CEES (5 μL) + base (NaOH to pH = 12) in SDS-5T. Note the slight shift in the maximum for the SAS merocyanine upon dilution indicating a change in microemulsion structure. The base + picoline + CEES control (black trace) has been scaled to reveal detail. Figure supplied by Prof. Ian Fallis and Dr Andrew Wood.

To verify that the merocyanine was being formed *in-situ*, ESI MS (+ve mode) spectra were analysed, an example of which is presented in Figure 3.6. Most rewardingly we observe that the base peak, even higher in intensity than the usually observed SDS sodium ion adducts, in the spectrum corresponds to the desired dye product (**6**, **7**). This is indicative that indeed the assembly of the dye has been promoted by the addition of the analyte. Reassuringly we also observed the protonated precursors 4-picoline (**1**) and 4-(dimethylamino)benzaldehyde (**4**). The absence of a peak for alkylated picoline in the mass spectrum is interesting as this species was clearly seen previously at m/z 182.14 in the preliminary mass spectrometry studies of various weak acids. This suggests that

the formation of the merocyanine dye is fast compared to the alkylation of 4-picoline by simulant. While it is not possible from this data to extract a conversion of analyte into the product, it seems likely that the extent of reaction is substantial and may prove useful in future studies.

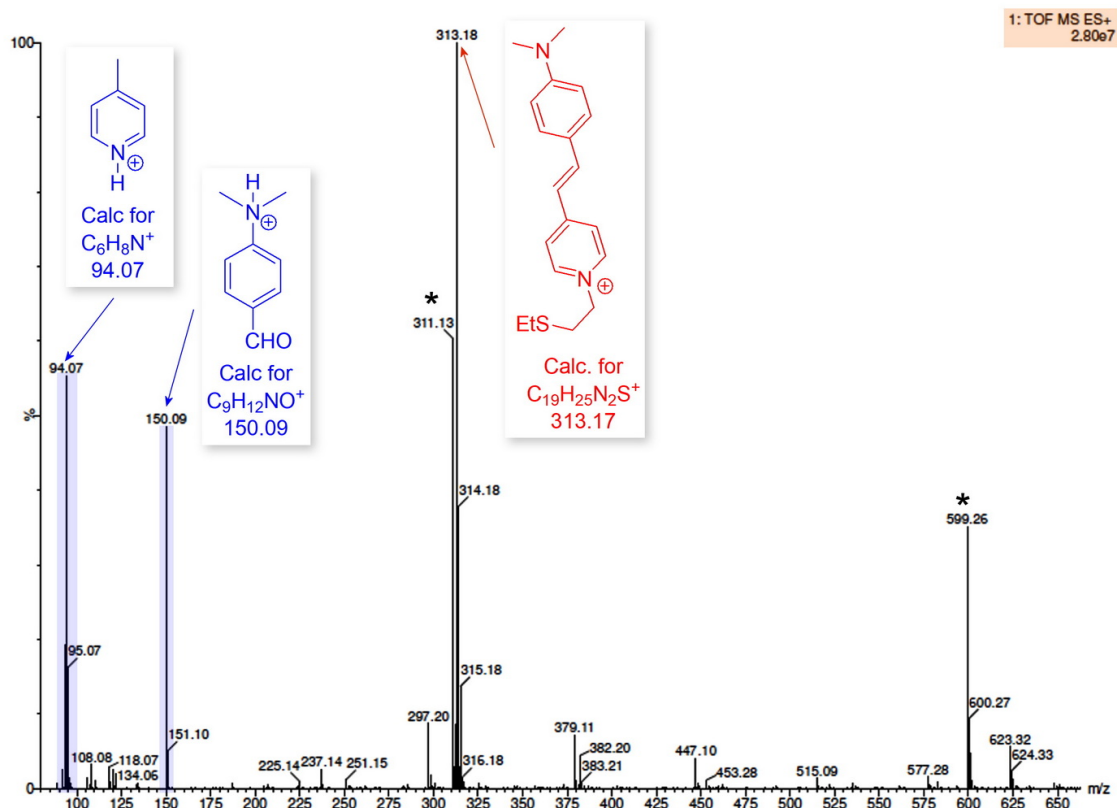


Figure 3.6. ESI MS (+ve mode) of 4-picoline + 4-Me₂NC₆H₄CHO + CEES + base in SDS-5T after 10 minutes with the reaction quenched by dilution with methanol. Note that the target cyanine dye is the base peak and the high ion count. *Clusters arising from the surfactant are marked. Figure supplied by Prof. Ian Fallis and Dr Andrew Wood.

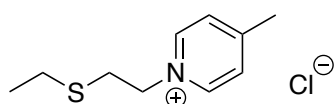
3.5. Experimental

Reagents were purchased from commercial suppliers and used as received without further purification unless stated otherwise. ¹H and ¹³C NMR spectra were run on Bruker Ultrashield FT-NMR spectrometers with a field strength of 300 MHz. NMR chemical shifts (δ) are reported in ppm and are referenced to the residual solvent signal. Spin-spin coupling constants *J* are given in Hz. Mass spectra were performed by the Analytical Services staff at Cardiff University School of Chemistry on a Waters Xevo G2-XS QToF mass spectrometer. UV-vis studies were performed on an Agilent Technologies Cary 60 UV-vis spectrophotometer using quartz cells.

3.5.1. Procedure for simulant and analyte testing

Prior to testing formulations with simulant or other toxic analytes, a bleach bath must be prepared to decontaminate all equipment and glassware that come in contact with hazardous chemicals during testing experiments. This decontaminating solution is prepared with thick bleach, IPA and water in a 1:1:2 ratio with NaOH pellets to maintain a high pH. Furthermore, coloured crepe paper is attached to the fume hood sash to demonstrate the level of extraction. Testing involving simulants should always be conducted with a supervisor or other qualified person in attendance. A glass petri dish is utilised as a secondary container to store the simulant bottle. In addition to standard laboratory PPE, two pairs of gloves of opposing colours are worn to handle simulants in order to identify any tears in the material. Once the stimulant has been carefully added to the formulation and the necessary equipment contaminated in the bleach bath, gloves are inspected for contamination. If contaminated, the gloves are placed in the bleach bath for decontamination.

3.5.2. Synthesis of 1-(2-(Ethylthio)ethyl)-4-methylpyridinium chloride (1a)



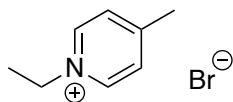
Tetraethyl ammonium iodide (0.062 g, 0.24 mmol) was dissolved in acetonitrile (5 mL) with heating. 4-picoline (2.34 mL, 24.1 mmol) and 2-chloroethyl ethyl sulfide (2.80 mL, 24.1 mmol) were added to the solution. The reaction mixture was heated at reflux in a pressure tube for 24 hours. The reaction was allowed to cool to room temperature. The residue was washed with petroleum ether, the mixture was then sonicated, and the solvent was decanted off. This was repeated twice to remove excess 2-chloroethyl ethyl sulfide. The dark brown oil was purified by Kugelrohr distillation at 50 °C for 2 hours (2.891 g, 13.3 mmol, 55 %). **¹H NMR** (400 MHz, MeCN-*d*₃) δ_{H} (ppm) = 9.09 (d, *J* = 6.7 Hz, 1H, Ar-**H**), 7.86 (d, *J* = 6.4 Hz, 2H, Ar-**H**), 4.86 (t, *J* = 6.6 Hz, 2H, RN-**CH**₂-), 3.13 (t, *J* = 6.6 Hz, 2H, RN-**CH**₂-**CH**₂-), 2.60 (q, *J* = 7.4 Hz, 2H, RN-**CH**₂-**CH**₂-**S-CH**₂), 2.61 (s, 3H, Ar-**CH**₃), 1.17 (t, *J* = 7.4 Hz, 3H, RN-**CH**₂-**CH**₂-**S-CH**₂-**CH**₃). **¹³C NMR** (400 MHz, MeCN-*d*₃) δ_{C} (ppm) = 160.83, 145.20, 129.14, 60.11, 32.85, 26.11, 22.14, 15.00. **HRMS (ES⁺)** found *m/z* 182.1008, calculated *m/z* 182.1003 for [C₁₀H₁₆NS⁺].

General Procedure 1. Synthesis of Pyridinium Salts

4-picoline (1.04 mL, 10.7 mmol) and alkyl halide (12.8 mmol) were dissolved in acetonitrile (10 mL) and heated at reflux for 24 h. The reaction was allowed to cool to

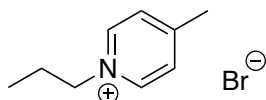
room temperature and the volatiles removed *in vacuo* to give an orange-pink oil. The crude product was dissolved in minimum dichloromethane and triturated with hexane to give an off-white solid.

Synthesis of 1-Ethyl-4-methylpyridinium bromide (1b)



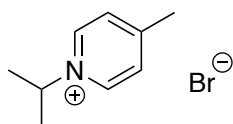
Compound **1b** was synthesised according to *General Procedure 1* using bromoethane (0.96 mL, 12.8 mmol). Yield: 1.961 g, 9.48 mmol, 89 %. **¹H NMR** (400 MHz, DMSO-*d*₆) δ_{H} (ppm) = 9.07 (2H, d, $^3J_{\text{HH}} = 6.7$ Hz, Ar-**H**), 8.01 (2h, d, $^3J_{\text{HH}} = 6.3$ Hz, Ar-**H**), 4.62 (2H, q, $^3J_{\text{HH}} = 7.3$ Hz, R-N-**CH**₂-), 2.60 (3H, s, Ar-**CH**₃), 1.49 (3H, t, $^3J_{\text{HH}} = 7.3$ Hz, R-N-**CH**₂-**CH**₃). **¹³C NMR** (101 MHz, DMSO-*d*₆) δ_{C} (ppm) = 158.55, 143.49, 128.26, 55.28, 21.31, 16.32. **LRMS (ES+)** found *m/z* 122.10 calculated *m/z* 122.10 for [C₈H₁₂N⁺].

Synthesis of 1-Propyl-4-methylpyridinium bromide (1c)



Compound **1c** was synthesised according to *General Procedure 1* using 1-bromopropane (0.96 mL, 12.8 mmol). Yield: 1.081 g, 7.94 mmol, 62 %. **¹H NMR** (400 MHz, MeCN-*d*₃) δ_{H} (ppm) = 9.11 (2H, d, $^3J_{\text{HH}} = 6.7$ Hz, Ar-**H**), 7.87 (2H, d, $^3J_{\text{HH}} = 6.4$ Hz, Ar-**H**), 4.64 (2H, t, $^3J_{\text{HH}} = 7.4$ Hz, R-N-**CH**₂-), 2.56 (3H, s, Ar-**CH**₃), 1.89 (2H, h, $^3J_{\text{HH}} = 7.3$ Hz, R-N-**CH**₂-**CH**₂-), 0.83 (3H, t, $^3J_{\text{HH}} = 7.4$ Hz, R-N-**CH**₂-**CH**₂-**CH**₃). **¹³C NMR** (101 MHz, MeCN-*d*₃) δ_{C} (ppm) = 159.46, 143.23, 128.84, 59.91, 22.12, 19.09, 13.1. **LRMS (ES+)** found *m/z* 136.11 calculated *m/z* 136.11 for [C₉H₁₄N⁺].

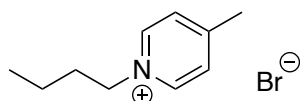
Synthesis of 1-Isopropyl-4-methylpyridinium bromide (1d)



Compound **1d** was synthesised according to *General Procedure 1* using 2-bromopropane (1.20 mL, 12.8 mmol). Yield: 1.370 g, 6.34 mmol, 59 %. **¹H NMR** (400 MHz, MeCN-*d*₃) δ_{H} (ppm) = 9.14 (2H, d, $^3J_{\text{HH}} = 6.8$ Hz, Ar-**H**), 7.89 (2H, d, $^3J_{\text{HH}} = 6.4$ Hz, Ar-**H**), 5.12 (1H, hept, $^3J_{\text{HH}} = 6.7$ Hz, R-N-**CH**-), 2.60 (3H, s, Ar-**CH**₃), 1.62 (6H, d, $^3J_{\text{HH}} =$

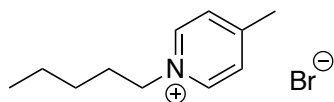
6.8 Hz, R-N-CH-(CH₃)₂). ¹³C NMR (101 MHz, MeCN-d₃) δ_C (ppm) = 160.37, 142.96, 129.42, 64.54, 22.93, 21.86. LRMS (ES+) found m/z 136.11 calculated m/z 136.11 for [C₉H₁₄N⁺].

Synthesis of 1-Butyl-4-methylpyridinium bromide (1e)



Compound **1e** was synthesised according to *General Procedure 1* using 1-bromobutane (1.37 mL, 12.8 mmol). Yield: 2.411 g, 10.5 mmol, 98 %. ¹H NMR (400 MHz, DMSO-d₆) δ_H (ppm) = 9.06 (2H, d, ³J_{HH} = 6.6 Hz, Ar-**H**), 8.01 (2H, d, ³J_{HH} = 6.3 Hz, Ar-**H**), 4.60 (2H, t, ³J_{HH} = 7.4 Hz, R-N-CH₂-), 2.60 (3H, s, Ar-CH₃), 1.86 (2H, p, ³J_{HH} = 7.5 Hz, R-N-CH₂-CH₂-), 1.25 (2H, h, ³J_{HH} = 7.4 Hz, R-N-CH₂-CH₂-CH₂-), 0.87 (3H, t, ³J_{HH} = 7.4 Hz, R-N-CH₂-CH₂-CH₂-CH₃). ¹³C NMR (101 MHz, DMSO) δ_C (ppm) = 158.67, 143.70, 128.28, 59.44, 32.55, 21.34, 18.64, 13.29. LRMS (ES+) found m/z 150.13 calculated m/z 150.13 for [C₁₀H₁₆N⁺].

Synthesis of 1-Pentyl-4-methylpyridinium bromide (1f)



Compound **1f** was synthesised according to *General Procedure 1* using 1-bromopentane (1.59 mL, 12.8 mmol). Yield: 1.395 g, 5.71 mmol, 53 %.

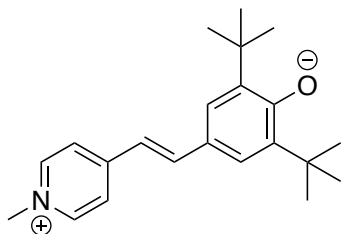
¹H NMR (300 MHz, MeCN-d₃) δ_H (ppm) = 8.92 (2H, d, ³J_{HH} = 6.7 Hz, Ar-**H**), 7.87 (2H, d, ³J_{HH} = 6.2 Hz, Ar-**H**), 4.61 (2H, t, ³J_{HH} = 7.5 Hz, R-N-CH₂-), 2.61 (3H, s, Ar-CH₃), 2.01 – 1.85 (2H, m, R-N-CH₂-CH₂-), 1.43 – 1.20 (4H, m, R-N-CH₂-CH₂-CH₂-CH₂-CH₃), 0.86 (3H, t, ³J_{HH} = 6.8 Hz, R-N-CH₂-CH₂-CH₂-CH₂-CH₃). ¹³C NMR (101 MHz, MeCN-d₃) δ_C (ppm) = 159.52, 143.33, 128.85, 70.78, 30.11, 29.45, 22.31, 21.42, 14.96. LRMS (ES+) found m/z 164.14 calculated m/z 164.14 for [C₁₁H₁₈N⁺].

General Procedure 2. Synthesis of Merocyanine Dyes

1-Alkyl-4-methyl pyridinium bromide (1 equiv.), 3,5-di-tert-butyl-4-hydroxybenzaldehyde (1 equiv.) and piperidine (1.2 equiv.) were dissolved in EtOH/MeCN (30 mL, 1:1 v/v). The reaction mixture was heated at reflux for 16-24 h. The completion of the reaction was determined by TLC. The reaction was stopped and allowed to cool to room temperature

and volatiles were removed *in vacuo* to give an intensely coloured deep blue oil. KOH in EtOH (0.2 M, 50 mL) was added to the oil and the solution was heated at 65 °C for 1 h. The reaction mixture was stopped and allowed to cool to room temperature and volatiles were removed *in vacuo* to give a deep blue oil. The crude product was purified by various methods described below.

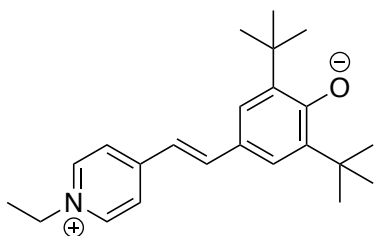
Synthesis of 4-(3,5-Di-*tert*-butyl-4-hydroxystyryl)-1-methylpyridinium (2a)



Compound **2a** was synthesised according to *General Procedure 2* using 1,4-dimethylpyridinium iodide (1.500 g, 6.38 mmol). The crude product was purified by recrystallisation in MeOH/H₂O (9:1, 50 mL) to yield a green solid (1.359 g, 4.20 mmol, 63 %).

¹H NMR (400 MHz, DMSO-*d*₆) δ_H (ppm) = 7.71 (2H, d, ³J_{HH} = 7.1 Hz, Ar-**H**), 7.53 (1H, d, ³J_{HH} = 14.5 Hz, R=C-**H**), 7.42 – 6.88 (4H, m, Ar-**H**), 6.17 (1H, d, ³J_{HH} = 14.5 Hz, R=C-**H**), 3.71 (3H, s, R-N-CH₃), 1.30 (18 H, s, Ar-*t*Butyl). ¹³C NMR (101 MHz, DMSO-*d*₆) δ_C (ppm) = 180.56, 154.83, 150.37, 143.61, 140.02, 129.29, 115.25, 104.12, 48.58, 43.54, 34.68, 29.63. **UV-Vis** (Toluene): λ_{max} (ε / L mol⁻¹ cm⁻¹) 628 (37600), 578 (54400), 543(39600). **HRMS (ES⁺)** found *m/z* 324.2322, calculated *m/z* 324.2327 for [C₂₂H₂₉NO+H⁺].

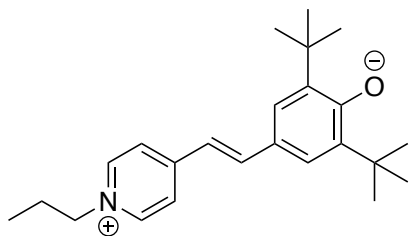
Synthesis of 2,6-Di-*tert*-butyl-4-(2-(1-ethylpyridinium-4-yl)vinyl)phenolate (2b)



Compound **2b** was synthesised according to *General Procedure 2* using 1-ethyl-4-methylpyridinium bromide (**1b**) (1.500 g, 7.42 mmol). The crude product was purified by slow evaporation in acetone (~100 mL) over 72 h to give green crystals (0.822 g, 1.96 mmol, 26 %). ¹H NMR (400 MHz, MeOH-*d*₄) δ_H (ppm) = 7.95 (2h, d, ³J_{HH} = 7.1 Hz, Ar-**H**), 7.63 (1H, d, ³J_{HH} = 14.9 Hz, R=C-**H**), 7.46 – 7.34 (4H, m, Ar-**H**), 6.50 (1H, d, ³J_{HH} =

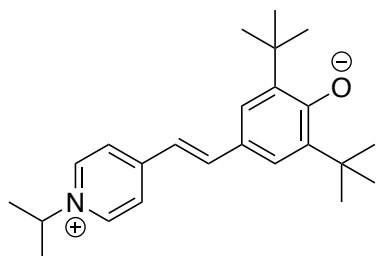
14.9 Hz, R=C-*H*), 4.12 (2H, q, $^3J_{\text{HH}} = 7.5, 5.6$ Hz, RN-CH₂-), 1.47 (3H, t, $^3J_{\text{HH}} = 7.2$ Hz, RN-CH₂-CH₃), 1.41 (18H, s, Ar-*t*butyl). $^{13}\text{C NMR}$ (101 MHz, MeOH-*d*₄) δ_{C} (ppm) = 154.73, 146.45, 141.80, 141.72, 141.34, 141.22, 129.06, 120.14, 110.34, 54.69, 35.90, 30.59, 16.43. **UV-Vis** (Toluene): λ_{max} ($\epsilon / \text{L mol}^{-1} \text{cm}^{-1}$) 628 (22900), 578 (32300), 543 (23000). **HRMS (ES⁺)** found m/z 338.2486, calculated m/z 338.2484 for [C₂₃H₃₁NO+H⁺].

Synthesis of 2,6-Di-*tert*-butyl-4-(2-(1-propylpyridinium-4-yl)vinyl)phenolate (**2c**)



Compound **2c** was synthesised according to *General Procedure 2* using 1-propyl-4-methylpyridinium bromide (**1c**) (2.312 g, 10.7 mmol). The crude product was purified by recrystallisation in MeOH/H₂O (95:5 v/v) to give a green solid (0.902 g, 2.57 mmol, 24 %). $^1\text{H NMR}$ (500 MHz, DMSO-*d*₆) δ_{H} (ppm) = 7.78 (2H, d, $^3J_{\text{HH}} = 7.4$ Hz, Ar-*H*), 7.54 (1H, d, $^3J_{\text{HH}} = 14.4$ Hz, R=C-*H*), 7.25 – 7.09 (4H, m, Ar-*H*), 6.19 (1H, d, $^3J_{\text{HH}} = 14.4$ Hz, R=C-*H*), 3.91 (2H, t, $^3J_{\text{HH}} = 7.1$ Hz, RN-CH₂-), 1.74 (2H, h, $^3J_{\text{HH}} = 7.3$ Hz, RN-CH₂-CH₂-), 1.30 (18H, s, Ar-*t*butyl), 0.86 (3H, t, $^3J_{\text{HH}} = 7.3$ Hz, RN-CH₂-CH₂-CH₃). $^{13}\text{C NMR}$ (101 MHz, DMSO-*d*₆) δ_{C} (ppm) = 154.45, 146.66, 142.03, 141.22, 119.44, 119.10, 108.97, 60.63, 35.94, 30.58, 29.74, 27.97, 26.20, 25.27, 10.87. **UV-Vis** (Toluene): λ_{max} ($\epsilon / \text{L mol}^{-1} \text{cm}^{-1}$) 628 (28900), 578 (40600), 543 (28800). **HRMS (ES⁺)** found m/z 352.2642, calculated m/z 352.2640 for [C₂₄H₃₃NO+H⁺].

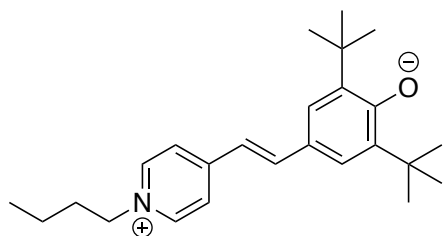
Synthesis of 2,6-Di-*tert*-butyl-4-2-(1-isopropylpyridinium-4-yl)vinyl)phenolate (**2d**)



Compound **2d** was synthesised according to *General Procedure 2* using 1-isopropyl-4-methylpyridinium bromide (**1d**) (0.500 g, 2.31 mmol). The crude product was purified by recrystallisation in EtOH to give a dark blue solid (0.495 g, 1.41 mmol, 61 %). $^1\text{H NMR}$ (400 MHz, DMSO-*d*₆) δ_{H} (ppm) = 7.87 (2H, d, $^3J_{\text{HH}} = 7.1$ Hz, Ar-*H*), 7.55 (1H, d, $^3J_{\text{HH}} = 14.5$ Hz, R=C-*H*), 7.26 – 7.09 (4H, m, Ar-*H*), 6.19 (1H, d, $^3J_{\text{HH}} = 14.5$ Hz, R=C-*H*), 4.34

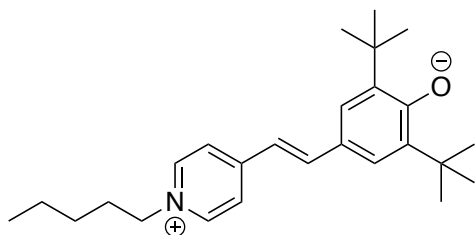
(1H, hept, $^3J_{\text{HH}} = 6.6$ Hz, RN-CH₂-), 1.41 (6H, d, $^3J_{\text{HH}} = 6.7$ Hz, RN-CH-(CH₃)₂), 1.30 (18H, s, Ar-*t*butyl). **¹³C NMR** (101 MHz, DMSO-*d*₆) δ_{C} (ppm) = 180.55, 150.85, 145.23, 143.68, 137.25, 133.49, 128.43, 115.35, 104.15, 58.51, 34.70, 29.64, 22.01. **UV-Vis** (Toluene): λ_{max} ($\epsilon / \text{L mol}^{-1} \text{cm}^{-1}$) 628 (49300), 578 (67900), 543 (47200). **HRMS (ES+)** found *m/z* 352.2640, calculated *m/z* 352.2640 for [C₂₄H₃₃NO+H⁺].

Synthesis of 2,6-Di-*tert*-butyl-4-2-(1-butylpyridinium-4-yl)vinylphenolate (**2e**)



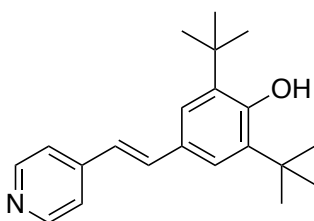
Compound **2e** was synthesised according to *General Procedure 2* using 1-butyl-4-methylpyridinium bromide (**1e**) (1.500 g, 6.52 mmol). The crude product was purified by recrystallisation in EtOH to give a green solid (2.138 g, 5.85 mmol, 90 %). **¹H NMR** (400 MHz, MeOH-*d*₄) δ_{H} (ppm) = 7.90 (2H, d, $^3J_{\text{HH}} = 6.9$ Hz, Ar-**H**), 7.63 (1H, d, $^3J_{\text{HH}} = 14.9$ Hz, R=C-**H**), 7.41 – 7.34 (4H, m, Ar-**H**), 6.44 (1H, d, $^3J_{\text{HH}} = 14.9$ Hz, R=C-**H**), 4.09 (2H, t, $^3J_{\text{HH}} = 7.3$ Hz, RN-CH₂-), 1.83 (2H, p, $^3J_{\text{HH}} = 7.5$ Hz, RN-CH₂-CH₂-), 1.40 (18H, s, Ar-*t*butyl), 1.38 – 1.32 (2H, m, RN-CH₂-CH₂-CH₂-), 0.98 (3H, t, $^3J_{\text{HH}} = 7.4$ Hz, RN-CH₂-CH₂-CH₂-CH₃). **¹³C NMR** (400 MHz, MeOH-*d*₄) δ_{C} (ppm) = 154.20, 146.51, 142.23, 141.21, 140.04, 129.45, 124.76, 119.26, 108.70, 58.90, 35.88, 33.91, 30.56, 20.39, 13.74. **UV-Vis** (Toluene): λ_{max} ($\epsilon / \text{L mol}^{-1} \text{cm}^{-1}$) 628 (11200), 578 (15700), 543 (11100). **HRMS (ES+)** found *m/z* 366.2797, calculated *m/z* 366.2804 for [C₂₅H₃₅NO+H⁺].

Synthesis of 2,6-Di-*tert*-butyl-4-(2-(1-pentylpyridinium-4-yl)vinyl)phenolate (**2f**)



Compound **2f** was synthesised according to *General Procedure 2* using 1-pentyl-4-methylpyridinium bromide (**1f**) (2.613 g, 10.7 mmol). The crude product was purified by recrystallisation in MeOH/H₂O (95:5 v/v) to give a green crystalline solid (0.472 g, 1.24 mmol, 7 %). ¹H NMR (400 MHz, DMSO-*d*₆) δ_H (ppm) = 7.77 (2H, d, *J* = 7.0 Hz, Ar-**H**), 7.53 (1H, d, *J* = 14.4 Hz, R=C-**H**), 7.42 – 6.78 (4H, m, Ar-**H**), 6.17 (1H, d, *J* = 14.5 Hz, R=C-**H**), 3.92 (2H, t, *J* = 7.2 Hz, RN-CH₂-), 1.72 (2H, p, *J* = 7.1 Hz, RN-CH₂-CH₂-), 1.30 (18H, s, Ar-*t*butyl), 1.26 – 1.20 (4H, m, RN-CH₂-CH₂-CH₂-), 0.86 (3H, t, *J* = 7.1 Hz, RN-CH₂-CH₂-CH₂-CH₃). ¹³C NMR (101 MHz, DMSO-*d*₆) δ_C (ppm) = 180.69, 150.40, 146.94, 143.62, 139.10, 129.46, 127.52, 115.43, 104.12, 56.22, 46.80, 34.66, 27.72, 21.60, 13.79. UV-Vis (Toluene): λ_{max} (ε / L mol⁻¹ cm⁻¹) 628 (30500), 578 (42600), 543 (30100). HRMS (ES⁺) found *m/z* 380.2953, calculated *m/z* 380.2953 for [C₂₆H₃₇NO+H⁺].

Synthesis of 2,6-di-*tert*-butyl-4-(2-(pyridin-4-yl)vinyl)phenol (MCP, **3**)



4-Bromo-2,6-di-*tert*-butylphenol (0.500 g, 1.75 mmol), 4-vinylpyridine (0.23 mL, 2.10 mmol) and tri-*o*-tolylphosphine (0.107 g, 0.35 mmol) were placed in a flask and dissolved in triethylamine/DMF (20 mL, 1:1 v/v). The reaction mixture was degassed by freeze-pump-thaw method (3 cycles) and Pd(OAc)₂ (0.044g, 0.18 mmol) was subsequently added under N₂. The reaction mixture was heated at 90 °C for 16h. The reaction was stopped and allowed to cool to room temperature. Distilled water (100 mL) was then added and the reaction mixture was extracted with DCM (3 x 50 mL). The organic layer was washed with distilled water (3 x 100 mL) to remove excess DMF and then washed with weak acid to remove excess triethylamine. The organic layers were combined and washed with brine (50 mL), then dried over magnesium sulfate, filtered and the volatiles

removed *in vacuo*. The crude oil was triturated with hexane to give a brown solid (0.190 g, 0.61 mmol, 35 %). **¹H NMR** (400 MHz, DMSO-*d*₆) δ_H (ppm) = 8.49 (2H, d, *J* = 5.1 Hz, Ar-**H**), 7.54 (2H, d, *J* = 5.5 Hz, Ar-**H**), 7.49 (1H, d, *J* = 16.4 Hz, R=C-**H**), 7.40 (2H, s, Ar-**H**), 7.26 (1H, s, Ar-O**H**), 7.01 (1H, d, *J* = 16.4 Hz, R=C-**H**), 1.42 (18H, s, Ar-*t*butyl). **LRMS (ES+)** found *m/z* 310.22, calcd *m/z* 310.22 for [C₂₁H₂₇NO+H⁺].

References

- 1 L. G. S. Brooker, G. H. Keyes and D. W. Heseltine, *J Am Chem Soc*, 1951, **73**, 5350–5356.
- 2 L. G. S. Brooker, G. H. Keyes, R. H. Sprague, R. H. VanDyke, E. VanLare, G. VanZandt, F. L. White, H. W. J. Cressman and S. G. Dent, *J Am Chem Soc*, 1951, **73**, 5332–5350.
- 3 H. W. Gibson and F. C. Bailey, *Can J Chem*, 1975, **53**, 2162–2170.
- 4 G. L. Gaines, *Anal Chem*, 1976, **48**, 450–451.
- 5 L. Beuze, *J Phys Chem*, 1986, **90**, 192.
- 6 N. S. Bayliss and E. G. McRae, *J. Amer. Chem. Soc*, 1952, **74**, 5803–5804.
- 7 E. G. McRae, *Spectrochimica Acta*, 1958, **12**, 192–210.
- 8 L. G. S. Brooker, G. H. Keyes, R. H. Sprague, R. H. VanDyke, E. VanLare, G. VanZandt, F. L. White, H. W. J. Cressman and S. G. Dent, *J Am Chem Soc*, 1951, **73**, 5332–5350.
- 9 L. G. S Brooker, G. H. Keyes, D. W. Heseltine and B. L. G S Brooker, *Org. Chhtn*, 1951, **73**, 2023.
- 10 C. Reichardt, *Chem Rev*, 1994, **94**, 2319–2358.
- 11 J. Catalán, E. Mena, W. Meutermans and J. Elguero, *Chem. Phys. Lett*, 1992, **96**, 2122–2166.
- 12 M. Tsukada, Y. Mineo and K. Itoh, *J. Phys. Chem*, 1989, **93**, 7989–7992.
- 13 H. Muströph, K. Reiner, B. Senns, J. Mistol, S. Ernst, D. Keil and L. Hennig, *Chemistry – A European Journal*, 2012, **18**, 8140–8149.
- 14 J. O. Morley, R. M. Morley and A. L. Fitton, *J Am Chem Soc*, 1998, **120**, 11479–11488.
- 15 C. J. MacNevin, D. Gremyachinskiy, C. W. Hsu, L. Li, M. Rougie, T. T. Davis and K. M. Hahn, *Bioconjug Chem*, 2013, **24**, 215–223.
- 16 A. V. Kulinich, E. K. Mikitenko and A. A. Ishchenko, *Physical Chemistry Chemical Physics*, 2016, **18**, 3444–3453.
- 17 P. R. Dragsten and W. W. Webb, *Biochemistry*, 1978, **17**, 5228–5240.
- 18 P. I. Lelkes and I. R. Miller, *J Membr Biol*, 1980, **52**, 1–15.
- 19 A. Mishra, M. K. R. Fischer and P. Büberle, *Angewandte Chemie International Edition*, 2009, **48**, 2474–2499.
- 20 N. Robertson, *Angewandte Chemie International Edition*, 2006, **45**, 2338–2345.
- 21 H. Bürckstümmer, N. M. Kronenberg, M. Gsänger, M. Stolte, K. Meerholz and F. Würthner, *J Mater Chem*, 2009, **20**, 240–243.
- 22 S. Basu, S. De and B. B. Bhowmik, *Spectrochim Acta A Mol Biomol Spectrosc*, 2007, **66**, 1255–1260.

- 23 P. Kaschny and F. M. Goñi, *Eur J Biochem*, 1992, **207**, 1085–1091.
- 24 K. F. Donchi, G. Peter Robert, B. Ternai and P. J. Derrick, *Aust J Chem*, 1980, **33**, 2199–2206.
- 25 S. S. Shah and M. J. Minch, *Journal of Organic Chemistry*, 1979, **44**, 3252–3255.
- 26 M. Mukhopadhyay, C. sen Varma and B. B. Bhowmik, *Colloid Polym Sci*, 1990, **268**, 447–451.
- 27 K. Yamamoto and S. Motomizu, *Talanta*, 1991, **38**, 477–482.
- 28 H. Sato, M. Kawasaki, K. Kasatani, Y. Kusumoto, N. Nakashima and K. Yoshihara, *Chem Lett*, 1980, 15529–1532.
- 29 R. Humphry-Baker, M. Grätzel and R. Steiger, *J Am Chem Soc*, 1980, **102**, 847–848.
- 30 T. Wolff, *Berichte der Bunsengesellschaft für physikalische Chemie*, 1981, **85**, 145–148.
- 31 K. K. Rohatgi-Mukherjee, R. Chaudhuri and B. B. Bhowmik, *J Colloid Interface Sci*, 1985, **106**, 45–50.
- 32 B. B. Bhowmik, R. Chaudhuri and K. K. Rohatgi-Mukherjee, *Indian J Chem*, 1987, **2**, 95–98.
- 33 B. B. Bhowmik and M. Mukhopadhyay, *Colloid Polym Sci*, 1988, **266**, 672–676.
- 34 S. Samim Ali, A. Gangopadhyay, A. Kumar Pramanik, U. Narayan Guria, S. Kumar Samanta and A. Kumar Mahapatra, , DOI:10.1016/j.dyepig.2019.107585.
- 35 T. J. Dale and J. Rebek, *J Am Chem Soc*, 2006, **128**, 4500–4501.
- 36 T. J. Dale and J. Rebek, *Angewandte Chemie*, 2009, **121**, 7990–7992.
- 37 R. Gotor, S. Royo, A. M. Costero, M. Parra, S. Gil, R. Martínez-Máñez and F. Sancenón, *Tetrahedron*, 2012, **68**, 8612–8616.
- 38 L. G. S. Brooker and G. H. Keyes, *J Am Chem Soc*, 1951, **73**, 5356–5358.
- 39 M. J. Minch and S. S. Shah, *J Chem Educ*, 1977, **54**, 709.

Chapter 4. Smart Devices for Chemical Warfare Agent (CWA) Detection

4.1. Introduction

4.1.1. Existing field detectors

The chemical weapons convention came into force in 1997 by the Organisation for the Prohibition of Chemical Weapons (OPCW) to control and ban CWAs. However recent uses of these agents in the Syrian civil war (2013-2018)¹ and in the UK (2018) with the use of nerve agents suggest the continued illicit synthesis and stockpiling of CWAs. In light of present threats, it is vital that analytical methods are adapted for on-field identification of suspected CWA samples. The rapid, sensitive, and selective identification of these agents is important in protecting first responders and medical personnel as well as the effective treatment of patients.² Current methods for on-site CWA detection largely involve using standalone devices or hand-held detectors for the determination of multiple target analytes. Detectors are based on a variety of techniques including ion mobility spectroscopy, flame photometry, infra-red spectroscopy, raman spectroscopy, surface acoustic wave, photo ionisation detection, and flame ionisation detection.³ Apart from this, gas chromatographs (GC) and GC combined with mass spectrometry detectors (GC/MS) are also available. However, these instruments suffer from several of the following limitations including high cost, non-portability, lack of selectivity and sensitivity, complicated operations, and long response times.² To overcome these disadvantages, colorimetric detection technology is an elegant solution as they are usually inexpensive, lightweight and easily operated in the field. However, there is very little purely colorimetric chemistry in this area with most sensors based on equipment. When a target analyte encounters certain reagents, a response can be observed visually in the form of a colour change or spectroscopically by fluorescence of UV-vis spectroscopy. These reagents can be incorporated into various devices such as papers, tubes, or kits. Papers are employed for detecting suspect liquids on a surface whereas, detector tubes are utilised for detecting vaporous agents. Detection kits are manufactured to contain a combination of papers and tubes for multi-analyte detection. Chemical detection papers are impregnated with soluble dyes and pH indicator to produce a visible colour change upon absorption of a liquid CWA. A yellow colour signifies the presence of G-type nerve agents, red denotes a blister agent and green signifies a V-type nerve agent. Figure 4.1 demonstrates the employment of these papers in the field. These user friendly and portable alternatives have rapid detection response times and were utilised by the military for decades before being discontinued to the mutagenicity of the dyes.^{4,5}



Figure 4.1. Colorimetric detection paper.

Colorimetric detection tubes such as Dräger tubes, shown in Figure 4.2, are glass tubes containing specific reagents impregnated into a silica gel support.⁶⁹ This technology requires a pump to draw the vaporous agent through the impregnated silica, causing a change in colour depending on the class of agent present.^{3,6,7} Phosphoric acid ester tubes experience a colour change from yellow to pink after exposure to nerve agent and yellow thioether tubes generate an orange colour upon exposure to HD. These tubes are able to quantitatively detect live agent as the intensity of colour production is proportional to the concentration of agent. These tubes can be combined in a manifold as a simultaneous testing set.



Figure 4.2. Commercially available colorimetric tubes.

Despite their promising features, colorimetric detection techniques lack specificity and suffer from many false positives caused by common chemicals such as bleach, brake fluid, and antifreeze. To overcome this limitation, efforts have been focused on the development of novel chemical probes for CWAs based on colorimetric or fluorogenic

detection. These nucleophilic probes exploit the electrophilic nature of nerve agents and blister agents to cause a change in their optical properties. However, there is less colorimetric chemistry capable of rapid detection at ambient temperature and also detectable by the naked-eye.

4.1.3. Colorimetric swab technology

Swab technology is an effortless approach to incorporate existing homogeneous chemistry into a hand-held device that can be easily deployed in the field. These swab systems have a lower risk of live agent contamination compared to paper-based technology as they allow a greater distance between the user and a potential hazard. Furthermore, following saturation of the swab tip, the entire swab is placed into a protective casing which prevents any potential leaking of the formulation containing live agent. These point-of-use devices can be deployed by both military personnel and first responders for rapid detection of hazardous chemicals in real-life scenarios. Colorimetric hand-held technology must have the following attributes to be an effective system; inexpensive reagents and materials, easy to use, portable, rapid response times, sensitive, selective, and disposable. Furthermore, the technology must generate a distinct colour change with the intention that the end user requires no prior chemical or laboratory knowledge to both operate the system and to understand the result.

4.2. Aims

The purpose of the work described below was to explore the performance of the mustard detection formulation in real-life scenarios. The applicability of the sensing formulation developed in Chapter 2 for the determination of CEES from spiked soil samples and contaminated surfaces. These solution-based formulations were developed into suitable field-deployable systems for the colorimetric determination of blister agents.

4.3. Results and Discussion

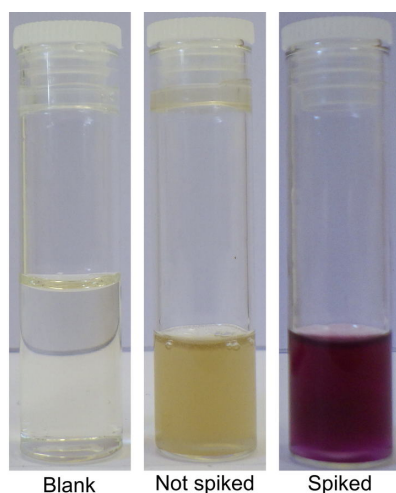
4.3.1. Detection in real-life scenarios

The requirement for easy-to-use field deployable devices for the detection of chemical warfare agents (CWAs) has become a necessary field of research due the illicit use and stockpiling of these highly toxic agents. Once deployed, sulfur mustard (SM) is dispersed into the environment and can remain active from hours to even weeks and it has been found to persist in soil and water for decades.^{8,9} Thus, it is crucial that sensing protocols are developed into easy-to-use devices to detect the presence of live agent in real-life scenarios.

4.3.2. Sensing Mustard Agents in Soil

To determine the practical application of NBP, the presence of CEES in soil was investigated. A sample of soil was spiked with CEES and treated with the anionic microemulsion formulation and allowed to react at ambient temperature for 5 minutes. Furthermore, a sample of soil not spiked with CEES was also treated in a similar manner. Images were taken after 5 minutes of exposure to soil samples and the supernatant was subsequently collected (Figure 1.4). This removal of soil from the solution allowed any changes in colour to be better perceived by the naked-eye.

The development of a purple colour characteristic of the conjugated dye indicated the presence of CEES. Although the colour is strong here, the previously high performance of the formulation with CEES has not transferred to soil studies. It is also worth noting the turbidity of the treated formulations compared to the blank solution. However, these details do not affect the visibility of the colour. The soil sample not spiked with CEES gave a slight colour change compared to the blank solution which is not unexpected after treatment with impure soil particles. Encouragingly, the solution does not produce the characteristic blue-purple colour of the dye and thus clearly showing the absence of CEES. The total volume of the solution after the removal of soil particles was lower due to the soil absorbing the formulation. Despite this, a clear colour change occurs after 5 minutes of exposure.



Component	Volume / μL
NBP (0.4 M)	100
NaOH (0.4 M)	200
Anionic microemulsion	1700
CEES	2

Figure 1.4. Performance of SDS-5T formulation with spiked and not spiked soil samples. Vials are from left to right: Blank; filtered solution after exposure to control soil sample; filtered solution after exposure to CEES-spiked soil sample.

4.3.3. Sensing on surfaces

The development of a swab device permits the incorporation of the existing formulation solution into a simple, inexpensive, and disposable device that can be used by untrained first responders. The cotton swab can be wiped over a suspected contaminated surface before being placed back into the swab chamber. The snap valve can subsequently be broken to allow the bulb solution to flow down the hollow tube of the swab to react with the analyte absorbed on the swab tip. A colour is generated if the target CWA is present.

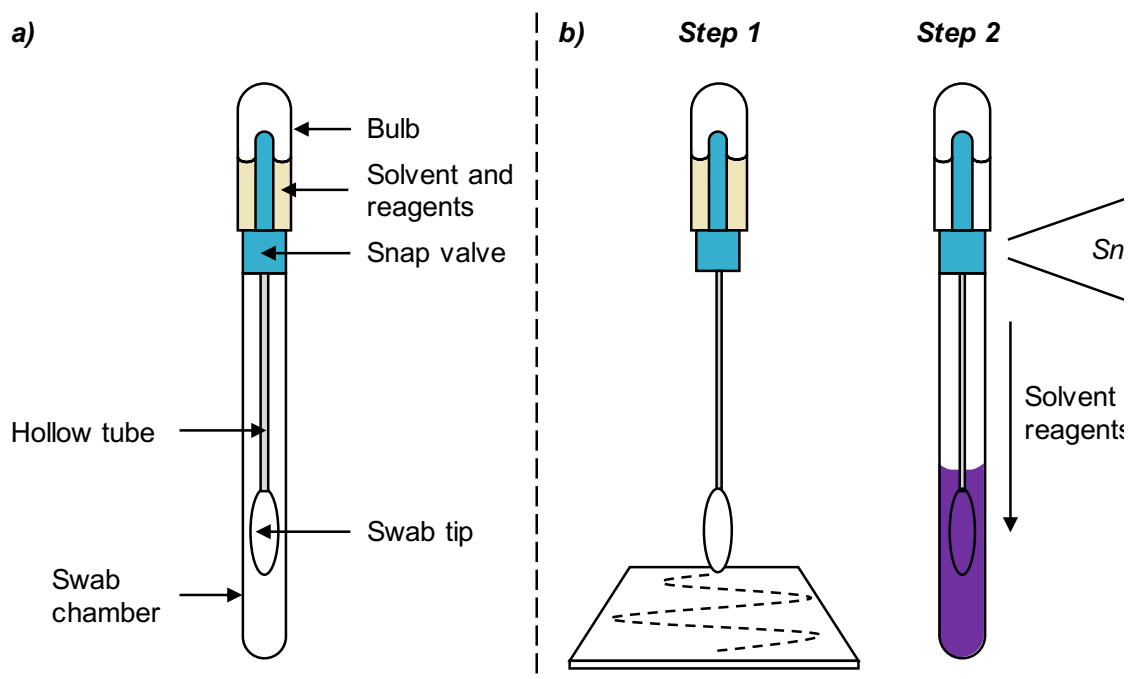
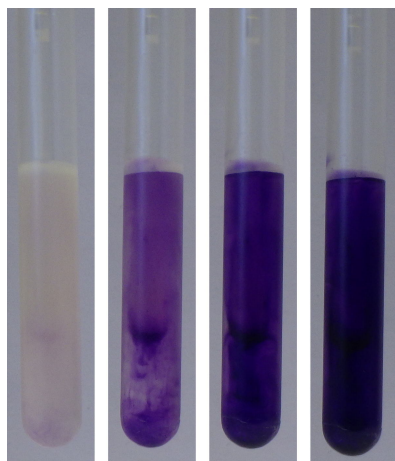


Figure 4.5. Illustration of a) swab components and b) method for detection of a contaminated surface.

To gain a better understanding of how the device works, initial tests with the swab were carried out using a control sample of SDS-5T. This system was deemed a challenging solution as the inherent saponaceous nature of the surfactant mixture could lead to dispensing difficulties. Hence, giving time to solve any issues at the initial stages of manufacture. Challenges arose when emptying the bulb of solvent because the system behaved as a pipette and as a result, solvent was drawn back up the hollow tube and returned to its initial location in the bulb. This caused the microemulsion to become susceptible to foaming which made the transfer of solution more challenging. To overcome this problem, a small hole was placed in the hollow tube of the swab to equalise the pressure. This simple remedy worked well with the microemulsion staying at the bottom of the swab chamber in repeated test runs. This was implemented in all future swab manufacturing. The NBP formulation was incorporated into a swab device as seen in Figure 4.5. and subsequently used to determine the presence of CEES from a contaminated surface.

4.3.3.1. Swab Device for The Detection of Mustard Agents



Component	Volume (μL)
NBP (0.4 M)	100
NaOH (0.4 M)	200
Anionic microemulsion	1700
CEES	2

Figure 4.6. Colorimetric response of swab device containing SDS-5T formulation after detection of CEES on a surface. Swabs are from left to right in each image: immediately after CEES exposure, 1 min exposure, 3 min exposure, and 5 min exposure.

It is evident from the images in Figure 4.6 that NBP in anionic microemulsion performs to a similar high standard to that of the initial solution tests executed in glass vials whereby a colour change occurs instantaneously upon exposure to CEES and the colour continued to intensify over the 5-minute monitoring period.

The swabs were not shaken during this period in order to observe the dispersion of colour. Although the colour takes approximately 3 minutes to sufficiently disperse, the recognisable colour of the NBP-CEES dye is unmistakable for the presence of CEES. Furthermore, the swab tip is nearly unperceived at the 5-minute mark due to the intensity of the colour produced.

4.4. Experimental

4.4.1. Procedure for CEES testing

Prior to testing formulations with CEES, a bleach bath must be prepared to decontaminate all equipment and glassware that encounter hazardous chemicals during testing experiments. This decontaminating solution is prepared with thick bleach, IPA and water in a 1:1:2 ratio with NaOH pellets to maintain a high pH. Furthermore, coloured

crepe paper is attached to the fume hood sash to demonstrate the level of extraction. Testing involving simulants should always be conducted with a supervisor or other qualified person in attendance. A glass petri dish is utilised as a secondary container to store the simulant bottle. In addition to standard laboratory PPE, two pairs of gloves of opposing colours are worn to handle simulants in order to identify any tears in the material. Once the simulant has been carefully added to the formulation and the necessary equipment contaminated in the bleach bath, gloves are inspected for contamination. If contaminated, the gloves are placed in the bleach bath for decontamination.

4.4.2. Procedure for preparation of spiked soil sample

Soil sample (2.0 g) was mixed with CEES (2 μ L) in diethyl ether (2 mL) and the mixture was allowed to stand for 20 min. The solvent was evaporated by nitrogen blow down to obtain a dry sample of soil spiked with CEES. This soil sample was treated with 2 mL of the appropriate formulation and allowed to react at ambient temperature for 5 minutes. Moreover, a soil sample not spiked with CEES was also treated in a similar manner.

4.4.3. Manufacture of swab devices

The swab device consists of 4 components: a bulb, a snap valve, a cotton swab, and a swab chamber (Figure 4.8). These materials are purchased from Medical Packaging Corp. (Hygiene, UK). The sensing formulation is placed in the bulb and the snap valve is tightly inserted using a custom-made swab press instrument. The snap valve is available in two types: single and double which denotes the amount of times required to break the snap valve to release the formulation down the swab shaft.

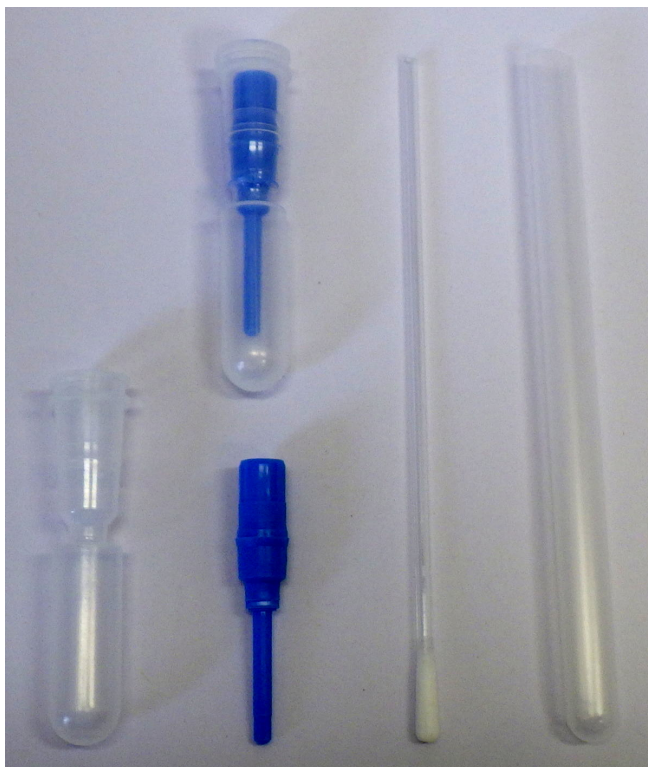


Figure 4.8. Swab components. Anti-clockwise from the top: Snap valve inserted into bulb; bulb; snap valve; swab; swab chamber.

4.4.4. Procedure for swabbing a CEES contaminated surface

CEES (2 μL) was placed onto a glass petri dish to mimic a real-life scenario of a contaminated surface. The swab chamber was removed, and the cotton swab tip of the device was wiped over the surface several times to ensure maximum absorption of the CEES. The swab was placed back into the chamber and the valve was snapped to release the appropriate sensing formulation, which was allowed to react at ambient temperature for 5 minutes.

References

- 1 R. Pita and J. Domingo, *Toxics*, 2014, **2**, 391–402.
- 2 T. Okumura, K. Suzuki, A. Fukuda, A. Kohama, N. Takasu, S. Ishimatsu and S. Hinohara, *Academic Emergency Medicine*, 1998, **5**, 618–624.
- 3 R. Sferopoulos, *Australian Government Department of Defence*, 2009, 98.
- 4 D. Thoraval, J. W. Bovenkamp, R. W. Bets and B. V. Lacroix, *Development of Paper, Chemical Agent Detector, 3-way Liquid Containing Non-Mutagenic Dyes. II-Replacement of The Blue Indicator Dye Ethyl-bis-(2,4-dinitrophenyl) acetate (EDA)*, Canada, 1988.
- 5 E. R. Nestmann, D. J. Kowbel and J. A. Wheat, *Carcinogenesis*, 1981, **2**, 879–883.
- 6 A. Bussey, A. Clarke and J. Lambert, PCT/GB2004/001083 WO/2004/081561, March 11, 2004.
- 7 1962.
- 8 Y. C. Yang, L. L. Szafraniec, W. T. Beaudry and R. J. Way, *Journal of Organic Chemistry*, 1988, **53**, 3293–3297.
- 9 G. W. Wagner and B. K. MacIver, *Langmuir*, 1998, **14**, 6930–6934.

Chapter 5. Concluding Remarks

5.1. Conclusion and Future Remarks

The research presented in this thesis highlights the potential of NBP and merocyanine dye, MCP, 3 as point-of-use sensors for mustards. The below discussion is presented as a summary of the work presented in this thesis, as well as to act as a critical evaluation of the results and to comment on the future direction of the work.

Expanding upon previous patented work by Fallis and Morgan,¹ NBP was incorporated into surfactant systems to improve upon the reactivity of NBP as a colorimetric assay for mustard agents. The use of NBP as the sensor meets the design criteria of incorporating inexpensive commercial reagents with relatively small quantities of all reagents required to prepare the formulation.

Upon exposure to CEES, NBP in micellar, swollen micellar and microemulsion formulations produced a positive blue-purple colour. The SDS systems were found to have the highest performance compared to the cationic and non-ionic systems with the greatest overall combined conversion of NBP to NBP-CEES dye. This advancement was achieved through the compartmentalised nature of the SDS structure in water which allowed NBP and base to be formulated in a one-pot system.

NBP was found to detect a small volume of CEES, with 2 μL of simulant detected which is the design criteria threshold. The target of 0.1 μL CEES was not met due to the lack of equipment with no small volume pipettes available. However, we predict that the formulation can detect such small volumes as intense colour changes have been generated rapidly with 2 μL of simulant. Furthermore, the formulation remained coloured for up to 24 hours after exposure to positive. Longer monitoring periods were not investigated as this is sufficient time for a colour change to remain when considering potential transportation of the formulation to a separate location. Conversely, the formulation remained colourless for up to 24 upon exposure to negative. The formulations were not monitored for longer time periods however this is sufficient time when considering transportation of the formulation.

Given that one of the target design criteria relates to colour persistence with larger volumes of CEES (20 μL), the solvation of the simulant was investigated in anionic swollen micelle. This system was chosen to act as best-case scenario in which the oil content of the system was solely derived from CEES. SDS-0T was found to dissolve a large quantity of CEES with 6.2 mL of simulant incorporated at ambient temperature. Although solubility studies were not conducted with SDS-5T microemulsion, it is predicted that the presence of toluene would allow this formulation to dissolve a higher volume of CEES as this hydrophobic, greasy material will be easily solvated in the toluene oil-core.

Unfortunately, NBP exhibited instability in SDS formulations with the production of $[\text{H}_{25}\text{C}_{12}\text{-NBP}]^+$ observed in mass spectrometry analysis of the formulation after 1 month of storage. The substitution of the more stable SDBS surfactant eliminated this instability and its incorporation into a formulation with NBP was able to detect CEES at a similar rate and colour intensity. Due to the time constraints of the project, thorough shelf-life investigations into the alternative SDBS formulation could not be carried out. Thus, we cannot confidently say that this alternative surfactant generates a formulation with a target shelf-life of two years. Upon comparison of the conversion of NBP to NBP-CEES dye, the SDBS formulation displayed an approximate 50 % decrease compared to SDS which was attributed to the increased viscosity of the system. Further work on the rheological properties of both systems is required to confirm this theory.

However, both SDS and SDBS formulations eliminated the prior limitations experienced by Epstein and Turner.^{2,3} The previous NBP assays required harsh conditions for the treatment of NBP with an alkylating agent. The enhancement of the electrophilicity of mustard agents is promoted by the negatively charged droplet of the anionic microemulsion. As a result, sulfur and nitrogen mustards react rapidly at ambient temperature. The compartmentalised character of the microemulsion allow incompatible reagents to be formulated together in a one-pot aqueous system. This advancement has identified the NBP formulation as a potential smart device for deployment in real-life scenarios.

The characteristic fluorescent behaviour of pyrene was exploited to investigate the location of NBP in the microemulsion. The 3/1 ratio plotted as a function of NBP concentration showed invariance of the measured values suggesting that NBP resides in the oil-core of the SDS droplet.

Many false positives were tested against NBP including reactive electrophiles, blister and nerve agent simulants and several known false positive analytes of discontinued colorimetric detection paper. Although a couple of these species produced an undesirable response, the observed colour was not the characteristic blue-purple of the NBP-CEES dye. Thus, we can confidently say that NBP is selective towards sulfur and nitrogen mustards and thus meets the last target criteria of generating a sensor that is effective against all common false positives.

The latter study of merocyanine dyes as alternative self-assembled sensors (SAS) was presented in its early stages of development. However, the colour change observed upon reaction of the merocyanine precursor with CEES is promising. Future work in this area requires focus on the purification of merocyanine reagents to eliminate the inherent colour of the blank formulation which would also increase the solubility of

the merocyanine in the droplet core. Hence, allowing meaningful and thorough investigations into the behaviour of the merocyanine in microemulsion formulations.

Unfortunately, the strong solvatochromism of the systems derived from the parent Brooker's merocyanine renders this type of system less useful in potential point-of-use applications where a 'fixed' colour response is most desirable, particularly if the method were to be used by inexperienced personnel. These types of material may however be used as solvent polarity probes as alternatives to more expensive Reichardt's dyes. The successful formation of an analyte-induced dye is an exciting development. While the colour of the dye observed in the formulation examined is not ideal, it does show that from commercially available precursors a relatively complex dye can be formed *in-situ* by the addition of the target analyte. This holds good future promise as it is relatively straightforward to vary the components to, for example, incorporate a higher degree of conjugation to shift the spectra observed towards the photopic maximum and hence more intensely perceived colours.

The established formulation for mustards developed in Chapter 2 was successfully manufactured into a field-deployable swab system for use by first responders. These swabs are an advancement on current equipment-based techniques for the determination of CWAs as they are inexpensive to manufacture and portable. Furthermore, the simple observation of colour within 1 minute provides non-experts in the field with an easy-to-use system for the determination of mustard agents. The formulation exhibited a high performance when exposed to CEES which were comparable to previous solution-based testing in glass vials. Slight adaptation was required in assembling the swab components with the requirement of creating a small hole in the swab shaft to prevent the formulation from transferring back into the swab bulb. Further studies are required regarding swab manufacture by integrating alternative components such as the introduction of filters and adjusting the swab length and material of the swab tip. Soil studies were performed on the NBP formulation exhibited moderately high success. The presence of soil produced a turbid final solution however this did not impede on the chemistry of the system and a coloured response was produced upon exposure to CEES-spiked soil and the formulation remained colourless when exposed to a control soil sample. Although the colour intensity was not comparable to previous solution-based tests with CEES, the difference in colour after 5 minutes of exposure was clearly observed by the naked eye.

As commercial colorimetric chemical papers are another interesting branch of smart devices, the development of these established formulations would be required. We postulate that the manufacture of paper-based products with impregnated reagents

will be a challenging venture, particularly with the NBP system as the compartmentalised nature of the formulation would be difficult to transfer to a “dry” device.

References

- 1 WO 2012/052747 A2, *PCT Int. Appl.*, 2012, 1–46.
- 2 C. R. Turner, *Analyst*, 1974, **99**, 431–434.
- 3 J. Epstein, R. W. Rosenthal and R. J. Ess, *Anal Chem*, 1955, **27**, 1435–1439.

Appendix

Compound	Merocyanine 2b
Formula	C ₂₃ H ₃₁ NO
$D_{calc.}/g\ cm^{-3}$	1.101
μ/mm^{-1}	0.066
Formula Weight	337.49
Colour	dark green
Shape	block
Size/mm ³	0.08×0.05×0.03
T/K	100(2)
Crystal System	monoclinic
Space Group	<i>P</i> 2 ₁ / <i>c</i>
<i>a</i> /Å	9.7065(5)
<i>b</i> /Å	13.1999(9)
<i>c</i> /Å	15.9901(8)
$\alpha/^\circ$	90
$\beta/^\circ$	96.289(4)
$\gamma/^\circ$	90
<i>V</i> /Å ³	2036.4(2)
<i>Z</i>	4
<i>Z'</i>	1
Wavelength/Å	0.71075
Radiation type	MoK α
$\theta_{min}/^\circ$	2.006
$\theta_{max}/^\circ$	25.003
Measured Refl.	14505
Independent Refl.	3590
Reflections with <i>I</i> > 2(<i>I</i>)	2323
<i>R</i> _{int}	0.1408
Parameters	233
Restraints	0
Largest Peak	0.344
Deepest Hole	-0.270
GooF	0.941
<i>wR</i> ₂ (all data)	0.1879
<i>wR</i> ₂	0.1587
<i>R</i> ₁ (all data)	0.1051
<i>R</i> ₁	0.0628

Table 1. Crystal data of compound **2b** (Chapter 2)